Dissecting the neutralising antibody response to the porcine reproductive and respiratory syndrome virus to identify novel vaccine targets



Jack W P Hayes

St Hugh's College

University of Oxford

A thesis submitted for the degree of

Doctor of Philosophy

Hilary Term 2024

Acknowledgments

I would first like to thank each member of my supervisory team: Professor Simon Graham, Professor Ray Owens, Dr. Jay Calvert, Professor Jonathan Grimes, and Professor John Hammond for their contributions throughout this project. In particular, I would like to highlight the exemplary support and guidance provided by Simon and Ray, who served as my primary supervisors. Their patience and encouragement have shaped both the project and my own personal development. For this and much more, I am sincerely grateful.

I would also like to thank all the of PRRS Immunology group members, past and present, placement and post-doc, I can't think of any team I'd have rather been a part of. Thank you especially to Dr. Jane Edwards who, whether it was part of Dead Cell Immunology, The COVID-19 Dream Team, or the hypothetical PRRS Immunology tent, was always there to provide a good laugh and sage advice, both in science and in life; and to Dr. Rory Fortes de Brito, a phenomenal drinking buddy and constant positive presence in the office, I'm sorry we could never bring home the rounders trophy.

Thanks must also be given to many collaborators. Dr Jean-Pierre Frossard (Animal and Plant Health Agency, UK) for provision of the essential PRRSV-1 strains; Dr Barbara Klupp (Friedrich-Loeffler-Institut, Isle of Riems, Germany) for provision of the anti-GP3 mAb; Dr Andra Corder (Seppic, France) for provision of the Montanide ISA 201 VG; Dr Jonathan Lovell (University of Buffalo, USA) for provision of the CoPoP/PHAD/QS21 liposomes; Prof. Robin Shattock, and Dr. Kostas Paschos (Imperial College London, UK) for provision of the saRNA-

vectored GP3, and the accompanying data; and Jordan Young (Zoetis, Michigan, USA), for serving as my host and mentor during my time visiting Kalamazoo.

I would like to thank several members of the Immunological Toolbox at The Pirbright Institute, who were instrumental in many aspects of this project: thank you Drs. Sylvia Crossley, Kevan Hanson, Danish Munir. Thank you also to members of the Immunogenetics Group, Drs. Kristel Ramirez-Valdez, and Mike Jarman, who were equally instrumental. I would especially like to thank Dr. Marie Di Placido, who was a constant presence across this project, always providing advice, help troubleshooting, reagents, and time. I am indebted. Thank you to Dr. Joe Newman of the Viral Glycoproteins Group, for provision of the SARS-CoV-2 S RBD; and thank you also to Chris Chiu and Dr. Katy Moffat of the Flow Cytometry Team for training in the machines, long hours of sorting, and good company. Thank you to the Bioimaging Team at Pirbright for the confocal training and troubleshooting; to The Core Sequencing Unit at The Pirbright Institute for transcriptome library preparation and sequencing data generation; and thank you to Drs. Jemma Wadsworth and Hayley Hicks for their exceptional support with the single cell sequencing data generation; even so close to Christmas they were willing to squeeze me in.

To my Mum, thank you for being my biggest cheerleader in everything I have done from day one, when I first set my sights on a science career, to now. Dad for enthusiastically supporting me through these four+ years. Thank you both for never letting me lose sight of my goals and serving a guiding light throughout my life. To all the rest of my family, although I cannot name you all personally, thank you for your encouragement and listening to me prattle on, your support always

spurred me on. Knowing there is a laminated copy of my silly “COVID-busters” poster hanging up will always brighten my day.

Thank you to all my friends who have supported me over the years. To the many members of the Tuesday night’s dinner club, and all those who have come and gone from Pirbright across my nearly seven years here. To Samuel and Chloe, without whom I would not have survived lockdown, your generous support, food parcels, and consideration have been indispensable through the past four years.

To Ginger, Sean, Lewis, the Amys, and my brother Charles, the fond memories forged with you have been equally important in my development, as both a scientist and as a person, as the work detailed in this thesis, I would not have reached this point without you. And to Arturo, for guiding me through many misadventures over the years, wild to think a “quick” campaign will last longer than my entire PhD! Thank you, I love you all.

Finally, to Emily:

If I were to list everything I was grateful for across these four years, my acknowledgments would end up being longer than the thesis itself. I would not have managed without your endless support, both in and out of the lab. From to being a sympathetic ear to helping with pipetting, from coffee runs to cooking dinners, from leaving little notes to a warm hug after a hard day; you always went above and beyond to help in any way that you could. Your love really has made every day better, and all the late nights worth suffering through. From the very bottom of my heart, thank you.

“I did my best. I have no regrets.”

Declaration

I, Jack Hayes, declare that this thesis and the work to which it refers are the results of my own efforts, and any contributions that have not been produced myself are clearly indicated. Any ideas, data, images, or text resulting from the work of others (whether published or unpublished) are fully identified as such with the work and attributed to their originator in the text, bibliography or footnotes. This thesis has not been submitted in whole or in part for any other academic degree or professional qualification. I agree that the University has the right to submit my work to the neoplagiarism detection service TurnitinUK for originality checks. Whether or not the drafts have been so assessed, the University reserves the right to require an electronic version of the final document (as submitted) for assessment as above.



Jack Hayes

11/01/2024

Abstract

Porcine reproductive and respiratory syndrome viruses (PRRSV) continue to cause major economic losses to the global swine industry. The high degree of variability among circulating PRRSV strains, facilitated by an inherent propensity for rapid mutation, poses a significant challenge to the development of effective vaccines. Antibodies capable of broadly neutralising PRRSV strains are of great interest as tools to guide next-generation vaccine design. The conserved neutralising epitopes on PRRSV glycoproteins, however, remain unknown, and our understanding of the mechanisms behind antibody-mediated neutralisation of PRRSV is incomplete. To address this, recombinant soluble forms of the PRRSV-1 minor envelope complex glycoproteins, GP2, GP3, and GP4, were produced using a mammalian cell expression system. Serum from hyperimmunised pigs were screened for binding to these proteins and GP3 was identified as the most highly recognised by antibodies in these sera. Fluorescently tagged GP3-tetramers were therefore constructed and used to isolate single B cells from a hyperimmune pig by flow cytometry. mRNA encoding immunoglobulin VH and VL regions was amplified using a semi-nested RT-PCR workflow, sequenced, and complementarity-determining regions annotated using the IgMAT tool. Fifteen unique heavy and light chain pairs were cloned and expressed as recombinant monoclonal antibodies (mAbs). mAbs were evaluated for their specificity, cross-reactivity and neutralising potency by ELISA, immunostaining of PRRSV-infected cells, and virus-neutralisation tests. The binding epitope of selected anti-GP3 mAbs was mapped to a conserved sequence but did not show neutralising activity *in vitro*. It is speculated that the binding site may represent a

decoy epitope. A pilot study investigating the immunogenicity of GP3 further demonstrated a lack of a neutralising antibody response despite high titres of GP3-binding antibodies. A workflow has been established for the isolation of porcine mAbs that could be used in future work to further dissect the immune response to PRRSV infection and vaccination.

Table of Contents

Dissecting the neutralising antibody response to the porcine reproductive and respiratory syndrome virus to identify novel vaccine targets 1

Acknowledgments 3

Declaration 6

Abstract 7

Table of Contents 9

List of figures 12

List of tables 16

List of abbreviations 18

Chapter 1. General Introduction 21

1.1 Porcine reproductive and respiratory syndrome 22

1.2 Porcine reproductive and respiratory syndrome viruses 23

1.3 The immune response to PRRSV 31

1.4 Vaccines against PRRSV 38

1.5 Structural vaccinology 41

1.6 PRRSV proteins as targets of neutralising antibodies 44

1.7 Aims and objectives 53

Chapter 2. Materials and methods 55

2.1 Design of PRRSV minor glycoproteins 56

2.2 Polymerase chain reaction 59

2.3 Agarose gel electrophoresis 60

2.4 DNA purification 61

2.5 Sanger sequencing 62

2.6 Cloning 62

2.7 Mammalian cell lines 66

2.8 Transfection 68

2.9 Flow cytometry 69

2.10 Confocal microscopy 72

2.11 SDS-PAGE 73

2.12 Protein purification by affinity chromatography 78
2.13 Generation of recombinant monoclonal antibodies 81
2.14 Enzyme-Linked Immunosorbent Assays 85
2.15 Bio-layer interferometry 89
2.16 PRRSV infection assays 90
2.17 Experimental PRRSV infection of pigs 93
2.18 Immunogenicity study 94
2.19 Whole antibody repertoire analysis 98
2.20 Analysis 100
Chapter 3. Cloning and expression of recombinant PRRSV-1 GP2, GP3, and GP4 102
3.1 Rationale 103
3.2 Designing recombinant PRRSV glycoproteins 104
3.3 Expression of full-length recombinant PRRSV glycoproteins 112
3.4 Expression and purification of secreted soluble biotinylated PRRSV glycoproteins 123
3.5 Discussion 131
Chapter 4. Characterisation of the antigenicity of soluble recombinant PRRSV-1 GP2, GP3, and GP4 ectodomains 138
4.1 Rationale 139
4.2 Assessment of recombinant PRRSV glycoprotein antigenicity using polyclonal sera 141
4.3 Identifying PRRSV-specific B cells utilising tetramerised recombinant PRRSV glycoproteins 152
4.4 Discussion 158
Chapter 5. Isolation and characterisation of PRRSV-1 GP3 specific porcine monoclonal antibodies 163
5.1 Rationale 164
5.2 Amplification of paired V(D)J genes from single sGP3-specific B cells 165
5.3 Annotation and comparison of sequences 169
5.4 Cloning, expression, and purification of recombinant mAbs 172
5.5 Characterising mAbs 180
5.6 Whole antibody repertoire analysis 192

5.7 Discussion 198
Chapter 6. Evaluation of the immunogenicity of PRRSV-1 GP3 203
6.1 Rationale 204
6.2 Vaccine preparation 207
6.3 Characterisation of immune response 215
6.4 Discussion 226
Chapter 7. General discussion 232
7.1 Summary 233
7.2 Discussion of limitations and future direction 234
7.3 Conclusion 242
Appendix 243
Bibliography 256

List of figures

Figure 1.1: Schematic overview of PRRSV genome organisation 25

Figure 1.2: PRRSV replication cycle 29

Figure 1.3: Cartoon depicting immunoglobulin structure and genetic encoding 34

Figure 1.4: Typical timeline representing the humoral immune response to PRRSV infection 36

Figure 1.5: Schematic overview of PRRSV envelope organisation..... 44

Figure 2.1: Western blotting transfer stack set up 76

Figure 2.2: Schematic demonstrating primer design enabling amplification of VH and VL antibody chain genes from isolated single cells..... 81

Figure 3.1. Protein folding was predicted by inputting amino acid sequences for PRRSV-1 Olot/91 glycoproteins GP2, GP3, and GP4 into Phyre2 105

Figure 3.2: Protein folding was predicted by inputting the amino acid sequences for PRRSV-1 Olot/91 glycoproteins GP2, GP3, and GP4 into AlphaFold..... 108

Figure 3.3: Overlayed model of PRRSV-1 Olot/91 glycoproteins GP2, GP3, and GP4 sequences with the transmembrane (TM) region onwards, and sequences with the TM and signal peptide (SP) regions removed were compared to the full-length version of each respective GP 110

Figure 3.4: Cartoon depicting the design rationale for generating recombinant PRRSV glycoproteins 112

Figure 3.5. Expression of recombinant PRRSV-1 glycoproteins GP2, GP3, and GP4 fused to GFP in transiently transfected HEK293T cells was determined by confocal microscopy 113

Figure 3.6: Expression of recombinant PRRSV-1 glycoproteins GP2, GP3, and GP4 in transiently transfected HEK293T cells was quantified by flow cytometry..... 114

Figure 3.7: HEK293T cells transiently transfected to express recombinant PRRSV glycoproteins were assessed by live cell fluorescence microscopy..... 116

Figure 3.8: Co-expression of recombinant PRRSV glycoproteins assessed by flow cytometry following transient transfection of HEK293T individually, in pairs, and triplets 118

Figure 3.9: Following cytometric analysis of HEK293T transiently transfected with individual, paired, or triplicate recombinant PRRSV glycoproteins, proportion of cells expressing each fluorescent protein-fused rec-GP were compared 119

Figure 3.10: Co-localisation of recombinant PRRSV glycoproteins was assessed by confocal microscopy, following transient transfection of HEK293T cells in pairs and triplets..... 121

Figure 3.11: Transiently transfected HEK293T cell lysate and culture supernatants were assessed for presence of rec-GP2, -GP3, or -GP4 by western blot..... 123

Figure 3.12: Use of a receptor-type protein-tyrosine phosphatase μ leader sequence was compared to the native signal peptide for expression of recombinant soluble PRRSV glycoproteins (sGPs), cut off at the first transmembrane domain 124

Figure 3.13: In vitro biotinylation of recombinant PRRSV glycoprotein ectodomains following co-transfection of HEK293T cells with BirA ligase was assessed by western blot..... 126

Figure 3.14: Protein extracted from cell lysate was treated with PNGase F before assessment by western blot, to investigate potential N-glycosylation heterogeneity . 128

Figure 3.15: Affinity purification of recombinant PRRSV sGPs from transiently transfected Expi293F cell culture supernatants was performed using the ÄKTA Pure Protein Purification System 129

Figure 4.1: Indirect ELISA comparing serum antibody reactivity to recombinant PRRSV-1 sGP2, sGP3 and sGP4 141

Figure 4.2: Deglycosylated aGP3 protein was assessed by ELISA to determine differences in binding by PRRSV immune sera..... 143

Figure 4.3: Recognition of recombinant PRRSV-1 sGP2, sGP3, and sGP4 was assessed by ELISA using sera collected from pigs (n=6) sequentially inoculated with diverse strains of PRRSV, across a 148-day challenge study..... 145

Figure 4.4: Pearson r correlation coefficients between mean antibody response to recombinant PRRSV sGP2, sGP3, and sGP4 and neutralising antibody titres (ND_{50}) 148

Figure 4.5: Antibody recognition of recombinant sGP2, sGP3, and sGP4 was assessed by indirect ELISA, using porcine sera from a collection of PRRSV studies..... 151

Figure 4.6: Flow cytometric assessment of the percentage of live peripheral blood mononuclear cells following cellular staining with an established antibody panel used to identify porcine B cells, and/or tetramerised sGP3..... 153

Figure 4.7: Representative gating strategy used to determine sGP-tetramer specific IgG, IgM, and IgA B cells..... 155

Figure 4.8: Representative flow cytometric dot plots of IgG, IgM and IgA expressing B cells stained with recombinant sGP tetramers..... 156

Figure 4.9: Proportion of recombinant PRRSV glycoprotein-specific B cells were identified by tetramer staining 157

Figure 5.1: Gating highlighting single B cells isolated using sGP3-tetramers 166

Figure 5.2: Representative gel electrophoresis image of GAPDH amplicons from isolated single cell cDNA..... 167

Figure 5.3: Representative gel electrophoresis image of V(D)J amplicons of IgG heavy chains and either kappa or lambda light chains from isolated single B cells..... 168

Figure 5.4: Colony PCR of recombinant mAb clones 173

Figure 5.5: Recombinant monoclonal antibody expression from transfected Expi293F cells was assessed by western blot 175

Figure 5.6: mAbs were treated under reducing conditions with the aim of breaking the disulfide bonds responsive for VH-VL chain interactions, enabling their individual visualisation by western blot 176

Figure 5.7: Assessment of concentration and specificity of mAbs in culture supernatants from transfected Expi293F cells 177

Figure 5.8: Following isolation by affinity chromatography, the purity of mAbs was assessed 179

Figure 5.9: sGP3 ELISA to investigate whether purified recombinant mAbs retained antigen-specificity 180

Figure 5.10: Recognition of native PRRSV antigen by recombinant mAbs was assessed by intracellular staining of PRRSV infected MARC-145 cells..... 182

Figure 5.11: Recognition of native PRRSV antigen by recombinant mAbs was assessed by intracellular staining of porcine alveolar macrophages (PAMs)..... 184

Figure 5.12: Assessment of cross-reactivity of recombinant mAbs using recombinant PRRSV-1 and PRRSV-2 sGP3 by ELISA..... 185

Figure 5.13: Overlapping linear peptides spanning the PRRSV-1 GP3 ectodomain were screened for mAb recognition by ELISA..... 187

Figure 5.14: Bio-layer interferometry was performed to determine the affinity of recombinant mAbs against PRRSV-1 recombinant sGP3 189

Figure 5.15: Neutralisation capacity of PRRSV sGP3-specific mAbs was tested by VNT 191

Figure 5.16: VH and VL genes were amplified from RNA isolated from whole blood, from six animals across five timepoints from a heterologous challenge study to establish a library for sequencing..... 192

Figure 5.17: Percentage each germline and allele contribute to 9 clusters, seen to represent the 15 antibody sequences investigated 195

Figure 5.18: The nine clusters associated with each recombinant mAb were investigated over time with sequence numbers reflecting expression 197

Figure 6.1: Affinity purification of recombinant sGP3 from transfected Expi293F cell culture supernatants was performed using ÄKTA Pure Protein Purification System followed by assessment by SDS-PAGE 208

Figure 6.2: Western blot analysis of bulk concentrated sGP3 to assess multiple bands observed by Coomassie staining 210

Figure 6.3: CoPoP liposome formation was assessed by Coomassie staining following native-PAGE 212

Figure 6.4: saRNA-vectored GP3 expression was assessed in HEK293T cells 214

Figure 6.5: GP3-specific T cell IFN-γ responses from animals vaccinated with PRRSV-1 GP3 were assessed by ELISpot assay 215

Figure 6.6: Assessment of GP3-specific antibody responses 216

Figure 6.7: Endpoint antibody titres from each serum were calculated following sGP3 ELISA 218

Figure 6.8: Immunostaining of sera from GP3-immunised pigs against PRRSV-1 Olot/91 infected MARC145-cells 219

Figure 6.9: ELISA assessing recognition of overlapping GP3 sequence peptides to identify linear epitopes by sera from GP3-immunised pigs 220

Figure 6.10: Neutralisation capacity of sera from animals vaccinated with PRRSV-1 GP3, using three vaccine delivery platforms, was assessed by VNT 222

Figure 6.11: Antibody depletion was assessed by ELISA, determining proportion of sGP3 binding from sera depleted using either recombinant PRRSV-1 GP3, recombinant SARS-CoV-2 S-RBD, or with a mock depletion using no antigen 223

Figure 6.12: The effect of antibody depletion on neutralisation capacity was assessed by VNT 225

Appendix Figure 1: pOPINEneo-3c-GFP plasmid map. Used for generating recombinant PRRSV GP-GFP fluorescent fusions 244

Appendix Figure 2: pOPINEneo plasmid map 245

Appendix Figure 3: pOPINTTneo plasmid map 246

Appendix Figure 4: pOPINTTneo plasmid map also encoding for a biotin acceptor peptide tag 247

Appendix Figure 5: Overall pLDDT confidence scores of AlphaFold predictions from Figure 3.3 248

Appendix Figure 6: pNeoSec_SsFc_IgG1 plasmid map 250

Appendix Figure 7: pNeoSec_SsFc_IgG1 plasmid map 251

Appendix Figure 8: pNeoSec_SsFc_IgG1 plasmid map 252

Appendix Figure 9: Structure of the six mAbs that were characterised throughout Chapter 5 was predicted using SAbPred 254

List of tables

Table 2.1: Human codon-optimised PRRSV-1 Olot/91 GP2, GP3, and GP4 sequences, to be used as templates to generate recombinant proteins. Start codons are in green, stop codons in red 57

Table 2.2: Summary of primers designed for the generation of recombinant PRRSV-1 GP2, GP3, and GP4 58

Table 2.3: Summary of plasmids used for generation of recombinant PRRSV-1 GP2, GP3, and GP4 and the subsets of each 59

Table 2.4: Detailed of the standard PCR protocol/thermocycler program used 60

Table 2.5: Restriction endonucleases used for double digestion of vectors 63

Table 2.6: Standard mixture used for colony PCR of bacteria following transformation. 65

Table 2.7: Quantities of transfection reagents at different scales used on day 2 of Expi293F cell transfection 68

Table 2.8: Volumes of transfection reagents at different scales used on day 3 of Expi293F cell transfection 69

Table 2.9: Standard antibody panel used to identify B cell isotypes by flow cytometry. All antibodies were titrated to determine optimal dilution before use. 71

Table 2.10: Components used to cast 2x 12.5% polyacrylamide gels 74

Table 2.11: List of antibodies used for western blot analysis of proteins used throughout this project 77

Table 2.12: Reverse transcription mixture used to generate cDNA from isolated single cells. 82

Table 2.13: PCR mixture for the amplification of glyceraldehyde-3-phosphate dehydrogenase (GAPDH) as a reference gene for assessing cDNA quality. 83

Table 2.14: PCR thermocycler program for the amplification of glyceraldehyde-3-phosphate dehydrogenase (GAPDH) as a reference gene for assessing cDNA quality. 83

Table 2.15: Summary of parameters for Octet® R8 platform bio-layer interferometry analysis 90

Table 2.16: List of PRRSV strains used for infection-based assays 90

Table 2.17: GP3 immunogenicity study vaccination groups and timeline 95

Table 2.18: Matrix of Illumina primers used for index addition for sequencing of a whole antibody repertoire library 99

Table 3.1: Signal peptide and transmembrane regions of each glycoprotein were predicted using SignalP 5.0 and TMHMM 2.0, respectively 106

Table 3.2: Yields of recombinant soluble PRRSV glycoprotein/litre of transfected Expi293F cell culture supernatant..... 131

Table 4.1: P value confidence scores for the slope of best-fit lines were generated as a measure of correlation between recombinant PRRSV sGP binding and neutralising antibody titres..... 149

Table 4.2: R squared scores for goodness of fit for lines generated as a measure of correlation between recombinant PRRSV sGP binding and neutralising antibody titres. 149

Table 5.1: Complementarity determining regions for each VH IgG sequence were annotated utilising the international ImMunoGeneTics information system® 169

Table 5.2: Complementarity determining regions for each VL IgK and IgL sequence were annotated utilising the international ImMunoGeneTics information system® 170

Table 5.3: Closest germline V gene was assigned to each VH sequence from isolated single cells 171

Table 5.4: Closest germline V gene was assigned to each VL sequence from isolated single cells 171

Table 5.5: Fifteen recombinant mAbs were expressed in Expi293F cells by co-transfecting with paired VH and VL plasmids..... 174

Table 5.6: Yields of recombinant monoclonal antibody following purification from transfected Expi293F cell culture supernatants were determined by spectrophotometry 178

Table 5.7: Kinetic binding constants for recombinant mAbs binding to recombinant sGP3 were determined by Octet® analysis software 190

Table 5.8: Summary of whole antibody repertoire sequences generated, including proportions of each isotype, and overall number of sequences..... 193

Table 5.9: Summary of which cluster each recombinant mAb described in this chapter was associated with 194

Appendix Table 1: List of primers kindly provided by the Immunological Toolbox, The Pirbright Institute, UK, enabling amplification of VH and VL genes..... 249

Appendix Table 2: Peptide library comprising overlapping sequences (16mers offset by 4 amino acids) representing PRRSV-1 Olot/91 GP3, up to the first transmembrane domain..... 253

Appendix Table 3: List of Illumina i7 and i5 index primer sequences used for whole antibody repertoire VH and VL sequence indexing..... 255

List of abbreviations

AA: amino acid

ASN: asparagine

APS: ammonium persulfate

BAP: biotin acceptor peptide

BCR: B cell receptor

BLI: bio-layer interferometry

bnAb: broadly neutralising antibody

BSA: bovine serum albumin

CD: cluster of differentiation

CDR: complementarity determining regions

CTL: cytotoxic T lymphocytes

CoPoP: cobalt porphyrin phospholipid

DAPI: 4′,6-diamidino-2-phenylindole

DMEM: Dulbecco's modified Eagle medium

Dpi: days post-infection

Dpv: days post-vaccination

E: PRRSV envelope protein

E. coli: Escherichia coli

EDTA: ethylenediaminetetraacetic acid

ELISA: enzyme linked immunosorbent assay

ER: endoplasmic reticulum

FACS: fluorescence-activated cell sorting

FBS: foetal bovine serum

FR: framework region

GAPDH: glyceraldehyde 3-phosphate dehydrogenase

GFP: green fluorescent protein

GP: glycoprotein

H+L: heavy and light antibody chain-specific

HEK: human embryonic kidney

HF: high fidelity

HIV: human immunodeficiency virus

HRP: horseradish peroxidase

IFN: interferon

IRF3: interferon regulatory factor 3

ISGF3: IFN-stimulated gene factor 3

Ig: immunoglobulins

IgH: immunoglobulin heavy chain

IgL: immunoglobulin light chain

IMAC: immobilised metal affinity chromatography

IMGT: ImMunoGeneTics information system

kb: kilobases

kDa: kilodalton

LB: Luria lysogeny broth

LNP: lipid nanoparticles

M: PRRSV membrane protein

mAb: monoclonal antibody

mCh: mCherry fluorescent protein

MFI: mean fluorescent intensity

MLV: modified live virus

N: PRRSV nucleocapsid protein

nAb: neutralising antibody

ND_{50}: Fifty percent neutralising dilution

NSP: non-structural protein

NT: nucleotide

OD: optical density

ORF: open reading frames

PAGE: polyacrylamide gel electrophoresis

PAM: porcine alveolar macrophage

PBMC: peripheral blood mononuclear cells

PBS: phosphate buffered saline

PCR: polymerase chain reaction

PDB: protein data bank

PE: r-phycoerythrin

PFA: paraformaldehyde

PRDC: porcine respiratory disease complex

PRRS: porcine reproductive and respiratory syndrome

PRRSV: porcine reproductive and respiratory syndrome virus

PVDF: polyvinylidene fluoride

RBD: receptor-binding domain

RMSD: root mean square deviation

RNA: ribonucleic acid

RSV: respiratory syncytial virus

RT: reverse transcription

rt: room temperature

RTC: replication and transcription complex

saRNA: self-amplifying ribonucleic acid

SDS: sodium dodecyl sulphate

sg: sub-genomic

sGP: soluble glycoprotein

SRCR: scavenger receptor cysteine-rich

Ss: *Sus scrofa*

Ta: Annealing temperature

$TCID_{50}$: median tissue culture infectious dose

TEMED: N,N,N,N tetramethylethylenediamine

TM: transmembrane

Tm: melting temperature

Treg: regulatory T cell

VH: heavy chain variable region

VL: light chain variable region

VNT: virus neutralisation test

YFP: yellow fluorescent protein

Chapter 1. General Introduction

1.1 Porcine reproductive and respiratory syndrome

Porcine reproductive and respiratory syndrome (PRRS) represents one of the greatest threats to the swine industry worldwide, causing an estimated loss of over US$ 650 million per annum in the USA alone [1, 2]. As the name suggests, clinical features of PRRS manifest two-fold: reproductive failure and respiratory disease, with the former primarily impacting breeding age gilts, sows, and boars, and the latter particularly impacting young, growing, and finishing pigs [3]. PRRS reproductive failure is characterised by increased abortion rates, up to 40% incidence rate in late-pregnancy sows in some reported cases [4], and the birth of mummified and weak piglets in which often succumb to respiratory disease [5]. The severity of the reproductive failure in sows depends on the viral strain/virulence, the pregnancy stage of the female, the presence of pre-existing neutralising antibodies (nAbs), and the general health status of the farm [4]. PRRS in growing pigs is characterised by dyspnoea, lethargy, anorexia/weight loss, reduced growth performance due to systemic disease, cyanosis of the ears (leading to PRRS previous moniker of blue ear disease), and PRRS-induced interstitial pneumonia [1, 5]. Lesion formation in the lungs is a common histological finding, ranging from mild to severe, with microscopic lung lesions resulting in type 2 pneumocytic hypertrophy and hyperplasia [6], and gross lung lesions leading to failure of the lung to total lung collapse [6]. PRRS-induced pneumonia is more severe in young pigs compared to adults and may be further complicated by concurrent bacterial infections [7]. PRRSV is considered an immunosuppressive virus, enabling infection of opportunistic bacterial pathogens, such as *Pasteurella multocida, Mycoplasma hyopneumonia,* and

Streptococcus suis [8, 9]. Damage to peripheral immune organs as a result of highly pathogenic PRRSV, for example, has been demonstrated to lead to increased susceptibility to *S. suis*, resulting in further reduced performance as well as elevated mortality [10, 11]. PRRSV, consequently, has been shown to be a key etiological contributor to the porcine respiratory disease complex (PRDC).

Spread of PRRS is known to occur by several routes of exposure; with transmission most commonly occurring by close contact between animals, as aerial transmission, or through contaminated bodily fluids i.e., semen, blood, secretions, or indirectly through fomites [12]. Additionally, vertical transmission (across the placental barrier) is a well-documented route of exposure, further contributing to the spread of PRRS within herds [12, 13]. These routes of exposure, further, also often result in spread of PRRS between herds and occasionally from wild boar in close proximity to farms [14].

The severity and duration of PRRS outbreaks is highly variable, with some herds being devastated by high production losses and severe-fatal respiratory disease, whereas other herds may have few to no losses, and display no observable clinical signs [15]. While pig genetic susceptibility, environmental conditions, and frequency of infection are all factors that influence these differences [16, 17], the impact of variability between virus strains cannot be overstated.

1.2 Porcine reproductive and respiratory syndrome viruses

The causative PRRS virus (PRRSV) is a small, enveloped, positive-sense single-stranded RNA virus, classified under the order *Nidovirales*, and *Arteriviridae* family [18]. PRRSV exists as two species: *Betaarterivirus suid 1* (PRRSV-1),

originally emerging from Europe, and *Betaarterivirus suid 2* (PRRSV-2), emerging from North America [19-21]. The two species of PRRSV share approximately 60% nucleotide sequence identity [22]; molecular analysis of the prototype PRRSV Lelystad and VR-2332 strains (PRRSV-1 and PRRSV-2, respectively) has suggested that divergently evolved strains emerged almost simultaneously, explosively increasing among domesticated swine in the 1980s [23-25]. Within species, strains are further classified into distinct subtypes: PRRSV-1 strains into four subtypes (subtype 1 (Global), 2, 3, and 4 (Eastern Europe – Russia, Belarus, Poland)) and PRRSV-2 strains into nine lineages (lineage 1-9) [26-28]. While PRRSV-1 subtype 1 has been reported across Europe, America, Asia, and recently in Africa [29, 30], the other subtypes have not been reported outside of Europe. Distribution of PRRSV-2 lineage strains spreads across America and Asia most prevalently, with one lineage appearing most prevalent in each area, i.e., PRRSV-2 lineage 3 historically being mainly identified in southern China (including Taiwan and Hong Kong) [31, 32] and lineage 4 being mainly identified in Japan [26]. PRRSV-2 lineage 1, conversely, has become the most prevalent and diverse lineage within the American and Asian swine industries [33, 34], representing 75% of all strains in Peru during 2015-2017 [35], and according to the latest reports [36] lineage 1 accounts for 64% of strains in China.

For both species, the PRRSV genome, approximately 15 kilobases (kb) in size, encodes at least 10 open reading frames (ORFs), flanked by the 5' and 3' untranslated regions (UTRs) (**Figure 1.1**).

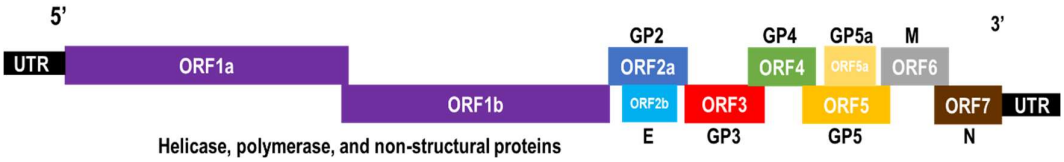


Figure 1.1: Schematic overview of PRRSV genome organisation. Open reading frames (ORFs) are represented 5' to 3' and annotated with the respective proteins encoded. Both 5' and 3' ends are flanked by untranslated regions (UTR). ORF1a and 1b encode for non-structural proteins, ORF2-4, including the alternative reading frame of ORF2bencode the minor envelope proteins, ORF5-6, including the alternative reading frame of ORF5a encode the major envelope proteins, and ORF7 encodes the nucleocapsid protein.

Like other single-stranded RNA viruses, the UTRs of PRRSV has been demonstrated to play a key role in the regulation of genomic RNA replication, transcription, and mRNA translation [37]. The 5′ UTRs consist of 220 and 190 nucleotides for PRRSV-1 and PRRSV-2 respectively and share approximately 60% sequence homology [22, 23]. Highly conserved stem-loop structures identified in the leader of PRRSV are believed to be essential for viral replication, with the 5' UTR providing the binding site for RNA-dependent RNA polymerase [37]. Unlike most arteriviruses, the 5' leader sequence of PRRSV consists of the entire 5' UTR [38]. ORF1a and 1b compose the majority of the genome [39], and encode polyproteins that are cleaved to generate the non-structural proteins (NSP) required for transcription and replication [40]. ORFs 2-6 encode for the structural proteins which make up the viral envelope: the non-glycosylated matrix (M) proteins, the N-glycosylated glycoproteins (GPs) GP2, GP3, GP4 and GP5 [39, 41]. Additionally, PRRSV adopts a unique discontinuous transcription mechanism for sub-genomic (sg) mRNA transcription, enabling the generation of the small, hydrophobic envelope (E), and GP5a/ORF5a proteins encoded in an alternative reading frame of sg mRNA 2, and 5 respectively [42, 43]. E, GP5a, GP2, GP3, and GP4 form a non-covalently linked heteropentameric complex

referred to as the minor envelope complex [44, 45], whereas the GP5 and M proteins form a disulphide-linked heterodimer referred to as the major envelope complex [46]. Additionally, ORF7 encodes for the structural nucleocapsid (N) protein, which encapsulates the viral RNA [47, 48]. The 3' UTR of PRRSV consists of 114 and 151 nucleotides for PRRSV-1 and PRRSV-2 respectively [49]. Like the 5' UTR, the 3' UTR of PRRSV is crucial for viral replication. Following binding of the RNA-dependent RNA polymerase, the replication and transcription complex (RTC) binds to the 3' UTR and initiates viral negative-strand RNA synthesis [49]. Recent studies have suggested that mutations within the 3' UTR may also contribute to the enhanced replicative ability of emerging highly pathogenic strains of PRRSV [50].

Despite the differences in sequence identity, the genomic organisation, gross clinical pathology, and disease phenotype are largely very similar between the majority of PRRSV-1 and -2 [39, 51]. A high mutation rate and recombination potential has resulted in highly diverse PRRSV populations, both genetically and antigenically [42]. PRRSV is an incredibly rapidly evolving virus, stemming from a lack of proofreading mechanisms; it has been calculated that PRRSV has a mutation rate between 4.71 - 9.80 × 10^{-2}/synonymous sites/year [23, 51], which equates to around one mutation per replication cycle [52]. For comparison, other viruses known for their rapid mutation rate, such as SARS-CoV-2 exhibits an evolutionary rate of 1.12 - 6.25 × 10^{-3} [53, 54], while seasonal influenza virus has comparatively lower evolutionary rate of 0.60 - 2.00 × 10^{-6} [55]. This exemplifies one of the most challenging aspects of PRRSV control, making both natural and

vaccine-induced humoral immune responses largely limited in their neutralising capacity.

Virulence, furthermore, can differ greatly between field strains of each subtype/species [56, 57]. The emergence a highly pathogenic PRRSV-2 strain in 2006-2007 in China is perhaps the most extreme example of how sudden and uncontrolled emergence of higher virulence strains can result in catastrophic effects on the global pig population, leading to the deaths of an estimated 20 million pigs [31, 58, 59]. Historically, PRRSV-1 has been considered less virulent than PRRSV-2 [60], however this notion has been challenged with the discovery of highly virulent PRRSV-1 strains. For example, PRRSV-1 subtype 3 strains Lena and SU1-Bel, which have been shown to be more pneumovirulent than PRRSV-1 subtype 1 strains, inducing a stronger early inflammatory response which resulted in more severe clinical disease and lung pathology [61-63]. Additionally, severe PRRSV outbreaks characterised by increased mortality, and high abortion rates have been increasingly reported first in Italy – attributed to the emergence of PRRSV-1 PR40 [64, 65] - and most recently in north-eastern Spain with the colloquially known “Rosalía” strain [66]. These examples, and many others, thoroughly highlights the importance of developing more efficacious vaccines.

Swine are the only natural host of PRRSV and, like other members of the family *Arteriviridae*, PRRSV has a very narrow cell tropism demonstrating preference for cells of the monocyte/macrophage lineage, and specific subsets of differentiated macrophages in the lung, lymphoid tissues, and placenta [67]. Whilst PRRSV has been shown to have a relatively restricted tropism for

macrophages with an M1 phenotype [68], the virus is able to infect the vast majority of macrophages with an M2 phenotype [69], and has even been shown to skew macrophage polarisation towards an M2 phenotype [70]. Further, it has been reported that specific subsets of dendritic cells are also susceptible to PRRSV infection, particularly monocyte-derived dendritic cells [69, 71].

Replication of the PRRSV RNA genome is a multistep process [72] involving a replication complex that is formed not only from components of viral and cellular origin but also from the viral genomic RNA template (**Figure 1.2**).

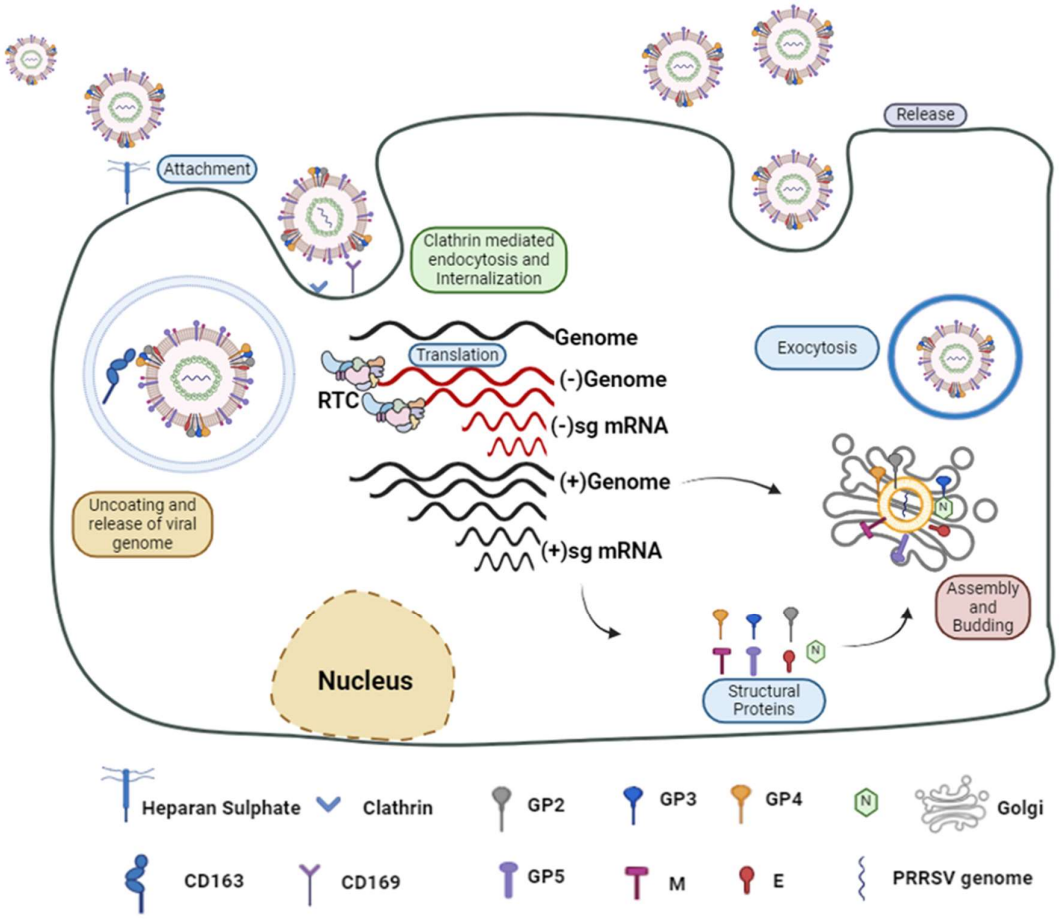


Figure 1.2: PRRSV replication cycle. Cartoon depicting PRRSV attachment, internalisation, and entry by receptor-mediated endocytosis. Uncoating of the virion followed by recruitment of RNA-dependant RNA polymerase, translation, and assembly of the replication and transcription complex (RTC) follows. Amplification of genomic and sub-genomic (sg) mRNA, encapsidation by the nucleocapsid (N) protein, and virion budding/egress are also depicted. Adapted from "Porcine Reproductive and Respiratory Syndrome Virus (PRRSV): Pathogenesis and Interaction with the Immune System". J. K. Lunney, et al., 2016, *Annual review of animal biosciences, 4(1):129-154.* Copyright 2015 of Annual Reviews. Adapted with permission.

PRRSV infection is initiated by the attachment of virions to heparan sulfate, in conjunction with sialoadhesin, also referred to as CD169. Together these serve as receptors that enable concentration of virions on the cell surface [73], and facilitate viral entry following interactions with the PRRSV major envelope proteins [74]. The importance of CD169 remains unclear and has been a topic of some debate. Some studies claim it is not essential for attachment and/or

internalisation [75], with CD169-knock out pigs demonstrating similar viraemia to wild-type pigs [76]. Other studies, conversely, have suggested CD169 is critical for viral endocytosis, demonstrating that PRRSV infection can be blocked by use of CD169-specific mAbs [77, 78].

Following attachment, PRRSV enters by receptor-mediated endocytosis, mediated by CD163. CD163 is a member of the scavenger receptor cysteine rich (SRCR) super family and has been determined to be the major receptor in mediating PRRSV viral uncoating, internalisation, and genome release [79-82].

Recently, CD163 has been edited in pig zygotes using CRISPR/Cas9, to remove the viral interaction domain while maintaining protein expression and biological function [83, 84]. These pigs were resistant to PRRSV-1 as well as PRRSV-2 infection *in vitro*. When these animals, moreover, were challenged with a highly virulent PRRSV-1 subtype 2 strain, the edited pigs showed no signs of infection or viremia or antibody response indicative of a productive infection, which contrasted with the wild-type control group. Follow ups to these studies, investigating CD163-knock out pigs [85, 86], showed similar results, and demonstrated its importance in the viral lifecycle.

Following disassembly and genome release into the cytoplasm, RNA-dependant RNA polymerase binds to the 5' UTR, as early described. Translation of the ORF1a and ORF1b yields replicase polyproteins pp1a-nsp2TF, pp1a-nsp2N, pp1a, and pp1ab [2, 72]. These polyproteins are cleaved by viral internal proteinases to generate 14 non-structural proteins, which are then assembled into the RTC [87]. The RTC directs both genome amplification, and sg mRNA

synthesis [88]. These sg mRNAs serve as templates for the synthesis of plus-strand sg mRNAs required to express the structural protein genes, as described above [88]. At the late stage of replication, multiple copies of the N protein bind to the newly synthesised RNA genomes and form a nucleocapsid complex [72, 89]. These complexes then become enveloped by budding from smooth intracellular membranes in the ER/Golgi complex [72, 90], and acquire the mature viral envelope proteins [44, 91]. The progeny virions accumulate in the intracellular membrane compartments, and are released from the cell using the exocytic pathway [72].

1.3 The immune response to PRRSV

PRRSV has evolved multiple strategies to evade and modulate the immune response. PRRSV infection induces alterations of immunoregulatory cytokines, leading to prolonged delay in the activation of cytotoxic T lymphocytes (CTLs) and antibody production. Thus, PRRSV infection frequently causes host immune response disorders, transiently diminishing T-cell immunity, and delayed protective antibody responses, which prolongs viremia and virus shedding [92-95].

1.3.1 Innate immune responses

PRRSV infection often results in poor activation of innate immune responses, prolonging/preventing viral clearance [39, 96]. PRRSV preferential tropism for macrophages, which form a major component in the sensing of pathogens, controlling inflammation, and activating the adaptive immune response often leads to suppression as a result of infection [97].PRRSV NSP2 has been shown

to antagonise the activation of interferon (IFN) regulatory factor 3 (IRF3) by inhibiting its phosphorylation and translocation [98], resulting in downregulation of the innate immune response. Furthermore, it has been shown that PRRSV uses multiple strategies to antagonize the JAK-STAT signalling pathway [99], such as the inhibition of type I IFN-induced elevation of STAT2 levels and IFN-stimulated gene factor 3 (ISGF3) nuclear translocation as a result of PRRSV N protein expression [100]. PRRSV infection has also been shown to induce significant suppression and dysregulation of NK-cell cytotoxic activity, with previous studies demonstrating a significant reduction in NK-cell cytotoxicity against PRRSV-infected macrophages [101].

1.3.2 Adaptive cell-mediated immune responses

The cell mediated adaptive immune response has been implicated in protection against PRRSV. T cells may play a role in the development of anti-PRRSV immunity stemming from their cytotoxic effector functions in clearing infected cells from the body and in providing help and regulating antigen-specific immune responses. Further, CTL responses have been shown to correlate with protection against PRRSV-1 transplacental infection [102], and early induction of CTL responses have been shown to lead to greater frequency of nAb positive animals [103].

Despite this, however, the suppressed innate immune response in early phase of PRRSV infection can potentially lead to the generation of poor adaptive immune responses, such as abnormal B-cell and T-cell proliferation, and poor induction of PRRSV-specific IFN-γ-secreting cells [104]. In addition to this knock-on effect from suppressing the innate immune response, PRRSV can also directly target T

cell responses as a method for evasion. Throughout the course of PRRSV infection, type I IFN responses often remain low [105] reducing inflammation and T-cell activation. It has been observed that experimental exposure to PRRSV resulted in little to no effect on dendritic cell maturation [75, 106], hence impairing antigen-presentation to T cells. Previous studies suggest that PRRSV further impairs dendritic cell function through the downregulation of MHC class I and II molecules, following infection of monocyte-derived dendritic cells [69, 107, 108], thus impairing antigen presentation. PRRSV, additionally, has been shown to replicate in lymphoid organs and cause lymph nodes lesions, which affect the host's cell-mediated immune response to PRRSV at these sites also [109].

Regulatory T cells (Tregs) are responsible for modulating the immune response and maintaining homeostasis. The induction of Tregs has been documented as one of the mechanisms used by viruses such as human immunodeficiency virus (HIV) and hepatitis C virus to induce immunosuppression [110, 111]. It was found that PRRSV-infected dendritic cells significantly increased the amount of $FoxP3^{+}CD25^{+}$ T cells, enhancing Tregs in secondary lymphoid organs such as the tonsils and mediastinal lymph nodes [112], which could further play a role in delaying cellular immune responses in PRRSV-infected pigs. It has been further detailed that PRRSV can induce Tregs in the lung and tracheobronchial lymph nodes of infected pigs [113], resulting in a significant increase in interleukin-10 production.

1.3.3 Adaptive humoral immune response

Antibody-mediated protection against pathogens induced by vaccines or infections is crucial in host defence, particularly pathogens as genetically variable

and rapidly evolving as PRRSV. Antibodies – or immunoglobulins (Ig) - consist of four polypeptides: two heavy (IgM, IgG, IgA, IgD, or IgE) and two light chains (either lambda (λ) or kappa (κ) (**Figure 1.3**).

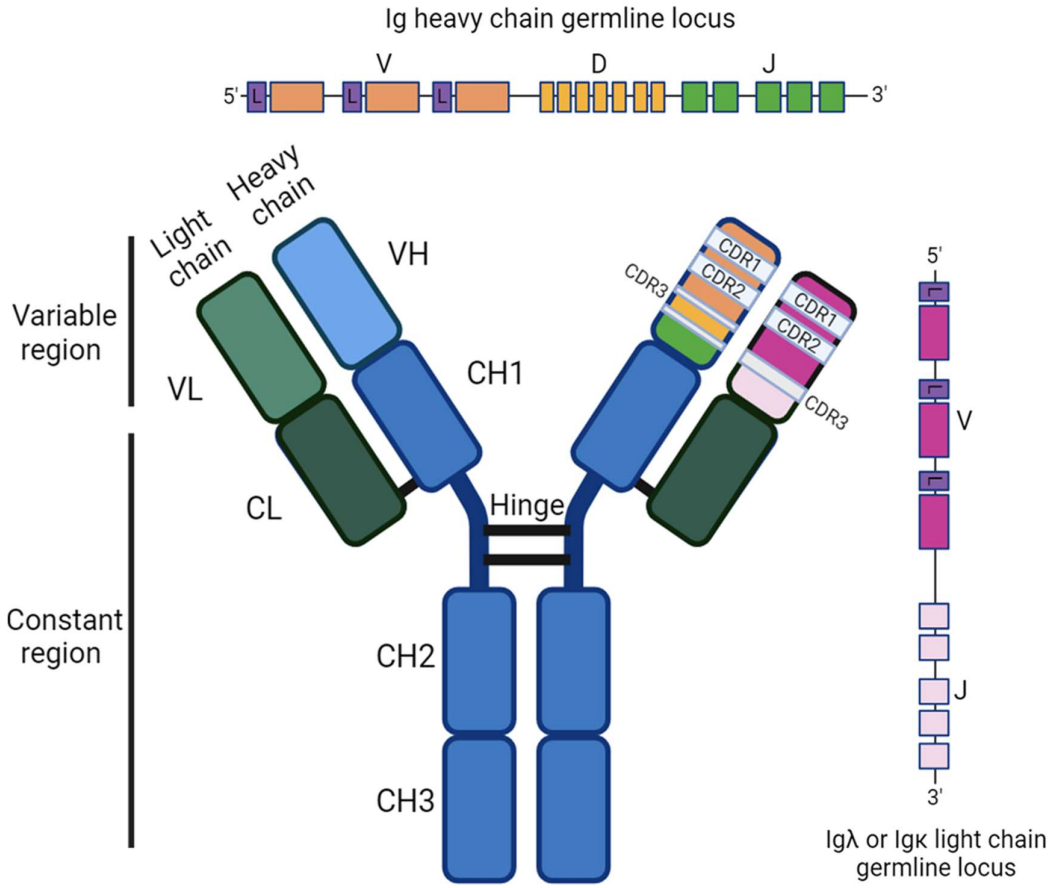


Figure 1.3: Cartoon depicting immunoglobulin structure and genetic encoding. Germline (unrearranged) genomic DNA configuration of the heavy and light chain loci are depicted. Stepwise rearrangement results in joining of the V(D)J segments (not to scale), and therefore determines the randomised complementarity-determining regions (CDRs) responsible for antigen specificity. The constant regions (CH1, CH2, and CH3 for the heavy chain, and CL for the light chain) are encoded by downstream exons and are joined to the rearranged V(D)J gene by mRNA splicing. Disulphide bridges joining protein chains in the full antibody structure are shown with black line segments.

Antibodies serve a dual function, with the fragment antigen-binding (Fab) determining antigen recognition/binding, and the fragment crystallisable region (Fc) mediating biological activity [114]. Each of the four chains has a variable (V)

region at its terminus, which contributes to the antigen-binding site, and a conserved constant (C) region, which determines the isotype and in turn determines the functional properties of the antibody [114]. Stepwise rearrangement of the germ line DNA results in the joining of a heavy chain D and J gene segment, followed by joining of a V segment to the D-J product, to generate the DNA encoding the heavy chain variable region. In the process of rearrangement, the ends of the gene segments are subject to variable amounts of exonuclease digestion, and randomised non-templated bases are added at the segment ends, to produce additional sequence diversity at the VDJ junctional region that encodes the complementarity-determining region (CDR) loops, CD1, CDR2, and CDR3. CDR3 is often the region of the antibody heavy chain that has the greatest impact on antigen specificity, and therefore neutralisation capacity, but all three motifs determine specificity. Similarly, the rearrangement of light chains V and J genes with diversification of the VJ junction to produce the rearranged light chain gene [115].

nAbs have been shown to protect against PRRSV infection; passive transfer experiments of serum from PRRSV-immune animals to naïve ones have demonstrated that PRRSV-nAbs can confer sterile immunity [116, 117]. This protection, however, was shown to be dose-dependent: while PRRSV-nAb titres of 1:8 was seen to block viraemia, it was not sufficient to prevent tissue seeding and transmission [116], even at titres of 1:32 sterilising immunity was only observed in 50% of animals tested. This demonstrates one of the key challenges associated with the humoral response to PRRSV. PRRSV is characterised by a delayed nAb response, and prolonged to persistent viraemia (**Figure 1.4**).

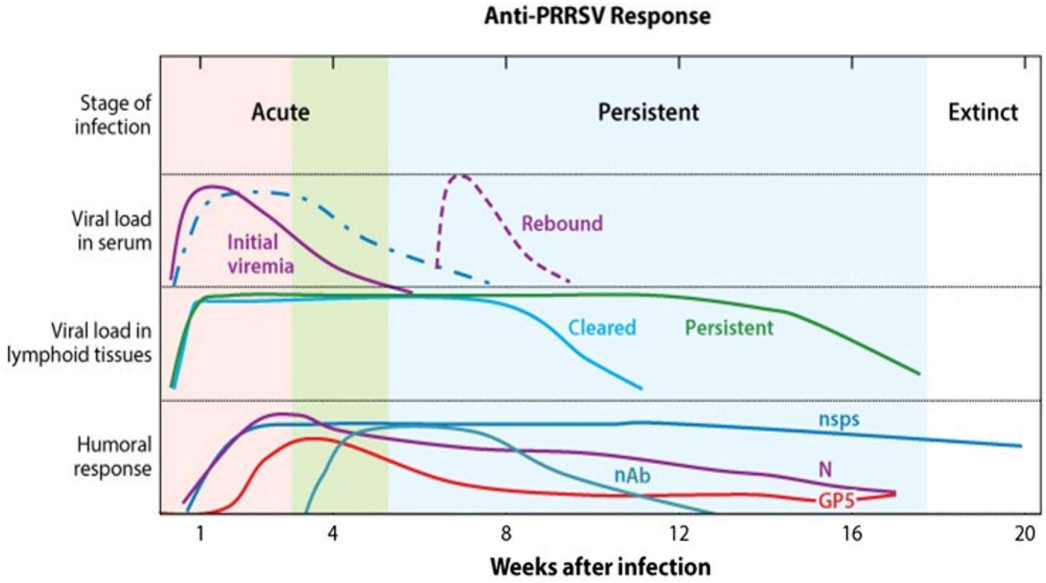


Figure 1.4: Typical timeline representing the humoral immune response to PRRSV infection. Time points are approximate and could be changed depending on the virus isolate. Viral load in serum is indicated by a range of responses (solid purple for fast serum clearance and dashed blue for slower clearance, dashed purple for rebound virus). The timing of the humoral response is shown as neutralising antibodies (nAb), additional antibody responses against nucleocapsid (N), GP5, and non-structural proteins (nsps) are also represented. Reprinted from "Porcine Reproductive and Respiratory Syndrome Virus (PRRSV): Pathogenesis and Interaction with the Immune System". J. K. Lunney, et al., 2016, *Annual review of animal biosciences, 4(1):129-154.* Copyright 2015 of Annual Reviews. Reprinted with permission.

While PRRSV infection elicits an antibody response by 7-9 days post-infection (dpi) [2, 118], these responses often do not correlate with protection, targeting abundant, immunodominant antigens that are largely non-neutralising (i.e. PRRSV nucleocapsid protein) [94, 116]. Further, antibodies that arise at this stage that are capable of neutralising, often offer little protection against genetically heterologous strains [119]. nAbs will often not occur until >28 dpi [39], and though they remain elevated throughout the persistent phase of infection [118] this response is often insufficient for protection; prolonged viraemia and shedding of PRRSV has been demonstrated for as long as 120-157 dpi [120, 121]. Additionally, it is well documented that PRRSV is capable of persisting in

lymphoid tissues (primary and secondary), for as long as 250 dpi [120, 122]. This prolonged shedding and persistence in tissues, consequently, often leads to an almost indefinite persistence of the virus within positive herds [123].

The high degree of observed variability among PRRSV isolates combined with the inherent propensity for rapid mutation and evolution, means those nAbs that do arise are either restricted in their breadth of protection, often poorly recognising heterologous strains. Further, escape mutants can arise, evading existing nAb responses [63, 124]. Broadly neutralising antibodies (bnAbs), that can confer cross-protection against PRRSV strains/species, consequently, are an area of great interest. PRRSV bnAbs have been documented, both naturally occurring and experimentally. Sera from U.S. sow herds repeatedly vaccinated and exposed to field strains were shown to neutralise a genetically diverse range of PRRSV strains, including PRRSV-1 and -2 [124], despite no prior evidence of PRRSV-1 exposure. It has been further demonstrated that bnAb responses can be promoted through the experimental repeat inoculation of pigs with homologous PRRSV strains [125].

PRRSV, however, has several strategies for modulating/evading the nAb response. Non-neutralising, immunodominant ‘decoy’ epitopes within the GP3, GP5, and – though debated – GP4, exist, which reduce induction of nAbs against nearby neutralising epitopes [74, 126, 127]. Moreover, it has been reported that PRRSV further modulates this response through the shielding of neutralising epitopes with glycans [128, 129]. While this has most prominently been reported in GP3, hypoglycosylated forms of GP5 have also been shown to induce significantly higher levels of nAbs in infected piglets [130]. Neutralising epitopes

that have been documented are linear and have been seen to reside within hypervariable regions of the virus [82, 131, 132] with NSP2, GP3, and GP5 being particularly notable examples.

It is worth noting that even non-neutralising antibodies serve a purpose in the control and detection of PRRS. Routine diagnostics of PRRS utilises the non-neutralising response mounted against the immunodominant N protein, abundant during PRRSV infection [133]. Structural analysis of antibodies that target non-neutralising epitopes, can also improve our understanding, and help inform future vaccine development.

It is the discovery and characterisation of bnAbs, however, that will be required to make truly substantial steps towards an effective PRRSV vaccine.

1.4 Vaccines against PRRSV

As has been highlighted, PRRSV genetic heterogeneity, its long persistence within the host population and the weak immune response of pigs make control and/or eradication of PRRSV in infected herds highly challenging. Endemically infected herds will typically experience cyclic clinical outbreaks whenever susceptible individuals are introduced, but also whenever a different strain enters the herd because of the low cross-protection and poor immune memory induced by the virus [134]. Generally, PRRS management strategies must, therefore, rely on a combination of biosecurity measures aimed at avoiding the entry of new strains (e.g., adoption of all-in/all-out flows, quarantine of replacement boars and gilts, disinfection protocols, diagnostic screening) and on immunisation approaches [135, 136]. Antiviral strategies, such as PRRSV entry receptor-

specific entry blockers [137], immune stimulating adjuvants for use with current vaccines [138], and microRNA-based therapies targeting the PRRSV genome [139, 140], have all shown promise in experimental settings. None, however, have progressed to commercially licensed treatments, and so there is still a reliance on conventional vaccines.

Though available for decades, current vaccination strategies for controlling PRRSV are limited in efficacy. Despite constant efforts to study the pathogenicity and immunology of PRRSV, it has been a substantial challenge to design effective vaccines. Both modified live virus (MLV) and inactivated PRRSV vaccines have been licenced, and are commercially available; however, both have advantages and disadvantages. MLV vaccines are generally preferred, serving as the predominating vaccines in the field, and have demonstrated efficacy in reducing disease severity, duration of viraemia, and viral shedding [141-143]. MLV vaccines have been used to combat PRRSV for decades, with examples such as the Porcilis PRRS MLV (Merck, Madison, NJ, USA) for PRRSV-1, and the Ingelvac PRRS MLV (Boehringer Ingelheim, Ingelheim am Rhein, Germany) for PRRSV-2 being commercially available, and still widely used since 2000 and 1994 respectively [144, 145]. However, no current PRRSV vaccine is capable of completely preventing disease: despite conferring protection against clinical diseases caused by closely related strains, MLVs have been shown to offer partial, or no, protection against more genetically distant strains [146]. The majority of PRRSV MLV vaccines are attenuated through serial propagation, upwards of 100 passages [147], in permissive continuous cell lines such as MA104 or the progeny MARC-145 lines [148] resulting in altered, low

virulence strains still capable of inducing an immune response. As MLV PRRSV strains can still replicate, and due to error-prone replication of its RNA genome, there are safety concerns regarding reversion of MLVs to virulence. Recombination between field and vaccine strains are points of contention [142, 149], with the epidemic of PRRSV-2 in the previously unaffected pig population in Denmark [150] being a notable example of a vaccine strain reverting to virulence.

Furthermore, there is evidence that maternally derived antibodies may impair the response of weaned piglets towards MLVs [151, 152]. These piglets are particularly susceptible to PRRSV, and as such are key populations for vaccination. Inactivated PRRSV vaccines, conversely are safer, with reversion to virulence not being a consideration following chemical (i.e. formaldehyde or β-propiolactone) or physical (heat or UV radiation) inactivation [153].

Inactivated PRRSV vaccines have been shown to boost immunity and are a particularly useful alternative when aimed at increasing levels of maternally derived antibody [64], and so could be seen as a safe alternative in this context.

Alone, however, these vaccines often fail to elicit significant induction of PRRSV-specific nAbs and cell-mediated immunity [146] and have been demonstrated to be limited in efficacy in the face of major antigenic shifts, or the emergence of novel strains, even against challenge from closer related strains [154]. Recent studies have investigated the efficacy of immunising with both MLV and inactivated vaccines [155], but have yet to demonstrate significant difference

between a single injection MLV vaccine and MLV plus inactivated virus boost vaccination scheme.

As such, exploring other alternative strategies to develop safer and more broadly protective vaccines is an area of great interest. Virus-vectored, subunit, and DNA vaccines have all been explored as potential alternatives, utilising antigenic PRRSV proteins as targets. In almost all instances, however, vaccines developed using these techniques have proven to be equally, or less effective than MLVs [146, 156-158]. Consequently, vaccines based on these techniques, though promising, are still far from practical application, and have little potential to replace MLVs without a major technological breakthrough.

1.5 Structural vaccinology

Another avenue towards developing a broadly protective PRRSV vaccine is by utilising a structural vaccinology approach. Through structural characterisation techniques such as X-ray crystallography and cryogenic electron-microscopy, the 3-dimensional (3D) structures of whole viruses, viral proteins, and antigen-antibody complex structures can be elucidated. As discussed earlier, the very basis of antibody recognition is determined largely by the topological complementarity between the CDRs of the antibody variable domain and those of the molecule being recognised [159]. Identifying which specific sites on an antigen to target, for potent neutralisation, is fundamental to a structure-based vaccine design. Identification of these sites, largely, can be achieved through the isolation of monoclonal antibodies (mAbs) with broad neutralisation capacity, utilising methods such as flow cytometry, i.e., as described by Young et al. [160].

Once these epitopes have been identified, ideally those that are targets for bnAbs, engineered *de novo* mimics can be used as immunogens to elicit antibodies with the original specificity [161] and therefore serve as a potential vaccine. The advantage of isolating mAbs is that, unlike whole serum, they are homogenous, consistent, each mAb will have a defined target and sequence. As such, isolated mAbs serve as powerful, replicable tools for identifying neutralising epitopes. The ability to selectively boost nAbs against subdominant, broadly protective epitopes could overcome long-standing obstacles in the development of vaccines against pathogens such as PRRSV.

Respiratory syncytial virus (RSV) is a key example of utilising such approaches for the design of novel vaccines. Through the design of *de novo* proteins mimicking the pre-fusion conformation of RSV F protein, in a stabilised form, and using these as immunogens, RSV-specific mAbs were isolated that demonstrated broad neutralisation against infection [162]. While approaches towards RSV vaccination have been investigated since the 1960s [163, 164] it is only now, with the use of structure-based vaccine concepts, that the first licensed human vaccine is available [165]. While RSV is perhaps the most successful example to date, structural vaccinology approaches have been employed for several viruses, such as West Nile virus [166], influenza A virus [167], and HIV [168]. No broadly protective vaccine for any of these viruses, however, has yet been produced.

No high-resolution structural information is available for the PRRSV envelope proteins, which makes it difficult to understand the structural basis of the virus-receptor interactions or antibody-mediated neutralisation [169], and is just another limitation of PRRSV vaccine development. The field, consequently, is

reliant on bioinformatic predictions largely based on cryo-electron microscopy experiments [170]. Neutralising epitopes have been described in PRRSV structural proteins GP3, GP4, GP5 and M, however there are inconsistencies between these findings, and more comprehensive studies are required to understand their contribution to a protective immune response [171, 172]. As discussed, cross-neutralising targets of PRRSV are likely to be structural or functional regions critical for essential pathogen/host cell interactions, conserved between PRRSV strains/ species. Isolation of mAbs that target these conserved regions, therefore, would greatly facilitate the development of broadly protective vaccines. Several approaches towards understanding the antibody-antigen complex of PRRSV have been attempted across the years. Historically, phage display libraries have been utilised to map both linear and discontinuous B cell epitopes [173, 174], and recent studies have successfully isolated mAbs from either hybridomas in immunised mice [93], or through the isolation and genetic re-programming of live single B-cells [160]. The isolation of PRRSV-specific mAbs, in the context of a structural vaccinology approach has recently been reported [175], utilising recombinant PRRSV-1 GP2, GP3, GP4, GP5, and M, generated in a prokaryotic expression system. The recombinant mAbs generated in this study demonstrated significant binding to the recombinant proteins, but no further data, i.e., on recognition of native virus, cross-reactivity, or neutralisation capacity have been reported since. Despite the progress in this field, regardless of approach, broadly neutralising epitopes remain largely undefined.

1.6 PRRSV proteins as targets of neutralising antibodies

The glycoproteins of PRRSV, especially GP5 and GP3, are the most variable proteins of any known virus [26, 176, 177], which poses significant difficulty in defining epitopes. As described above, PRRSV proteins form either a multimeric, non-covalently linked minor envelope complex [44, 45] or a disulphide-linked heterodimer referred to as the major envelope complex [46] (**Figure 1.5**).

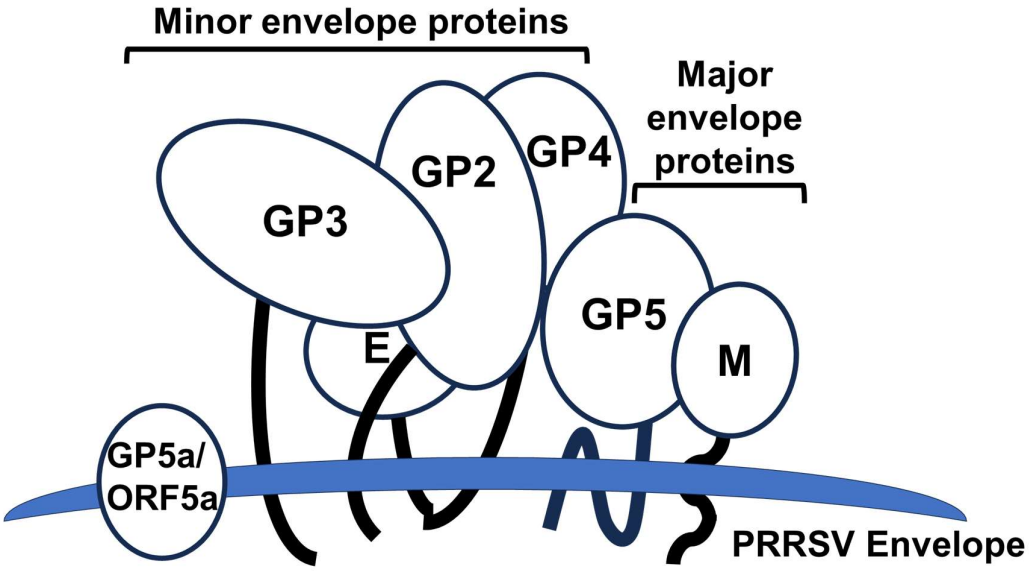


Figure 1.5: Schematic overview of PRRSV envelope organisation. Proteins of the multimeric minor envelope complex are represented on the left, and proteins of the major envelope complex represented on the right. Adapted from "The minor envelope glycoproteins GP2a and GP4 of porcine reproductive and respiratory syndrome virus interact with the receptor CD163*"*. P. B. Das, et al., 2010, *Journal of Virology, 84(4):1731-40*. Copyright 2010 American Society for Microbiology. Adapted with permission.

The formation of these complexes adds further challenge to understanding PRRSV: is it poorly understood how complex formation affects epitope availability, as well as the formation of discontinuous epitopes. Despite this, PRRSV proteins still represent key targets for neutralising antibodies.

1.6.1 Non-structural and nucleocapsid protein

In addition to the above envelope proteins, non-structural proteins and the genome-encapsulating nucleocapsid protein have also been explored as potential targets for PRRSV vaccine development.

1.6.1.1 Non-structural protein 2

Compared to PRRSV structural proteins, NSP2 has a high number of immunodominant B cell epitopes as shown in mapping studies [178]. NSP2 is comprised of an amino-terminus-cysteine-protease-domain, thought to be required for NSP2 and NSP3 cleavage. Moreover, NSP2 functions as cofactor in the protease activity of NSP4 for cleavage of the polyprotein-1a and polyprotein-1b. Recent studies have explored the use of NSP2-based designs in conjunction with GP5, M, and GP3, in order to enhance the neutralising response [179] [180], however so far these have been limited to *in vitro* studies. NSP2 undergoes remarkable genetic variation, and so is often used alongside GP3 and GP5 for phylogenetic analysis for the genetic variation and molecular epidemiology [181, 182].

1.6.1.2 Nucleocapsid protein

The most abundant protein in the PRRSV virion is the N protein [49, 183], and has a molecular mass of approximately 15 kilodalton (kDa) [49]. The N protein of PRRSV-1 has 128 amino acids (AA) while PRRSV-2 has 123 AAs [49, 184]. In the endoplasmic reticulum-Golgi complex, homodimerisation of the N protein occurs through disulfide-linkage via a cysteine residue at position 27 and 23 in PRRSV-1 and PRRSV-2 strains respectively [185]. This cysteine, moreover, has

been shown to be crucial for infectious virus production and viral genome replication [186]. The N protein is a serine phosphoprotein and is highly immunogenic; however, to date no N-specific-nAbs have been isolated, with some arguing that nAbs cannot be induced by this protein [184].

1.6.2 The major envelope proteins

While the minor envelope proteins and their interaction with CD163 drives the viral uncoating and genomic release, it is the major envelope proteins – M and GP5 – and their interactions with CD169 and heparan sulfate that drive viral attachment. Consequently, these proteins have also been an area of great interest, in developing next-generation PRRSV vaccines. Having the highest relative abundance of the PRRSV structural proteins, the major envelope proteins are also the most well studied of those described in this chapter.

1.6.2.1 Glycoprotein 5

GP5 is the most abundant glycoprotein on the surface of the PRRSV virion and considered the most variable protein of PRRSV [142, 187]. It has been predicted that GP5 possesses a 31-35 residue signal sequence, followed by a short 28-30 residue ectodomain, and a 65-69 residue hydrophobic domain. Though historically of some debate, this hydrophobic domain is predicted to comprise three transmembrane helices [188-190]. Finally, common amongst major envelope proteins of nidoviruses, PRRSV GP5 possess a long hydrophilic cytoplasmic tail region extending up to 65-70 residues [188]. There are two and three N-glycosylation sites on PRRSV-1 and -2 GP5, respectively [190]. Previous studies have revealed that these glycan moieties are necessary for preventing

recognition by nAbs [191]. GP5 has historically been favoured as the most relevant antigen for vaccine development [94], and has been considered the main protective antigen targeted by nAbs induced by PRRSV vaccination or prior infection [192].

The protein has six antigenic determinants and contains two major B cell epitopes: an immunodominant non-neutralising epitope A and a neutralising epitope B [126, 193, 194]. It is hypothesised that the combination of epitope A serving as a decoy epitope, and the presence of a hypervariable region – HVR-2 – in epitope B [195] result in most of the response to GP5 being non-neutralising. Epitope B has been described as possessing many features of a broadly neutralising epitope [74], with several studies lending support to this, [74, 160, 196], however in all instances the nAb response described in these studies is against homologous strains. A recent study demonstrated that an IgM mAb isolated from a GP5 immunised mouse demonstrated broadly neutralising potential [93].

This has also been met with conflicting studies, which suggest that the GP5-specific antibody response is non-neutralising, i.e., Li and Murtaugh [197] demonstrated that while immunisation of pigs with polypeptides of the GP5-M ectodomain could induce PRRSV-specific antibodies, they demonstrated no neutralisation against PRRSV virions. Epitope B, furthermore, has been argued to not contain any neutralising antigen region [198]. It is hypothesised therefore, that the nAb response against GP5 may not be enough to confer protection, and it is the complex interplay between PRRSV viral proteins that elicits a neutralising response. It is unclear whether these discrepancies are due to improvements in

techniques over time, or from gaps in knowledge of these proteins, but what is clear is how this highlights the complexities of PRRSV proteins and their interactions with the immune response.

1.6.2.2 Matrix protein

For Arteriviruses, the M protein is the most conserved structural protein [199]. It is a non-glycosylated, triple membrane spanning protein, 160-170 residues in length, with a molecular weight of 18-19 kDa [183]. The M protein consists of a short, 15-17 residue extracellular domain, followed by three putative hydrophobic transmembrane domains each 18-20 residues in length connected by 6-9 AAs, and – like GP5 - a long 84-89 residue C-terminal endodomain [188]. Unlike the PRRSV GPs, the short N-terminal ectodomain of the M protein does not contain a signal peptide or a consensus sequence for the attachment of N-linked glycans [200]. Even though there is no clear evidence, the M protein is assumed to be crucial for virus assembly and egress. It has been shown that mutations in the M protein-encoding ORF6 enabled escape from pre-existing bnAbs [47], suggesting that M protein does serve a role in viral neutralisation. Additionally, binding analysis revealed residue 70 of the M protein plays an important role in regulating the susceptibility to nAbs in porcine serum [131]. As previously discussed, however, these GP5-M-specific antibodies were non-neutralising and so, as with GP5, this is an area of debate. Studies have shown that in conjunction with NSP2, GP5-M contributes to a neutralising response including, albeit weakly, against heterologous strains [180], contributing further to the hypothesis that response to these proteins alone is insufficient for protection.

1.6.3 The minor envelope proteins

As PRRSV research continues to advance, more focus has been placed on the minor envelope proteins as the major determinant of a broadly neutralising response. As has been discussed throughout, CD163 is the major viral receptor for PRRSV. GP2 and GP4 have been shown to be essential for the interactions with CD163 [82, 128], with recent evidence suggesting GP3 plays a role in this interaction also [201], and so could represent a key target for vaccine development.

1.6.3.1 Glycoprotein 2

GP2 comprises 249 and 256 residues in PRRSV-1 and -2, respectively, and a molecular weight of 29 – 30 kDa [202]. Four domains have been detailed in GP2: an N-terminal signal sequence between residues 1 and 40 (PRRSV-1) and 1 to 37 (PRRSV-2), an estimated 168 residue ectodomain, a 20-residue transmembrane (TM) helix, and a 20-residue endodomain [190]. GP2 exhibits a typical type I membrane topology, passing once through the membrane, and demonstrating signal peptide cleavage upon translation [188]. Two N-glycosylation sites are recognized in both PRRSV-1 (asparagine (Asn) 173 and Asn 179), and PRRSV-2 (Asn 178 and Asn 174) [203, 204]. The role of N-glycosylation on PRRSV infectivity is unclear; however, it has also been demonstrated that the N-glycosylation of the asparagine residue at position 184 was essential for infectious PRRSV-1 virus production [190], later confirmed in PRRSV-2 based on the FL12 strain [203].

GP2 does represent a potential vaccine target, however, its role in the induction of broadly reactive nAbs remains largely unknown [125], and cross-neutralising GP2-specific mAbs have yet to be isolated. From pepscan analysis of PRRSV-1 Lelystad, it was found that GP2 possessed two neutralising epitopes. [205], these were not observed until 141 dpi, and so the neutralising response of these antigenic regions is likely of minor importance. This study, largely focussed on the use of linear peptides and so do not represent the conformation of the native protein structure. Consequently, conformational epitopes formed as a result of secondary/tertiary structure, and as part of the minor envelope complex, remain unstudied.

1.6.3.2 Envelope and GP5a proteins

The E protein is a non-glycosylated structural protein with a length of 70-73 residues, with a molecular weight of 10 kDa [206]. The E protein has a single cross-helical structure and provides ion channel activity for the virion [207]. The E protein has been shown to be vital for virus infectivity but not for virion particle assembly [208, 209]. Despite playing an important putative role in the infection no literature exists indicating presence of immunogenic epitopes, neutralising or otherwise.

GP5a/ORF5a, similarly, is underrepresented in literature. GP5a/ORF5a is a more recently described structural protein in PRRSV that is present in all Arteriviruses [43]. It is a non-glycosylated and hydrophobic, with a length of 46–52 residues, and a mass of 5.4 kDa [210]. The GP5a/ORF5a protein is predicted to have a type III membrane typology, possessing no canonical N-terminal signal peptide [188].Studies have shown that GP5a/ORF5a protein is essential for viral viability

and infectivity [211, 212], and is well conserved amongst PRRSV strains [181]. Despite this, a follow up to these studies has reported the contrary: that immunisation of pigs with GP5a/ORF5a protein did not induce a nAb response [213]. As such, the true role GP5a/ORF5a protein plays in the context of nAbs remains poorly understood.

1.6.3.3 Glycoprotein 3

GP3 of PRRSV-1 and -2 is composed of 265 and 254 AAs, respectively. While historic evidence has suggested that GP3 exhibits a type II membrane topology with an N-terminal anchor and a C-terminal ectodomain [214, 215], however it is now widely accepted that instead GP3 is a classic type I membrane protein possessing a unique hairpin-like topology, with the hydrophobic C-terminus spanning the membrane alongside two transmembrane regions to anchor the protein [188]. 27-29 residues comprise the signal sequence, 150-181 residues comprise the endodomain, 13-25 comprise the hydrophobic transmembrane/anchor region, and 27-37 residues comprise the C-terminal sequence [188] for PRRSV-1 and PRRSV-2 respectively. GP3 is extensively glycosylated with six glycosylation sites predicted in the putative ectodomain [216]. It has been shown that a small fraction of GP3 can be found secreted in a soluble, membrane free form as a result of its hairpin-like topology [217, 218]; it is believed that both virion-associated and soluble-forms of GP3 can elicit immune responses in infected pigs [219]. GP3 has been demonstrated to display a high level of immunogenicity [219-222], despite its significantly lower relative abundance compared to the major envelope proteins. A multitude of linear antigenic regions were identified in GP3 from both PRRSV-1 and PRRSV-2

strains, but antibodies directed against most of these epitopes do not neutralise viral infectivity [178, 223-225]. GP3 possesses a well-documented neutralising epitope [129, 191, 226], however, access to this epitope by antibodies is often greatly restricted, with the N-glycan of GP3 reducing immunogenicity and often preventing neutralisation [227].

GP3 is also well documented for possessing hypervariable regions. It has been observed that escape variants of PRRSV from experimentally infected pigs contain mutations in GP3 [228], [229], lending support that it does serve a role in the neutralising antibody response. These characteristics make GP3 a particularly appealing for study. As mentioned earlier, recent work has, demonstrated the use of recombinant baculovirus-expressed GP3 protein as immunogens to isolate GP3-specific mAbs from immunised mice [230]. One of the mAbs isolated from this study has been shown to exhibited broad-spectrum recognition and neutralising activities against PRRSV-1 and PRRSV-2 strains *in vitro*, however, there has been no reported evidence of its efficacy *in vivo.*

1.6.3.4 Glycoprotein 4

GP4 of PRRSV-1 and -2 are composed of 183 and 178 AAs, respectively, with a molecular weight of 31–35 kDa. Like GP2, GP4 is predicted to be a type I integral membrane protein [204], possessing a 24-21 residue signal sequence, a 143-130 residue endodomain, a short transmembrane domain of 15-11 residues, and a very short 7-4 AA endodomain tail for PRRSV-1 and PRRSV-2 respectively. GP4 and is highly glycosylated during transport through the endoplasmic reticulum-Golgi complex [231]. GP4 has four predicted glycosylation sites: Asn 37, Asn 88, Asn 124, and Asn 130 for PRRSV-1 and Asn 37, Asn 84, Asn120, and Asn 130

for PRRSV-2 [183]. One PRRSV-neutralising epitope has been identified in GP4 [202], however like GP2, no mAbs have been isolated to date. Although the described epitopes of GP4 have been shown to be highly immunogenic [174, 202], it has also been shown to be highly variable [232]. Studies have clearly demonstrated that the neutralising epitope on GP4 is susceptible to mAb-induced immunoselection *in vitro* [132, 233], no evidence that it is susceptible to antibody selection *in vivo* has been shown. Conversely, other studies have demonstrated that GP4 from PRRSV-1 Lelystad was able to elicit nAbs that were protective against closely related strains, but these offered no protection against more heterologous strains [127].

1.7 Aims and objectives

Despite their importance, key gaps exist in our knowledge of PRRSV glycoproteins. The minor envelope proteins, specifically, remain some of the least understood viral proteins, despite the promise they hold as targets for novel vaccine design. It was decided that this project, therefore, would focus on the proteins of the minor envelope complex of PRRSV-1.

Four primary objectives were set on this basis:

1. Produce novel recombinant PRRSV glycoproteins to use as tools to support mAb isolation and characterisation (**Chapter 3**).
2. Characterise the antigenicity of recombinant PRRSV glycoproteins (**Chapter 4**).
3. Identify and characterise naturally occurring porcine mAbs capable of neutralising PRRSV (**Chapter 5**).

4. Evaluate the immunogenicity of novel recombinant PRRSV glycoproteins (**Chapter 6**).

Chapter 2. Materials and methods

2.1 Design of PRRSV minor glycoproteins

2.1.1 Protein modelling and prediction

Recombinant protein design was informed using several protein fold and topology prediction software:

Phyre2 version 2.0 (Imperial College London, London, UK, [234]), SignalP version 5.0 (Department of Health Technology, Lyngby, Denmark, [235]) and TMHMM version 2.0 (Department of Health Technology, Lyngby, Denmark, [236]) were used for signal peptide, transmembrane domain prediction, and folding predictions. AlphaFold and AlphaFold2 (European Bioinformatics Institute (EMBL-EBI), Hinxton, UK, [237]) were used in addition to the above software for protein folding predictions and comparing planned recombinant GP subsets with portions of sequences removed. RCSB PDB Mol* 3D Viewer (RCSB Protein Data Bank, [238], [239]) was used to visualise and align protein models.

2.1.2 Recombinant GP sequences and primer design

Human codon-optimised sequences of PRRSV-1 Olot/91 (GenBank: KF203132.1) GP2 (GenBank: AGW23405.1), GP3 (GenBank: AGW23404.1), and GP4 (GenBank: AGW23406.1) were generated by Integrated DNA Technologies (IDT Inc., California, USA) as synthetic gene fragments (**Table 2.1**). Sequences were codon optimised for expression in human cells, using Integrated DNA Technologies optimisation tool.

	Gene sequence
GP2	ATGCAATGGGGTCACTGTGGCGCTAAAAGCGCATCCTGTAGCTGGACTCCTTCTTTG TCATCTTTGTTGGTCTGGTTGACGCTCAGCTTCAGCTTGCCATATTGTCTTGGCTCA CCATTGCCAGCTGGATACTGGTCATTCTTTTCCGAGTGGTTCGCACCTCGCTTTAGC GTCAGGGCACTTCCGTTCACTCTGCCGAATTACCGGCGGTCCTACGAAGGCCTTCTG CCCAACTGTCGCCCCGACGTGCCCCAGTTCGCGGTGAAACATCCGCTTGGAATGTTT TGGCACATGAGGGTAAGTCACCTGATAGATGAGATGGTTTCTCGCCGGATATATCAA ACTATGGAACACTCTGGTCAAGCGGCTTGGAAACAAGTGGTATCCGAGGCGACACTG ACTAAATTGAGCGGCCTCGATATAGTGACTCACTTCCAGCACTTGGCTGCCGTGGAA GCCGACAGTTGCAGATTTCTGTCCTCCAGGCTCGTCATGCTGAAAAACCTTGCGGTT GGAAATGTTAGCTTGCAGTACAACACTACACTCGACAGGGTGGAGCTGATATTTCCA ACTCCAGGTACCCGCCCAAAACTCACAGACTTCAGACAATGGTTGATTAGTGTTCAC GCCAGTATATTTTCAAGTGTAGCGAGCAGCGTTACCCTGTTCATCGTCCTTTGGCTT CGCATTCCGATACTTCGCTACGTGTTCGGTTTTCATTGGCCTACAGCTACGCATCAT TCCTCCTAA
GP3	ATGGCTCATCAGTGTGCGCGATTTCATTTCTTCTTGTGCTCATTCATCTGCTACTTG GTACATTCCGCGTTGGCCTCAAATTCCAATTCAACTCTGTGTTTTTGGTTTCCGCTC GCACACGGCAATACCTCTTTTGAGCTTACCATTAATTACACAATATGCATGCCTTGC AGTACCTCCCAGGCGGCTCACCAGAGACTGGAGCCTGGGAGAAATATGTGGTGTCGC ATCGGACATGATCGCTGTGAAGAGAGGGACCACGACGAACTTTCCATGTCCATCCCC TCCGGGTATGACAATCTCAAATTGGAGGGATACTATGCATGGTTGGCTTTCCTTTCC TTTTCCTACGCTGCGCAGTTTCATCCAGAGCTCTTTGGGATCGGAAACGTGTCCAGG GTGTTCGTGGACAAACAACATCAGTTTATTTGTGCAGAGCACGATGGGCGAAACTCT ACGATATCAACTGAATACAATATTAGTGCGCTGTACGCAGTGTATTATCATCACCAG ATTGATGGCGGTAACTGGTTTCATCTGGAATGGCTCCGGCCCTTTTTCTCCTCTTGG CTGGTACTTAACATATCTTGGTTCCTCCGGCGGTCTCCCGTCTCACCAGTATCAAGA AGGATTTACCAGATTCTTAGGCCTACGAGGCCGCGCCTCCCCGTAAGCTGGTCATTT AGAACAAGCATAGTCTCCGATCTCACTGGCAGTCAACAACGCAAGAGGACATTCCCA TCAGGATCAAGATTGAATGTCGTAAAACCCAGCGTGTTCCCGTCCACTCTTAGATAA
GP4	ATGGCGGCGGCGATACTCTTTCTGTTGGCGGGAGCCCAGCATTTTATGGTATCTGAG GCATTTGCCTGTAAGCCGTGTTTCTCTACTCACCTTTCTGATATTAAGACTAACACG ACCGCCGCGGCAGGCTTCATGGTCTTGCAGAATATTAATTGTCTTAGGCCGCACGGA GTCAGCACAGCTCAAGAGAACATATCATTCGGAAAGCCCTCACAGTGCAGGGAAGCC GTAGGGATACCTCAATATATAACCATTACCGCAAATGTTACCGACGAATCATATTTG TATAACGCGGACCTTCTGATGCTGTCAGCGTGTCTCTTTTACGCATCCGAAATGTCA GAGAAGGGCTTCAAAGTAATCTTTGGTAATGTTAGTGGAGTAGTTAGTGCGTGTGTG AATTTCACTGATTACGTGGCACATGTAACCCAGCATACTCAGCAGCACCACCTTGTG ATAGACCATATCAGGCTGCTTCACTTCTTGACCCCATCAACAATGCGCTGGGCAACT ACCATCGCCTGCCTGTTTGCGATCCTGTTGGCTATTTGA

Table 2.1: Human codon-optimised PRRSV-1 Olot/91 GP2, GP3, and GP4 sequences, to be used as templates to generate recombinant proteins. Start codons are in **green**, stop codons in **red**.

Primers were designed to generate three subsets of each PRRSV-1 GP: full-length, up to the first transmembrane domain only, and with or without the native signal peptide (**Table 2.2**).

Primer name	Sequence (5' to 3')	Target sequence
OPPF22380fwd	aggagatataccatgCAATGGGGTCACTGTGGCG	5' of GP2 sequence (start of predicted signal peptide)
OPPF22380rev	gtgatggtgatgtttGGAGGAATGATGCGTAGCTG	3' of full GP2 sequence
OPPF22382rev	cagaacttccagtttGGAGGAATGATGCGTAGCTG	3' of full GP2 sequence with overhangs for fluorescent protein fusion
OPPF22383fwd	gcgtagctgaaaccggcCCATTGCCAGCTGGATACTG	5' of nucleotide position 117 of GP2 (predicted signal peptide removed)
OPPF22383rev	gtgatggtgatgtttTTGTCTGAAGTCTGTGAGTTTTG	3' of GP2 nucleotide position 603 (encoding predicted ectodomain only)
OPPF22385fwd	aggagatataccatgGCTCATCAGTGTGCGCGATTTC	5' GP3 sequence (start of predicted signal peptide)
OPPF22385rev	gtgatggtgatgtttTCTAAGAGTGGACGGGAACACG	3' of full GP3 sequence
OPPF22386rev	cagaacttccagtttTCTAAGAGTGGACGGGAACACG	3' of full GP3 sequence with overhangs for fluorescent protein fusion
OPPF22387fwd	gcgtagctgaaaccggcAATTCCAATTCAACTCTGTGTTTTTG	5' of nucleotide position 81 of GP3 (predicted signal peptide removed)
OPPF22387rev	gtgatggtgatgtttTTCCAGATGAAACCAGTTACCGC	3' of nucleotide position 543 of GP3 (encoding predicted ectodomain only)
OPPF22389fwd	aggagatataccatgGCGGCGGCGATACTCTTTC	5' of GP4 sequence (start of predicted signal peptide)
OPPF22389rev	gtgatggtgatgtttAATAGCCAACAGGATCGCAAAC	3' end of full GP4 sequence
OPPF22390rev	cagaacttccagtttAATAGCCAACAGGATCGCAAAC	3' of full GP4 sequence with overhangs for fluorescent protein fusion
OPPF22391fwd	gcgtagctgaaaccggcGCCTGTAAGCCGTGTTTCTC	5' of nucleotide position 66 of GP4 (predicted signal peptide removed)
OPPF22391rev	gtgatggtgatgtttCCTGATATGGTCTATCACAAGG	3' of nucleotide position 571 of GP4 (encoding predicted ectodomain only)
OPPF22383-BAP-rev	gtcattcagcaagctTTGTCTGAAGTCTGTGAGTTTTG	3' of GP2 nucleotide position 603 for addition of BAP tag
OPPF22387-BAP-rev	gtcattcagcaagctTTCCAGATGAAACCAGTTACCGC	3' of GP3 nucleotide position 543 for addition of BAP tag
OPPF22391-BAPrev	gtcattcagcaagctCCTGATATGGTCTATCACAAGG	3' of GP4 nucleotide position 571 for addition of BAP tag

Table 2.2: Summary of primers designed for the generation of recombinant PRRSV-1 GP2, GP3, and GP4. For all GPs, full-length and shortened forms cut-off at the first predicted transmembrane domain were generated. All sequences were also designed to enable alternative signal peptide use. Lower case nucleotides represent the overhang sequences, designed to enable cloning into the respective vectors.

All primers were designed with overhangs to enable cloning into the pOPIN-suite expression vectors, provided by Prof. Ray Owens, Protein Production UK (PPUK), Rosalind Franklin Institute, Harwell, UK [240] (**Table 2.3**). Plasmid maps of these expression vectors are detailed in **Appendix Figures 1 – 4**, with the exception of pOPINE-YFP and pOPINE-mCherry, which were not provided.

Vector	Protein(s) expressed
pOPINEneo	Full length recombinant GPs with a hexahistidine tag
pOPINTTGneo	Full length and ectodomain only recombinant GPs with a hexahistidine tag and receptor-type protein-tyrosine phosphatase μ signal peptide in place of the native signal peptide
pOPINEneo-3C-GFP	Full length recombinant GPs with a green fluorescent protein (GFP) fusion and a hexahistidine tag
pOPINE-YFP	Full length recombinant GPs with a yellow fluorescent protein (YFP) fusion and a hexahistidine tag
pOPINE-mCherry	Full length recombinant GPs with an mCherry fusion and a hexahistidine tag
POPINTTG-BAP	Ectodomain only recombinant GPs with a hexahistidine tag, receptor-type protein-tyrosine phosphatase μ signal peptide in place of the native signal peptide and an additional biotin acceptor peptide (BAP) tag site

Table 2.3: Summary of plasmids used for generation of recombinant PRRSV-1 GP2, GP3, and GP4 and the subsets of each. All plasmids listed were kindly provided by the Ray Owens Group, PPUK, Rosalind Franklin Institute/University of Oxford.

2.2 Polymerase chain reaction

Polymerase chain reaction (PCR) was used to amplify DNA for cloning, investigating the size and presence of plasmid inserts and to generate DNA samples for cloning/sequencing. Working stocks of forward and reverse primers were diluted to 10 μM in nuclease-free distilled water (dH_2O) (Merck, Darmstadt, Germany, ref W4502) before use. Different DNA polymerases were used for

different PCR purposes based on their proof-reading abilities. For analysis, sequencing, and colony PCR, 1× ReadyMix™ Taq PCR Reaction Mix (Merck, ref P4600) was used. For cloning, Q5® High-Fidelity DNA Polymerase (New England BioLabs, ref M0494S) was used due to comparative low error rates and proof-reading ability. As standard, PCR was performed using a Veriti™ 96-Well Fast Thermal Cycler (Applied Biosystems, Thermo Fisher Scientific ref 4375305). PCR reactions contained varying amounts of template (2-50 ng), primers at a final concentration of 0.5 µM, the DNA polymerase and its respective buffer diluted to 1×, and nuclease-free dH_2O to make a final volume of either 25 or 50 µL. A standard thermocycler program was followed throughout (**Table 2.4**), with deviations from this program being detailed throughout.

Stage	Temperature/Time	Number of cycles
1	95-98 °C for 2-3 minutes	1
2	95-98 °C for 20 seconds	25-40
3	57-72 °C for 30 seconds	
4	72 °C for 30 seconds	
5	72 °C for 2 minutes	1
6	4 °C hold	∞

Table 2.4: Detailed of the standard PCR protocol/thermocycler program used. Annealing temperatures, extensions times and number of cycles were adjusted based on primer melting temperature (Tm) and PCR product length. Extension time was based on 30 seconds per kb.

Following amplification 1-5 µL of each PCR product was analysed on a 1% (w/v) agarose gel.

2.3 Agarose gel electrophoresis

Agarose gels were used to visualise and purify DNA. To make a 1% (w/v) gel, 500 milligrams (mg) of agarose (Meridian Bioscience, London, UK, ref BIO-

41025) was added to 50 mL of 1× TBE buffer (Invitrogen™, ref 15581044) diluted in deionised water and heated to dissolve the agarose. 5 µL of either GelRed® Nucleic Acid Gel Stain (Cambridge Bioscience, ref BT41003) or SYBR™ Safe DNA Gel Stain (Thermo Fisher Scientific, ref S33102) was mixed in before pouring into a sealed gel tray. The gel was left to set at room temperature (rt). Before loading, the appropriate volume of Gel Loading Dye, Purple (6×) (New England BioLabs, ref B7024S) was added to each sample. 1 µL of 1 kb Plus DNA Ladder (New England BioLabs, ref N3200) was used as a marker for each gel. Gels were loaded and run at 90 V. Gels were imaged using a BioRad GelDoc Go Gel Imaging System (BioRad Laboratories, California, USA, ref 12009077).

2.4 DNA purification

2.4.1 Purification from agarose gels

Following agarose gel electrophoresis, PCR products or digests were purified using either the QIAquick Gel Extraction Kit (QIAGEN, Manchester, UK, ref 28704), or GFX PCR DNA and Gel Band Purification Kit (Cytiva Life Sciences, ref 28903471). Portions of gels containing the desired DNA fragments were excised using a sterilised scalpel blade and subsequently processed according to the manufacturer's protocol. DNA samples were eluted in DNase/RNase/protease free dH_2O (Merck, ref W4502).

2.4.2 Quantification of DNA

Concentrations of plasmid preparations were calculated using a NanoDrop One Microvolume UV-Vis Spectrophotometer (Thermo Fisher Scientific, ref ND-ONE-W). The machine was first blanked with 2 µL of DNase/RNase/protease free dH_2O

before a 2 µL sample of plasmid was added and concentration read using absorbance measurements at wavelengths of 260 and 280 nm. Purity was assessed using the A260/280 nm measurements, anything outside of the range of 1.7-2.0 was considered impure.

2.5 Sanger sequencing

Cycle sequencing PCR amplification utilising a BigDye™ Terminator v3.1 Cycle Sequencing Kit (Applied Biosystems, ref 4337455) was performed on 1 µL of product in a 20 µL reaction volume containing 1x Sequencing Buffer, BigDye™ Terminator 3.1 Ready Reaction Mix, nuclease-free H_20, and 4 pmol forward or reverse primers from the first round of PCR. Amplification used the following protocol: 96 °C for 1 minutes (min), 30 cycles of 96 °C for 10 seconds (s), 50 °C for 5 s, and 60 °C for 4 min. Products were then precipitated with 125 mM ethylenediaminetetraacetic acid (EDTA) and 100% ethanol for 15 minutes at room temperature, followed by centrifugation at 2000 rpm for 45 min at 4 °C. Pellets were washed with 60 µL 70% ethanol, and precipitated by centrifugation at 1650 rpm for 15 min at 4 °C. Pelleted material was then vacuum dried, resuspended in Hi-Di™ Formamide (Applied Biosystems, ref 4311320), denatured at 95 °C for 2 min, and submitted to Dr. Jemma Wadsworth, The Molecular Epidemiology Group at The Pirbright Institute for sequencing.

2.6 Cloning

2.6.1 Digestion

A standard cleavage reaction contained 1-3 µg of DNA, 1 µL of restriction enzyme, 5 µL rCutSmart® Buffer (New England BioLabs, ref B6004S) (kept on

ice) and dH_2O to make a final volume of 50 µL. If enzymes were compatible (at least 75% cutting efficiency in the recommended buffer), double digests were carried out with both enzymes present simultaneously in the reaction. If not, sequential digests were performed with a heat inactivation step in-between. Digestion protocols were based on NEBCutter V2.0 (New England BioLabs), typically incubating for 30 min-2 hours (h). Temperatures used were in accordance with the manufacturer's recommendations. The full list of restriction enzymes used throughout have been detailed (**Table 2.5**).

Vector	Enzyme 1	Enzyme 2
pOPINEneo	NcoI-HF (New England BioLabs, ref R3193)	PmeI-HF (New England BioLabs, ref R0560)
pOPINTTGneo	PmeI-HF (New England BioLabs, ref R0560)	KpnI-HF (New England BioLabs, ref R3142)
pOPINEneo-3C-GFP	NcoI-HF (New England BioLabs, ref R3193)	PmeI-HF (New England BioLabs, ref R0560)
pOPINE-YFP	NcoI-HF (New England BioLabs, ref R3193)	PmeI-HF (New England BioLabs, ref R0560)
pOPINE-mCherry	NcoI-HF (New England BioLabs, ref R3193)	PmeI-HF (New England BioLabs, ref R0560)
POPINTTG-BAP	KpnI-HF (New England BioLabs, ref R3142)	HindIII-HF (New England BioLabs, ref R0104)
pNeoSec_SsFc_IgG1	EcoRI-HF (New England BioLabs, ref R0101)	PstI-HF (New England BioLabs, ref R0140)
pNeoSec_SsVL_kappa	EcoRI-HF (New England BioLabs, ref R0101)	PstI-HF (New England BioLabs, ref R0140)
pNeoSec_SsVL_lambda	EcoRI-HF (New England BioLabs, ref R0101)	PstI-HF (New England BioLabs, ref R0140)

Table 2.5: Restriction endonucleases used for double digestion of vectors. New England BioLabs Inc. product codes are also detailed. HF indicates high fidelity restriction endonuclease. pOPIN-suite plasmids listed were kindly provided by Prof Ray Owens, Rosalind Franklin Institute/University of Oxford. The expression vectors pNeoSec-SsFc-IgG1, pNeoSec-SsLC-κ and pNeoSec-SsLC-λ were provided by the Immunological Toolbox (The Pirbright Institute, UK). The vectors are derived from pNeoSec and encode the porcine constant domain regions for each immunoglobulin gene.

2.6.2 Ligation

Ligation of inserts was carried out using InFusion® cloning following the Vazyme ClonExpress® Ⅱ One Step Cloning Kit (Generon Ltd., Slough, UK, ref C115-01) protocol.

2.6.3 Transformation

Following ligation, bacteria were transformed for scale-up and purification of each plasmid. Laboratory adapted *Escherichia coli* (Stellar Supercompetent™ Cells, Takara Bio, ref. 636763) were utilised. 3 µg of ligated plasmid was mixed into 10 µL of thawed bacteria and kept on ice for 30 min. Bacteria were heat shocked at 42 °C for 45 s and immediately placed on ice for 3 min. 900 µL of S.O.C. Medium (Thermo Fisher Scientific, ref 15544034) was added to each transformed culture, and placed in a shaking incubator at 37 °C for 1 h at 200 rpm. 100 µL of cultures were plated onto Luria lysogeny broth (LB) agar plates prepared by Central Services Unit, The Pirbright Institute. LB powder (Merck, ref L3397) was added to agar (Merck, ref A1296) at 15 grams per litre (g/L) and autoclaved to sterilise. Depending on vector used, the antibiotic kanamycin (Merck, BP861) or ampicillin (Merck, ref A9518) was used, at 50 µg/mL and 100 µg/mL respectively. Antibiotics were added after autoclaving and cooling of the agar. Cultures were incubated at 37 °C for a minimum of 12 h, until colony formation was observed.

2.6.4 Colony PCR

Representative colonies were picked using a sterile pipette tip, mixed with 30 µL dH_2O and added to a standard PCR mix, detailed in **Table 2.6**.

Component	Final concentration
Q5® 5x Reaction Buffer (NEB, ref B9027S)	1x
Q5® 5x High GC Enhancer (NEB, ref B9028A)	1x
10 µM Forward Primer (selected from Table 2.1)	100 nM
10 µM Reverse Primer (selected from Table 2.1)	100 nM
10 mM dNTPs (Thermo Fischer Scientific, ref 18427013)	0.25 mM
Nuclease-Free Water	-
Q5® High-Fidelity DNA Polymerase (New England BioLabs, ref M0491S)	0.02 U/µl
Template DNA	< 1,000 ng

Table 2.6: Standard mixture used for colony PCR of bacteria following transformation.

PCR amplification was then performed using the reaction parameters described in **Section 2.2**. Remaining dH_2O-bacteria mixture was stored for up to 7 days at 4 °C and all constructs were submitted for Sanger sequencing prior to further work. Following sequencing results, selected cultures were taken forward for scale-up.

2.6.5 Scale-up of cultures

Bacteria were grown in LB broth supplemented with the required antibiotic. Similar to what was described in **Section 2.6.3**, LB powder was added at 15 g/L dH_2O and autoclaved to sterilise. Depending on how much plasmid was to be purified, cultures ranging from 50-500 mL were established and grown in shaking incubators at 37 °C for 12-16 h, until cultures were cloudy.

2.6.6 DNA purification

Plasmids were extracted using the QIAprep Plasmid Prep Kits (QIAGEN). Depending on the quantity of plasmid required, the QIAGEN Plasmid Mini (ref 12123) Midi (ref 12143), or Maxi (ref 12162) kits were used. For proteins used in the immunogenicity trial detailed in **Section 2.17**, an EndoFree® Plasmid Maxi Kit (ref 12362) was used. All kits were used according to the manufacturer's protocol and eluted in DNase/RNase/protease free dH_2O.

2.7 Mammalian cell lines

2.7.1 Cell culture

All cell lines described were available as part of The Pirbright Institute PRRS Immunology Group's pre-existing cryopreserved stocks, unless stated otherwise. All cell lines were cultured at 37 °C, 95% humidity, and 5% CO_2. Adherent cell lines were passaged using 0.25% trypsin-EDTA (Thermo Fisher Scientific, ref 25300054)

Human embryonic kidney (HEK) 293T cells were used to assess small-scale production of the recombinant GPs, utilised in the initial flow cytometry and confocal microscopy experiments. The cells were grown as adherent monolayers using Dulbecco's Modified Eagle Medium (DMEM) (high glucose, GlutaMAX™ Supplement, HEPES) (Thermo Fisher Scientific, ref 32430100) supplemented with 10% heat-inactivated Brazilian foetal bovine serum (FBS) (Thermo Fisher Scientific, ref 10270106) and 1% Penicillin-Streptomycin (100 units/ml penicillin and 100 µg/ml streptomycin) (Merck, ref P4333). Cells were passaged every 3-4 days.

Expi293F™ cells (Thermo Fisher Scientific, ref A14527) were used for the large-scale production of recombinant proteins. Cells grown in suspension in either 125 mL or 1 L Erlenmeyer non-baffled cell culture shaker flasks (Corning®, New York, USA, ref CLS431405/CLS431403) depending on the size required. Cells were grown on an orbital shaker at 200 rpm, using Expi293™ Expression Medium (Thermo Fisher Scientific, ref A1435101), without any additional supplementation. Cells were typically kept at 3-5 × 10^5 viable cells/mL and passed every 3-4 days.

MARC-145 cells were used for PRRSV-infection based assays, such as immunostaining or virus neutralisation assay. MARC-145 is a continuous cell line derived from the African Green Monkey kidney cell line MA-104, and are routinely used for PRRSV isolation and vaccine production, being well established as being permissive to PRRSV infection [241, 242]. The cells were grown as adherent monolayers in DMEM, again supplemented with 10% FBS and 1% Penicillin-Streptomycin. Cells were passaged every 3-4 days.

Porcine alveolar macrophages (PAMs) were used for PRRSV-infection assays utilising strains that could not effectively replicate in MARC-145 cells (i.e. PRRSV-1 SU1-Bel). PAMs isolated by bronchoalveolar lavage were cultured using RPMI-1640 Medium (Thermo Fisher Scientific, ref 11875093), supplemented with 10% FBS and 1% Penicillin-Streptomycin. As primary cells, PAMs were not cultured for an extended period of time, and only used for PRRSV-infection assays.

2.8 Transfection

For transfection, 10% FBS and 1% Penicillin-Streptomycin were not supplemented into the culture medium, as this had a negative impact on transfection efficiency.

HEK293T cells were transfected using TransIT®-LT1 Transfection Reagent (Mirus Bio LLC., Madison, Wisconsin, USA, ref MIR 2304) following the manufacturer's recommended protocol. Cells were incubated following transfection for 2-3 days.

Expi293F cells were transfected across a 5-day period. Cell volumes were adjusted to 0.8-1.0 × 10^6 viable cells/mL on day 1, before transfection on day 2. Transfection mixtures were prepared by mixing 1/10^{th} volume of Opti-MEM™ Reduced Serum Medium (Thermo Fisher Scientific, ref 31985062) with final concentrations of 0.91 µg/mL total DNA and 4.85 µg/mL PEI MAX® - Transfection Grade Linear Polyethylenimine Hydrochloride (Polysciences Inc., Pennsylvania, USA, ref 24765-1) and leaving the mixture for 10 min at rt before adding to the cells. Mixtures prepared for each scale of cultures used are detailed (**Table 2.7**).

Scale (Volume of cells)	Volume of Opti-MEM (mL)	Plasmid DNA vector (µg)	Volume of 1 mg/mL PEI40K
30 mL	3	15	160 µL
100 mL	10	50	533 µL
300 mL	30	150	1.6 mL

Table 2.7: Quantities of transfection reagents at different scales used on day 2 of Expi293F cell transfection. PEI40K was prepared beforehand and sterile filtered. Scale used was dependent on how much protein was required.

At 16 h following transfection, cell growth supplement mixtures were prepared. All solutions were 0.2 µm filter sterilised before addition, prepared v/v in Expi293 Expression medium. Final volumes of 0.76 mg/mL of sodium propionate (Merck, ref P1880), 0.61 mg/mL of valproic acid sodium salt (Merck, ref P4543) and 0.75 % D-(+) Glucose solution (Merck, ref G8769-100) were added to each culture. Mixtures prepared for each scale of cultures used are detailed (**Table 2.8**).

Scale (Volume of cells)	Volume of 50 mg/mL valproic acid	Volume of 100 mg/mL sodium propionate	Volume of 45% D-(+) Glucose Solution
30 mL	500 µL	200 µL	550 µL
100 mL	1.67 mL	0.67 mL	1.83 mL
300 mL	5 mL	2 mL	5.5 mL

Table 2.8: Volumes of transfection reagents at different scales used on day 3 of Expi293F cell transfection. Valproic acid and sodium propionate were prepared beforehand and sterile filtered. 45% glucose used was available from Merck (ref G8769-100). Scale dependent on how much protein was required.

Cultures were incubated for an additional two days before harvest on day 5. Cells were centrifuged at 4,000 × *g* for 30 min. Supernatants were stored for purification and cell pellets were either kept for analysis or discarded.

2.9 Flow cytometry

Standard flow cytometry experiments were performed using a minimum of triplicate wells for each condition, with a minimum of 1.0×10^6 cells per replicate. Samples were analysed using the BD LSRFortessa™ Cell Analyzer (Becton, Dickinson and Company, New Jersey, USA) or the Bigfoot Spectral Cell Sorter (Thermo Fisher Scientific). Single colour controls were included for all experiments, to enable spectral unmixing/compensation. For all experiments,

FACS buffer (PBS supplemented with 1% FBS) was used for washes and antibody dilutions.

2.9.1 Tetramer assembly

Biotinylated recombinant GPs were tetramerised with either Brilliant Violet 421 (BV421)-labelled streptavidin (BioLegend, ref 405225) or Brilliant Violet 650 (BV650)-labelled streptavidin (BioLegend, ref 405232) at a 4:1 molar ratio, introducing 1-part biotinylated protein every 12 minutes on ice until the desired ratio was achieved. Volumes were calculated based on the molarity of the protein to be tetramerised and compared to the molarity of the fluorochrome-conjugated streptavidin.

An additional control decoy, biotinylated SARS-CoV-2 spike protein receptor-binding domain [243] provided by the Viral Glycoproteins Group at The Pirbright Institute, was tetramerised with PerCP-Cy5.5-labelled streptavidin (BioLegend, ref 405214) at a 8:1 molar ratio. Excess biotinylated antigen was added to bind any free streptavidin-BV421/streptavidin-B650 that may have been present following GP-tetramer assembly, thereby further reducing non-specific staining. Tetramers were prepared one week in advance of sorting.

2.9.2 Staining panels

An established panel of antibodies [243], designed to enable identification of IgM, IgG, and IgA expressing porcine B cells, was used for the majority of flow cytometry experiments detailed in Chapters 3-6 (**Table 2.9**). Due to the limitations of commercially available antibodies, a R-Phycoerythrin (PE) Conjugation Kit -

Lightning-Link® kit (Abcam, ref ab102918) was used to conjugate an anti-pig IgM antibody with PE.

Antibodies	Target	Final concentration
Mouse IgG2a monoclonal-PE-Cy7 conjugate (BD Bioscience, ref 561477)	Porcine CD3	2 µg/mL
Recombinant human IgG1 monoclonal-PE-Vio 770 conjugate (Miltenyi Biotec, ref 130-110-521)	Human CD14 (cross-reactive against porcine CD14)	2 µg/mL
Mouse IgG1-PE conjugate (BioRad, ref MCA637GA)	Porcine IgM	2.5 µg/mL
Mouse IgG1 monoclonal-Alexa Fluor 647 conjugate (Generon ref CSA3841)	Porcine IgG	2.5 µg/mL
Goat IgG polyclonal-FITC conjugate (Bio-Rad, ref AA140F)	Porcine IgA	2.5 µg/mL
LIVE/DEAD fixable dead cell stain (Thermo Fisher Scientific, ref L34957)	Cell viability stain	1.25 µg/mL

Table 2.9: Standard antibody panel used to identify B cell isotypes by flow cytometry. All antibodies were titrated to determine optimal dilution before use.

2.9.3 Fluorescence-activated cell sorting

Cryopreserved peripheral blood mononuclear cells (PBMCs) (detailed in **Section 2.17**) were thawed and washed using RPMI-1640 Medium, supplemented with 10% FBS and 1% Penicillin-Streptomycin.

Single colour controls for each tetramer were included by first staining 1.0×10^6 cells with mouse anti-porcine CD8α-biotin (Cambridge Bioscience, ref 4520-08) diluted 1/200 (v/v), followed by the three streptavidin-fluorochrome conjugates used for tetramer assembly, detailed in **Section 2.9.1**. Tetramers were diluted 1/20 (v/v) before staining cells in conjunction with the antibody panel detailed in **Section 2.9.2**. All staining was performed on ice. Sorted cells were collected in cell collection buffer: 0.01M Tris (pH 8.0), 100 units RNasin® Ribonuclease

Inhibitor (Promega, Wisconsin, USA, ref N2115), diluted in RNase-free water, and frozen for subsequent analysis. Flow cytometric cell sorting was performed using a BD FACSAria™ III Cell Sorter by either Dr. Katy Moffat, or Chris Chiu, Flow Cytometry Facility, The Pirbright Institute.

2.10 Confocal microscopy

Coverslips were washed in 70% (v/v) ethanol and dried upright individually in wells of a 24-well plate. HEK293T cells were cultured overnight on coverslips treated with Poly-L-Lysine solution (Merck, ref P4707) in 24 well culture plates at density of 8 × 10^4 cells/well. Cells were transfected with 500 ng of DNA using TransIT®-LT1 Transfection Reagent as previously described (**Section 2.8**) and cultured for an additional 2 days. Cells were washed with PBS (Central Services Unit, The Pirbright Institute) and fixed with 4% paraformaldehyde (PFA) solution (Thermo Fisher Scientific, ref 15670799) containing 0.1% Triton X-100 (Merck, ref 9036-19-5) for 15 min at 37 °C. Cells were subsequently blocked with PBS containing 0.1% bovine serum albumin (BSA) (Thermo Fisher Scientific, ref 9048-46-8) for 30 min at rt. Cells were stained with 100 µL/well Alexa Fluor™ 647 Phalloidin (Thermo Fisher Scientific, ref A22287) diluted 1:500 (v/v) in PBS for 10 min at rt. Cells were washed, and subsequently stained with 100 µl/well 300nM 4′,6-diamidino-2-phenylindole (DAPI) (BioLegend, ref 422801) diluted in PBS. Following additional washes, coverslips were mounted with 7 µL Vectashield® Antifade Mounting Media (Vector Laboratories, California, USA, ref H-1000-10), were left overnight at 4 °C, dried to remove excess Vectashield®, and then sealed using clear nail varnish. Slides were imaged within one week of staining and

analysed with use of a Leica TCS SP2 confocal microscope (Leica Microsystems, Wetzlar, Germany).

2.11 SDS-PAGE

2.11.1 PAGE conditions

SDS-PAGE and western blotting were used to screen cultures for recombinant protein expression, assess glycosylation and biotinylation, and determine the quality of purified protein.

In all instances, 12.5 %,1.0 mm polyacrylamide gels were used and were cast in-house using the BioRad Mini-PROTEAN Tetra Cell system (BioRad, ref 1658000) (**Table 2.10**). Tris buffers were made using Trizma® base (Merck, ref 93362) in dH_2O, pH adjusted using 1 mol/L hydrochloric acid (HCl) (Merck, ref 1.09057) as measured using an Orion Star™ A211 Benchtop pH Meter (Thermo Fisher Scientific, ref STARA2110).

Reagents	Volume (mL) for 2x resolving gels	Volume (mL) for 2x stacking gels
40% acrylamide (BioRad, ref 1610140)	3.0415625	0.6083125
2% BIS-acrylamide (BioRad, ref 1610142)	1.66875	0.33375
1M Tris pH 8.8	3.75	-
1M Tris pH 6.8	-	0.625
10% SDS solution (Thermo Fisher Scientific, ref 15553027)	0.1	0.05
dH_2O	1.3978375	3.3454375
N,N,N,N tetramethylethylenediamine (Merck, ref 1.10732)	0.00835	0.0125
10% w/v ammonium persulfate (Thermo Fisher Scientific, ref 17874) in dH_2O	0.0335	0.025

Table 2.10: Components used to cast 2x 12.5% polyacrylamide gels. Resolving gels were cast and left to polymerise before adding N,N,N,N tetramethylethylenediamine and ammonium persulfate to stacking gels. Tris solutions were prepared in house. Gels were cast in pairs to facilitate use with the BioRad Mini-PROTEAN Tetra Cell system.

PAGE gels were run using 10x Tris/Glycine/SDS running buffer (BioRad, ref 1610732) diluted 1/10 (v/v) in dH_2O, at 40 amperes (A). For sample loading, three parts of each sample was mixed with one part 4× Laemmli sample buffer (BioRad, ref 1610747) supplemented with either β-mercaptoethanol (BioRad, ref 1610710) or dithiothreitol (Thermo Fisher Scientific, ref R0861). For non-reducing gels, sample buffers were prepared without either supplemented reducing agent. Samples were compared to 7 µL per gel of PageRuler™ Plus Prestained Protein Ladder (Thermo Fisher Scientific, ref 26619) loaded alongside.

2.11.2 Coomassie staining

Once gel electrophoresis was complete, PAGE gels were removed and mixed with 5 mL of InstantBlue® Coomassie Protein Stain (Abcam, Cambridge, UK, ref ab119211). Gels were left to stain for 2 h-overnight atop a benchtop orbital shaker (60 rpm), thoroughly washed with dH_2O once the staining period was complete, then imaged using a BioRad GelDoc Go Gel Imaging System equip with a White Sample Tray for GelDoc Go Gel Imaging System (BioRad, ref 12012165).

2.11.3 Western blotting

PAGE gels to be used for western blotting, following electrophoresis, were taken forward for transfer. A semi-dry transfer protocol was used, utilising the Trans-Blot® Turbo™ Transfer System (BioRad, ref 1704150). Transfer buffer was prepared from 100 mL 10x Tris/Glycine Buffer (BioRad, ref 1610734), 200 mL 99.8% methanol (Thermo Fisher Scientific, ref 10285131), and 700 mL dH_2, mixed and diluted 1/10 (v/v) of dH_2O. 0.83 mm thick blotting paper (Thermo Fisher Scientific, ref 84783) was pre-soaked in transfer buffer. 0.45 µm polyvinylidene fluoride (PVDF) transfer membrane (Thermo Fisher Scientific, ref 88518) was activated for 1 min in 99.8% methanol before being washed and pre-soaked in transfer buffer. Transfer stacks were then assembled, layering the activated PVDF and PAGE gel between the blotting paper (**Figure 2.1**).



Figure 2.1: Western blotting transfer stack set up. Proteins were transferred from the gel onto a PVDF membrane at 0.6 A in transfer buffer. Polyvinylidene fluoride membrane was first activated using 99.9% methanol. Filter paper and membrane were all pre-soaked in transfer buffer prior to transfer.

Following transfer, blots were blocked for 1 h at rt in 15 mL PBS supplemented with 5% (w/v) skimmed milk powder and 0.1% (v/v) Tween-20 (Merck, ref 9005-64-5). Once blocked, blotted proteins were screened for using antibodies as probes, on a benchtop roller. Western blotting was used to assess several proteins throughout this project, antibodies used are detailed in **Table 2.11.**

Antibody	Target	Purpose	Protocol
Mouse IgG1 monoclonal (BioRad, ref MCA1396)	Hexahistidine tag	Screening for recombinant glycoproteins	1 µg/mL diluted v/v in PBS (5% milk, 0.1% Tween20) at 4 °C overnight
Goat IgG-HRP cross-adsorbed polyclonal (Thermo Fisher Scientific, ref A16072)	Mouse IgG H+L	Secondary antibody for screening recombinant glycoproteins, to enable chemiluminescent development of blots	0.2 µg/mL diluted v/v in PBS (5% milk, 0.1% Tween20) for 1 hour at room temperature
Streptavidin-HRP (Thermo Fisher Scientific, ref N100)	Biotin	Assessing biotinylation of recombinant glycoproteins	1.25 µg/mL diluted v/v in PBS (5% milk, 0.1% Tween20) at 4 °C overnight
Goat IgG-HRP polyclonal (Abcam, ref ab6915)	Pig IgG H+L	Screening for recombinant mAbs	0.4 µg/mL diluted v/v in PBS (5% milk, 0.1% Tween20) at 4 °C overnight
Mouse mAb (Clone HyP10-C40-C1) provided by Dr Barbara Klupp, Friedrich-Loeffler-Institut, Isle of Riems, Germany	PRRSV-1 GP3	Assessing additional bands observed following purification of recombinant GP3	1 µg/mL diluted v/v in PBS (5% milk, 0.1% Tween20) at 4 °C overnight

Table 2.11: List of antibodies used for western blot analysis of proteins used throughout this project. All antibodies were titrated to determine optimal dilution before use.

Blots were washed for three 5-min intervals in PBS supplemented with 0.1% Tween20 between every step. Blots were developed with 3 mL Pierce™ ECL Plus Western Blotting Substrate (Thermo Fisher Scientific, ref 32106). Blots were imaged first by bright field to capture the protein ladder, then chemiluminescence was imaged, both using a BioRad GelDoc Go Gel Imaging System. Exposure time varied for each antibody, ranging from seconds up to 10 min. Images were merged later for analysis.

2.11.4 Deglycosylation

Deglycosylation of proteins was performed by PNGase F digestion (New England BioLabs, ref P0704) of N-glycan chains. Typical reaction conditions and protocol was followed according to the manufacturer's recommendations, mixing 100 µL of protein with 1 µL of PNGase F, 2 µL 10X GlycoBuffer 2 (New England BioLabs, ref B3704SVIAL), 2 µL 10% NP-40 (New England BioLabs, ref B2704SVIAL) and up to 6 µL dH_2O. Samples undergoing denaturing conditions were first heated for 10 min at 100 °C, then incubated for 2 h at 37 °C followed by analysis. Products undergoing non-denaturing conditions were not initially heated, and instead incubated for 24 h at 37 °C, followed by analysis. Products were assessed by western blotting.

2.12 Protein purification by affinity chromatography

2.12.1 Purification of the recombinant glycoproteins with a hexahistidine tag

300 mL transfected Expi293F cell cultures were used as standard for recombinant GP purification. Protein from clarified culture supernatants (as detailed in **Section 2.8**) was purified using immobilised metal affinity chromatography (IMAC), through use of HisTrap HP His tag protein Ni-NTA resin purification columns (Cytiva, ref 17524801) and the ÄKTA Pure Protein Purification System (Cytiva). Buffers for purification were prepared in-house using the following reagents: imidazole powder (Merck, ref S56750), sodium chloride (Merck, ref 1.06404.100), sodium phosphate dibasic (Merck, ref S7907-

500G), sodium phosphate monobasic (Merck S5011-100G), and sterile filtered through Nalgene™ PES MF75 75 mm × 0.2 µm × 500 mL Bottle Top Filters (Thermo Fisher Scientific, ref 167-0045). pH and conductivity of all buffers was measured using a SevenCompact Duo pH/Conductivity Meter (Mettler-Toledo, Ohio, USA, ref S213-Kit).

Prior to loading, supernatants were adjusted to 0.5 M sodium chloride and 30 mM imidazole by addition of 8x Phosphate Buffer (4 M sodium chloride, 0.16 M sodium phosphate pH 7.5) and 2 M imidazole solution. Samples were mixed and conductivity monitored, 8x Phosphate buffer was added until conductivity was the same as the equilibration buffer (30 mM imidazole, 20 mM sodium phosphate pH7.5) ± 1 mS/cm, typically 42-44 mS/cm. 1 mL Aliquots of pre-load samples were taken for controls for subsequent western blot analysis. Samples were loaded onto the Ni-NTA resin purification column and eluted into either 2.5 mL, 5 mL, or 10 mL fractions with elution buffer (20 mM sodium phosphate pH 7.5) ranging from 50 mM – 0.2 M imidazole as required. Columns were stripped using strip buffer (0.5 M imidazole, 20 mM sodium phosphate pH 7.5) into a final 15 mL fraction. Flow through was also collected throughout for subsequent western blot analysis.

Following western blot analysis, select fractions were taken forward for concentration and buffer exchange using Amicon® Pro Purification System with 10 kDa Amicon® Ultra-0.5 Device (Merck, ref ACS501024), in accordance with the manufacturer's specifications. Samples underwent three rounds of buffer exchange, suspended in a final 10 mM sodium chloride solution.

2.12.2 Purification of recombinant monoclonal antibodies with protein G

100 mL transfected Expi293F cell cultures were used as standard for recombinant mAb purification. mAbs from clarified supernatants (as detailed in **Section 2.8**) were purified using HiTrap Protein G HP (Cytiva, ref 17040501) utilising the ÄKTA Pure Protein Purification System (Cytiva). Buffers for purification were prepared in-house using the following reagents: Sodium chloride (Merck, ref 1.06404.100), sodium hydroxide (Thermo Fisher Scientific, ref J/7800/15), glycine (75.07 g/mol) (VWR International, ref 101194M), PBS and sterile filtered as detailed in **Section 2.12.1**. PBS was used as wash/equilibration buffer and so no pH/conductivity adjustment was required. Supernatants were loaded onto the protein G columns and eluted into 5 mL fractions using elution buffer (0.1 M glycine-HCl pH 2.7). Columns were stripped into a final 15 mL fraction using strip buffer (0.1 M glycine-HCl pH 2.3). Immediately following elution, eluate pH was neutralised with a minimum of 1/10 v/v of 1 M TRIS pH 8.0 to prevent denaturation of the mAbs. Following western blot analysis, fractions were dialysed for buffer exchange using 5-15 mL Slide-A-Lyzer 10K G2 dialysis cassettes (Thermo Fisher Scientific, ref 87731) overnight at 4 °C in accordance with the manufacturer's specifications. Samples underwent two rounds of buffer exchange, suspended in a final PBS solution.

2.12.3 Quantification of purified proteins

Protein concentrations were determined using a Pierce™ BCA Protein Assay Kit (Thermo Fisher Scientific, ref 23225) in accordance with the manufacturer's specifications. A minimum of three technical replicates were used in all instances. Standard curves were calculated based on known concentrations of BSA, and

concentration of samples interpolated using GraphPad Prism v9.3.1 (GraphPad Software Inc., La Jolla, USA). For recombinant mAbs, in addition to BCA assay, concentrations were calculated based on the A280 of the eluate using a Multiskan GO spectrophotometer (Thermo Fisher Scientific, ref PIP16079). UV280 nm with a 1 cm pathlength was divided by an extinction coefficient of 1.4 to give an estimation of IgG concentration in mg/mL Concentrations given by the two methods were compared.

2.13 Generation of recombinant monoclonal antibodies

Methods for reverse transcription of RNA and nested PCR of porcine IgG, Igκ, and Igλ genes, in addition to primers, were all provided by Dr Marie Di Placido, the Immunogenetics Group/Immunological Toolbox at The Pirbright Institute. This workflow was designed to enable amplification using a universal forward primer against a conserved region of the V gene segment, and complimentary reverse primer specific for each isotype's C gene segment (**Figure 2.2**)

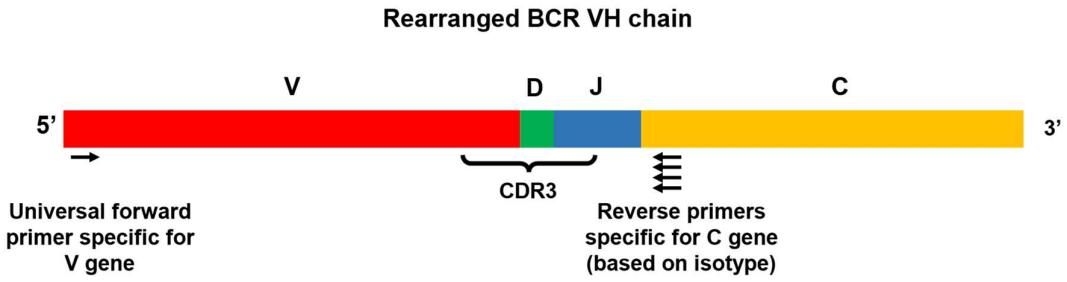


Figure 2.2: Schematic demonstrating primer design enabling amplification of VH and VL antibody chain genes from isolated single cells.

2.13.1 Generation of cDNA

Total RNA from single cells isolated by flow cytometric cell sorting was reverse transcribed in a final volume of 20 µL (**Table 2.12**) for 1 h at 37 °C using a

Sensiscript® Reverse Transcription Kit (Qiagen, ref 205213), in accordance with the manufacturer's protocol. To comply with biosecurity protocols of The Pirbright Institute's biocontainment facility, samples were further heated to 56 °C for 1 h, followed immediately by 95 °C for 5 min.

Component	Final concentration
Nuclease-free H_20	-
10x Buffer RT (Qiagen, ref205213)	1x
5 mM dNTP mix (Qiagen, ref205213)	0.5 mM each dNTP
RNAsin® Ribonuclease Inhibitor (Promega, ref N2115)	125U
Oligo d(T)23 VN (New England Biolabs, ref S1327S)	1 µM
Random Primer 9 (New England Biolabs, ref S1254S)	1 µM
Sensiscript® Reverse Transcriptase (Qiagen, ref205213)	
Template RNA	<50 ng (per reaction)

Table 2.12: Reverse transcription mixture used to generate cDNA from isolated single cells.

Following reverse transcription, each sample was taken through a reference gene PCR, testing for glyceraldehyde-3-phosphate dehydrogenase (GAPDH) amplification. Primers *Sus scrofa* (ss)GAPDH_F: ACCCAGAAGACTGTGGATGG and ssGAPDH_R: ACGCCTGCTTCACCACCTTC, kindly provided by Dr. Kristel Ramirez, The Pirbright Institute, were used. Amplification mixture (**Table 2.13**) and thermocycler program (**Table 2.14**) are detailed.

Component	Final concentration
5x HotStart Taq Reaction Buffer (NEB, ref B9014S)	1x
10 µM Forward Primer	100nM
10 µM Reverse Primer	100nM
10 mM dNTPs (Thermo Fischer Scientific, ref 18427013)	0.25 mM
Nuclease-Free Water	-
Hot Start Taq DNA Polymerase (NEB, ref M0495S)	0.02 U/µl
Template cDNA	< 1,000 ng

Table 2.13: PCR mixture for the amplification of glyceraldehyde-3-phosphate dehydrogenase (GAPDH) as a reference gene for assessing cDNA quality. Template cDNA was generated from isolated single B cells.

Stage	Temperature/Time	Number of cycles
1	95 °C for 15 minutes	1
2	94 °C for 30 seconds	40
3	55 °C for 30 seconds	
4	72 °C for 45 seconds	
5	72 °C for 10 minutes	1
6	4 °C hold	∞

Table 2.14: PCR thermocycler program for the amplification of glyceraldehyde-3-phosphate dehydrogenase (GAPDH) as a reference gene for assessing cDNA quality.

2.13.2 Semi-nested PCR amplification of VH and VL genes

Variable regions of the IgG heavy chain (HC) locus, lambda (LCλ) or kappa (LCκ) light chain loci were next amplified separately from each single cell cDNA by two rounds of nested PCRs. The first round of PCR was performed on 4 µL cDNA in a 25 µL reaction volume containing 1x Q5® reaction buffer (NEB, ref B9027S), 1x Q5® High GC Enhancer (NEB, ref B9028A), 0.25 mM dNTPs (Thermo Fischer Scientific, ref 18427013), 0.02 U/µL Q5® High-Fidelity DNA Polymerase (NEB, ref M0491S), nuclease-free H_20, and 100nM of primers (see **Appendix Table 1**

for primer sequences), amplification used the following protocol: 98 °C for 30s, 25 cycles of 98 °C for 10s, 64 °C for 20s, and 72 °C for 20s, followed by a final elongation step at 72 °C for 2 min.

Products from the first round were then diluted 1:10 in nuclease-free dH_2O and further amplification was performed on 1 µL diluted product, in a 25 µL reaction volume containing the same contents as described above, though with different primers (see **Appendix Table 1** for primer sequences). Amplification used the following protocol: 98 °C for 30s, 5 cycles of 98 °C for 10s, 65 °C for 20s, 72 °C for 15s, then 25 cycles of 98 °C 10s, 68 °C for 20s, 72 °C for 15s, followed by a final elongation step at 72 °C for 2 min. PCR products from each single cell were then run and imaged on a 1% agarose gel, as described in **Section 2.3**. Following imaging, products were taken forward for Sanger sequencing, as described in **Section 2.5.**

2.13.3 Sequence annotation by IMGT and mAb design

Following sequencing of VH and VL amplicons, the international ImMunoGeneTics information system (IMGT®) [244-246] was used to annotate each sequence, enabling identification of each V-, V-J-, or V-D-J region, identification of complementarity-determining regions, and determining which germline gene and allele the sequences were closest in identity to. Based on these annotations, sequences were either submitted for bioinformatics analysis (in the case of the whole antibody repertoire analysis, detailed in **Section 2.18**), or generated as synthetic genes from Twist Bioscience (Twist Bioscience, California, USA). Sequences taken forward for cloning were trimmed to enable

cloning into the pNeoSec-suite of vectors: pNeoSec_SsVL_kappa, pNeoSec_SsVL_lambda, pNeoSec_SsFc_IgG1, provided by the Immunological Toolbox at The Pirbright Institute, for the VL and VH sequences respectively. Sequences starting at the 5' end of the Framework Region 1 (FR1) motif and ending with a small portion of the C terminus of the constant region with the appropriate overhangs for cloning were generated.

Cloning of these synthetic genes followed methods detailed in **Section 2.6** with amplified VH and VL sequences being cloned into. Cloning was confirmed by colony PCR and Sanger sequencing as described above. Paired VH and VL-expressing constructs were transfected into Expi293F cells following methods detailed in **Section 2.8**. Expression was assessed by western blotting (**Section 2.11**) and ELISA (**Section 2.14**).

2.14 Enzyme-Linked Immunosorbent Assays

All ELISA results presented were measured at an absorbance of 450nm, with an additional reading at 595nm being recorded and subtracted to account for background.

2.14.1 Recombinant PRRSV glycoprotein ELISAs

Purified recombinant GPs (detailed in **Sections 2.1** and **2.12**) were used to assess binding by serum or mAbs. A coating GP concentration of 100 ng/well was found to be optimal for this protocol. For all GP ELISAs, recombinant SARS-CoV-2 spike protein RBD, provided by the Viral Glycoprotein Group, The Pirbright Institute, was used as a negative control. All final ELISA results presented have

had the optical density (OD) values from RBD-coated wells subtracted from the ODs from GP-coated wells to account for background from non-specific binding.

Clear flat-bottom nonsterile 96-well MaxiSorp plates (Thermo Fisher Scientific, ref 442404) were coated with 100 ng/well of protein diluted in 100 µL /well of carbonate-bicarbonate coating buffer, 0.6 M, pH 9.6 (Merck, ref SRE0102) and incubated at 4 °C overnight. On the following day coating buffer was removed, plates blocked with PBS supplemented with 5% w/v of skimmed milk powder for 2 h at 37 °C, then washed three time with PBS supplemented with 0.05% Tween-20. 50 µL/well of serum/mAb, diluted in PBS supplemented with 2.5% w/v of skimmed milk powder, was added, and incubated for 1 h at 37 °C. Plates were washed five times, before the addition of 100 µL/well goat anti-porcine IgG-HRP polyclonal antibody (Abcam, ref ab6915), diluted 1/10,000 (v/v) in PBS supplemented with 5% w/v of skimmed milk powder, incubated for 1 h at 37 °C. Following five additional washes, 50 µL/well of 3,3′,5,5′-Tetramethylbenzidine (TMB) Liquid Substrate System for ELISA (Merck, ref T0440) was added and left at rt for 5-10 min until colour change was observed. After which 50 µL/well of 1 M sulfuric acid solution (Thermo Fisher Scientific, ref 15644920) was added to stop the reaction. Absorbance was read on an Agilent BioTek ELx808 Absorbance Microplate Reader (Agilent Technologies, California, USA) or GloMax® Discover Microplate Reader (Promega).

2.14.2 IgG ELISAs

Total IgG in supernatant from Expi293F cells transfected to express recombinant mAbs, was measured using a Pig IgG ELISA Kit (Bethly Laboratories Inc., USA,

ref E101-104). Methods were followed in accordance with the manufacturer's specifications. Absorbance was measured as detailed above (**Section 2.14.1**). A standard curve was calculated, based on the dilution series of a standard of known concentration. IgG concentrations were interpolated using GraphPad Prism v9.3.1.

2.14.3 Peptide library screening

Overlapping biotinylated peptides, 16mers offset by 4 AAs, representing the ectodomain sequence of PRRSV-1 Olot/91 GP3 were generated by Mimotopes (MIMOTOPES Pty Ltd, Victoria, Australia). Full list of peptide sequences is detailed in **Appendix Table 2.**

MaxiSorp 96-well plates were coated with 100 µL of Neutravidin Protein (Thermo Fisher Scientific, ref 31000) at 500 ng/well diluted in carbonate-bicarbonate coating buffer, 0.6 M, pH 9.6 (Merck, ref C3041) and incubated at 4 °C overnight. The following day, the coating solution was removed, and plates washed with PBS supplemented with 0.2% Tween-20. Plates were blocked with 200 µL/well of PBS supplemented with 2% (w/v) skimmed milk powder for 1.5 h at 37 °C, followed by three washes. Peptides were diluted to a final concentration of 2.5 µg/mL in PBS supplemented with 1% (v/v) BSA (dilution buffer) and 100 µL were added to each well on the respective plates before incubation at 2 h at rt on a rocking table. Plates were washed three times and 50 µL/well of sera/mAbs tested, diluted in dilution buffer, were added and plates incubated at rt for 1 h. Plates were washed three times before 100 µL/well goat anti-porcine IgG-HRP polyclonal antibody (Abcam, ref ab6915), diluted 1/30,000 in dilution buffer, was

added and incubated for 30 min at rt. Plates were washed three final times before the addition of TMB Liquid Substrate (Merck, ref T0440) followed by 1 M sulfuric acid, as described in **Section 2.14.1**. Absorbance was read as detailed above.

2.14.4 Interferon gamma ELISpot assay

Multiscreen 96-wells filtration plates (Merck, ref MAIPS4510) were activated one day prior to each assay with 15 µL of 35% (v/v) ethanol per well for 1 min at rt. Wells were rinsed with 150 µL of sterile PBS three times and coated with 50 µL/well of mouse anti-porcine IFN gamma monoclonal (BD Pharmingen, ref 559961) diluted 1:500 in PBS. Following coating plates were incubated at 4 °C for 12-16 h. Wells were washed three times with 150 µL of sterile PBS, followed by a blocking step of 150 µL/well of RPMI 1640 Medium (supplemented with 10% FBS and 1% Penicillin-Streptomycin) and incubation at 37 °C, 5% CO_2 for 1h. Blocking solution was removed, and 2.5 × 10^5 freshly isolated porcine PBMCs were added per well. 50 µL of stimuli, 2 µg/mL of PRRSV GP3 peptides/RPMI 1640 Medium (negative control)/ 10 µg/mL of Concanavalin A (Merck, ref C5275) (positive control), were added in triplicate to the required wells and incubated for 18-20 h under normal cell culture conditions. Following incubation, wells were decanted, and cells lysed with 200 µL cold sterile dH_2O for 5 min at 4 °C, before being washed three times with PBS supplemented with 0.05% (v/v) Tween-20 (wash buffer). 50 µL of mouse anti-porcine IFN gamma-biotin monoclonal detection antibody (BD Pharmingen, ref 559958) was added per well, diluted 1:3000 in PBS supplemented with 0.05% (v/v) Tween-20 and 1% (v/v) FBS (incubation buffer), and plates were incubated for 1.5 h under normal cell culture

conditions. Wells were washed five times with 150 µL wash buffer followed by the addition of 50 µL of streptavidin-AP enzyme conjugate (R & D Systems, Minnesota, USA, ref SEL002-A), diluted 1:60 in incubation buffer, and incubation for 1.5 h at rt. Following three washes with wash buffer and three subsequent washes with PBS, 50 µL/well of BCIP/NBT ELISpot substrate (R & D Systems, ref SEL002-B) was added and incubated for 15-30 min at rt. Following spot development, reactions were stopped with 150 µL dH_2O, both sides of the membrane washed thoroughly with tap water, and plates dried at rt for 18-20 h. Once dried completely, plates were imaged and spots counted using a S6 FluoroCore™ M2 ImmunoSpot® Analyser (CTL Corporation, Oregon, USA).

2.15 Bio-layer interferometry

Bio-layer interferometry assays were performed using an Octet® R8 BLI Platform (Sartorius AG, Göttingen, Germany), to characterise recombinant mAb binding kinetics with recombinant GP3. Octet® Kinetics Buffer (Sartorius, ref 18-1105) was used to dilute all reagents, hydrate Ni-NTA biosensors (Sartorius, ref 18-5101) and establish baselines. Recombinant GP3 was loaded onto Ni-NTA Biosensors at 25 nM followed by 0.2% casein solution (Vector Labs, ref SP-5020-250), used to reduce non-specific binding, and an additional re-equilibration step in Kinetics Buffer. Each mAb was diluted to 125 nM for the association step, which was followed by the dissociation step. Step times are detailed in **Table 2.15**.

Step Number	Step Name	Reagents added	Step Time (seconds)
1	Baseline	Kinetics Buffer only	60.000
2	Loading	GP3	300.000
3	Baseline2 (block)	0.2 casein solution	300.000
4	Baseline3 (re-equilibration)	Kinetics Buffer only	300.000
5	Association	Recombinant mAbs	300.000
6	Dissociation	Kinetics Buffer only	300.000

Table 2.15: Summary of parameters for Octet® R8 platform bio-layer interferometry analysis. Standard parameters used for investigating kinetics between recombinant PRRSV-1 GP3 and recombinant mAbs.

Data were aligned to the association step, inter-step corrected to association and Savitsky Golay correction was applied. Data were fitted using a 1:1 stoichiometry model and R2 values > 0.98 were achieved. Data analysis was conducted using the Octet Analysis Software v12.2.1.23.

2.16 PRRSV infection assays

2.16.1 Viruses

All PRRSV strains used were available as part of the PRRS Immunology Group's pre-existing stocks, unless indicated otherwise. The following viruses were used in the infection assays detailed in this section:

Species	Strain	Subtype
PRRSV-1	Olot/91	Subtype-1, MARC-145 cell-adapted, attenuated Spanish strain
	215-06	Subtype-1, UK field isolate
	SU1-Bel	Subtype-3, higher pathology Belarus isolate
PRRSV-2	VR-2332	Lineage 1, prototype PRRSV-2 strain (USA origin)

Table 2.16: List of PRRSV strains used for infection-based assays. PRRSV-1 strains were kindly provided by Dr Jean-Pierre Frossard, Animal and Plant Health Agency, UK. PRRSV-2 VR-2332 was purchased from ATCC.

PRRSV-1 Olot/91 was first isolated from stillborn piglets born from a PRRSV-infected sow in 1991 [247] and has been attenuated by repeated passage on MA104 and MARC-145 cells. PRRSV-1 Olot/91 was chosen as the representative subtype-1 strain for the majority of infection assays due to ease study: adaption for growth in MARC-145 cells enabled generation of high titres of virus, and low virulence enabled study by immunostaining without excessive cytopathic effect or cell death. PRRSV-1 215-06 and PRRSV-1 SU1-Bel were both isolated at the Animal and Plant Health Agency (APHA), UK, in 2013 [248, 249] and are non-cell culture adapted subtype-1 and subtype-3 strains, respectively. PRRSV-2 VR2332 was first isolated from gnotobiotic piglets following an epizootic of PRRS in 1992 [250].

2.16.2 Virus neutralisation test

One day prior to investigation, 1.5×10^4 cells/100 µL MARC-145 cells or 1.0×10^5 cells/100 µL PAMs were seeded into a 96-Well, Nunc™ MicroWell™ 96-Well, Nunclon Delta-Treated, Flat-Bottom Microplate (Thermo Fisher Scientific, ref 167008) and cultured under normal conditions for 18-24 h. Following incubation, a 3-fold or 5-fold dilution series of either mAbs or serum was prepared, mixing material with 400 median tissue culture infectious doses ($TCID_{50}$) of PRRSV. An additional 10-fold dilution series from 400 to 0.004 $TCID_{50}$/well of PRRSV was also included in each assay as a back titration control. Virus-serum/mAb mixtures were incubated for 1 h at 37 °C, after which 50 µL was added to each well of cultured cells, before incubating for 48-72 h under normal culture conditions. Cells were washed with PBS supplemented with 0.2% (v/v) Tween-20, followed by fixation with PBS supplemented with 2% (v/v) PFA and 0.1% (v/v) Triton-X100 for

10 min at rt. Cells were washed three times and blocked using PBS supplemented with 10% (v/v) normal goat serum (Abcam, ref ab7481) and 0.2% (v/v) Tween-20 for 30 min at rt. Following blocking, 50 µL/well of SDOW17-A (mouse IgG1 monoclonal specific to PRRSV nucleocapsid (RTI Laboratories Inc., Michigan, USA) diluted 1:4000 (v/v) in PBS supplemented with 0.2% (v/v) Tween-20 was added for 1 h at rt. Following an additional three washes, 50 µL/well of Goat anti-Mouse IgG (H+L) Cross-Adsorbed Secondary Antibody, Alexa Fluor™ 488 (Thermo Fisher Scientific, ref A-11001) diluted 1:500 in PBS supplemented with 0.2% Tween-20 was added for 30 min at 4 °C. Following a final three washes, fluorescent readout was measured using the Incucyte® SX5 Live-Cell Analysis System (Sartorius), using whole well analysis parameters.

2.16.3 Immunostaining of PRRSV infected cells

The immunostaining methods used closely mirror those detailed above in **Section 2.16.2**. Key differences are highlighted below:

One day prior to investigation, 1.5×10^4 cells/100 µL MARC-145 cells or 1.0×10^5 cells/100 µL were seeded into a 96-Well, Nunc™ MicroWell™ 96-Well, Nunclon Delta-Treated, Flat-Bottom Microplate (Thermo Fisher Scientific, ref 167008) and cultured under normal conditions for 18-24 h. Following incubation, cells were infected with 400-1000 $TCID_{50}$/well of PRRSV and incubated under normal culture conditions for 48-72 h. An additional 10-fold dilution series from 400 - 0.004 $TCID_{50}$/well of PRRSV was also included in each assay as a control, to enable back titration. Following incubation, washes, blocking and fixation (as above in **Section 2.16.2**), a 50 µL/well of a dilution series of recombinant mAbs,

ranging from 10,000 – 20 ng/mL were added for 1 h at rt. Cells were again washed and a Goat Anti-Porcine IgG(H+L)-Alexa Fluor 488 (Cambridge Biosciences, ref 6050-30) was added at 1:500 for 30 min at 4 °C. Following final washes, fluorescent readout was measured using the Incucyte® SX5 Live-Cell Analysis System (Sartorius) as detailed in **Section 2.16.2**.

2.17 Experimental PRRSV infection of pigs

2.17.1 Heterologous PRRSV challenge study

A sequential heterologous infection study was carried out previously using six 12-weeks-old, PRRSV naïve, Large White/Landrace cross, female pigs. Animals were inoculated intranasally and intramuscularly with 10^6 $TCID_{50}$ of PRRSV-1 Olot/91. The pigs were then sequentially challenged at 35-day intervals by similar inoculation with 10^5 $TCID_{50}$ of PRRSV-1 SU1-Bel (day 35), PRRSV-1 215-06 (day 70) and PRRSV-2 KS06-72109 (day 105). Pigs were finally challenged with 10^7 $TCID_{50}$ PRRSV-1 Olot/91 (day 140) and the study terminated 7 days later (day 147-148). Clinical signs and rectal temperatures were measured daily, and blood samples collected at weekly intervals. Serum samples were stored at −80 °C for subsequent analysis and heparinised blood used for isolation of PBMCs, which were cryopreserved in 10% (v/v) dimethyl sulfoxide (DMSO) (Thermo Fisher Scientific, ref 15572393) in FBS. Full details of this study have been published [251].

2.17.2 Olot/91 hyperimmune pigs

An experimental infection and challenge study was previously carried out using 12-week-old, PCV-2 free, PRRSV antibody-negative Large White/Landrace

cross-bred pigs. This experiment was designed to enable a comparison of T cell responses following primary infection to those boosted following secondary exposure. Animals were inoculated intranasally with 10^6 $TCID_{50}$ PRRSV-1 Olot/91 (n = 5) or 10^4 $TCID_{50}$ PRRSV-1 SU1-Bel (n = 5). Thirty-five days post-inoculation, pigs were challenged with increased doses of the homologous virus, 10^7 $TCID_{50}$ PRRSV-1 Olot/91 and 10^5 $TCID_{50}$ PRRSV-1 SU1-Bel. Animals were monitored for clinical scores and rectal temperatures and blood samples were collected at intervals from 2 dpi until the end of the study at 60 dpi. Heparinized blood was used for isolation of PBMCs, and serum samples were stored at −80 °C for subsequent analysis. Full details of this study have been published [252]. Serum from two pigs (pigs 71 and 86) repeatedly infected with PRRSV-1 Olot/91 were used in the present study.

2.17.3 Additional PRRSV infected and MLV vaccinated pigs

Serum samples from an additional study previously performed by the PRRS Immunology Group, The Pirbright Institute, were additionally used. These included sera from a commercial study comparing a novel MLV with a licensed MLV, this included sera from animals that were (i) vaccinated with MLV, (ii) vaccinated with MLV and challenged with PRRSV-1, and (iii) unvaccinated with PRRSV-1.

2.18 Immunogenicity study

Animal work was approved by The Pirbright Institute and University of Reading Animal Welfare and Ethical Review Bodies and conducted in accordance with the

UK Animals (Scientific Procedures) Act 1986. Ethical endpoints were in place and were not reached.

This was a pilot study that aimed to evaluate the immunogenicity of PRRSV-1 GP3 delivered by a self-amplifying (sa)RNA vector and benchmarking this against adjuvanted recombinant GP3 protein formulations. GP3 used for this study was generated as described in **Sections 2.1 and 2.12**. Ten 300 mL cultures were established, purified, and screened prior to vaccination. Nine, PRRSV naïve (confirmed by pre-screening of a blood sample collected on the supplier farm), piglets were randomly assigned (by weight) to three treatment groups (n=3) and taken through the 56-day study. A prime-boost vaccination regiment was followed (**Table 2.17**).

Group (n=3)	Day 0	Day 28	Day 58
Group 1: 100 µg GP3 adjuvanted with Montanide ISA 201 VG (provided by Dr Andra Corder, Seppic, France)	Prime	Boost	Termination
Group 2: 100 µg GP3 adjuvanted with CoPoP/PHAD/QS21 liposomes (provided by Dr Jonathan Lovell, University of Buffalo, USA)			
Group 3: 3 µg saRNA-GP3 in lipid nanoparticles (provided by Prof Robin Shattock, Imperial College London, UK).			

Table 2.17: GP3 immunogenicity study vaccination groups and timeline. Blood samples for serum and PBMC isolation were collected weekly and fortnightly, respectively.

Prior to vaccine formulation, recombinant GP3 was tested using a Pierce™ Chromogenic Endotoxin Quant Kit (Thermo Fisher Scientific, ref A39552) in accordance with the manufacturer's recommendations to ensure safe use for vaccination. Endotoxin concentrations were interpolated from a standard curve.

0.2 mg/mL recombinant GP3 was diluted to a total of 13.5 mL in sterile PBS and mixed with 16.5 mL of Montanide ISA 201 VG at 32 °C, for a total 45/55% (v/v) mixture. Emulsification was performed by sheer mixing using an Ultra Turrax® Tube Drive mixer (IKA-Werke, Staufen, Germany, ref 0003646000) for 3 min at 1100 rpm. Following mixing, formulation was stored at 4 °C for a minimum of 1 h.

CoPoP/3D(6-acyl)-PHAD®/QS-21 (CPQ) liposomes were prepared by mixing 2 mL of 0.2 mg/mL GP3 diluted in PBS and incubating for 3 h at rt. Prior to vaccination, incorporation of GP3 was assessed by Ni-NTA competition assay using His Pur Ni-NTA Magnetic Beads (Thermo Fisher Scientific, ref 88831). Ni-NTA beads were added to the assembled liposomes, incubated for 30 min at rt, then removed by magnetic separator (Thermo Fisher Scientific, ref 12321D). Samples were assessed by native-PAGE followed by Coomassie staining to detect presence of recombinant GP3. Presence of GP3 attached to the Ni-NTA beads was indicative of incomplete liposome assembly. This work was performed by Dr. Jane Edwards, The Pirbright Institute.

Lipid nanoparticles (LNP) carrying saRNA vector expressing membrane displayed GP3 (PRRSV-1 Olot/91 GP3 ectodomain fused to the Ebola virus glycoprotein transmembrane domain) were generated and provided by Dr. Kostas Paschos and Prof. Robin Shattock, Imperial College London.

Pigs were immunised twice, at an interval of 28 days, by intramuscular injection into the brachiocephalic muscle. To characterise immune responses, blood samples were collected by venipuncture of the external jugular vein into SST™ BD Vacutainer® Tubes every 7 days for isolation of serum and into BD

Vacutainer® Heparin Tubes every 14 days for PBMC isolation. After 56 days, animals were culled by a Schedule 1 method.

Following termination, material was assessed using several methods detailed throughout this chapter. GP3 protein and peptide library antibody ELISAs and IFN-γ ELISpot assays were performed as detailed in **Section 2.14**. Virus neutralisation tests (VNTs) were performed as detailed in **Section 2.16**.

2.18.2 Serum depletion experiments

Serum depletions were performed to assess the contribution of GP3-specific antibodies to neutralisation. For each experiment performed immune and naïve sera were depleted with GP3, SARS-CoV-2 spike protein RBD [243], or beads only to serve as a control.

Dynabeads™ his-tag isolation and pulldown magnetic beads (Thermo Fisher Scientific, ref 10104D) were prepared in accordance with the manufacturer's protocol. 10 µg of each recombinant protein, or an equal volume of PBS for the beads only, were mixed in a total volume of 700 µL of binding buffer: dH_2O supplemented with 100mM (w/v) sodium phosphate pH 8.0 (Thermo Fisher Scientific, ref J60825.AK), 600mM (w/v) sodium chloride (Merck, ref 1.06404.100), and 0.02% (v/v) Tween-20 (Merck, ref 9005-64-5) in a 1.5 mL reaction tube. 2mg of magnetic beads were added to the 700 µL sample mix and incubated at rt on a benchtop roller for 10 min. Following binding, the tubes were placed in a 12-tube magnetic separation rack (New England BioLabs, ref S1509S) for 5 min, and supernatant was carefully discarded by pipetting. Beads were resuspended in dH_2O at 1 mg beads/mL, and washed three times with PBS

supplemented with 0.05% BSA, using the magnets as described above. Following the final wash, beads were resuspended at 1 mg/mL in PBS supplemented with 0.05% BSA. Beads were incubated at a 3:1 v/v ratio with each serum tested, and incubated for 12-16 h at 4 °C on a benchtop roller. Following this incubation, tubes were placed back in the magnetic separation rack, and the protein-specific antibody depleted sera taken forward for analysis by ELISA or VNT.

2.19 Whole antibody repertoire analysis

2.19.1 Library generation

RNA was isolated from frozen whole blood collected in PAXgene blood RNA tubes (QIAGEN, ref 762165) as part of the study detailed in **Section 2.17.1**, using PAXgene Blood RNA Kit (QIAGEN, ref 762174) for extraction, following the manufacturer's recommendations. Reverse transcription, quality control, and amplification of VH and VL genes was performed using methods detailed in **Section 2.13**. Following PCR III, amplicons were purified using a GFX PCR DNA and Gel Band Purification Kit as detailed in **Section 2.4**. Purified products were taken through an additional PCR stage to add NEBNext® Multiplex Oligos for Illumina® - dual-index i7 and i5 primers (New England BioLabs, ref E7600S), enabling next-generation sequencing. A matrix of index primers was used to enable simultaneous sequencing, following pooling of samples (**Table 2.18**). Primer sequences are also detailed in **Appendix Table 3**.

		Donor animal					
		Pig 60	**Pig 62**	**Pig 63**	**Pig 64**	**Pig 67**	**Pig 69**
Timepoint	**0 dpi**	i7_701 i5_S502	i7_702 i5_S502	i7_703 i5_S502	i7_704 i5_S502	i7_705 i5_S502	i7_706 i5_S502
	42 dpi	i7_701 i5_S503	i7_702 i5_S503	i7_703 i5_S503	i7_704 i5_S503	i7_705 i5_S503	i7_706 i5_S503
	78 dpi	i7_701 i5_S505	i7_702 i5_S505	i7_703 i5_S505	i7_704 i5_S505	i7_705 i5_S505	i7_706 i5_S505
	112 dpi	i7_701 i5_S506	i7_702 i5_S506	i7_703 i5_S506	i7_704 i5_S506	i7_705 i5_S506	i7_706 i5_S506
	148 dpi	i7_701 i5_S507	i7_702 i5_S507	i7_703 i5_S507	i7_704 i5_S507	i7_705 i5_S507	i7_706 5_S507

Table 2.18: Matrix of Illumina primers used for index addition for sequencing of a whole antibody repertoire library. Six animals, from five timepoints along a heterologous PRRSV challenge study are represented Following 0 dpi, each timepoint represents one-week post-challenge.

2.19.2 Sequencing

Indexed samples were submitted to Dr. Graham Freimanis and Dr. Noemi Polo, Bioinformatics, Sequencing & Proteomics Facility, The Pirbright Institute, and taken forward for library construction and sequencing using an Illumina MiSeq System (Illumina, California, USA). Resulting data was passed on to the bioinformatics team.

2.19.3 Bioinformatics

Bioinformatic analysis of these data were performed in collaboration with Dr. Mike Jarman as well as Dr. Marie Di Placido of the Immunogenetics Group at The Pirbright Institute. Full AA sequences were further clustered together using an AA identity rate of 97% using UCLUST v11.0.667 [253] and clusters were extracted for further processing. Single chains per cell were determined by

dominant clusters encompassing over 90% of the UCLUST input sequences. Where multiple dominant clusters were present, each dominant clusters' centroid was assigned as that sample's sequence. AA sequences determined from the single B cells isolated by flow cytometric cell sorting were also included in this analysis.

2.20 Analysis

2.20.1 Image capture and analysis

Confocal images were viewed and overlaid using Leica Application Suite X software (LAS-X). Agarose gels, PAGE gels, and western blots were imaged using Image Lab version 5.2.1 software (BioRad).

2.20.2 Sequence analysis

Nucleotide sequences obtained were analysed using a standard nucleotide basic local alignment search tool (BLAST). To analyse protein sequence, sequences were first translated in 3 reading frames using ExPASy translate tool software, the correct in frame sequence was then analysed using a standard protein BLAST. Sequence alignments, analysis, and pairing of VH-VL chains was performed using MEGA11: Molecular Evolutionary Genetics Analysis version 11.0.9 [254].

2.20.3 Statistics and Analysis software

Statistical analysis was performed using GraphPad Prism v9.3.1 (GraphPad Software, Inc., La Jolla, USA). ANOVA (Kruskal–Wallis) with Tukey's multiple comparisons, and Dunn's multiple comparisons tests were performed. Additional

statistical tests used for each comparison are indicated in the Results chapters. All flow cytometry data was analysed using FlowJo™ versions 6 - 10.8.1 Software (BD Life Sciences) (FlowJo™ Software for Windows, Version 10.8.1. Becton, Dickinson and Company). Biosensor Kinetic Assays were analysed using the Octet Analysis Studio software, version 12.2.1.23 (Sartorius AG, Göttingen, Germany).

Chapter 3. Cloning and expression of recombinant PRRSV-1 GP2, GP3, and GP4

3.1 Rationale

PRRSV envelope glycoproteins are essential for viral entry and replication and have been demonstrated to be a major inducer of nAbs [124, 125, 129, 230].

The use of recombinant proteins as a method for isolating mAbs has also been well documented, being recently employed as part of the response against the SARS-CoV-2 pandemic [243, 255]; enabling isolation of antigen-specific B cells with a much shorter generation time than other methods such as phage display, and hybridoma generation. Further, tetramerisation of antigens has been proven a useful method for the identification and isolation of rare, low frequency B cell populations, enhancing the avidity of ligand binding [256]. Generation of biotinylated antigens, which can be tetramerised to a streptavidin molecule, is a common approach for tetramer assembly [256-258], and so was employed for this project. Chemical biotinylation, however, often results in heterogeneous products [256], which may result in inconsistent findings. Generating recombinant proteins fused with the 15 amino acid biotin acceptor peptide (BAP) tag peptide, and co-transfection of cells with plasmid encoding BirA ligase, is a reliable approach for site-specific in vitro biotinylation [259] and so was also employed for this project.

Generation of recombinant PRRSV glycoproteins, however, has historically proven challenging with the few published studies utilising prokaryotic or insect cell expression systems [70, 157, 260, 261] and epitope mapping studies limited to using linear peptides [174, 205, 220]. By using a mammalian expression

system, over insect or prokaryotic, the resulting proteins should have more authentic folding, glycosylation, and other post-translational modifications [262].

Despite their importance, key gaps exist in our knowledge of PRRSV glycoproteins. The minor envelope proteins, specifically, remain some of the least understood viral proteins, despite the promise they hold as targets for novel vaccine design [82, 128, 201]. It was decided that this project, therefore, would focus on the glycoproteins of the minor envelope complex of PRRSV-1.

3.2 Designing recombinant PRRSV glycoproteins

PRRSV-1 Olot/91 (GenBank Accession: KF203132) was chosen as the base to design recombinant GPs, in part due to having annotated genome sequence data [263], but also as it served as a representative PRRSV-1 subtype 1 strain. Investigating this subtype of PRRSV-1 was considered most relevant due to its predominance in Europe and circulation in Asia, North America, and Africa [17, 30]. Furthermore, PRRSV-1 Olot/91 was used as both the initial prime and final boost in the hyperimmunisation of animals to be utilised in this project [251], as detailed in **Chapter 2.17.**

Recombinant PRRSV GP design was informed two-fold: cross-referencing with available literature [216, 226], and utilising protein fold prediction software, such as Phyre2 [234] (**Figure 3.1A**). In addition to model prediction, Phyre2 provided signal peptide and TM domain prediction (**Figure 3.1B).**

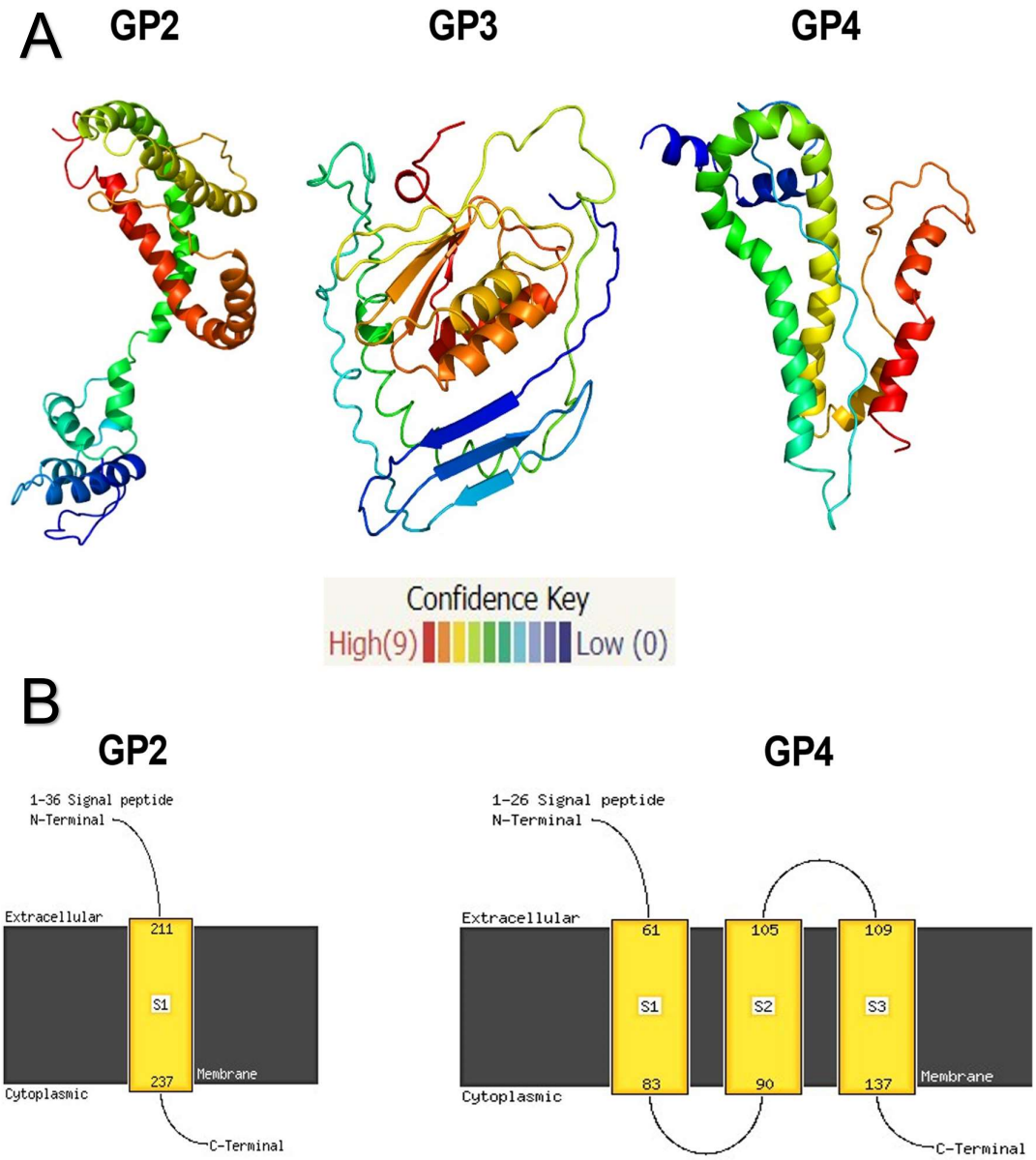


Figure 3.1. Protein folding was predicted by inputting amino acid sequences for PRRSV-1 Olot/91 glycoproteins GP2, GP3, and GP4 into Phyre2. Predicted structure was displayed as a final model (**A**), colour coded by a confidence key, and membrane topology was displayed as a cartoon (**B**). Topology could not be confidently predicted for GP3 and is therefore not included.

Phyre2 modelling resulted in low confidence models overall. Confidence in the models was 38%, 28%, and 41% for GP2, GP3, and GP4, respectively, and therefore much of the secondary structure was unable to be determined.

Modelling predicted a 36-residue signal peptide for GP2, and a 26-residue signal peptide for GP4, largely aligning with the literature [216]. It was also predicted that GP2 possessed a 26-residue TM domain, starting at residue 211; GP4 was predicted to possess three TM regions, 22, 15, and 28 residues starting at residues 61, 90, and 109, respectively. It has been described that GP2, GP3, and GP4 are single pass membrane proteins [226], however, the predictions made in Phyre2 conflict with this. Prediction confidence, furthermore, was also too low to predict the topology for GP3 and so overall these models were treated as highly speculative, and use of alternative software was explored.

A combination of SignalP 5.0 [235] and TMHMM – 2.0 [236] were employed to predict topology (**Table 3.1**).

Sequence	Signal peptide	Confidence	TM region	Confidence
GP2	1-37	0.756	205-227	0.976
GP3	1-26	0.968	182-195	0.828
GP4	1-21	0.952	158-179	0.721

Table 3.1: Signal peptide and transmembrane regions of each glycoprotein were predicted using SignalP 5.0 and TMHMM 2.0, respectively. The predicted residues for each are tabulated. Confidence scores, out of a maximum of 1.0, were assigned to each prediction.

The predictions generated utilising these tools aligned closer to what has been detailed in the literature [190, 226]. Each GP was predicted to possess a single TM region, 22 residues from amino acids 205-227 for GP2, 13 residues from amino acids 182-195 for GP3, and 21 residues from amino acids 158-179 for GP4. The signal peptide length either matched or was ±1-2 residues of what has been described the literature, and overall confidence levels were acceptable.

Based on these signal peptide and TM region predictions, sequences for each GP were trimmed removing either the TM region and endodomain, or, the TM region, endodomain and signal peptide. These trimmed sequences, in addition to the full length, were entered into AlphaFold [237] to investigate whether these truncated, ectodomain only forms were predicted to fold in a similar way to the native, full length, GPs (**Figure 3.2**).

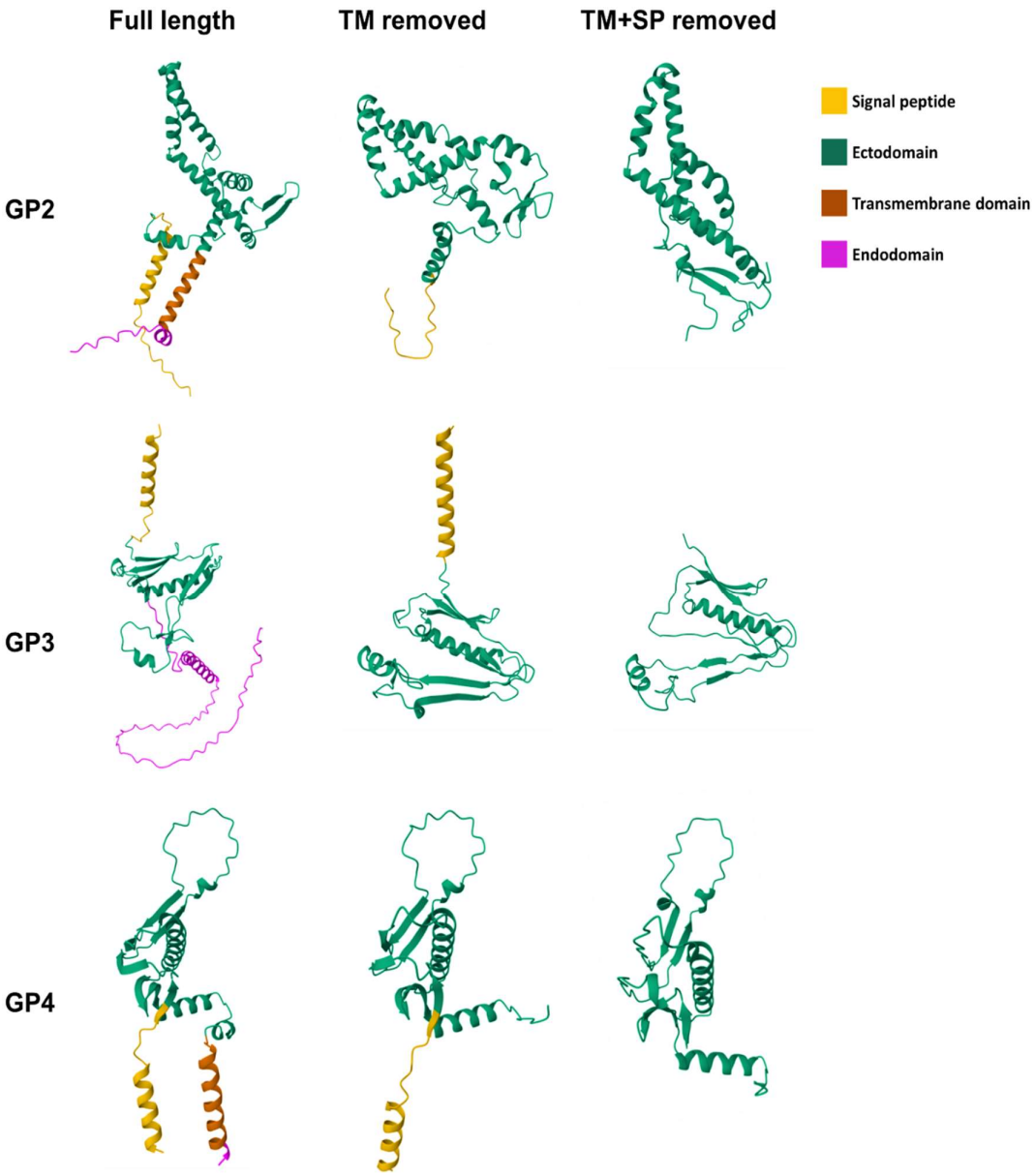


Figure 3.2: Protein folding was predicted by inputting the amino acid sequences for PRRSV-1 Olot/91 glycoproteins GP2, GP3, and GP4 into AlphaFold. Additionally, for each GP, sequences with the TM region onwards, and sequences with the TM and signal peptide regions removed were also modelled. n = 5 predictions were made per sequence, the highest ranked models are shown as cartoon representations. **Yellow** structures represent the predicted signal peptides, **green** represent the predicted ectodomain, **orange** represent the predicted transmembrane domains, and **pink** represent the predicted endodomains.

The overall pLDDT confidence scores were lowest for the predicted GP2 models, ranking 53.694%, 53.648%, and 54.353% for the full length; TM and

endodomains removed; and TM, endodomain, and SP removed sequences respectively. As a consequence of these low confidence scores, there was some considerable variation observed between the predicted models, with discrepancies in both folding, and predicitons of secondary structure. Corresponding average pLDDT score plots are detailed in **Appendix Figure 5**.

Despite much of the endodomain portion of the full length GP3 being modelled with low confidence, the overall pLDDT confidence score did not increase by more than 0.83% after removing the TM and endodomain in the second model. Confidence scores were 58.157%, 58.986% for the full length; TM and endodomains removed; and TM, endodomain, and SP removed sequences respectively. While residues 110-150 had high confidence scores (~80-90%), residues 35-100 were much more variable (~40-60%). Secondary structures appeared relatively similar between models.

GP4 had the highest overall confidence scores of the three GPs investigated, scoring 66.801%, 67.189%, and 68.148% for the full length, TM removed, and TM+SP removed sequences, respectively. Residues 50-70 scored very low (~40%), but otherwise confidence was ≥ 70% throughout, with the secondary structures in each model appearing largely homologous.

Regions with pLDDT between 50 and 70, however, are considered low confidence and should be treated with caution [264], and so the models for each GP were overlayed, to determine structural similarity between the trimmed sequences and the full length forms (**Figure 3.3**). The jFATCAT-rigid pairwise structure alignment algorithm was selected as it allowed for flexible protein

structure comparison, while only considering alignments with matching sequence order [265, 266]. The more stringent, rigid version of the algorithm was selected as it aligns the entire structure, without breaks, and resulted in fewer false positive matches.

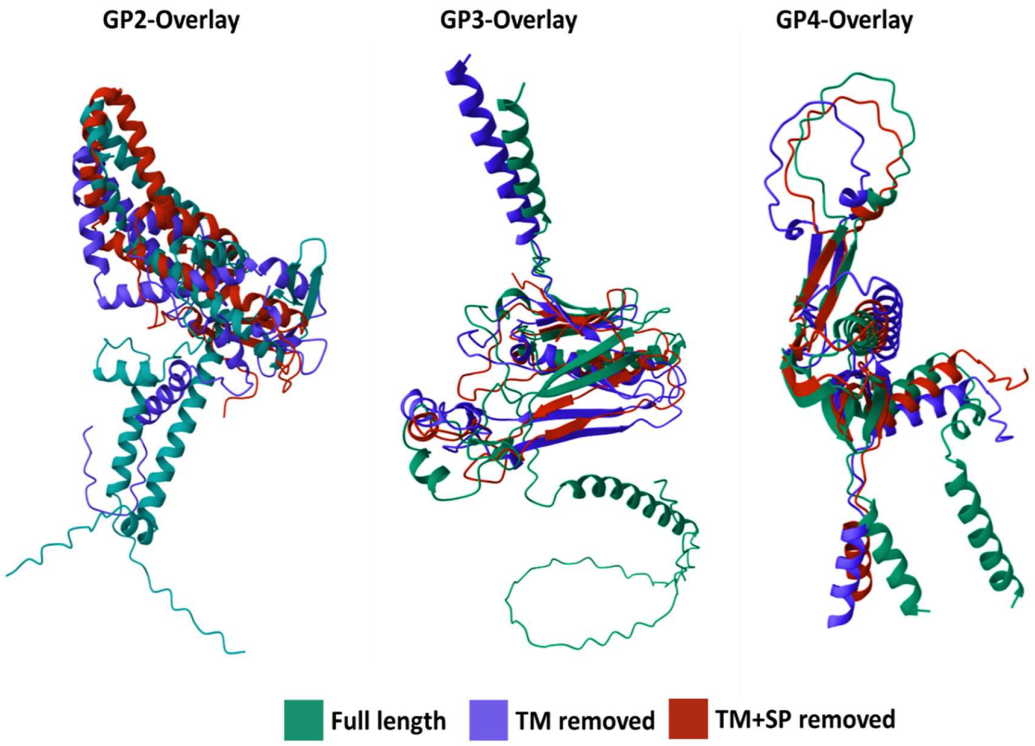


Figure 3.3: Overlayed model of PRRSV-1 Olot/91 glycoproteins GP2, GP3, and GP4 sequences with the transmembrane (TM) region onwards, and sequences with the TM and signal peptide (SP) regions removed were compared to the full-length version of each respective GP. Models were assigned aligned using the jFATCAT-rigid pairwise structure alignment algorithm.

Following alignment, each GP subset was given a root mean square deviation (RMSD) score. RMSD is one of the most commonly used parameters for the structural (dis)similarity between two conformations of a molecule; an RMSD value ≤ 3 angstroms (Å) is considered acceptable, 3-4 Å suggests differences in folding, and > 4 Å is considered poor. Mirroring the confidence data, GP4 demonstrated the highest homology between models, scoring 6.66 Å, and 3.36

Å for the full-length vs. TM removed, and full-length vs. TM+SP removed respectively. GP3 scored lower with 10.30 Å and 6.00 Å for the full-length vs. TM removed, and full-length vs. TM+SP removed respectively. GP2 scored the lowest, with 12.04 Å and 8.51 Å for the full-length vs. TM removed, and full-length vs. TM+SP removed respectively. These alignments overall suggested poor structural similarity between each GP and their respective subsets. Given the poor confidence score in the folding of these proteins, these results were interpreted cautiously. Use of alternative structure alignment algorithms, furthermore, such as Smith-Waterman 3D and jCE revealed dramatically different RMSD scores (data not shown).

Based on these data, multiple primer sets were designed (**Chapter 2.1**) with the aim of generating subsets of each glycoprotein based on the TM and signal peptide predictions from their respective full-length sequences (**Figure 3.4**). Genes were synthesised with human codon usage for expression in human embryonic kidney cell lines.

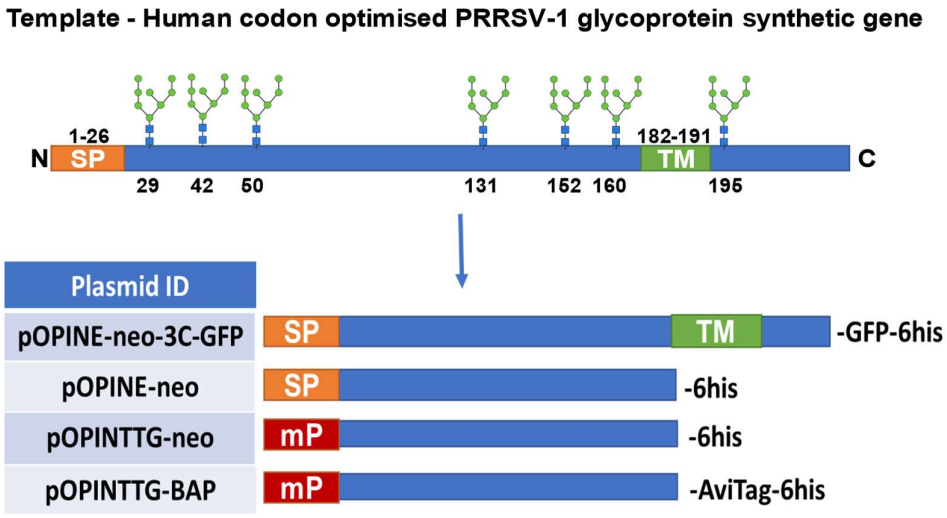


Figure 3.4: Cartoon depicting the design rationale for generating recombinant PRRSV glycoproteins. Gene fragments of each GP serve as the templates to produce a full-length sequence fused with a fluorescent protein (GFP in this example), and truncated sequences cut off at the transmembrane domain (TM). These truncated sequences were produced with either a native (SP) or receptor-type protein-tyrosine phosphatase μ (mP) leader sequence. All sequences include 5' and 3' sequence overhangs appropriate for cloning. GP3 is shown as a representative example.

Recombinant GP design was an iterative process, first starting with generation of a full-length GP fused to GFP. Using fluorescent protein fusions enabled assessment of expression by microscopy assays, and subsequent quantification by flow cytometry, crucial as immunolabelling was not a feasible option due to a lack of GP-specific antibodies.

3.3 Expression of full-length recombinant PRRSV glycoproteins

Expression was first investigated following transfection in HEK293T cells. A green fluorescent protein (GFP) control plasmid, containing no recombinant GP (rec-GP) insert, was used as a control for transfection conditions. Fluorescence was confirmed first by standard fluorescence microscopy imaging of live cells (data

not shown), and subsequently, in greater detail, by confocal microscopy (**Figure 3.5**)

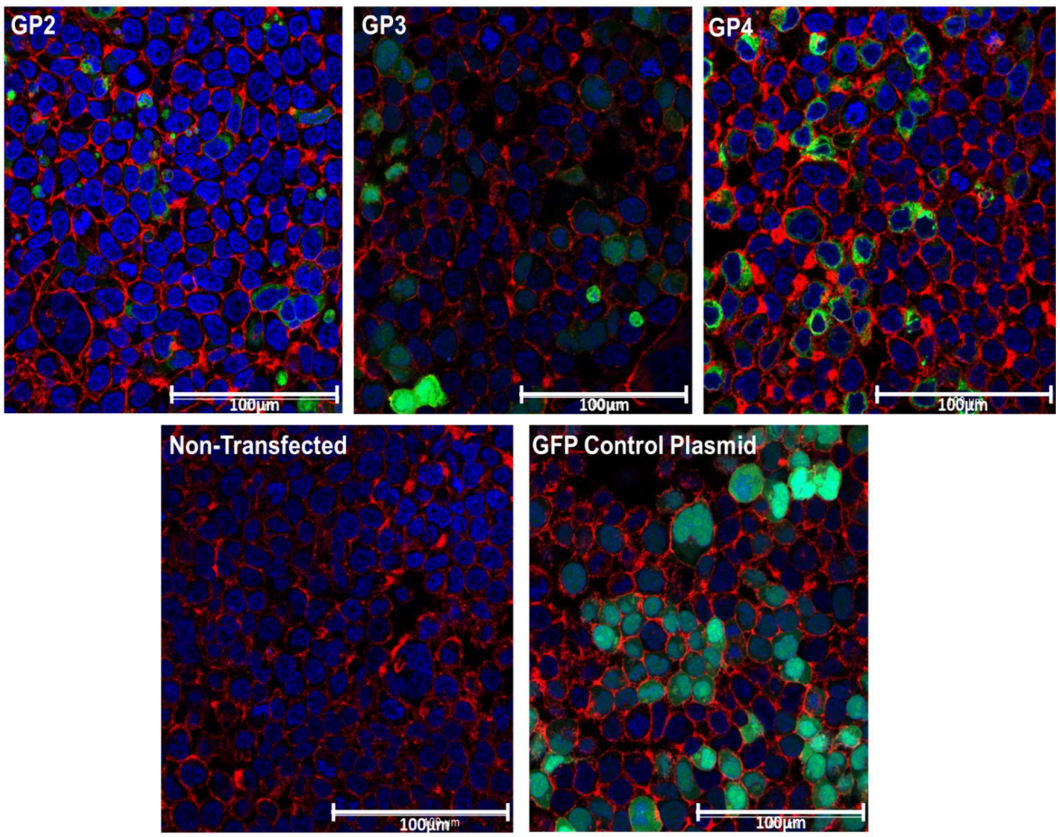


Figure 3.5. Expression of recombinant PRRSV-1 glycoproteins GP2, GP3, and GP4 fused to GFP in transiently transfected HEK293T cells was determined by confocal microscopy. Rec-GP expression was demonstrated by GFP expression (**green**), DAPI/nuclei staining (**blue**), and phalloidin/actin filaments (**red**). Scale bars are 100 µm.

It was observed that all three rec-GPs were expressed by transiently transfected HEK293T cells. To quantify transfection efficiency flow cytometric analysis was performed. A series of nine technical replicates for each rec-GP-GFP fusion were assessed (**Figure 3.6A, B**). Cells were transfected under the same conditions used for the initial microscopy experiments. Further, mean fluorescent intensity values (MFI) were extracted, enabling quantitative comparison in expression between the rec-GPs (**Figure 3.6C**).

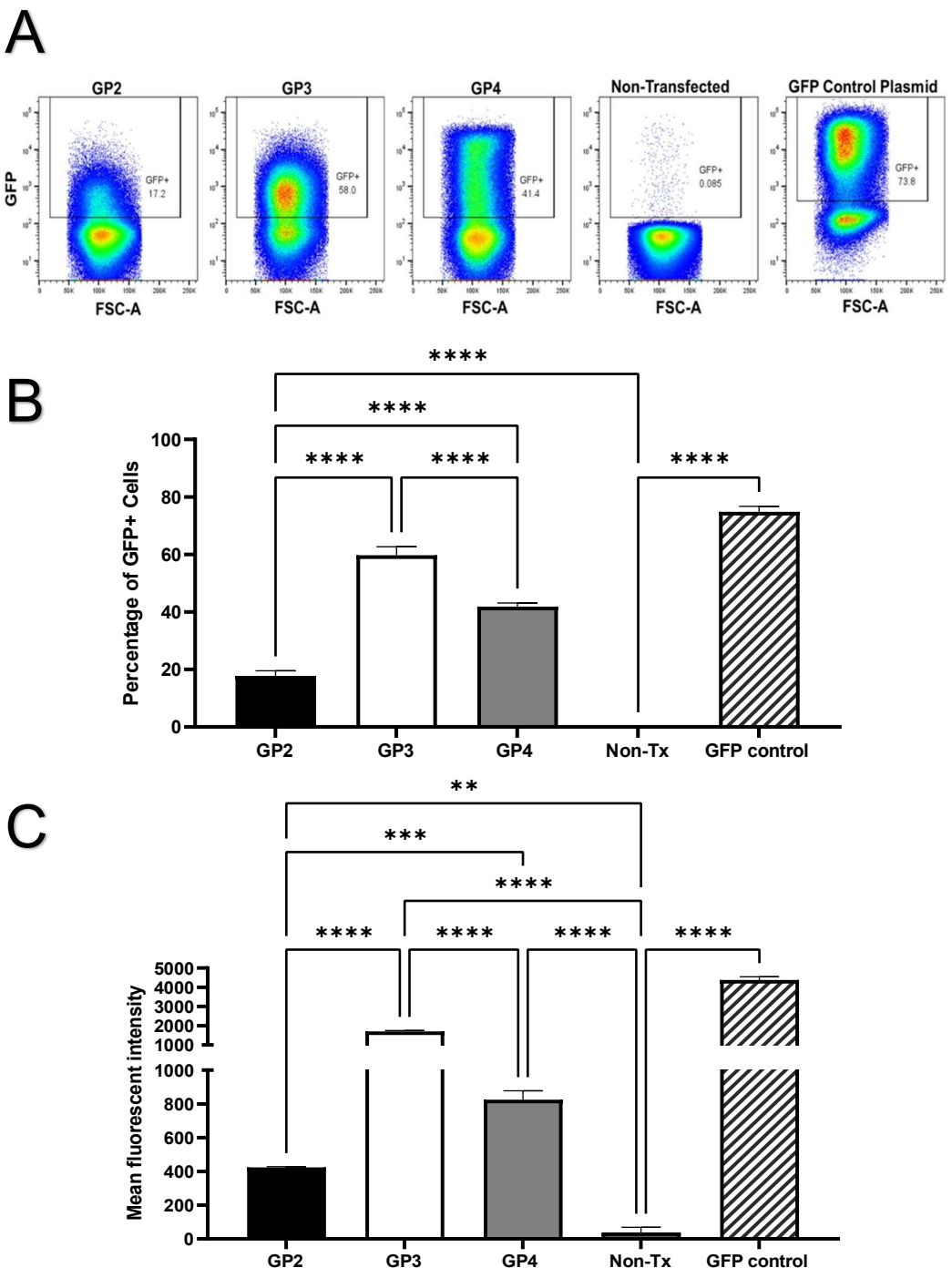


Figure 3.6: Expression of recombinant PRRSV-1 glycoproteins GP2, GP3, and GP4 in transiently transfected HEK293T cells was quantified by flow cytometry. Representative flow cytometry dot plots representing expression of each GFP-GP fusion compared to a GFP only control plasmid and non-transfected controls, are shown (**A**). Mean percentages of GFP$^+$ events, nine technical replicates ± SD, of the transfected cells are also shown (**B**) as well as mean fluorescent intensity of GFP$^+$ cells (**C**). **, ***, and **** represents a significance of P <0.01, P <0.001 and P <0.0001 respectively.

The average proportion of GFP^+ cells in the rec-GP2, GP3, and GP4 transfected samples were observed to be 17.78%, 59.68%, and 41.83%, respectively, compared to an average of 0% and 74.84% in the non-transfected and GFP-plasmid controls, respectively. Analysis by one-way ANOVA revealed a significant difference in proportion of GFP^+ events (adjusted *P* value <0.0001) between all three rec-GP transfection conditions. Significantly more rec-GP3-GFP^+ events were observed than rec-GP2 and GP4. The proportion of rec-GP4-GFP^+ events, in turn, was significantly greater than rec-GP2. Extraction of the MFI values for the rec-GP transfected cells demonstrated a similar trend. Analysis by one-way ANOVA revealed that the expression of rec-GP3 was significantly higher than rec-GP2 and rec-GP4 (adjusted *P* value <0.0001). Significantly higher expression of rec-GP4, similarly, was observed compared to rec-GP2 (adjusted *P* value =0.001).

Expression of the rec-GPs was investigated further, with the aim of assessing co-expression within transfected cells. To this end, additional fluorescent fusions were generated: GP2-mCherry, and GP3-yellow fluorescent protein (YFP), to use in conjunction with the previous GP4-GFP. HEK293T cells were transiently transfected with single (**Figure 3.7A-C**), paired, or with all three rec-GPs (**Figure 3.7D**), and assessed by fluorescence microscopy. Utilising the Incucyte® SX5 Live-Cell Analysis System and image analysis software, the number of fluorescent events for all conditions were recorded (**Figure 3.7E**). Due to hardware limitations, GFP^+ and YFP^+ events were indistinguishable, and so were combined for this initial experiment.

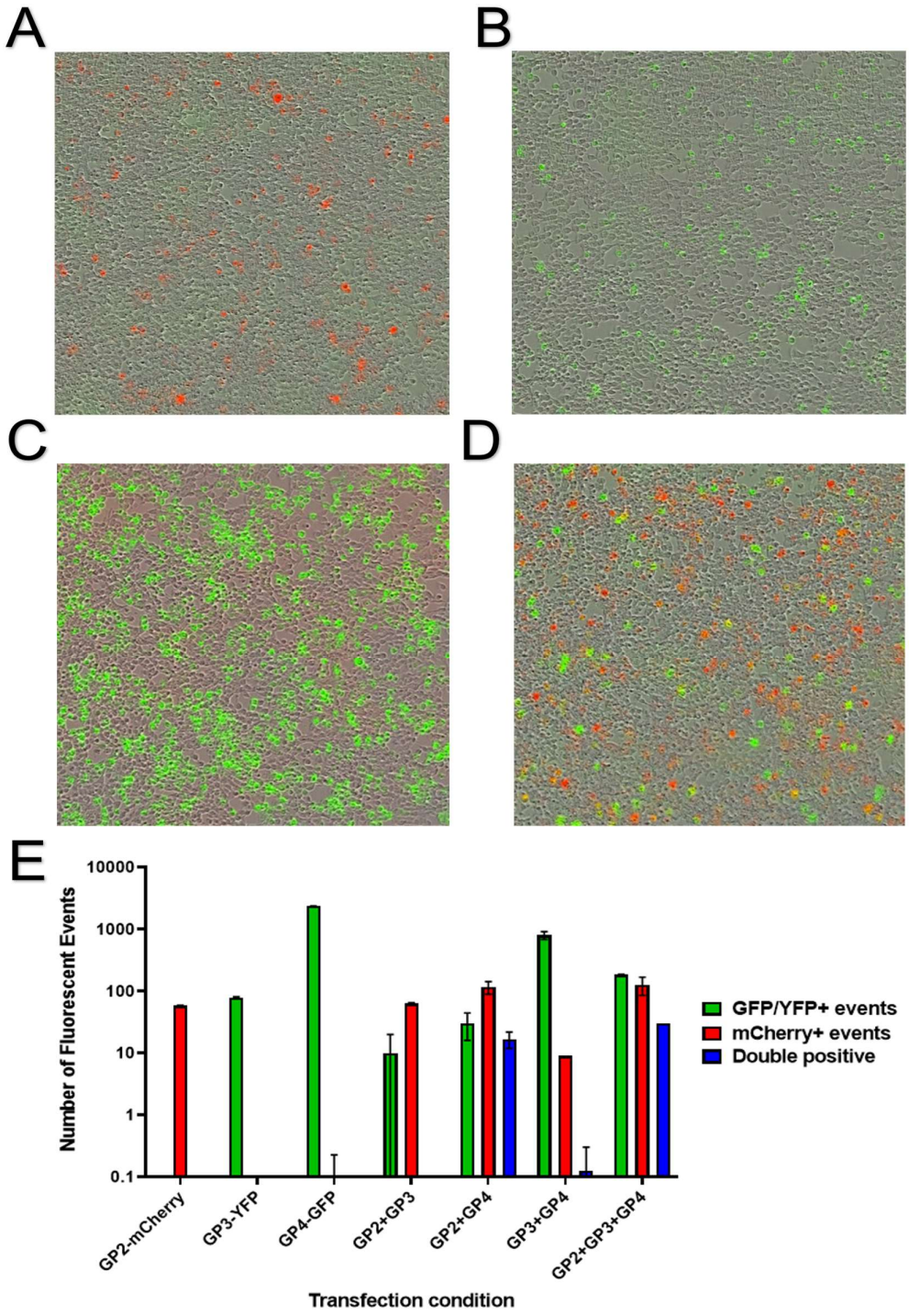


Figure 3.7: HEK293T cells transiently transfected to express recombinant PRRSV glycoproteins were assessed by live cell fluorescence microscopy. Shown are representative images of cells transfected with either individual rec-GPs: GP2-mCherry (**A**), GP3-YFP (**B**), or GP4-GFP (**C**), or co-transfected with all three simalteneously (**D**). Dual expression was assessed but not shown. All transfection conditions were quantified by detection of fluorescenct events by Incucyte® SX5 Live-Cell Analysis System (**E**). Mean data of three technical replicated technical replicates ± SD are shown.

Analysis by Tukey's multiple comparisons test revealed significantly more rec-GP4-GFP positive events were recorded than rec-GP2-mCherry or rec-GP3-YFP, when comparing the single transfections (adjusted *P* value <0.0001). In paired/triplet conditions, cells expressing both GFP/YFP-fusions and mCherry-fusions were observed, however co-transfection appeared to reduce expression overall. This trend was consistent across all transfection conditions, with a significant reduction (adjusted *P* value <0.0001 vs rec-GP2-mCherry, adjusted *P* value = 0.0124 vs rec-GP3-YFP and adjusted *P* value <0.0001 vs rec-GP4-GFP) being observed in the co-transfected cells compared to the individually transfected.

Through subsequent analysis, the issue of the overlap between the emission spectra of GFP and YFP was addressed by quantifying expression using spectral flow cytometric analysis, enabling differentiation between GFP^+ and YFP^+ events. Both individually, and co-transfected, conditions were investigated (**Figure 3.8**). Events that were both $mCherry^+$ and YFP^+ were then gated further to identify which of those events were also GFP^+ (therefore expressing all three rec-GPs).

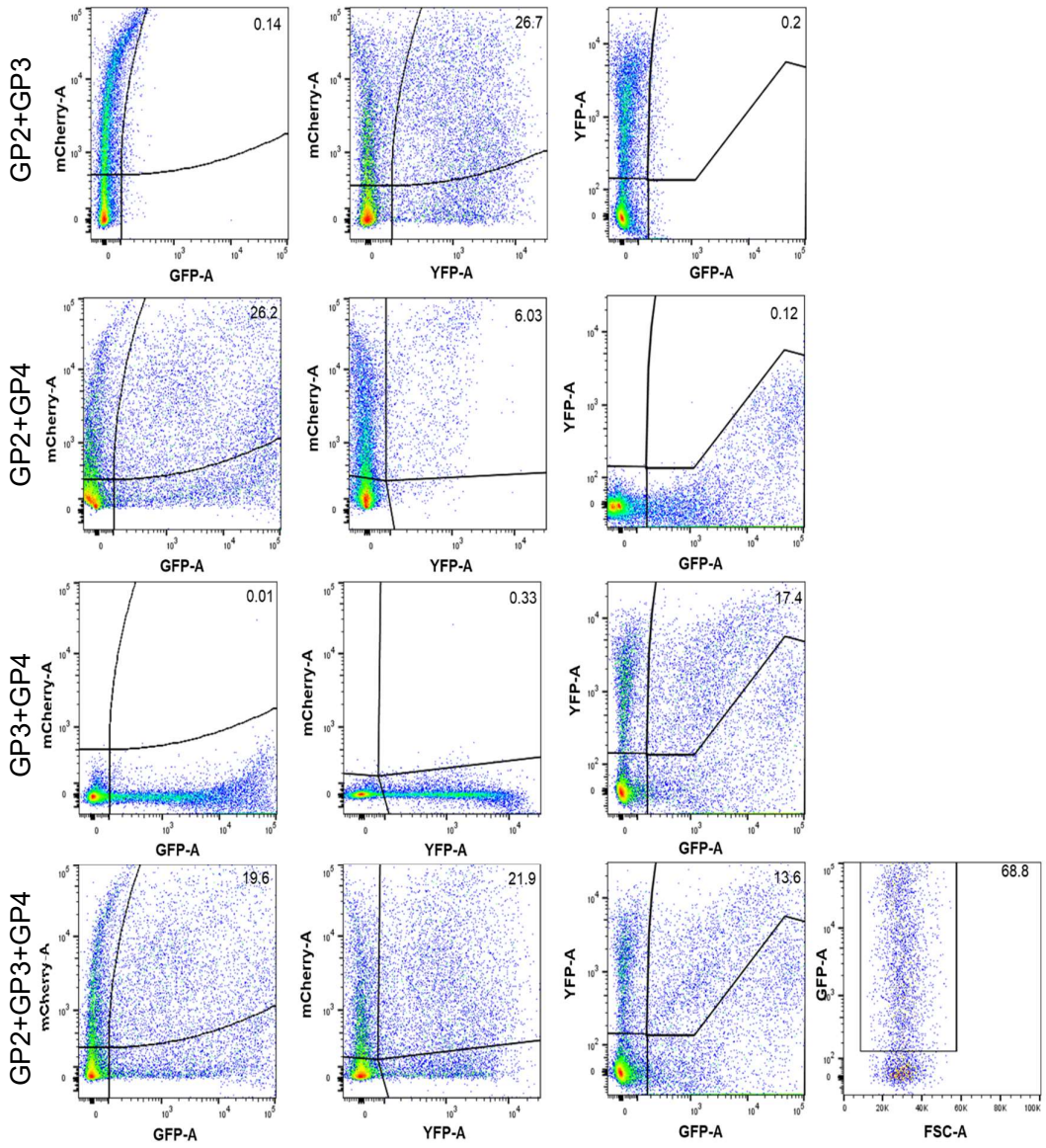


Figure 3.8: Co-expression of recombinant PRRSV glycoproteins assessed by flow cytometry following transient transfection of HEK293T individually, in pairs, and triplets. Paired GPs were compared, and double positive events were gated. Triple positive events were identified as mCherry$^+$ YFP$^+$ and GFP$^+$. Representative flow cytometry dot plots are shown.

Under each condition, double positive events were observed, indicating co-expression. Further, for cells that were co-transfected with all three rec-GPs, it was observed that by further gating on double positive cells, a small proportion of these were mCherry$^+$ YFP$^+$ GFP$^+$, indicating expression of all three rec-GPs

simultaneously. MFI values for cells expressing each protein were extracted and used for statistical analysis (**Figure 3.9**).

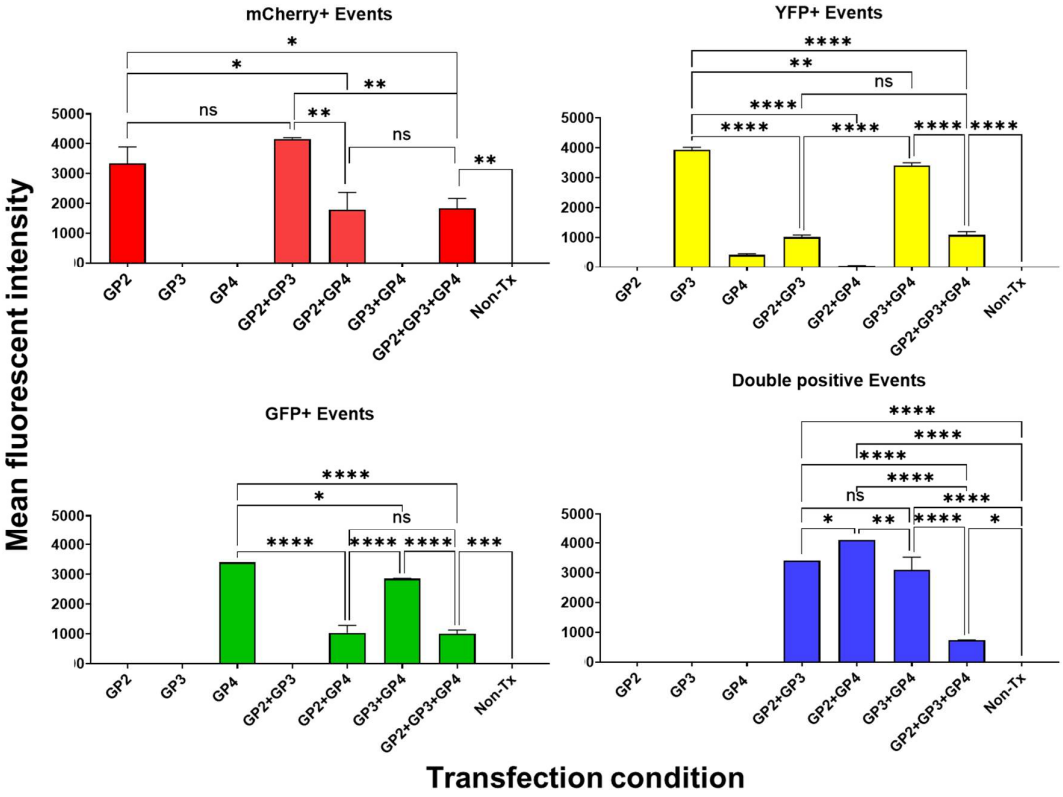


Figure 3.9: Following cytometric analysis of HEK293T transiently transfected with individual, paired, or triplicate recombinant PRRSV glycoproteins, proportion of cells expressing each fluorescent protein-fused rec-GP were compared. Means of three technical replicates are shown, with error bars representing standard deviation. Mean fluorescent intensity of fluorescent events were plotted to enable statistical analysis. *, **, ***, and **** represents a significance of P <0.05, P <0.01, P <0.001 and P <0.0001 respectively, and ns = not significant.

Statistical analysis of these extracted MFI values revealed that expression for each paired combination of rec-GPs varied greatly across transfection condition. Assessing mCherry$^+$ events first, there was no significant difference in MFI when rec-GP2 was paired with rec-GP3, compared to the rec-GP2 only, but a significant decrease was observed when paired with rec-GP4 (adjusted P value <0.05). This trend was true both for rec-GP2+GP4 transfection, and rec-GP2+GP3+GP4

transfection (adjusted *P* value <0.05). Interestingly, MFI values appeared to increase when co-transfecting with rec-GP2+GP3; while this increase was not statistically significant compared to the rec-GP2 only transfected cells, the rec-GP2+GP3 co-transfected events demonstrated a significantly higher MFI than any other transfection condition (adjusted *P* value <0.0005).

Looking at YFP^+ events, rec-GP3 demonstrated greater variation, with there being a statistically significant decrease in MFI in all conditions when paired with rec-GP2(adjusted *P* value <0.0001). When paired with only rec-GP4, there was a significant decrease in MFI observed (adjusted *P* value <0.001), though not as drastic as any of the rec-GP2 transfection conditions.

For GFP^+ events, similar to rec-GP3, MFIs demonstrated from rec-GP4 transfection appeared to decrease significantly in all instances when paired with rec-GP2 (adjusted *P* value <0.0001). Once again, when paired with rec-GP3 only, a less substantial decrease in MFIs was observed, though still significant (adjusted *P* value <0.05).

Looking only at the events which were double (or triple) positive, it appears that the addition of rec-GP3 significantly reduced the percentage of fluorescent cells in all instances, particularly when all three were co-expressed. Interestingly, all these data together suggest that there is little/no co-dependence for the expression of these rec-GPs, being able to be expressed individually.

To expand on these data, co-expression of rec-GPs was investigated further utilising confocal microscopy. This also enabled investigation of the localisation/co-localisation of the rec-GPs within transiently transfected cells

(**Figure 3.10**). Fluorescence was measured in all channels across each condition to compensate for any crossover between fluorescent channels.

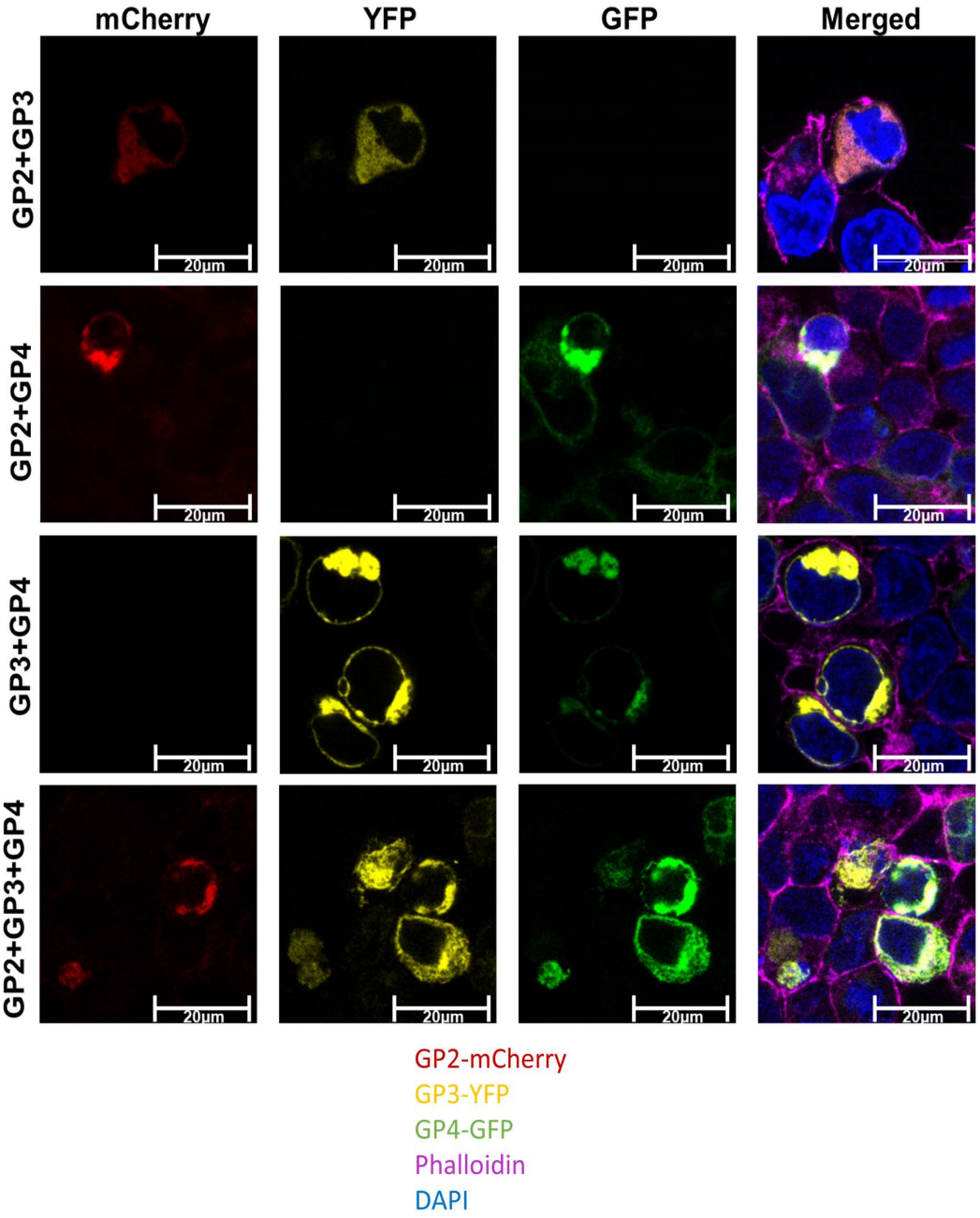


Figure 3.10: Co-localisation of recombinant PRRSV glycoproteins was assessed by confocal microscopy, following transient transfection of HEK293T cells in pairs and triplets. Expression of each Rec-GP was demonstrated by a respective fused-fluorescent protein: mCherry for GP2 (**red**), YFP for GP3 (**yellow**), and GFP for GP4 (**green**), cells also underwent DAPI/nuclei staining (**blue**), and phalloidin/actin filament staining (**purple**). Images are at 300% magnification. Scale bars are 20 µm.

It was observed that within co-transfected cells, in all experimental conditions, the rec-GPs appeared to co-localise. In all instances, there was no observable overlap between the rec-GPs and phalloidin staining, suggesting that the rec-GPs were not being surface expressed. Rather, rec-GPs appeared to localise primarily around the nuclear envelope, and within the endoplasmic reticulum (ER).

The rec-GPs being retained within the ER, particularly within the membrane of the ER, as these proteins appear to be, would pose considerable challenges for purification. Soluble, secreted proteins not only result in greater yields, but require significantly less processing to purify. Further, purification of proteins that failed to export from the ER could result in inconsistencies in post-translational modification and protein folding [267], influencing later results, particularly for proteins as heavily glycosylated as these rec-GPs.

To investigate whether any rec-GPs were secreted during culture, analysis of cell culture supernatant by western blot was performed and compared to whole cell lysate (**Figure 3.11**).

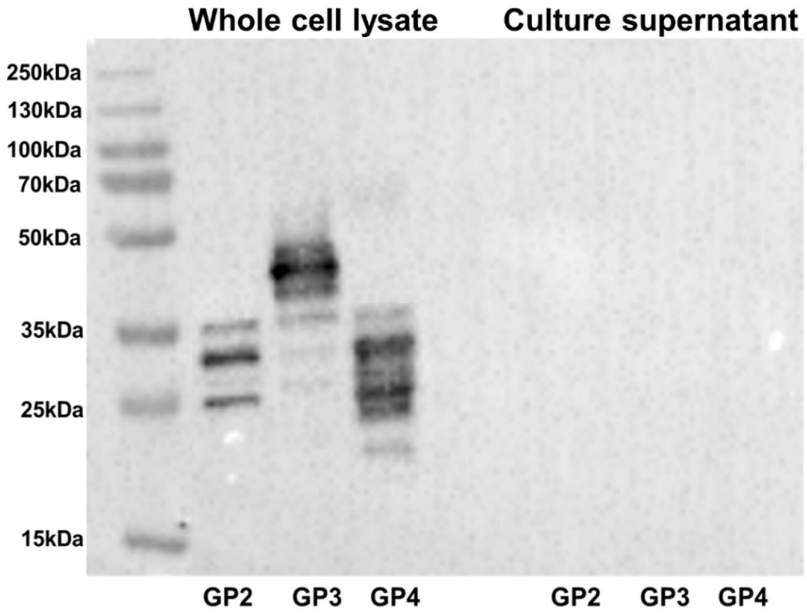


Figure 3.11: Transiently transfected HEK293T cell lysate and culture supernatants were assessed for presence of rec-GP2, -GP3, or -GP4 by western blot. Whole cell lysates and culture supernatants were collected three days post-transfection and proteins detected using an anti-His-HRP antibody.

No observable protein could be detected in the culture supernatant in any transfection conditions, and so it was concluded that the full-length rec-GPs were not secreted. It was observed in the cell lysate that each rec-GP was represented by multiple bands, likely indicating different levels of N-glycosylation occupancy. With no detectable secreted protein, focus therefore shifted to the generation of ectodomain only forms.

3.4 Expression and purification of secreted soluble biotinylated PRRSV glycoproteins

Soluble GPs (sGPs) were initially generated as two versions: each rec-sGP ending at the 5' end of the first transmembrane domain either with the native signal peptide, or with the signal peptide sequence removed to be cloned into

expression vectors encoding for the receptor-type protein-tyrosine phosphatase μ, referred to herein as μ-phosphatase, leader sequence. Cell lysates were first assessed by western blot, to compare expression with the two signal peptide sequences (**Figure 3.12A**), followed by assessment of cell culture supernatant to assess whether the proteins were secreted (**Figure 3.12B**).

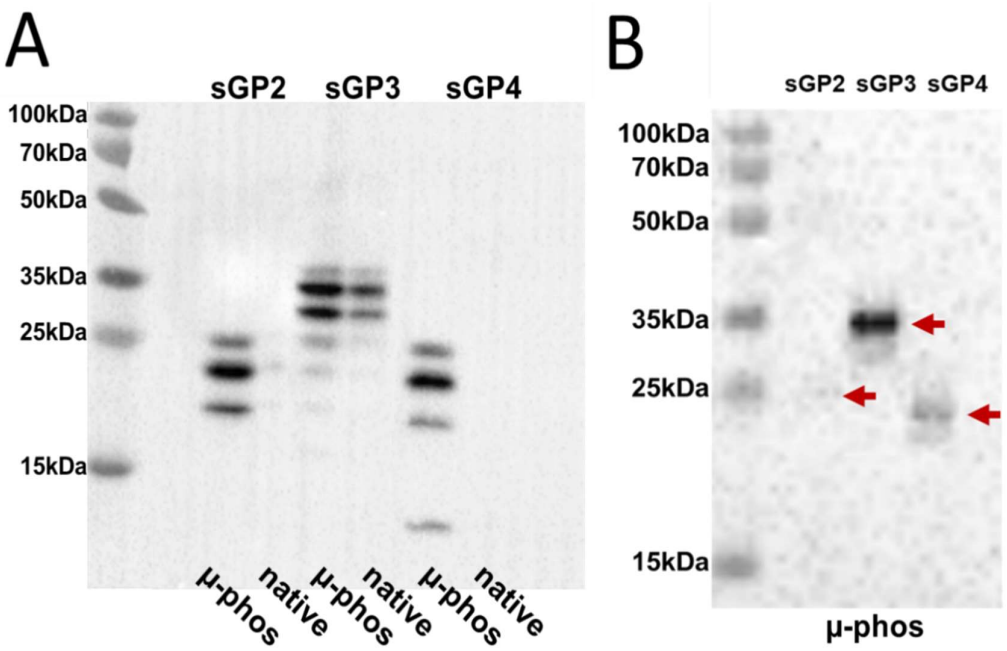


Figure 3.12: Use of a receptor-type protein-tyrosine phosphatase μ leader sequence was compared to the native signal peptide for expression of recombinant soluble PRRSV glycoproteins (sGPs), cut off at the first transmembrane domain. Cell lysate from HEK293T cells transiently transfected with each rec-GP/signal peptide combination were assessed by western blot (**A**). Cell culture supernatant from the μ-phosphatase leader sequence construct transfected cells was subsequently assessed to detect presence of the proteins (**B**).

It was observed that the rec-GPs generated with a μ-phosphatase leader sequence consistently expressed more efficiently than those with the native leader sequence, with stronger bands being observed for the sGP2 and sGP3. sGP4, furthermore, only appeared to be detectable by western blot when expressed using the μ-phosphatase leader sequence. Consequently, only the μ-

phosphatase versions were taken forward. Subsequent western blot assessment of the culture supernatants revealed that all three sGPs were detectable, though sGP3 was represented by much stronger bands than either sGP2 or sGP4, with sGP2 in particular appearing to be close to the limit of detection.

Based on these data, the sGP constructs with the μ-phosphatase leader sequence appeared to be secreted, and so a second iteration of each were generated with an additional BAP tag. HEK293T cells were transiently transfected with each new sGP construct, and an additional plasmid encoding for BirA ligase. The *in vitro* biotinylation of these rec-GPs was assessed by western blot; similar to the above, cell lysates (**Figure 3.13A**) and culture supernatants (**Figure 3.13B**) were screened by western blot using a streptavidin-HRP conjugate.

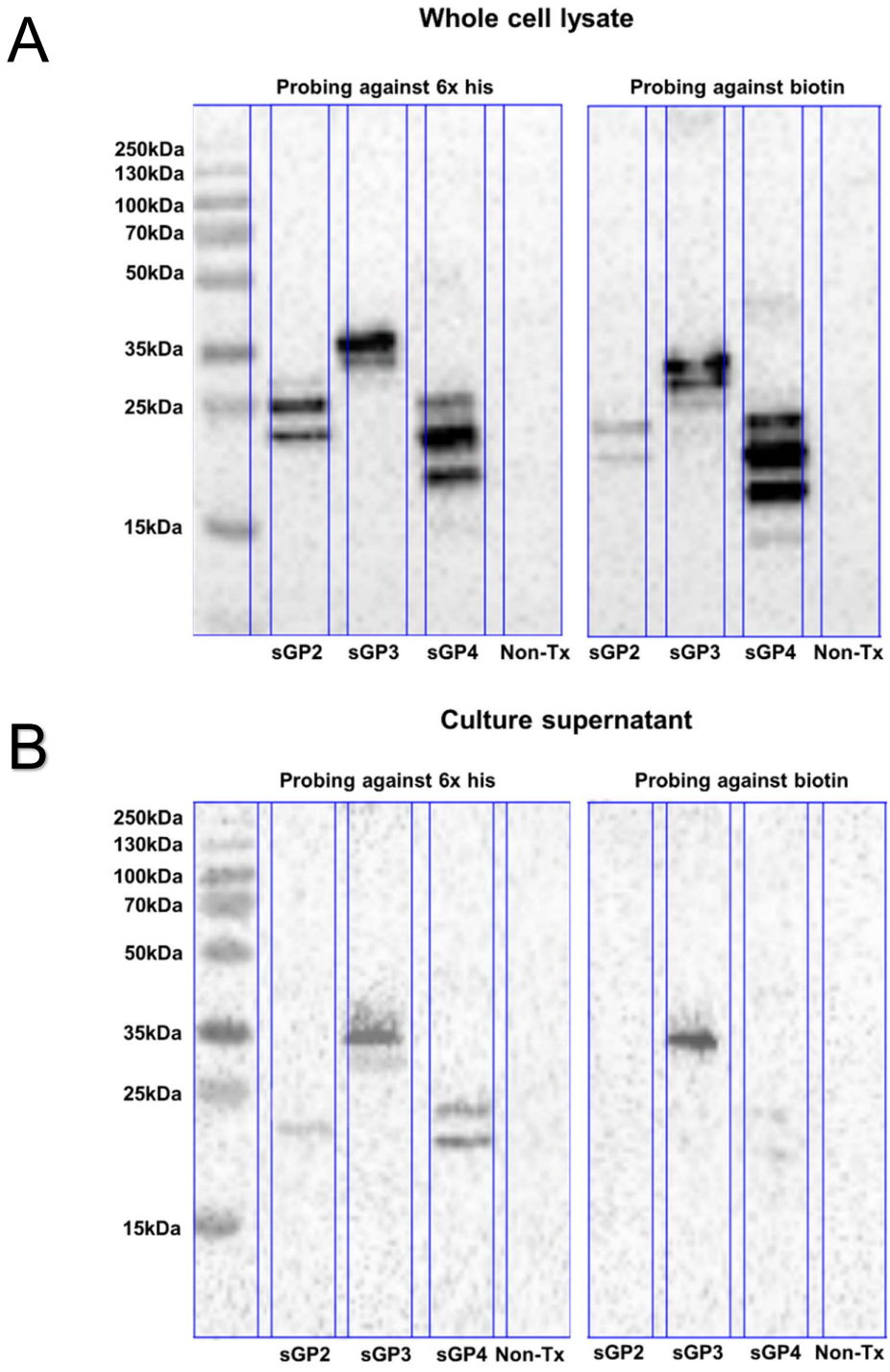


Figure 3.13: In vitro biotinylation of recombinant PRRSV glycoprotein ectodomains following co-transfection of HEK293T cells with BirA ligase was assessed by western blot. Protein from whole cell lysate (**A**) and secreted protein from cell culture supernatant (**B**), was assessed by probing with anti-6x his tag-HRP or streptavidin-HRP.

Western blot analysis of the cell lysate demonstrated that the majority of rec-GPs were biotinylated, though sGP2 appeared to have a smaller biotinylated proportion compared to sGP3 and sGP4. This analysis also revealed that all bands for each rec-GP appeared to be representatively biotinylated. For the cell supernatant samples, western blot analysis revealed that a) the BAP tag had not negatively affected the secretion of these rec-GPs, with all three being detectable in the supernatant; and b) that, like what was observed in the lysate, sGP2 appeared to have a smaller biotinylated proportion, being below the limit of detection for this assay. sGP4, also demonstrated a smaller biotinylated proportion, with weaker bands being observed in the anti-biotin blot compared to the anti-his. The majority of sGP3 appeared to be biotinylated.

An additional experiment was conducted to investigate the multiple bands observed both in the cell lysate and culture supernatant. As mentioned above, these bands were likely indicative of different levels of N-glycosylation occupancy, and so enzymatic removal of N-linked oligosaccharides was performed by incubation of cell lysate with PNGase F (**Figure 3.14**).

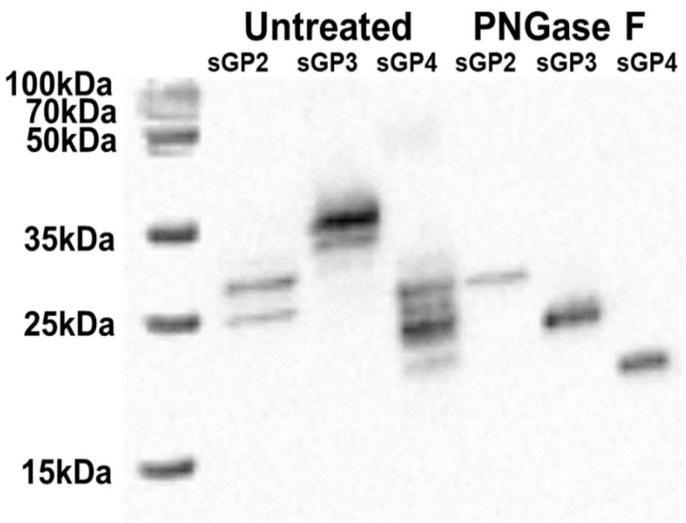


Figure 3.14: Protein extracted from cell lysate was treated with PNGase F before assessment by western blot, to investigate potential N-glycosylation heterogeneity. Samples were taken through the same protocol either with or without the PNGase F enzyme added, to ensure the two conditions were comparable.

Following N-glycan digestion by PNGase F, all three rec-sGPs were observed to be represented by one clear band. Compared to the untreated, and previous results detailed in this chapter, none of the additional bands could be observed, lending agreement to the hypothesis that these were different glycoforms of each rec-sGP.

These rec-sGPs were taken forward for large scale culture: 30 mL, and subsequently 300 mL cultures of Expi293F cells were established and tested. Cultures were transfected with each rec-sGP and BirA ligase, then purified by affinity chromatography. Assessment by western blot further informed eluted fraction selection for all three rec-sGPs (**Figure 3.15A**). Following this, the selected fractions were further concentrated and taken through buffer exchange. Purity of final products was assessed by a side-by-side western blot (**Figure 3.15B**) and Coomassie protein stain (**Figure 3.15C**). Finally, biotinylation of rec-sGPs was also assessed by western blot after purification (**Figure 3.15D**).

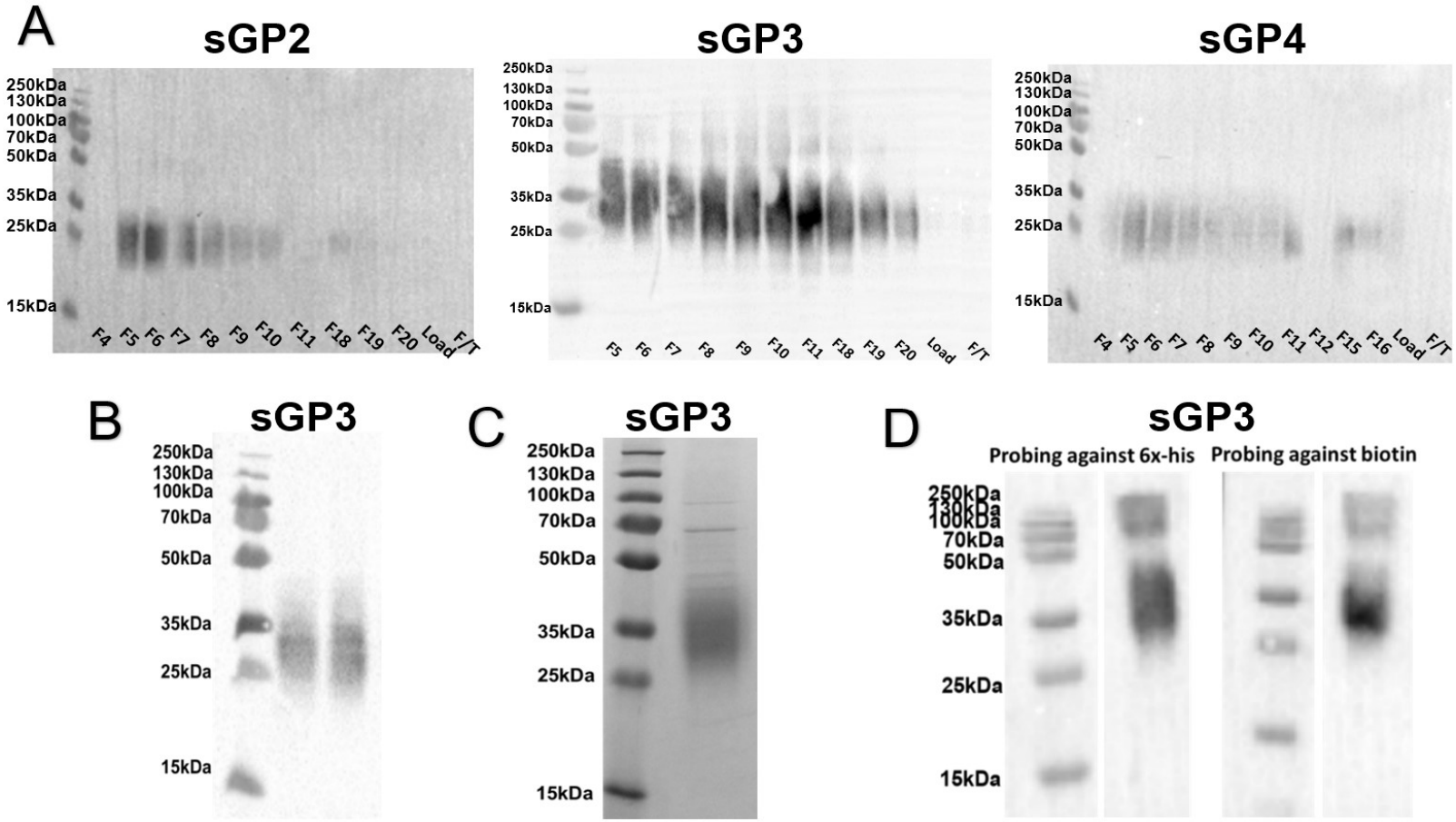


Figure 3.15: Affinity purification of recombinant PRRSV sGPs from transiently transfected Expi293F cell culture supernatants was performed using the ÄKTA Pure Protein Purification System. Eluted fractions were run on an SDS-PAGE gel and imaged via western blot (**A**). Fractions with the strongest bands were taken through concentration and buffer exchange, after which purity of the proteins was tested by western blot (**B**) and Coomassie protein stain (**C**). Biotinylation was also confirmed by western blot (**D**). Representative examples of sGP3 are shown for figures **B**, **C**, and **D**.

Across all three rec-sGPs, protein began to elute at fraction 5, with fainter bands being observed with each subsequent fraction. For sGP2 and sGP4, no observable protein was detected by fraction 12. For sGP3 however, large quantities of protein were observed in all fractions up until fraction 12, with the gradient seen in sGP2 and sGP4 not being observable. Smaller quantities of protein were detected at fractions 18 and 19 for sGP2, fractions 18-20 for sGP3, and fractions 15-17 for sGP4. This jump in fractions corresponds to the increase in imidazole concentration used throughout the IMAC purification step, with some protein not eluting until greater imidazole concentrations were introduced. Most of the rec-GPs would gradually elute at 75-100 mM of imidazole, not dissociating from the column all at once. Following buffer exchange and concentration, comparable results were seen between the three rec-GP. Coomassie stain analysis of the purified rec-GPs showed a major product at 25-40 kDa, mirroring the earlier data, and minor contaminants at 100 and ~70 kDa. These contaminants appeared more pronounced for sGP3, though this may be the result of higher overall yields. Purified sGP2, sGP3, and sGP4, additionally, all appeared to be reliably biotinylated, with all bands shown to possess a 6x-his-tag, also being biotinylated. This analysis also revealed that the contaminating bands at 100 and 70 kDa also appeared to be biotinylated, suggesting that these contaminants may be some form of sGP aggregate.

Following purification and processing, protein concentrations, and subsequently yields, were calculated by BCA assay. Concentrations were interpolated from a BSA standard curve (**Table 3.2**).

Protein	µg/litre (mean)	µg/litre (Q1)	µg/litre (Q4)
sGP2	115.61	103.71	141.80
sGP3	884.20	734.76	741.92
sGP4	133.33	116.71	155.53

Table 3.2: Yields of recombinant soluble PRRSV glycoprotein/litre of transfected Expi293F cell culture supernatant. Yields have been calculated from n = 6 batches, presented here as a mean, and range (lower and upper quartiles) for each recombinant glycoprotein.

Consistently across batches, greater yields of sGP3 were purified compared to sGP2 and sGP4, the two of which had comparable yields.

3.5 Discussion

The aim of this chapter was to demonstrate a mammalian cell expression system as a viable method to generate recombinant PRRSV glycoproteins.

The results presented in this chapter demonstrate that accurate protein structure predictions, enabled by recent advances in machine learning algorithms, provide an entry point to probing structural mechanisms, but have their limitations. While their use has facilitated greater understanding into structural vaccinology approaches, successful application of these structure prediction algorithms relies largely on similar structure found in the Protein Data Bank library. Even the most advanced tools available, i.e., AlphaFold2, still rely on identifying proteins that may have a similar structure to the input [237]. Predictions made using these tools can form the foundation, but the confidence scores in the structure of proteins largely decide their usefulness. All predictions made regarding the PRRSV GPs detailed throughout were treated with caution. Furthermore, it

should be noted that these predictions may offer conflicting results, and so their use alone is still insufficient. While the earlier detailed case of Phyre2 predicting multiple TM regions within GP4 is an example of this, it is not the only example. With the recent release of SignalP 6.0, it is now predicted with confidence that GP2 does not possess a signal peptide. Follow up study should be wary of these inconsistencies.

RMSD is the most commonly used quantitative measure of the similarity between two superimposed atomic coordinates and, as detailed above, was used for the comparison between the full-length, TM domain removed, and TM and signal peptide removed models for each GP. The main disadvantage of the RMSD, however, lies in the fact that it is dominated by the amplitudes of errors. Two structures that are identical with the exception of a position of a single loop or a flexible terminus typically have a large global backbone RMSD and cannot be effectively superimposed by any algorithm that optimises the global RMSD [268]. As such RMSD scores given, especially to low confidence models, should be interpreted cautiously, limiting the usefulness of the comparisons made as part of **Figure 3.3**.

As has been discussed, no high-resolution structural information is available for the PRRSV envelope proteins, and so understanding the structure of these proteins was largely reliant on predictive modelling. X-ray crystallography and cryo-electron microscopy experiments would provide much more reliable information than that generated through the use of the prediction software detailed here. Use of such methods was discussed for this project but were ultimately beyond the scope of what could be achieved.

Despite the lower confidence scores assigned to the predictive models, the results in this chapter denote, to my knowledge, the first use of a mammalian cell expression system for the generation of recombinant PRRSV glycoproteins. As introduced in **Chapter 1.5**, previous studies have generated similar recombinants, but have only explored prokaryotic or insect cell expression systems prokaryotic or insect cell expression systems [70, 157, 260, 261]. As highlighted these are limited by key differences in the post-translational modifications between proteins expressed in insect, and mammalian cell lines, especially for proteins as highly glycosylated as those presented in this chapter.

The full-length recombinant GPs, first explored as part of this project, appeared to possess similar properties to their native counterparts. The localisation data of the rec-GPs were consistent with previous findings, with ER localisation by PRRSV GPs being detailed following both transfection of MARC-145 and BHK-21 cells [46, 128, 191], and following PRRSV infection of MARC-145 cells [269]. Following infection, egression of the minor envelope proteins is normally initiated by a lipid raft-associated GP4, to which GP2, and subsequently GP3 form a complex with [270]. While this might explain why the individually expressed rec-GPs were not transported, this does not explain those that were successfully co-transfected with all three rec-GPs. Given the frequency of these cells was very low, it is possible that protein was being translocated, but in such small quantities it was below the sensitivity of the detection assays used.

There was a large proportion of cells in the co-transfected conditions that only expressed one or two rec-GPs. Incucyte analysis suggested significant differences in the expression of rec-GPs in transfected cells, however this was

not observed when analysed by flow cytometry. As mentioned in the preceding section, Incucyte image analysis was limited by the inability to distinguish between GFP^+ and YFP^+ events. Polycistronic vectors were discussed as a means to efficiently ensure cells could be transfected with all three rec-GPs equally. It was observed that when co-transfecting with multiple rec-GPs, overall expression was decreased. It is unknown why this was the case. The construction of a polycistronic plasmid for the purpose of expressing all three rec-GPs described in this project was discussed as a possibility, though ultimately was not investigated. The first description of the expression of an Arterivirus minor envelope heterotrimer in mammalian cells from a single plasmid was very recently described [271] and, though this study focussed on the closely related equine arteritis virus rather than PRRSV, it demonstrated promising results. The results detailed in this study also closely align with the observations made as part of this chapter, whereby expression levels of GP2 appeared to be negatively impacted upon combining with GP3 and GP4. Further, it was observed that intracellular transport of GP3 and GP4 were largely independent of whether the proteins were expressed individually, or together, in agreement with the results presented here.

In all instances soluble GP3 was secreted at higher levels than GP2 and GP4. One hypothesis for this is that GP3 has been shown to also exist as a soluble form [218, 222], that does not interact with GP2 and GP4, and so therefore has a greater propensity for secretion. As a consequence of this, purified yields of GP3 were higher across all replicates. Investigation of co-expression in this project was limited to the full-length rec-GPs, follow up work should investigate

whether co-expression of these soluble ectodomain only GPs results in complex formation, and whether they are still secreted when complexed.

Following purification, it became difficult to discriminate between these previously observed distinct glycoforms, with each GP appearing as one broad band. As described above, digestion by PNGase F resulted in removing all but one band. This suggests that this large band comprises multiple glycoforms. GP2, GP3, and GP4 are known to possess two, seven, and four potential N-glycosylation sites respectively [203, 260], with this being consistent between both PRRSV-1 and PRRSV-2. It has not been fully determined, however, to what extent the range of glycosylation states observed alters the conformation of these GPs, or how this affects their antigenicity. Highly glycosylated sites within the native PRRSV GPs have been shown to shield neutralising epitopes, with GP3 being the most prominently reported [203]. It has been shown that removal of N-glycans from GP5 reduced infectivity of PRRSV [272], however the influence of N-glycosylation for the minor envelope glycoproteins is more controversial. One study reported that the glycosylation of residues Asn42, Asn50, and Asn131 of GP3 is necessary for infectious virus production [203], while another study has reported that none of the individual glycosylation sites in GP3 have a vital effect on the production of infectious virus [273]. Both studies were conducted using two different PRRSV strains and, while N-glycosylation sites are shared between PRRSV-1 and PRRSV-2, it is possible that they serve different functions between the two species and could explain the discrepancy in reported results. For GP2 and GP4, several studies suggest that none of the individual N-glycosylation sites are essential for infection virion formation [190, 191, 226, 273]. The effect of

glycosylation on the antigenicity of the recombinant GPs was briefly investigated as part of the following **Chapter 4**.

This chapter also highlights several areas where information is lacking, which should be an emphasis for future research. Predictive modelling provided only a small insight into the native GPs and without more confident models of both the native, and these recombinant GPs, it is not possible to comment on how truly similar the recombinants are in terms of 3D structure. Greater understanding of the structure of these recombinant GPs is paramount to understanding their interactions with antibodies and so, as discussed above, greater investigation into the structure of these rec-GPs was of great interest, though ultimately beyond the scope of this project. Future work building upon the results presented in this thesis should strive to better characterise these recombinant GPs.

The soluble GP2 and GP4 demonstrated significantly lower yields than the GP3, consistently across this project. Future work focussing on promoting secretion could yield better results for GP2 and GP4. Work on this project has aimed to achieve this, i.e., utilising a μ-phosphatase signal peptide in place of the native signal peptide. Alternative methods have been described, however, such as the use of antisense long non-coding RNAs to increase translation of partially overlapping protein-coding mRNAs to increase production of secreted proteins [274], and are another possible avenue to improve secretion. Generation of stable cell lines was explored during this project; however, this did not result in greater yields than using transiently transfected cells. One hypothesis formed as to why GP3 demonstrated such greater yields as a soluble form, is that GP3 is naturally more soluble than GP2 or GP4. GP4 is often reported as being lipid-raft

associated [270], and there is no evidence for it, or GP2, existing as soluble forms during natural virion assembly. It is well documented, conversely, that GP3 commonly exists as a secreted form following both transfection and infection of PRRSV [218], which may account for the yields observed in this chapter.

Outside of investigating co-expression and co-localisation, this project yielded limited data these GPs as a complex. Secreted soluble forms were observed not to form the minor envelope complex, and as a result, any potential conformational epitopes exposed as part of complex formation, were not investigated. As previously discussed, expressing the three GPs in a polycistronic vector would be a potential method for efficient transfection. Introducing flexible protein linkers [275, 276] as part of this system could hold promise for expression of the whole minor envelope complex.

Overall, this chapter has demonstrated that a mammalian cell expression system can be utilised to generate recombinant PRRSV GPs. Furthermore, it was demonstrated that generating these GPs with the transmembrane and endodomain portions of the sequence removed still resulted in expressed protein. It can be assumed that, as all three of these secreted soluble forms are likely to be folded (and hence functional) protein, since they must have passed the quality control measures of the ER in order to be secreted [267].

There are still unanswered questions regarding how similar the structure of these recombinant GPs are to the native GPs, and so the results described in the next chapter aimed to better characterise the antigenicity of these rec-GPs.

Chapter 4. Characterisation of the antigenicity of soluble recombinant PRRSV-1 GP2, GP3, and GP4 ectodomains

4.1 Rationale

For recombinant minor envelope glycoproteins to be viable as tools to identify/isolate PRRSV-specific B cells, they must be able to elicit binding similar to that of the native protein. Consequently, the secondary and tertiary structures of these recombinant GPs must be the same, if not similar enough, to their native counterparts such that the same epitopes are accessible. Understanding the antigenicity of these recombinant glycoproteins, as a result, is imperative for their use as tools to isolate mAbs. There is evidence that a neutralising epitope located in the ectodomain of GP4 is considered immunodominant and responsible for the induction of nAbs upon infection, with high GP4-specific antibody titres arising 2-3 weeks post-infection with PRRSV-1 Lelystad [127]. Furthermore, a follow up study suggested that it was in fact GP3 that was the major target of nAbs from sera of PRRSV-infected pigs [205], suggesting that both of these GPs are targets for nAb responses, and therefore novel vaccine design. While there is less evidence for GP2, it is known to possess neutralising epitopes, as detailed in **Chapter 1**. With GP2, alongside GP4 playing such a crucial role in the interactions with CD163 it could still serve as a target of interest.

As highlighted in the previous chapter there are inconsistencies in, or an absence of, experimental structural information available for the PRRSV minor envelope proteins [169]. Furthermore, while PAGE and western blotting can be used to assess whether the recombinant proteins are of the expected molecular weight, little information on the structure of these recombinant sGPs can be ascertained. Outside of predictive modelling, it is therefore difficult to ascertain how similar the recombinant sGPs were structurally to the native viral GPs. This chapter,

therefore, investigated the antigenicity of these recombinant sGPs utilising serum from animals experimentally infected with PRRSV or MLV and PRRSV-naïve animals, to determine whether these recombinant proteins could elicit specific antibody binding.

For several experiments detailed in this chapter, material from a heterologous PRRSV challenge study, conducted by the PRRS Immunology Group at The Pirbright Institute, prior to this project was utilised. The details and experimental design of this study are outlined in **Chapter 2.17**.

As discussed in **Chapter 3**, antigen-tetramers have been shown to be a powerful method for the identification and isolation of specific B cells by flow cytometry, particularly for low frequency B cell populations [256-258]. Moreover, tetramers have been demonstrated as a reliable method to enable identification of PRRSV-specific cells, i.e., NSP7 tetramers have been used to identified PRRSV-specific B cells, despite only comprising a 0.001% frequency of total B cells [277, 278]. To date, however, there has been no experimental evidence of tetramerised minor envelope GPs being used for this purpose. Some previous studies have utilised virus-infected cells as a means to isolate PRRSV-specific cells [160], however the limitation of this is that antibodies against the more abundant, or immunodominant, antigens will likely eclipse those against the weaker, or less abundant antigens. For study of the minor envelope glycoproteins, which are significantly lower in relative abundance, this is a key benefit of rec-GP tetramers over whole virus. Utilisation of individual GP tetramers over whole virus, furthermore, enables greater dissection of B cell frequency against each glycoprotein separately. While these GPs likely possess conformational epitopes,

only presented as part of the minor envelope complex, fundamental understanding of each individual GP is still incomplete. This previously would have been limited to methods such as antigen-specific IgG ELISpot assays [279, 280], and so the methods described herein may provide a new approach to study the antigen-antibody interactions of each minor GP.

Before attempting to isolate mAbs, this chapter aimed to investigate whether these recombinant sGPs could be used to identify PRRSV-specific B cells.

4.2 Assessment of recombinant PRRSV glycoprotein antigenicity using polyclonal sera

Antigenicity of each sGP was first assessed by a small-scale ELISA, comparing sera from PRRSV-immune pigs to naïve pigs.

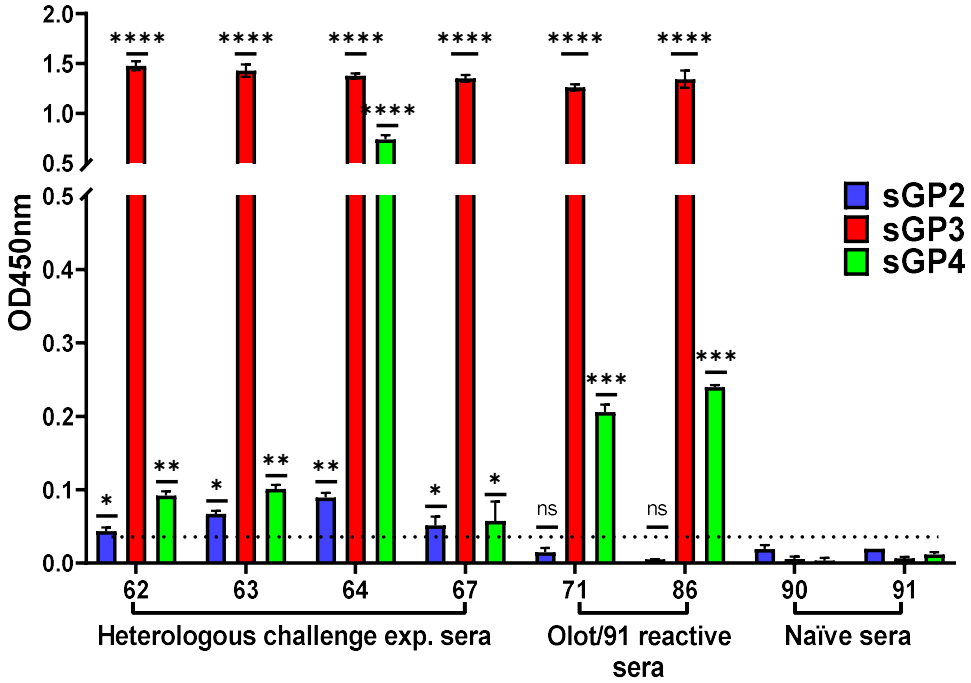


Figure 4.1: Indirect ELISA comparing serum antibody reactivity to recombinant PRRSV-1 sGP2, sGP3 and sGP4. Sera isolated from pigs sequentially inoculated with four heterologous PRRSV strains (n=4), pigs repeatedly inoculated with PRRSV-1 Olot/91 (Mokhtar et al, 2016) (n=2), and PRRSV-naïve pigs (n=2) were tested. Mean data of three technical replicates ± SD are shown, *, **, ***, and **** represent P <0.05, P <0.01, P <0.001, and P <0.0001 respectively, and ns = not significant.

Though close to the calculated threshold (mean OD for naïve sera + 3* SD), Dunnett's multiple comparisons test revealed that the response to sGP2 was statistically significant: adjusted *P* value <0.005 for pig 62, and adjusted *P* value <0.001 for the other three animals from the heterologous inoculation experiment. Interestingly, the response to sGP2 from the Olot/91 reactive animals was not significantly higher than the naïve sera. Recognition of sGP3 was shown by all PRRSV-reactive sera, compared to the naïve sera: adjusted *P* value <0.0001 for all animals in both the heterologous inoculation experiment and from the Olot/91 repeat inoculation experiment. The responses against sGP4 were more varied than those observed against sGP2 or sGP3. While the response from pig 67 was comparable to those seen against sGP2 (adjusted *P* value <0.005), the response from pig 64 was significantly higher than those observed from all other animals, being comparable to the response to sGP3 (adjusted *P* value <0.0001). It was observed that the response from the Olot/91 repeat inoculation experiment was higher, but still not as strong as that seen against sGP3.

As an additional experiment, the effect of glycosylation on antigenicity was investigated. sGP3 was used for this, due to the high antigenicity demonstrated above. N-linked oligosaccharides were removed from sGP3 by PNGase F digestion, and binding of immune sera was compared by ELISA (**Figure 4.2**).

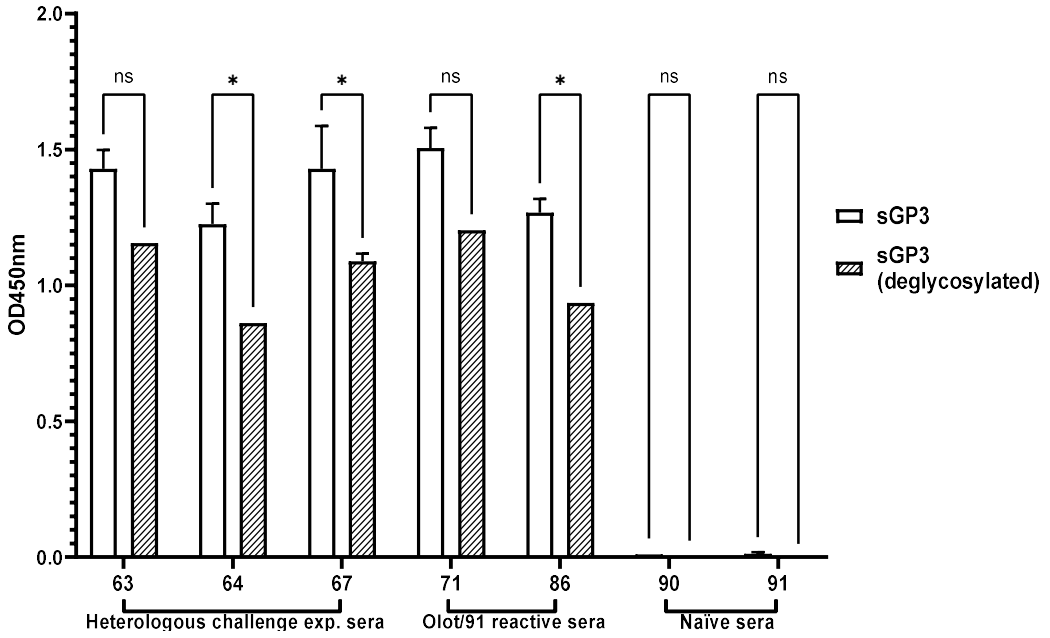


Figure 4.2: Deglycosylated aGP3 protein was assessed by ELISA to determine differences in binding by PRRSV immune sera. Mean data of two technical replicates ± SD are shown, * represents a significance of *P* <0.05 and ns = not significant.

By two-way ANOVA, Šídák's multiple comparisons test showed a significant difference in binding between conditions for sera from animals 64 (adjusted *P* value = 0.0269), 67 (adjusted *P* value = 0.0124), and 86 (adjusted *P* value = 0.0441), with the higher responses being observed against the glycosylated sGP3. No significant difference was observed between the two glycosylation conditions for animals 63, 71, 90, and 91. Further, by two-way ANOVA, all PRRSV-reactive sera showed significant binding above the naïve sera against both glycosylation conditions. While binding to the glycosylated sGP3 showed strong significance (adjusted *P* value < 0.0001) from all reactive sera tested, against the deglycosylated sGP3 sera from pig 64 and pig 86 gave a less significant response (adjusted *P* value = 0.0004 and = 0.0002 respectively).

These results suggest that glycosylation did have an effect on the antigenicity of recombinant GP3, but not consistently between animals.

Sampling was expanded to include the full longitudinal set of serum samples from the heterologous challenge study (n = 6 animals), and response to each sGP was assessed across the full 148-day study timeline and compared against the virus neutralising antibody titres (**Figure 4.3**).

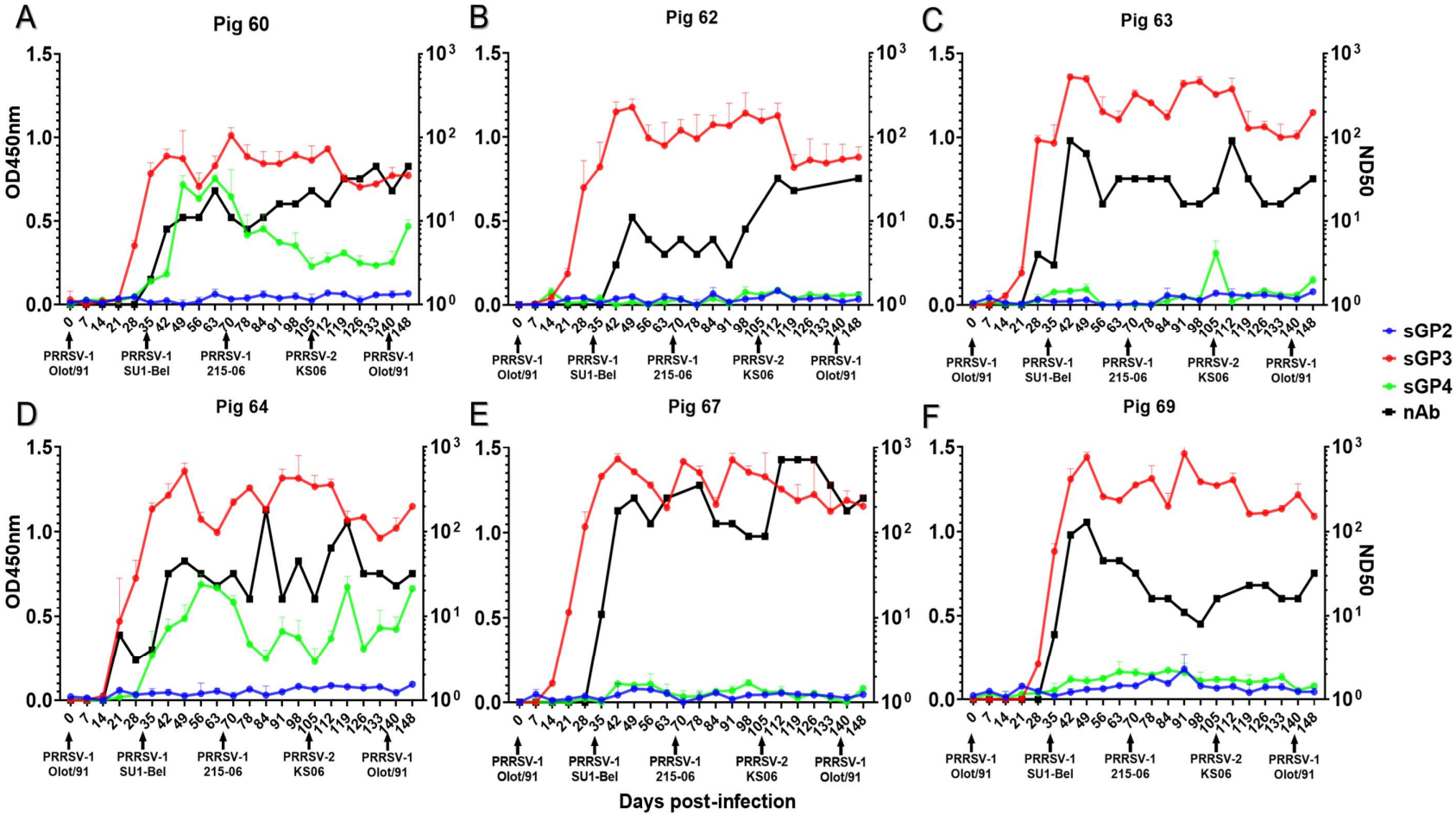


Figure 4.3: Recognition of recombinant PRRSV-1 sGP2, sGP3, and sGP4 was assessed by ELISA using sera collected from pigs (n=6) sequentially inoculated with diverse strains of PRRSV, across a 148-day challenge study. Mean data (OD_{450}) across two technical replicate wells ± SD are plotted and compared to neutralising antibody titres (ND_{50}) calculated from the same serum samples.

Tukey's multiple comparisons test revealed that response to sGP2 was seen to be low to negligible in pig 60-67 across the timeline of the study, with no data points being statistically significant compared to the response at 0 dpi. An increase was observed from sera from pig 69 at 91 dpi, which was significant (adjusted *P* value = 0.0066), this response fell below significance by 98 dpi.

Response to sGP3 was consistently strongest throughout, arising in each pig 14-21 dpi, and persisting until termination of the study, with all end point sera scoring significantly above 0 dpi (adjusted *P* value <0.0001). Despite the comparatively strong response throughout, the kinetics of responses against sGP3 did not appear to be influenced by later PRRSV challenges. An apparent lack of anamnestic response following the later PRRSV challenges seems a consistent trend between the six animals investigated. In all instances, while there was a clear boosting effect following challenge PRRSV-1 SU1-Bel, this was not the case following challenge with PRRSV-2 KS-06.

Response to sGP4 differed dramatically between animals. Starting 28 dpi and persisting until termination, serum from pig 60 and pig 64 showed significantly higher binding of sGP4 than the other animals in the cohort (adjusted *P* value <0.0001), with the response from the end point sera remaining significantly higher than 0 dpi (adjusted *P* value <0.0001). No significant binding from pig 62, pig 67, nor pig 69 was observed at any time point assessed. For most of the time points assessed, responses from pig 63 remained below significance. Immediately following challenge with PRRSV-2 KS06 (105 dpi), however, statistically significant sGP4 binding comparable to that seen by sera from pig 60 and pig 64 was observed, well above the responses observed 0-98 dpi (adjusted *P* value

<0.0001). This response, however, was short lived, being comparable to 0 dpi sera by 112 dpi. No significant response was observed until termination, at 148 dpi, were a weak, but significant sGP4 response was recorded (adjusted *P* value = 0.277). Similarly, the overall kinetics of sGP4 responses observed differed between animals. While responses from pig 60 appeared to largely align with those described against sGP3, responses from pig 64 differed greatly, with a clear boosting effect following each challenge.

The nAb titres observed were comparable across the majority of the animals tested, with the titres calculated from sera from pig 67 being significantly higher than the rest of the cohort (adjusted *P* value <0.0001). To investigate whether there was any correlation between sGP-specific response and nAb titres, correlation coefficients for each sGP response were calculated and plotted (**Figure 4.4**). Correlation coefficients were calculated for each animal, across all 22 time points. R squared and P values for each animal-sGP response are also detailed (**Table 4.1, Table 4.2**).

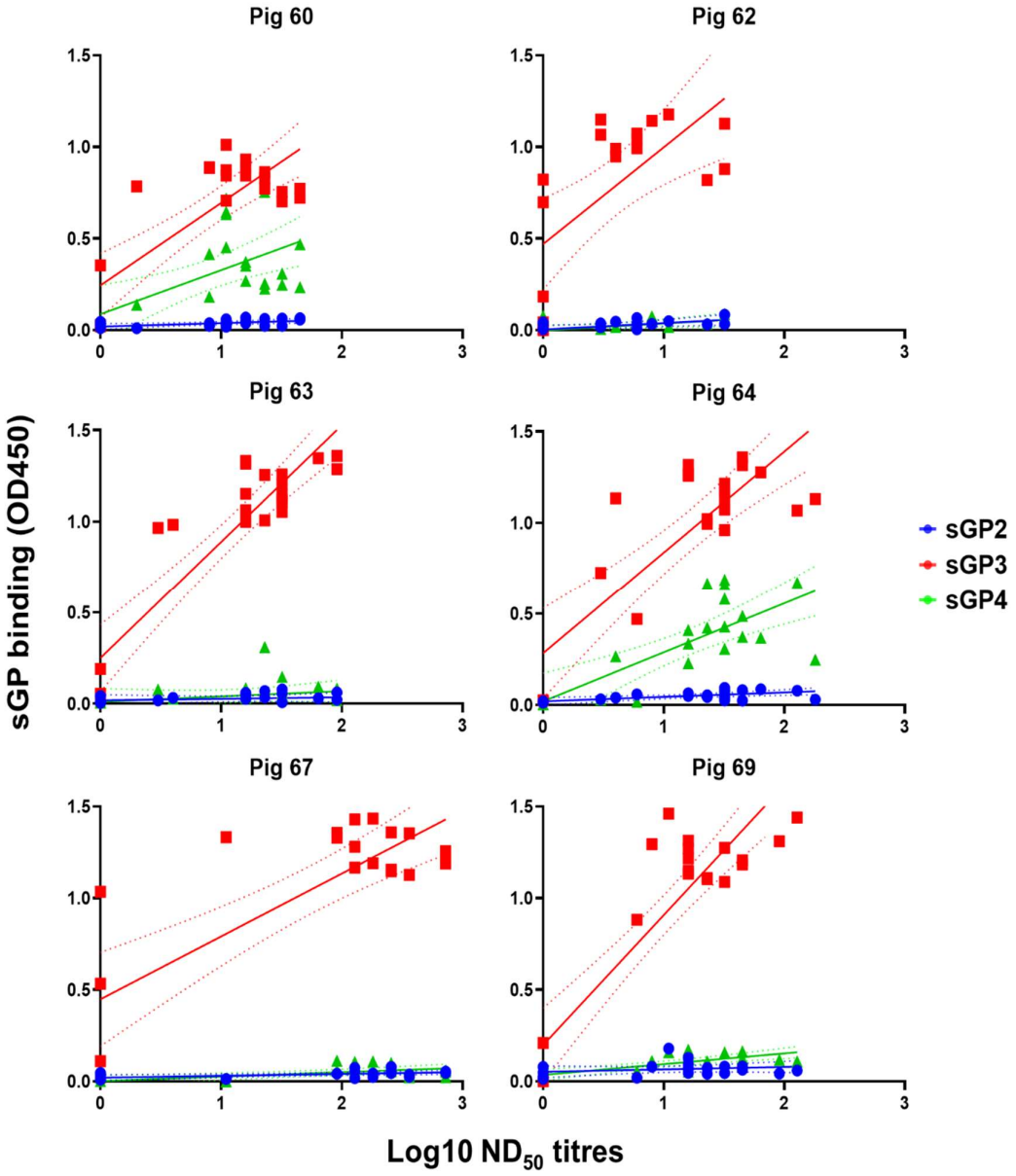


Figure 4.4: Pearson r correlation coefficients between mean antibody response to recombinant PRRSV sGP2, sGP3, and sGP4 and neutralising antibody titres (ND_{50}). Correlation coefficients were calculated and plotted for n = 6 animals from a 148-day heterologous PRRSV challenge study. 95% confidence bands of the best-fit lines are shown for each plot.

Pig number	P value for sGP2	P value for sGP3	P value for sGP4
60	0.0126	<0.0001	0.0025
62	0.0174	0.0026	0.0362
63	0.4858	<0.0001	0.3012
64	0.0039	<0.0001	<0.0001
67	0.0131	<0.0001	0.0036
69	0.3033	<0.0001	<0.0001

Table 4.1: P value confidence scores for the slope of best-fit lines were generated as a measure of correlation between recombinant PRRSV sGP binding and neutralising antibody titres.

Pig number	R^2 for sGP2	R^2 for sGP3	R^2 for sGP4
60	0.2729	0.6310	0.3742
62	0.3052	0.4421	0.2462
63	0.0246	0.8109	0.0533
64	0.3480	0.6699	0.5516
67	0.2827	0.6326	0.3677
69	0.0556	0.8107	0.5637

Table 4.2: R squared scores for goodness of fit for lines generated as a measure of correlation between recombinant PRRSV sGP binding and neutralising antibody titres.

Together these data demonstrated that for all six animals tested, there appeared to be a statistically significant correlation between sGP3 binding by ELISA and nAb titres. This correlation was noticeably weaker for the data generated from pig 62, however this was still significant. Despite the *P* values suggesting correlation, the R^2 suggest poor fit, with no values being above the 0.9 threshold set for this analysis. Further, interpreting these data as such suggests a significant correlation between sGP2 and nAb titres for pig 60, 62, 64, and 67, despite earlier ANOVA analysis suggesting that the sGP2 response, overall, was not statistically

significant. Caution, consequently, should be taken interpreting these results. Similarly, it was suggested that there was a positive correlation between sGP4 response and nAb titres in all animals other than pig 62. These results, again, should be interpreted cautiously.

The discrepancy in reactivity between animals, particularly to sGP4, highlighted the limited size of this cohort of animals. To assess whether the diversity of responses against these recombinant sGPs was consistent, a much greater number of sera was tested by ELISA (**Figure 4.5**). These sera were provided from previous studies conducted in the PRRS Immunology Group at The Pirbright Institute.

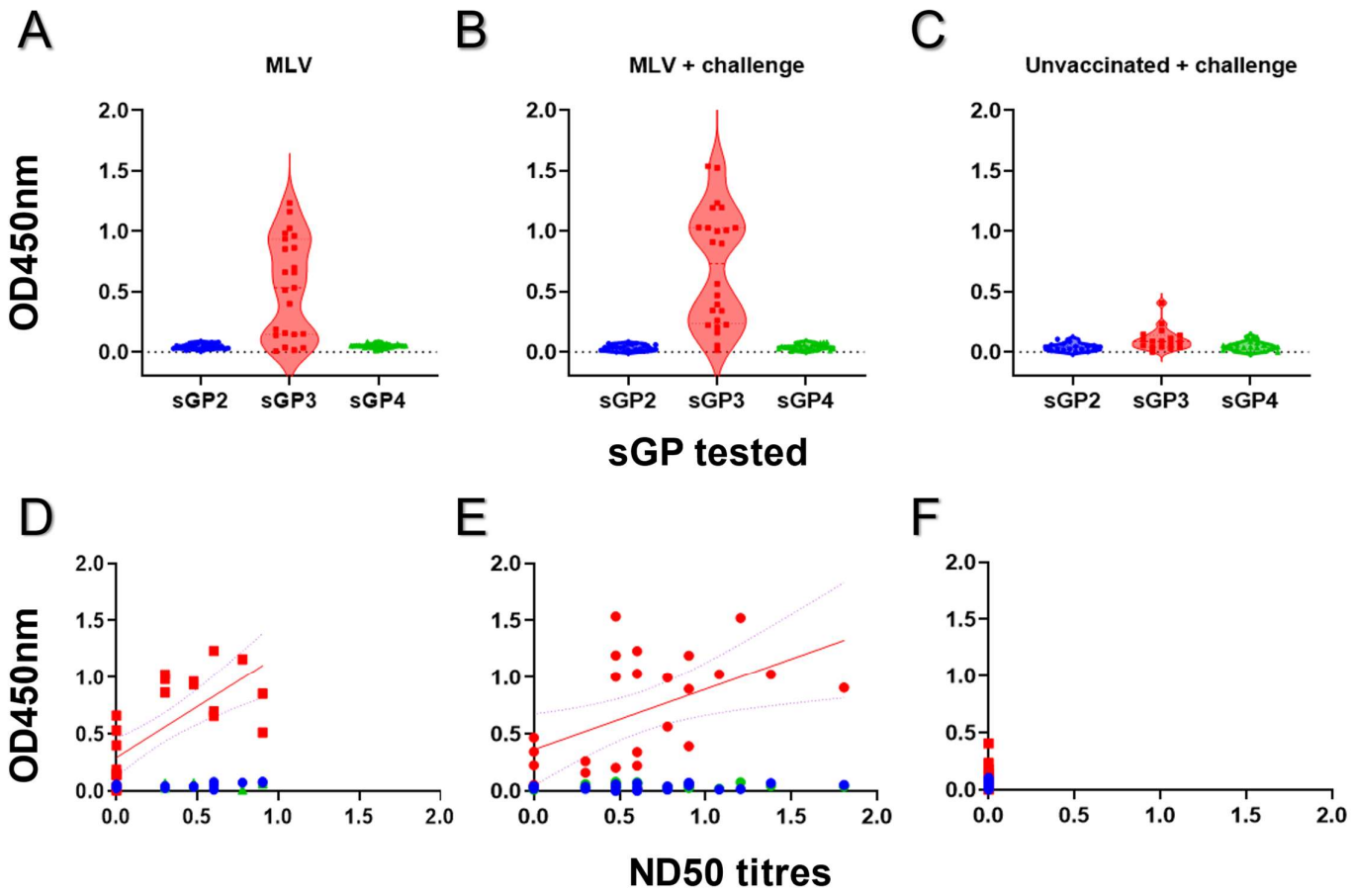


Figure 4.5: Antibody recognition of recombinant sGP2, sGP3, and sGP4 was assessed by indirect ELISA, using porcine sera from a collection of PRRSV studies. These comprised sera collected 49 days post-immunisation with a licensed or experimental MLV (n = 23) (**A, D**), sera collected 49 days post-immunisation with a licensed or experimental MLV with a PRRSV-1 challenge on day 35 (n = 24) (**B, E**) or sera collected 21 dpi following PRRSV-1 challenge (n = 17) (**C, F**). Correlation between recombinant sGP response and neutralising antibody titres was plotted for each experimental condition. 95% confidence bands of the best-fit lines are shown for each plot.

In all instances, the response to sGP3 appear to be the dominant response, eliciting significantly higher binding than sGP2 and sGP4, lending further support to the data generated using material from the heterologous challenge study. There was no significant correlation between sGP2 and nAb titres, nor for sGP4 and nAb titres. This was not the case for sGP3: there was a moderate correlation between the sGP3-specific response of the MLV vaccinated animals and nAb titres (adjusted *P* value *P* <0.0001, R^2 0.509), as well as the MLV vaccinated/PRRSV challenged animals (adjusted *P* value *P* <0.001, R^2 0.288). As expected, no nAb titres could be detected in the unvaccinated animals.

sGP3 appeared to consistently elicit binding from PRRSV-reactive polyclonal sera to a significant degree above naïve samples. While antibody reactivity sGP2 and sGP4 were less consistent, there was evidence that they could elicit binding from PRRSV-reactive sera. Consequently, it was then investigated whether these recombinant sGPs could elicit binding from live B cells isolated from hyperimmune pigs.

4.3 Identifying PRRSV-specific B cells utilising tetramerised recombinant PRRSV glycoproteins

For each sGP, two tetramers were assembled, utilising fluorophore-conjugated streptavidin. Streptavidin-BV421 and streptavidin-BV650 were selected as these fluorophores are on opposing end of the spectrum, and so this limited artifact caused by spectral overlap. Two tetramers for each sGP were used to increase the confidence of detecting true antigen-binding low frequency events. In addition to these tetramers, a decoy tetramer was assembled, utilising a recombinant SARS-CoV-2 spike protein RBD, provided by colleagues at The Pirbright Institute

[243], to facilitate the exclusion of non-specific cells binding tetramer components other than the recombinant sGPs.

Prior to attempting staining with the full tetramer panel, the recombinant sGP tetramers were tested for potential cytotoxic effects. sGP3 tetramers were used for this initial test due to the comparative abundance of sGP3 material compared to sGP2 and sGP4. Cryopreserved PBMCs from two PRRSV-naïve animals were resuscitated and stained, in triplicate, with different combinations of tetramer and/or an established antibody panel to be used to stain porcine B cell populations [243] (**Figure 4.6**).

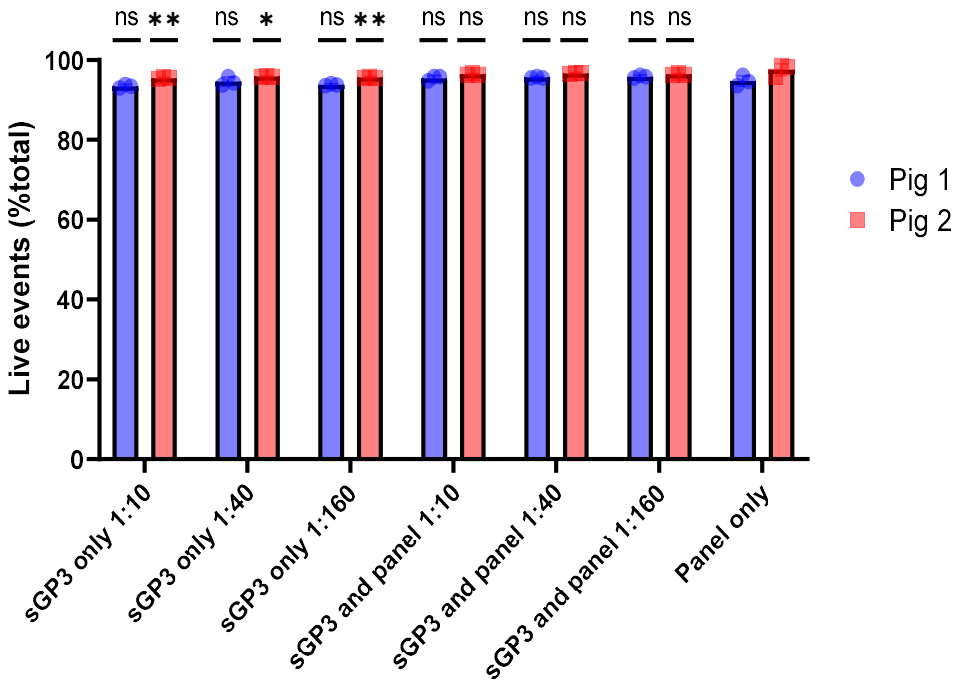


Figure 4.6: Flow cytometric assessment of the percentage of live peripheral blood mononuclear cells following cellular staining with an established antibody panel used to identify porcine B cells, and/or tetramerised sGP3. Conditions were run in triplicate, with the means being compared to the panel only (sGP3 tetramer negative) to assess potential reduction in viability. sGP3 tetramers were diluted either 1:10 or 1:160 (v/v) across conditions. Mean data of three technical replicates ± SD are shown, * represents P <0.05, ** represents P <0.01, and ns = not significant.

Dunnett's multiple comparisons test was performed, comparing mean data to the panel only for each pig. For pig 1 there was no statistically significant decrease in viability between any of the sGP3 conditions and the panel only. For pig 2, however, there was a significant reduction in all sGP3 only conditions, compared to the panel only (adjusted *P value* = 0.0033, = 0.0212, and = 0.0073 respectively). Whilst these are significant reductions, the reductions were small, and the overall percentage of viable cells remained very high.

Staining cells with the sGP3 tetramer and antibody panel together, however, did not significantly decrease viability for pig 2. As cells would always be stained using both the tetramerised sGPs and the full antibody panel, it was concluded the observed reduction in viability was acceptable, and the tetramers taken forward for subsequent study. Tetramers of sGP2 and sGP4 were also assembled and taken forward for staining. (**Figure 4.7**). Previously cryopreserved PBMCs from each of the six heterologous challenge animals were stained with each tetramer and the antibody panel designed to identify B cells expressing surface IgG, IgM, and IgA (**Figure 4.8**).

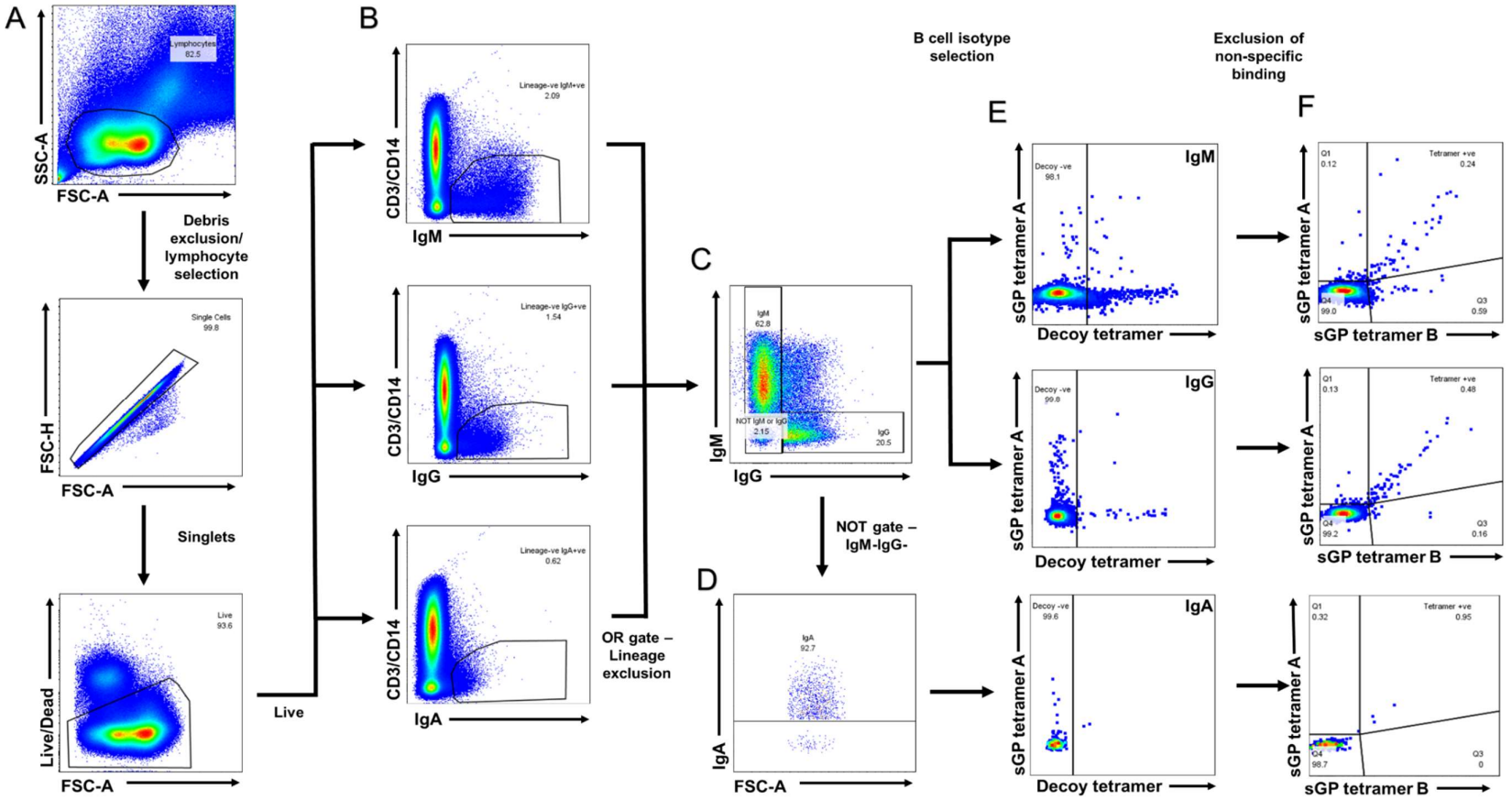


Figure 4.7: Representative gating strategy used to determine sGP-tetramer specific IgG, IgM, and IgA B cells. Cells were initially gated to exclude debris, non-lymphocyte cells, doublets, and dead/dying cells (**A**). B cells were identified as $CD3^-$ $CD14^-$ and BCR^+ (**B**). A Boolean OR gate enabled further separation of each B cell isotype (**C**). Using a Boolean NOT gate, any $CD3^-$ $CD14^-$ cells that were also IgM^- IgG^- were identified as IgA^+ (**D**). For each isotype, non-specific binding cells were excluded through use of a decoy antigen tetramer (**E**). Finally, cells that were double positive, binding both sGP tetramer A and B, were identified as antigen-specific (**F**). One biological repeat, using sGP3-tetramers, is shown.

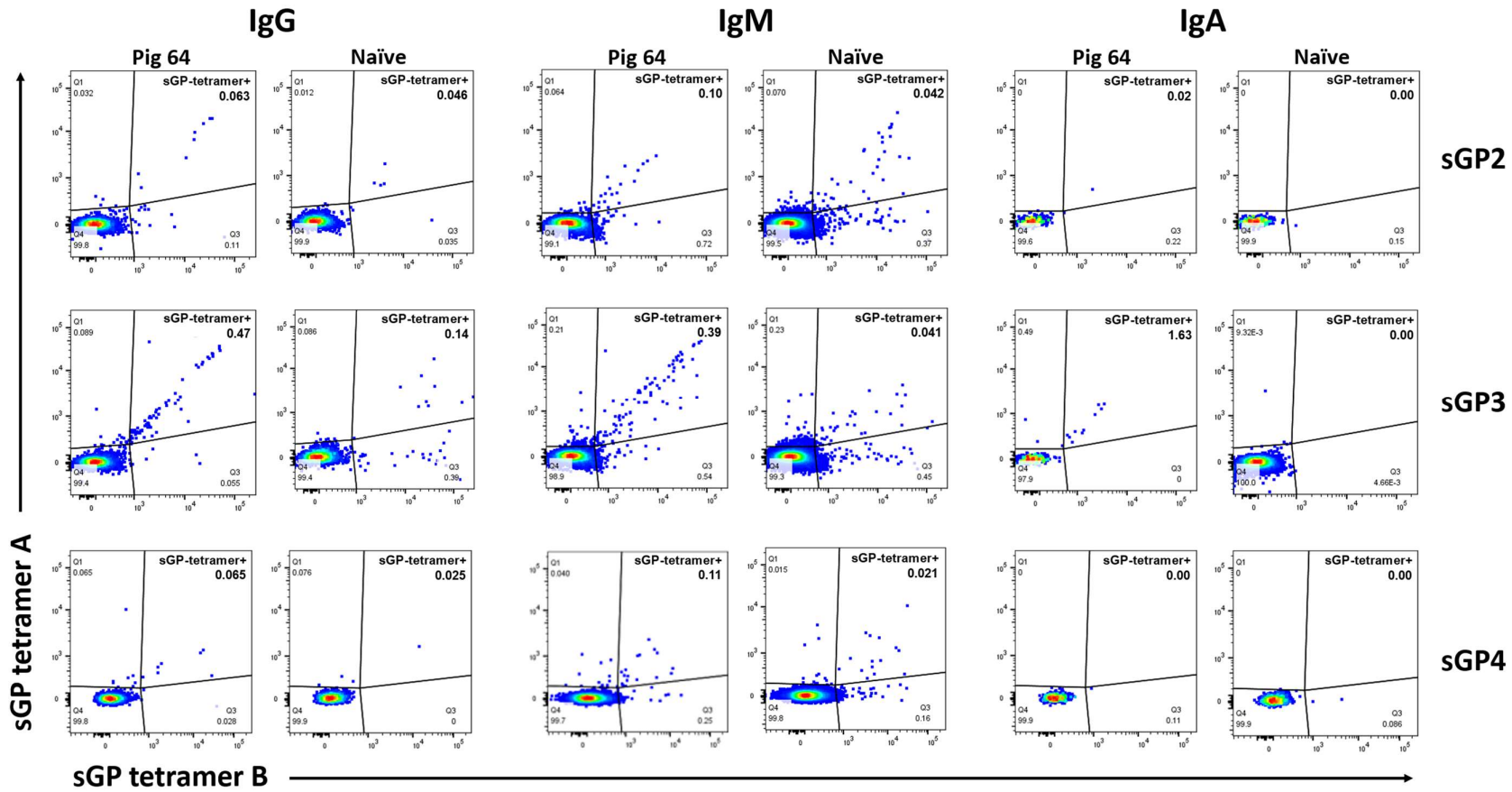


Figure 4.8: Representative flow cytometric dot plots of IgG, IgM and IgA expressing B cells stained with recombinant sGP tetramers. PBMCs from a PRRSV-immune pig (pig 64) are compared to a PRRSV-naïve pig (naïve). Cells binding to the decoy tetramer, assembled using a non-PRRSV antigen have been excluded. Cells in Q1 and Q3 (top left and bottom right respectively) are also excluded, with those in Q2 (top right) being considered true binders to the recombinant GP tested.

The proportion of double tetramer positive events from each B cell isotype was plotted to compare B cell staining amongst the six hyperimmune pigs and a naïve control (**Figure 4.8**).

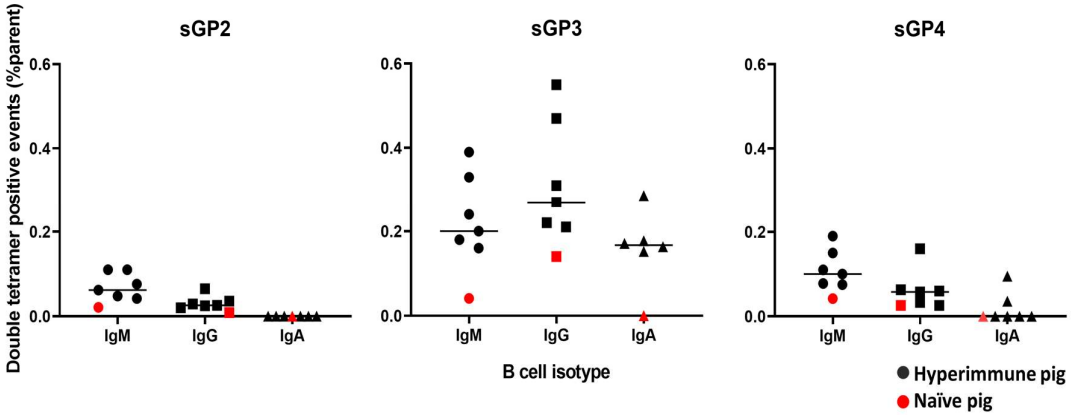


Figure 4.9: Proportion of recombinant PRRSV glycoprotein-specific B cells were identified by tetramer staining. Peripheral blood mononuclear cells isolated from a PRRSV-naïve pig and from the endpoint (148 dpi) of n = 6 pigs from a heterologous PRRSV challenge experiment were stained using an antibody panel including tetramerised recombinant PRRSV sGPs. IgM, IgG, or IgA expressing B cells that were dual labelled for the sGP tetramers and were negative for the decoy tetramer are shown.

As with the ELISA data, flow cytometric staining highlighted the lack of binding to sGP2, with only PBMCs isolated from pig 64 exhibiting significant IgG binding above the naïve animal. While there was no significant IgA binding, a comparatively large proportion of IgM^+ cells recognised sGP2, with PBMCs from pig 60, 62, 64, and 67 all demonstrating significant binding above the naïve animal (adjusted *P* value = 0.0078 for pigs 60, 64, and 67, and adjusted *P* value = 0.0445 for pig 62). The number of tetramer positive events demonstrated by the other two animals was not statistically significant. The sGP3 response appeared to remain the dominant between the three recombinant sGPs tested. PBMCs isolated from all six challenge study animals demonstrated a significantly higher proportion of IgM^+ and IgA^+ sGP3-tetramer positive events compared to

the naïve animal (adjusted *P* value = 0.026 for pig 60, = 0.0129 for pig 62, = 0.0153 for pig 64 and = 0.0578 for pig 67). Due to the high background staining observed, PBMCs from pig 63 and 69 did not demonstrate a statistically significant proportion of IgG^+ sGP3-tetramer positive events. Although comparable sGP4 responses were observed by ELISA from pig 60 and pig 64, this was not reflected in the PBMC staining data. While the PBMCs isolated from pig 60 showed significantly higher proportion of IgG^+ binding (adjusted *P* value = 0.0727), this was not consistent with IgM^+ and IgA^+, with only cells isolated from pig 69 demonstrating a significant proportion of staining for either isotype (adjusted *P* value = 0.0935 for both IgM^+ and IgA^+). Proportions of sGP4-tetramer specific cells isolated from pig 64 appeared to fall well within the average, being comparable to the naïve for all three isotypes.

4.4 Discussion

The aim of this chapter was to demonstrate recombinant PRRSV glycoproteins produced in a mammalian system were antigenic, and as such could be used as tools to elicit specific binding from PRRSV-reactive material.

Collectively the studies in this chapter showed that, compared to sGP2 and sGP4, sGP3 consistently elicited greater binding by serum antibodies from PRRSV-challenged/immunised animals, regardless of the infection regime. GP3 has been shown to possess the largest number of antigenic regions [205], which may contribute to the discrepancy in response between it and sGP2/sGP4. Much of these data reflect the responses of animals that have been MLV vaccinated, rather than exposed to natural infection. Even the animals detailed as part of

Figure 4.5, had received a combination of vaccinations as well as experimental challenge, and so it is possible that this is not representative of natural infection. While the immunogenicity of GP3 is well documented, considerably higher titres than those reported here against GP2 and GP4 have been detailed in other studies [219]. Though GP4 has been reported as possessing highly antigenic neutralising epitopes [127, 174, 202], this was not well reflected in the data presented in this chapter.

Another explanation for the difference in response between GP3 and GP2/GP4 is that despite possessing a large number of antigenic regions, the majority are non-neutralising [127], likely serving as decoy epitopes [218]. This may explain why the responses observed were so much higher than sGP2 or sGP4. There is some debate as to whether GP4 possess decoy epitopes [126, 127], which the results of this study could not address, but there is no evidence of GP2 possessing any.

Worth highlighting are the inconsistent results observed in the responses against sGP2 and sGP4 described throughout this chapter. Though some of the animals from the heterologous challenge study demonstrated significant sGP4-specific antibody responses, this was not the case for the larger cohort of animals. Furthermore, despite statistically significant responses being detected against sGP2 by sera from all four pigs from the heterologous challenge study in one assay, these responses were very low. No significant responses could be detected following subsequent analysis across the full duration of this study. This highlights the limitations of the assays described throughout this chapter. It is possible that the responses to sGP2 and sGP4 were close to the limit of detection

for ELISA, which would be one explanation for the inconsistencies in responses observed. Within assays, responses against sGP2 and sGP4 also appeared inconsistent. Particularly for sGP4, where some animals responded significantly higher than others in their cohort. It has been demonstrated experimentally that GP4-specific nAbs offer little protection against more heterologous strains [127]. It is possible that, as the recombinant sGP4 is based on the PRRSV-1 Olot/91 sequence, animals repeatedly infected with Olot/91 [252] demonstrated a greater average response than the other animals assessed in this chapter. This could potentially explain the discrepancies between the heterologous challenge study pig responses: pig 60 and pig 64, which demonstrated significantly higher sGP4 than the rest of the cohort, could possess a greater proportion of antibodies specific to the PRRSV-1 Olot/91 GP4 sequence.

This, however, would not explain the differences observed between the ELISA data and PBMC tetramer staining data. Despite the significant binding demonstrated by the end point pig 64 sera, PBMCs isolated from the same time point failed to demonstrate a statistically significant proportion of sGP4-tetramer binding B cells (of any isotype). Due to limitations of the panel used, it was not possible to differentiate between memory and plasma B cells by flow cytometry. While GP4-specific antibody titres were detected in the serum for some of these animals tested, it is possible that the majority of circulating B cells were memory B cells and so proportionally lower binding was seen following tetramer staining. For this workflow, only PBMC samples were analysed. Several other immune associated tissue samples, i.e., spleen, retropharyngeal lymph nodes, and bronchoalveolar lavage fluid, were stored as part of this challenge study. With the

results described in this chapter demonstrating that the recombinant sGPs are antigenic, attempting sGP4-tetramer staining with these additional tissues may help resolve the discrepancies observed between the two assays, and further determine which immune associated tissues are contributing most to the serum antibody titres observed.

A considerable proportion of PRRSV-specific IgM^+ cells were detected when screening with both sGP2 and sGP4. The proportion, on average, of sGP3-specific B cells were comparable between isotypes. It is interesting, furthermore, that such a relatively large proportion of PRRSV-specific IgA, usually a mucosal immunity associated antibody isotype [281], was detected in cells isolated from the blood. For the work presented throughout this chapter, a polyclonal anti-IgG H+L antibody was used in the detection of PRRSV-specific antibodies. While it was assumed that the majority of these responses would be IgG, it is possible that IgA and IgM antibodies were contributing to the ELISA responses observed. In hindsight, assessing responses against each sGP using IgA-, IgA-, and IgM-specific detection antibodies may have yielded a more complete dataset. This was discussed but, due to time constraints, was not explored.

Worth highlighting is the differences observed between responses against the glycosylated, and deglycosylated sGP3. As has been discussed in previous chapters, PRRSV GPs are heavily glycosylated proteins [282], with these glycans being implicated in the shielding of neutralising epitopes [128, 129] and discussed several times thus far is the different levels of N-glycosylation occupancy for these recombinant GPs. In literature it is not always clear whether the presence of glycans will alter the immunogenicity of the recombinant antigen [283, 284],

however if these recombinants, comprising multiple glycoforms, elicit varied binding based on their glycosylation state, this may limit their efficacy as tools. It is possible that the differences in serum binding observed may be an artifact of the non-specific binding to the glycan sugars, and as such this signal is reduced following PNGase F digestion. Another possibility may be that there are distinct confirmation epitopes which disappear when the protein is deglycosylated.

Overall, this chapter has demonstrated the potential of recombinant PRRSV GPs as tools to identify PRRSV-specific B cells and could be used to isolate mAbs with neutralising capacity. One must be cautious not to over-interpret these data, however. Without direct comparison to the native PRRSV GPs, the results detailed in this chapter largely demonstrate specific binding to the recombinant sGPs. While these responses were largely significant compared to those seen against control antigens, or by PRRS-naïve sera, they may not be truly representative of the responses against the native antigens.

sGP3 demonstrated the capability to elicit strong binding from PRRSV-reactive sera, and appeared to have kinetics that closely correlated with neutralisation titres, suggesting that sGP3-specific antibodies may contribute to the neutralising response. sGP2 and sGP4 also appear to have some potential, but clearly require greater optimisation. Though sGP2 largely failed to elicit binding from PRRSV-reactive sera, sGP2-tetramer specific B cells could still be identified and, as such, sGP2 could be used to isolate mAbs. This is a similar case for sGP4 and, though sGP3 was ultimately selected for use in the work detailed in the next chapter, with a workflow now established these two sGPs hold great potential for follow up investigation.

Chapter 5. Isolation and characterisation of PRRSV-1 GP3 specific porcine monoclonal antibodies

5.1 Rationale

To date, single antigen-specific human B cells have been efficiently isolated by flow cytometry based on fluorescently labelled antigens as rationally designed probes. Utilising tetramerised HIV-1 antigens of the trimeric envelope such as GP120 [285, 286], isolation of HIV-1 specific B cells has enabled the generation of mAbs capable of broad neutralisation. As has been discussed, isolation of single PRRSV-specific B cells has been demonstrated [175], utilising tetramerised recombinant PRRSV proteins, in a similar manner proposed for this project. Despite being isolated from a donor animal that had previously demonstrated broad PRRSV-neutralising capacity, none of the mAbs generated by that study were capable of neutralising PRRSV infectivity. It is worth noting that the antigens, PRRSV GP2, GP3, GP4, GP5, and M proteins, used in this study were generated in an *E. coli* expression system, and so lack the post-translational modification that would be seen in the native virus. This may have contributed to the lack of neutralising mAbs generated. The previous chapters in this thesis have highlighted the importance of proper folding and glycosylation for PRRSV glycoproteins, and the implications of these properties in immune recognition. The experiments described in the previous chapter established the potential of recombinant glycoproteins as a tool for isolating PRRSV-specific B cells and generating mAbs. This chapter, therefore, details the use of tetramerised sGP3 to isolate these B cells, and the subsequent generation and characterisation of recombinant mAbs. Only sGP3 was selected to be taken forward in the first instance, due to the greater yields produced, and observed greater antigenicity described in **Chapter 4**.

Of the six heterologous PRRSV challenge study animals, pig 64 was selected as the B cell donor, having demonstrated strong sGP3 binding by both ELISA and tetramer staining, detailed in **Chapter 4**. Further, serum and B cells from pig 64 also demonstrated sGP4 binding and so was also selected with the possibility of later isolating sGP4-specific B cells, if time allowed.

5.2 Amplification of paired V(D)J genes from single sGP3-specific B cells

Twenty million previously cryopreserved PBMCs isolated from pig 64 at 148 dpi were co-stained with the tetramer panel and established antibody panel [243] to determine BCR, described previously in **Chapter 4**. All decoy-tetramer positive events were excluded, and double sGP3-teramer positive events were isolated by flow cytometric single cell sorting into 96 well plates containing 10 µL/well of cell collection buffer: 0.01M Tris (pH 8.0), 100 units RNasin® Ribonuclease Inhibitor, diluted in RNase-free water. Sorted cells were backgated post-sorting to ensure only double-tetramer-positive, IgG-positive events were isolated (**Figure 5.1**).

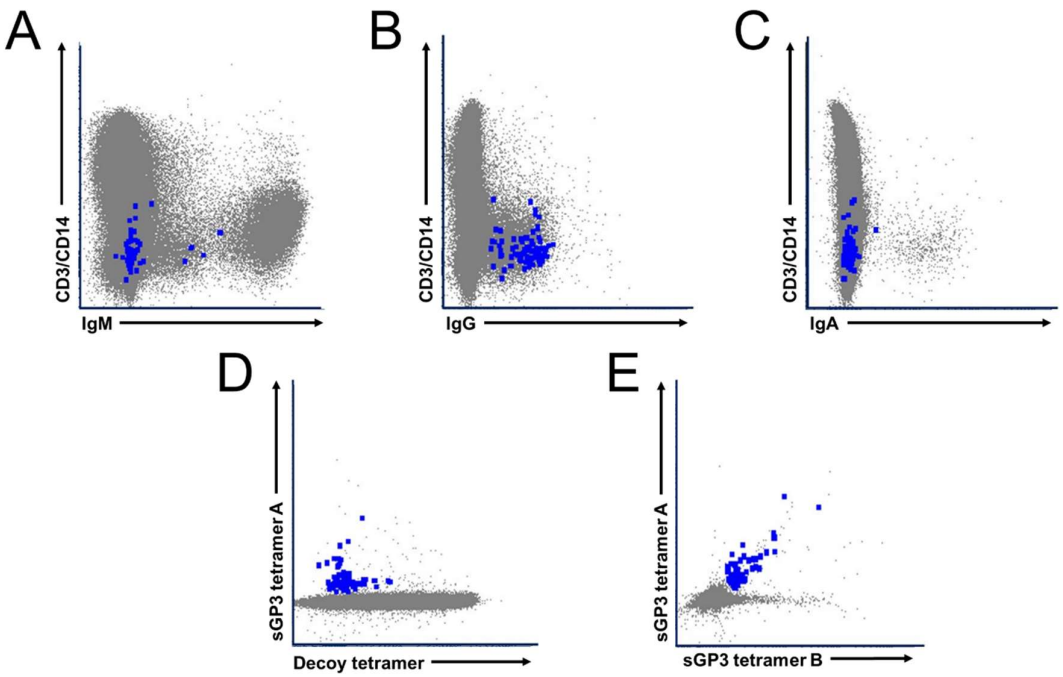


Figure 5.1: Gating highlighting single B cells isolated using sGP3-tetramers. Previously cryopreserved PBMCs from pig 64 were taken through flow cytometric analysis to identify PRRSV-1 sGP3 specific IgG^+ B cells. Live, $CD3/CD14^-$, IgM^- (**A**), IgG^+ (**B**), IgA^- (**C**), decoy $tetramer^-$ (**D**), sGP3 tetramer A/B^+ (**E**) cells were sorted as single cells; highlighted throughout in blue.

Back gating revealed a proportion of the tetramer sorted events were IgM^{dim}, despite the gating strategy focussing on IgG^+ cells only. Despite this, the majority of tetramer sorted events were $CD3/CD14^-$, IgG^+, IgA^-, decoy $tetramer^-$, double sGP3 $tetramer^+$, as intended. Of the 110 sorted single cell events, 96 were taken forward for processing. RNA was extracted from the sorted single B cells, and cDNA synthesised. Prior to VH and VL amplification, each sample was tested to assess cDNA quality, using a reference gene PCR designed by the Immunogenetics Group at The Pirbright Institute (**Figure 5.2**). GAPDH was selected as the reference gene.

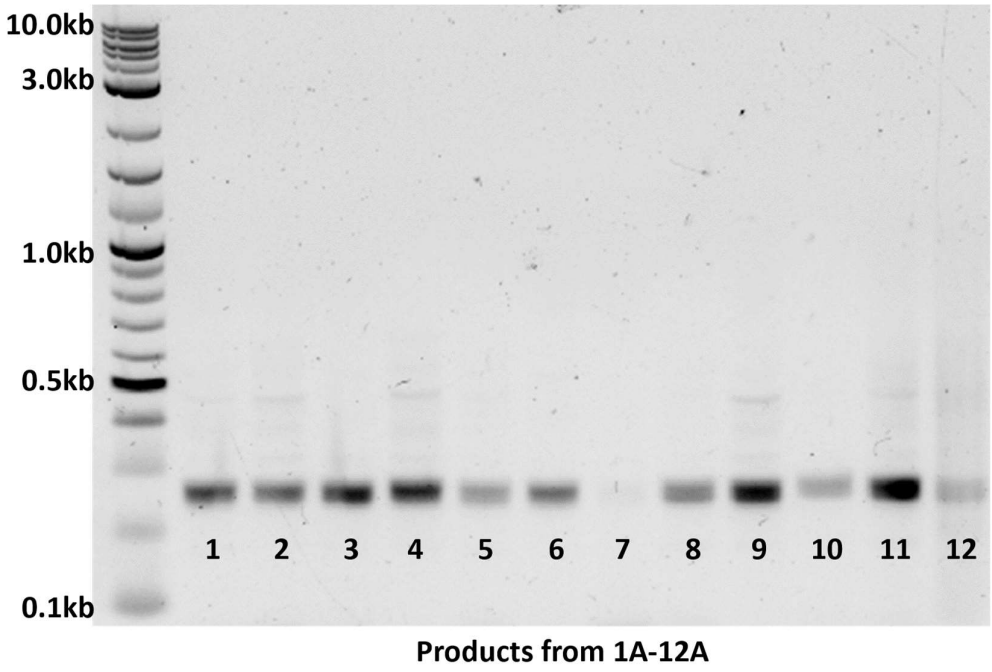


Figure 5.2: Representative gel electrophoresis image of GAPDH amplicons from isolated single cell cDNA. Cells isolated using sGP3-tetramers were used as a template. Twelve samples are shown (wells 1A – 12A); expected product size was 247bp.

This reference gene PCR revealed that on average cDNA from 70/96 wells were of high enough quality for GAPDH amplification. Subsequently, cDNA from all cells from which GAPDH could be amplified was taken through a semi-nested PCR, to amplify the variable region domains of IgG (VH) and, Igκ, and Igλ (VL). Final amplicons were imaged by gel electrophoresis to confirm successful amplification of products of the correct size (**Figure 5.3**).

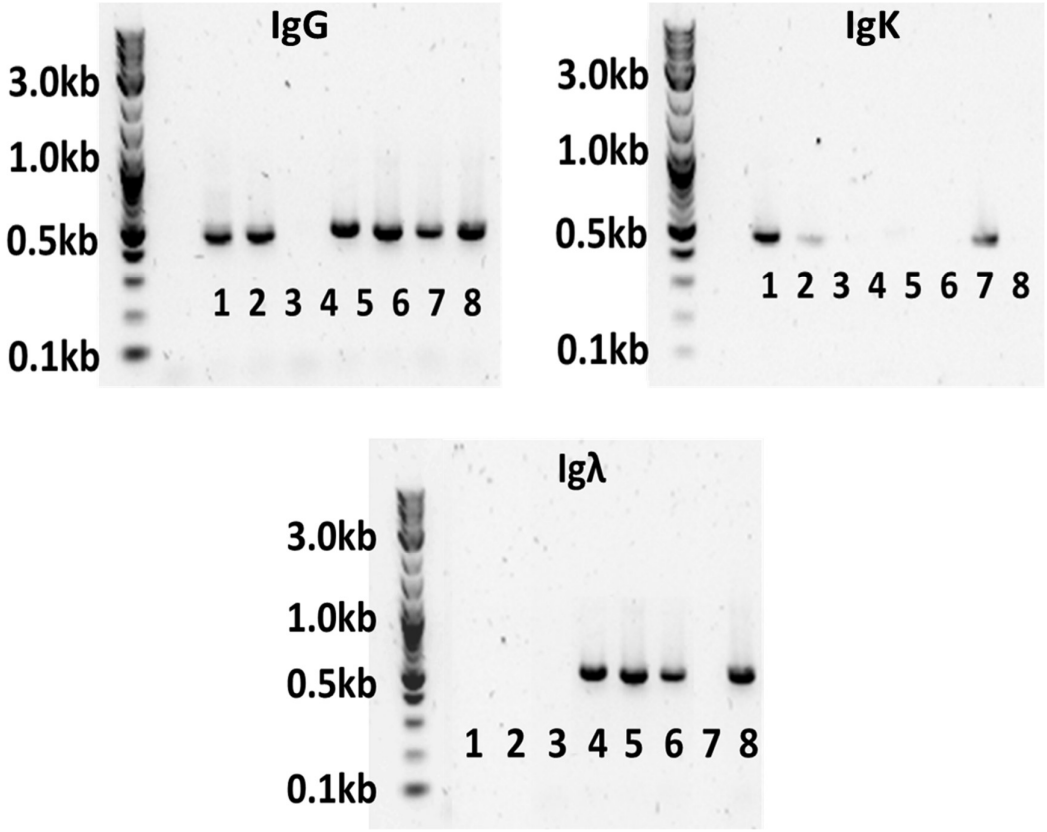


Figure 5.3: Representative gel electrophoresis image of V(D)J amplicons of IgG heavy chains and either kappa or lambda light chains from isolated single B cells. Representative images of each are shown for eight single cells (1 – 8). Cell 3 is an example whereby neither VH nor VL genes could be amplified, despite reference gene amplification. Expected product sizes were 472 bp for VH chains, 477-512 bp kappa chain, and 422-477 bp for lambda chain.

In total, 37 pairs of VH and VL amplicons were successfully amplified from single cells. VH alone was amplified from approximately 60% of isolated single cells, with 53 IgG VH chains being amplified. VL amplification was limited to approximately 40% of the isolated cells, with a total of 39 total VL chains being amplified. There were 2 instances whereby VL chains were amplified, with no corresponding VH chains.

Each amplicon was then submitted for Sanger sequencing. During imaging, conflicting Igκ, and Igλ amplicons were observed: suggesting there were isolated

single cells that appeared to express both Igκ, and Igλ VL chains simultaneously. Sequencing revealed the observed conflicting light chains were identical to those in other wells, and likely a result of cross-contamination during PCR. The conflicting sequences were disregarded and removed from further processing. In total 16 VH and VL pair sequences were identified.

5.3 Annotation and comparison of sequences

Utilising the IMGT® information system, each of the 16 paired sequences were annotated, enabling comparison of the complementarity determining regions (CDRs) for VH (**Table 5.1**) and VL (**Table 5.2**) sequences.

Code	CDR1-IMGT	CDR2-IMGT	CDR3-IMGT
IgG1-2G	GFDFSDNS	IATGDYDGGT	ATTPRLTIAVAIAVIGVAGYRPVMDL
IgG1-4D	**GFTFSSTY**	LTSSGSVT	AIGYIEGSATYYGMDL
IgG1-5E	RVTFSSIY	ISNSGSMT	ARCFGYGGGCYAGFYVMDL
IgG1-5F	GITFTNTY	MTTVGGVT	AIGYTGASATYYGMDL
IgG1-7A	**GFTFSSTY**	LTSSASVT	AIGYVGGSATYYGMDL
IgG1-7E	GFTFSSDF	ISNSGDNT	VRGCGGHALDL
IgG1-9D	EAISIYS	IGRSGTNT	EGSCSNCPSPSTVNL
IgG1-11A	RFTFSTYE	ISTRGSSF	TGGHRCYGLFGGCFGWFGDYYAMHL
IgG1-11B	**TRDIRRYG**	**IGSVSYLGST**	**ARVGCYCNGGSWYADRPVFMDL**
IgG1-11C	**HETSGVMA**	**IGSVSYLGST**	**ARVGCYCNGGSWYADRPVFMDL**
IgG1-11D	**HETSGVMA**	**IGSVSYLGST**	**ARVGCYCNGGSWYADRPVFMDL**
IgG1-11E	LRTSGVMA	**IGSVSYLGST**	**ARVGCYCNGGSWYADRPVFMDL**
IgG1-11F	RKQKTQAL	IGSVNYLGSS	QEWVATAMLVVGMLSGPSLWI
IgG1-12B	KRHQALWR	**IGSVSYLGST**	**ARVGCYCNGGSWYADRPVFMDL**
IgG1-12C	**TRDIRRYG**	**IGSVSYLGST**	**ARVGCYCNGGSWYADRPVFMDL**
IgG1-12D	**TRDIRRYG**	**IGSVSYLGST**	**ARVGCYCNGGSWYADRPVFMDL**

Table 5.1: Complementarity determining regions for each VH IgG sequence were annotated utilising the international ImMunoGeneTics information system®. Each isolated single cell was assigned a code to keep track of paired VH and VL sequences. Repeated sequences are highlighted in red.

Code	CDR1-IMGT	CDR2-IMGT	CDR3-IMGT
IgLC-κ2G	QSLLHTDGANY	YAT	FLSLQSPYG
IgLC-λ4D	LLDKKY	**KDS**	**QSADNIHNVI**
IgLC-λ5E	SLLDAK	**KDS**	QSADSLDSVP
IgLC-λ5F	FAGTKY	RTM	**QSADNIHNVI**
IgLC-λ7A	**YLLDKK**	**KDS**	**QSADNIHNVI**
IgLC-λ7E	**YLLDKK**	**KDS**	**QSADNIHNVI**
IgLC-λ9D	SGRNR	NDS	RSPDISGHLV
IgLC-κ11A	LTLPTNGAFG	RLP	**QQFKEFPRG**
IgLC-κ11B	RCRRMEHLR	**EAT**	**QQFKEFPRG**
IgLC-κ11C	**SDAADEWSLW**	**EAT**	**QQFKEFPRG**
IgLC-κ11D	**SDAADEWSLW**	**EAT**	**QQFKEFPRG**
IgLC-κ11E	ASDAADEPYR	ATN	**QQFKEFPRG**
IgLC-κ11F	AHLTLPTNGH	**GYQ**	**QQFKEFPRG**
IgLC-κ12B	**RCRRMEAIC**	**EAT**	**QQFKEFPRG**
IgLC-κ12C	DAADEWRFDN	**GYQ**	**QQFKEFPRG**
IgLC-κ12D	**RCRRMEAIC**	**EAT**	**QQFKEFPRG**

Table 5.2: Complementarity determining regions for each VL IgK and IgL sequence were annotated utilising the international ImMunoGeneTics information system®. Each isolated single cell was assigned a code to keep track of paired VH and VL sequences. Repeated sequences are highlighted in red.

Annotation of CDR motifs revealed several instances of repeated sequences. Furthermore, it was determined that, although some VH sequences (i.e., IgG1-11C and IgG1-11D) were identical, their respective VL sequences differed. Only one of each repeat was selected to be taken forward in each instance, resulting in 15 unique heavy and light chain pairs. All the amplified heavy chains were IgG1.

From these same annotations, distance of each sequence from the germline V gene, and which allele these sequences originated from, was also determined (**Tables 5.3, Table 5.4**).

VH Sequence	Closest germline V gene and allele	Identity (%)
IgG1-2G	IGHV1-6*01	94.56
IgG1-4D	IGHV1-10*01	92.01
IgG1-5E	IGHV1-4*02	93.75
IgG1-5F	IGHV1-10*01	93.40
IgG1-7A	IGHV1-10*01	90.97
IgG1-7E	IGHV1-4*02	90.97
IgG1-9D	IGHV1-8*01	89.58
IgG1-11A	IGHV1-14*01	92.36
IgG1-11B	IGHV1-11*01	94.56
IgG1-11C	IGHV1-11*01	94.22
IgG1-11D	IGHV1-11*01	94.90
IgG1-11E	IGHV1-11*01	94.22
IgG1-11F	IGHV1-11*01	93.20
IgG1-12B	IGHV1-11*01	94.56
IgG1-12C	IGHV1-11*01	94.90
IgG1-12D	IGHV1-11*01	94.56

Table 5.3: Closest germline V gene was assigned to each VH sequence from isolated single cells. Nucleotide identity between sequenced VH regions from isolated single cells and germline V genes were compared utilising the international ImMunoGeneTics information system®. The allele of each V gene is detailed following an asterisk (*).

VL Sequence	Closest germline V gene and allele	Identity (%)
IgLC-κ2G	IGKV2-10*02	93.54
IgLC-λ4D	IGLV3-3*01	96.42
IgLC-λ5E	IGLV3-3*01	87.81
IgLC-λ5F	IGLV3-3*01	97.49
IgLC-λ7A	IGLV3-3*01	96.77
IgLC-λ7E	IGLV3-3*01	96.77
IgLC-λ9D	IGLV3-3*02	93.55
IgLC-κ11A	IGKV2-13*02	70.79
IgLC-κ11B	IGKV2-13*02	68.42
IgLC-κ11C	IGKV2-13*02	69.10
IgLC-κ11D	IGKV2-13*02	67.01
IgLC-κ11E	IGKV2-13*02	67.01
IgLC-κ11F	IGKV2-13*02	68.04
IgLC-κ12B	IGKV2-13*02	71.93
IgLC-κ12C	IGKV2-13*02	68.04
IgLC-κ12D	IGKV2-13*02	71.93

Table 5.4: Closest germline V gene was assigned to each VL sequence from isolated single cells. Nucleotide identity between sequenced VL regions from isolated single cells and germline V genes were compared utilising the international ImMunoGeneTics information system®. The allele of each V gene is detailed following an asterisk (*).

Apart from IgLC-κ2G, all VL Igκ sequences had significantly lower nucleotide identity with their respective germline sequences than the VL Igλ, or VH IgG sequences, which (with the exception of IgLC-λ5E at 87.81% identity) all had >90% identity with their respective closest germline V gene.

Following annotation, each sequence was trimmed down starting at the FR1 motif in the V region and ending with a short, 15-18 nucleotide portion of the C region, and overhang sequences added to enable cloning into the pNeoSec suite of vectors (as detailed in **Chapter 2**). Synthetic gene blocks were generated for each VH and VL sequence and cloned into porcine expression vectors containing the full constant regions of the Igκ and Igλ VL chains and IgG1 VH chain [287] which could then be expressed.

5.4 Cloning, expression, and purification of recombinant mAbs

Following cloning and DNA plasmid preparation, insertion was confirmed by colony PCR, comparing bacteria transformed with the cloned cassettes and those transformed with the vector only, and imaged by gel electrophoresis (**Figure 5.4**).

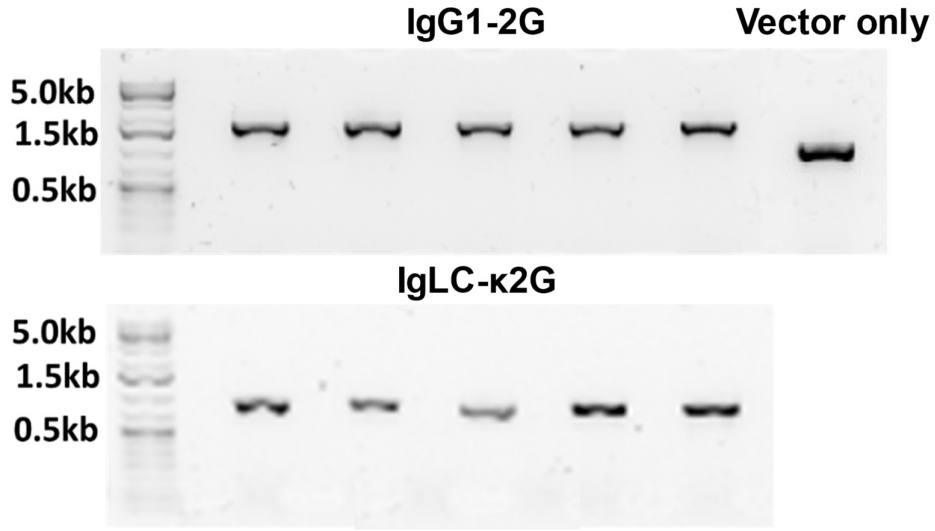


Figure 5.4: Colony PCR of recombinant mAb clones. Insertion of recombinant V(D)J genes was visualised on an agarose gel. Five replicate mAb 1 VH (IgG1-2G) and VL (IgLC-κ2G) clones are shown as representative images, compared to a IgG1-Fc vector only control.

Correct orientation of all clones was subsequently confirmed by submitting triplicates for each clone for Sanger sequencing. Sequencing revealed correct insertion of all VH and VL sequences, pairs of which were then taken forward for expression. Expi293F cells were co-transfected with the corresponding VH and VL constructs, to generate a total of 15 mAbs (**Table 5.5**).

mAb	VH clone	VL clone
1	IgG1-2G	IgLC-κ2G
2	IgG1-4D	IgLC-λ4D
3	IgG1-5E	IgLC-λ5E
4	IgG1-5F	IgLC-λ5F
5	IgG1-7A	IgLC-λ7A|7E
6	IgG1-7E	IgLC-λ7A|7E
7	IgG1-9D	IgLC-λ9D
8	IgG1-11A	IgLC-κ11A
9	IgG1-11B|11C|11D|12C	IgLC-κ11B
10	IgG1-11B|11C|11D|12C	IgLC-κ11C
11	IgG1-11B|11C|11D|12C	IgLC-κ11D
12	IgG1-11E	IgLC-κ11E
13	IgG1-11F	IgLC-κ11F
14	IgG1-11B|11C|11D|12C	IgLC-κ12C
15	IgG1-12B|12D	IgLC-κ12D

Table 5.5: Fifteen recombinant mAbs were expressed in Expi293F cells by co-transfecting with paired VH and VL plasmids.

Paired VH and VL sequences from together assigned a mAb number from 1 to 15, to make subsequent analysis simpler. Three days post-transfection, cell culture supernatants were tested for expression by western blot (**Figure 5.5**).

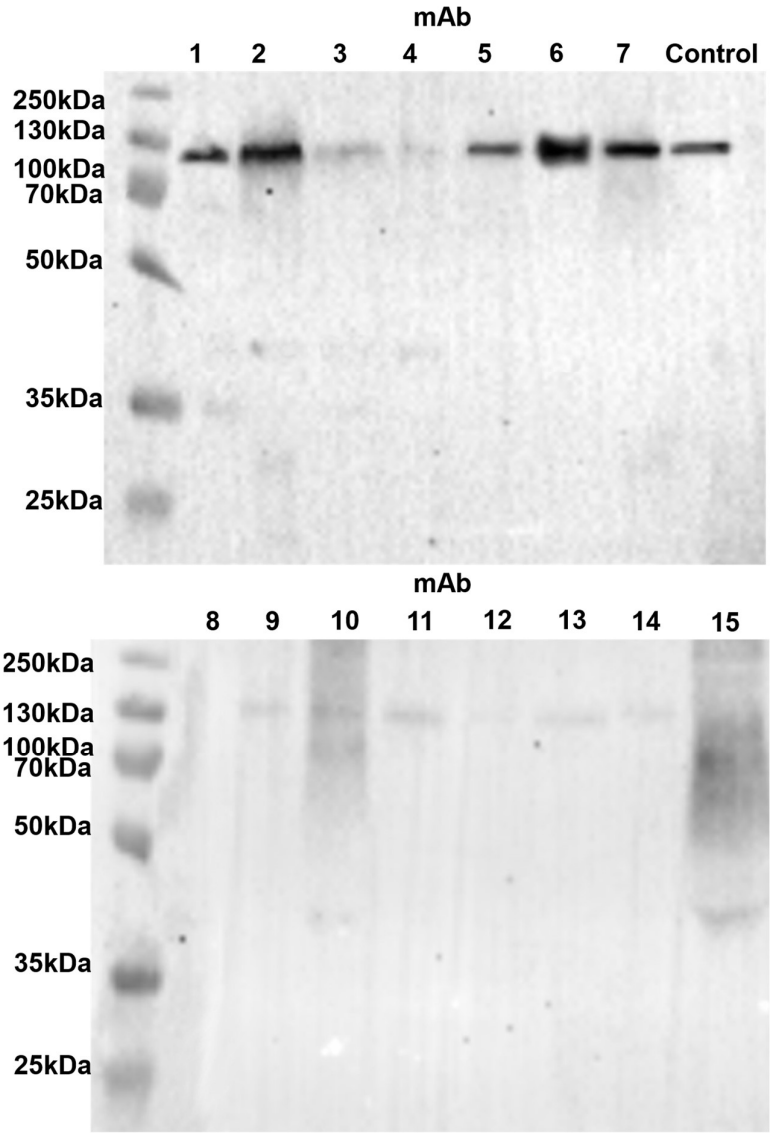


Figure 5.5: Recombinant monoclonal antibody expression from transfected Expi293F cells was assessed by western blot. Cell culture supernatant samples were run under non-reducing conditions and probed for with an IgG (H+L) secondary antibody. In addition to the 15 mAbs isolated from PRRSV-immune pig 64, a recombinant Nipah virus-glycoprotein specific mAb – generated by the PRRS Immunology Group, The Pirbright Institute, utilising the same methods – was included as a control.

Analysis by western blot highlighted some discrepancies in expression amongst the mAbs. mAbs 1, 2, 5, 6, and 7 were all represented by strong bands, comparable to the control mAb. mAbs 3, 4, 9, 11, 12, 13, and 14 were all detectable, but were represented by faint bands, with some being close to the

limit of detection. mAbs 10 and 15 were represented by several bands, suggesting issues during expression.

Samples were also run under standard reducing conditions side-by-side with non-reducing conditions (**Figure 5.6**).

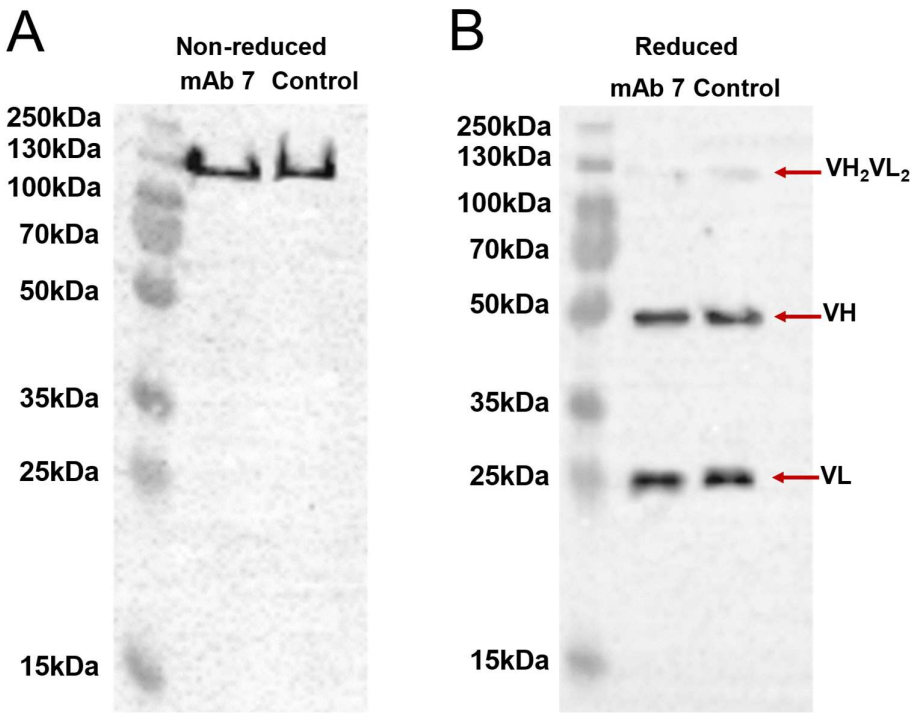


Figure 5.6: mAbs were treated under reducing conditions with the aim of breaking the disulfide bonds responsive for VH-VL chain interactions, enabling their individual visualisation by western blot. Representative gels comparing mAb 7 and a Nipah virus glycoprotein-specific control mAb shown. mAbs were run in parallel under either non-reducing (**A**) or reducing conditions (**B**). The constituent VH and VL chains are highlighted under the reduced conditions.

mAbs tested under non-reducing conditions were consistent with the previous data. The smearing and presence of several bands for mAb 10 and mAb 15 was also consistent between experiments (data not shown). Under reducing conditions, for both the experimental and control mAbs, two distinct bands could be observed. The bands at ~50 kDa likely represented the VH chains, and those

at ~25 kDa representing the VL chains, consistent with what has been described in the literature [114]. Larger bands could still be detected, comparable to the non-reduced samples, likely suggesting that there had been incomplete reduction of the mAbs. Following this, these supernatants were also assessed by ELISAs to determine the IgG concentration (**Figure 5.7A**) and reactivity against sGP3 (**Figure 5.7B**).

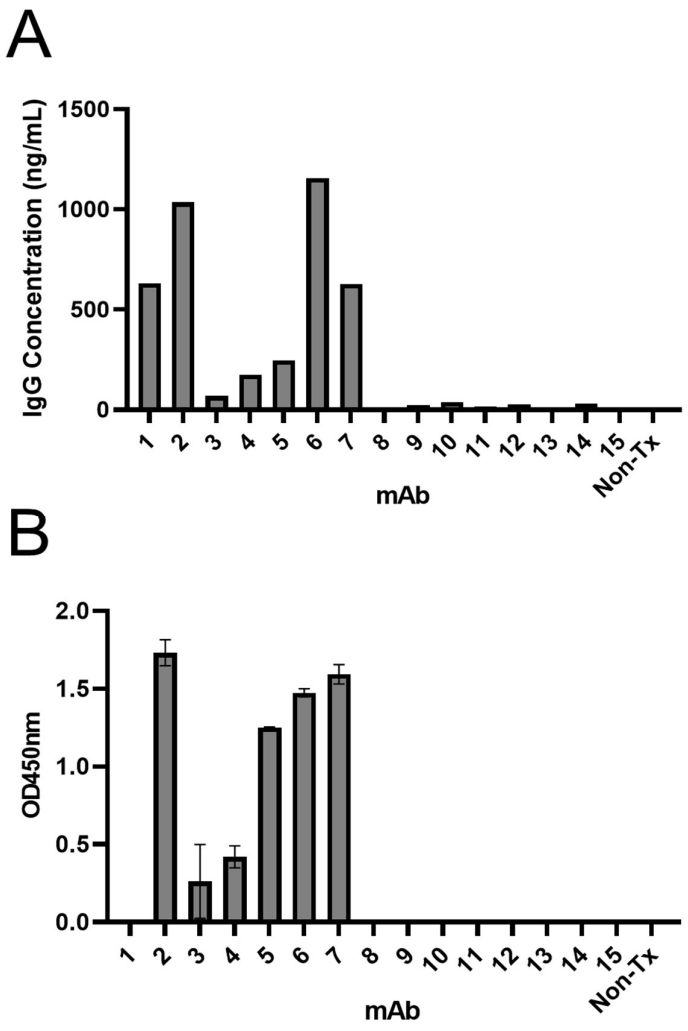


Figure 5.7: Assessment of concentration and specificity of mAbs in culture supernatants from transfected Expi293F cells. Following transfection, supernatants were screened by ELISA using an anti-pig IgG (H+L) secondary antibody, and OD values interpolated against a porcine IgG standard curve to determine concentration (**A**). Supernatants were also tested by ELISA for binding to PRRSV-1 sGP3 (**B**).

Consistent across repeats, it was observed that only half of the mAbs were expressed at a detectable level, with only mAb 1-7 giving IgG concentrations significantly above the non-transfected control (adjusted *P* value <0.0001). Interestingly, those that failed to express – mAbs 8-15 – shared highly homologous VH sequences. Despite the observation that mAb 1 expressed well, no reactivity against sGP3 could be detected by ELISA; mAbs 2 – 7 all demonstrated sGP3 reactivity.

The six mAbs that demonstrated reactivity were taken forward and more protein was produced by transfecting larger scale Expi293F cell cultures. mAbs were purified from culture supernatant utilising protein G affinity chromatography. Antibody yields were calculated by spectrophotometry, and later by BCA assay (**Table 5.6**). Yields varied greatly between mAbs, with mAb 3 and mAb 4 yields being significantly lower.

mAb	mg/litre
2	1.842
3	0.147
4	0.260
5	2.256
6	3.000
7	4.024

Table 5.6: Yields of recombinant monoclonal antibody following purification from transfected Expi293F cell culture supernatants were determined by spectrophotometry. 100mL cultures of transiently transfected Expi293F cells were established and mAb purified by protein G affinity chromatography.

Following purification, the purity of each mAb was assessed by western blot (**Figure 5.8A**) and Coomassie staining (**Figure 5.8B**) following non-reducing PAGE.

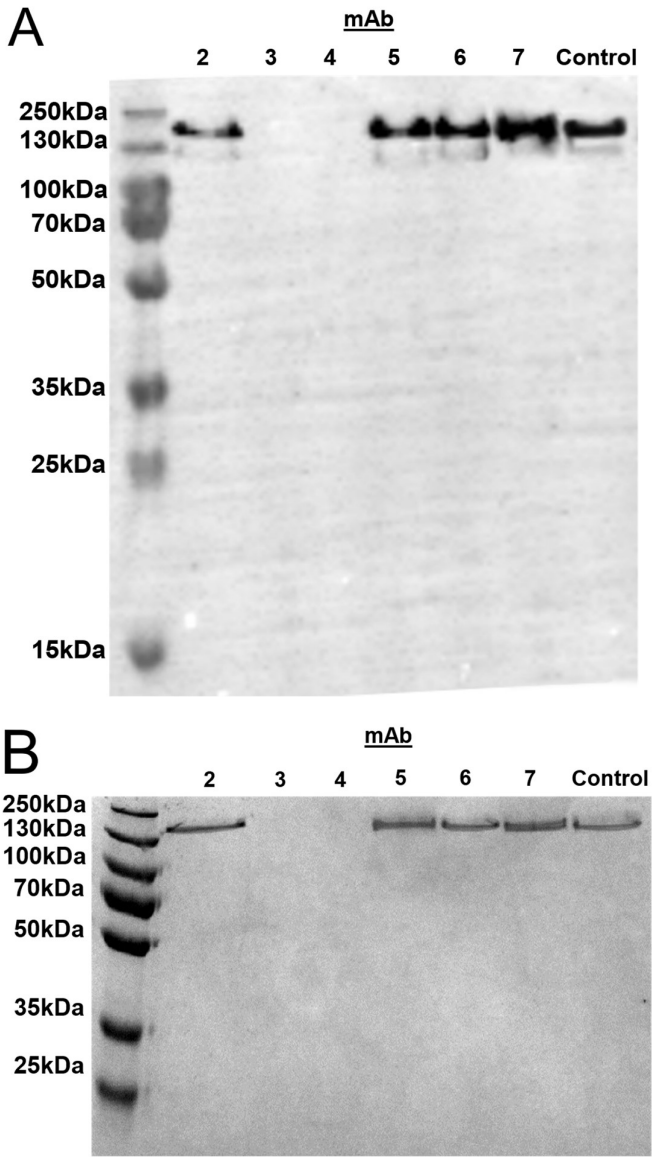


Figure 5.8: Following isolation by affinity chromatography, the purity of mAbs was assessed. mAbs 2-7, in addition to a Nipah virus glycoprotein-specific mAb –which served as a control, were assessed by western blot (**A**) and Coomassie staining (**B**). All mAbs were ran under non-reducing conditions; 10 µg of each mAb was loaded.

mAbs 3 and 4 could not be detected by this assay. mAbs 2, 5, 6, and 7 all looked comparable to the control. Despite the low protein concentration of mAbs 3 and 4, all seven mAbs were then taken forward for initial characterisation.

5.5 Characterising mAbs

Following expression, mAbs were characterised with the aim of assessing the breadth of their cross-reactivity and neutralisation capacity. The purified mAbs were first assessed for their ability to bind the recombinant PRRSV-1 sGP3 used to isolate the B cells by ELISA (**Figure 5.9**).

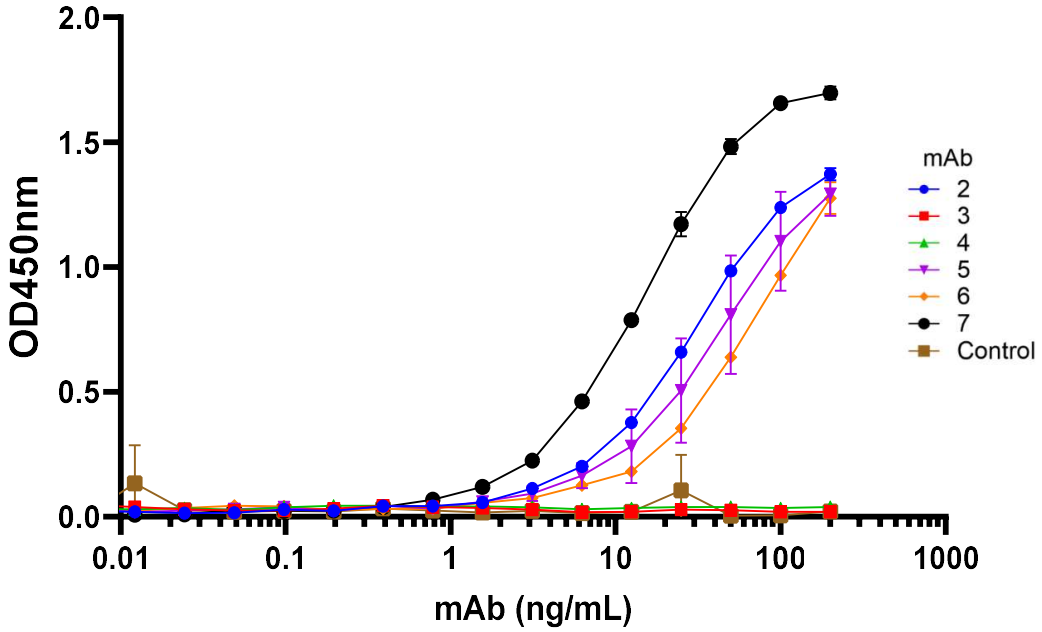


Figure 5.9: sGP3 ELISA to investigate whether purified recombinant mAbs retained antigen-specificity. Seral dilutions of mAbs from 200 – 0.1 ng/mL were tested. Mean data of two technical replicates ± SD are shown.

A two-way ANOVA revealed significant binding of mAb 2, mAb 5, mAb 6, and mAb 7 to sGP3 (adjusted *P* value <0.0001), compared to the control mAb. mAbs 3 and 4, however, did not elicit any binding that was statistically significant. The OD450

observed from mAb 7, further, was significantly higher than any of the other mAbs tested in this experiment (adjusted *P* value <0.0001). mAb 2, furthermore, showed significantly higher absorbance than mAb 5 (adjusted *P* value = 0.0258), and mAb 6 (adjusted *P* value <0.0001). There was no significant difference observed between mAb 5 and mAb 6.

The reactivity of these mAbs was tested further, investigating whether they could recognise native GP3, within PRRSV infected cells, and not restricted to recognising the recombinant sGP3. mAb binding was investigated using immunofluorescence staining of MARC-145 cells infected with PRRSV-1 Olot/91 (**Figure 5.10A**). The cross-reactivity of these mAbs was also investigated in the same assay, by utilising PRRSV-2 VR-2332 infected cells (**Figure 5.10B**).

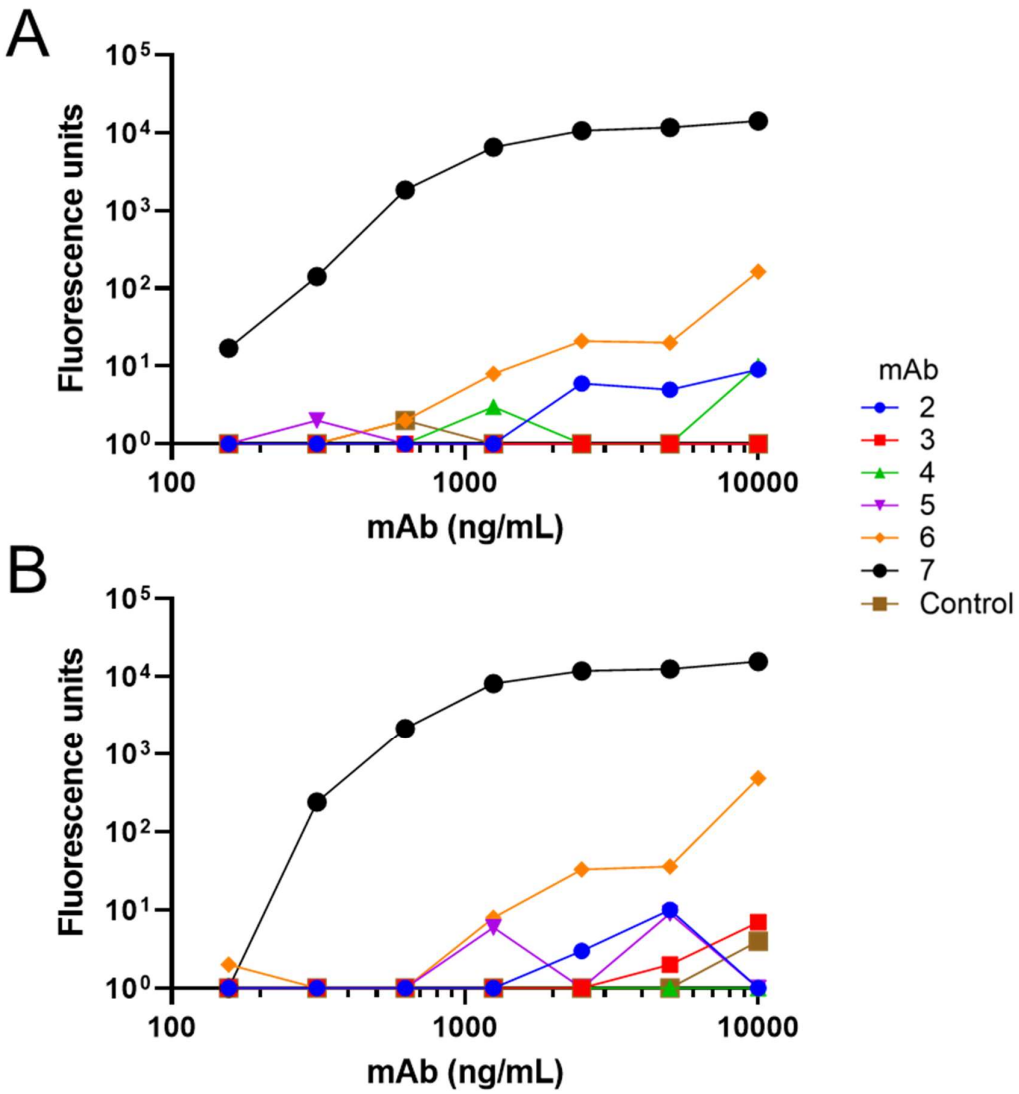


Figure 5.10: Recognition of native PRRSV antigen by recombinant mAbs was assessed by intracellular staining of PRRSV infected MARC-145 cells. Cells were infected with either PRRSV-1 Olot/91 (**A**) or PRRSV-2 VR-2332 (**B**). mAb binding was revealed by addition of a fluorescent secondary antibody and analysis using an Incucyte® SX5 Live-Cell Analysis System. Technical singlets are shown**.**

Cross-reactive recognition was observed by mAb 6 and 7, which demonstrated binding to both PRRSV-1 and PRRSV-2 infected cells. mAb 2 also demonstrated binding to PRRSV-1, however, was not seen to be capable of binding PRRSV-2 at the 10 µg/mL dilution. Worth noting is that these data were generated as technical singlets, and so likely skewed by the staining observed in a single well.

At 5 µg/mL and below, mAb 2 appeared to demonstrate significantly higher binding than what was observed at 10 µg/mL, and appear similar to what was observed against PRRSV-1. Caution should be made interpreting these data, without a greater number of replicates. mAb 3, 4, and 5 did not demonstrate any significant binding. Recognition of these mAbs against additional PRRSV-1 strains was also investigated utilising similar assays. Porcine alveolar macrophages were infected instead of MARC-145 cells due to the two strains used being non-adapted PRRSV-1 field strains. PRRSV-1 215-06 (**Figure 5.11A**) and PRRSV-1 SU1-Bel (**Figure 5.11B**) were chosen as these strains were used in the heterologous challenge study from which these mAbs were isolated.

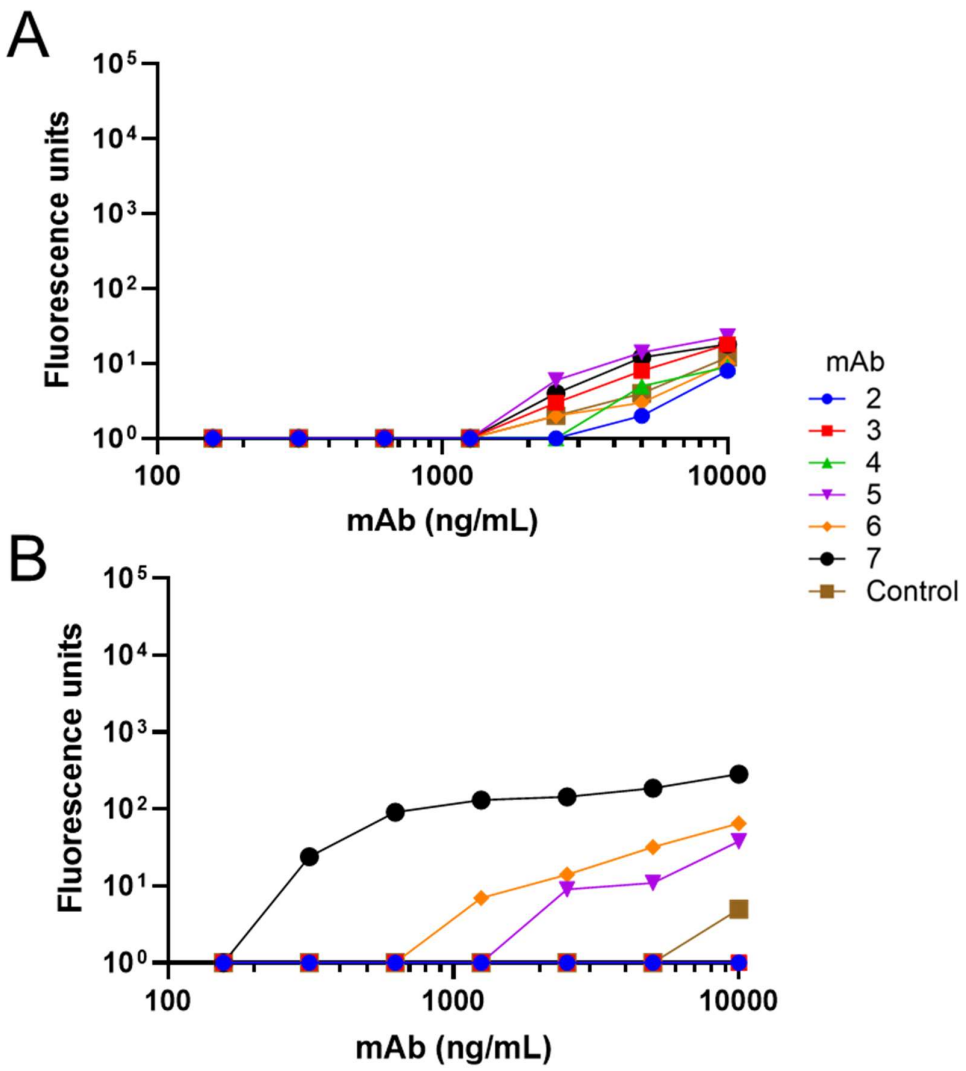


Figure 5.11: Recognition of native PRRSV antigen by recombinant mAbs was assessed by intracellular staining of porcine alveolar macrophages (PAMs). PAMs were infected with PRRSV-1 subtype 1 215-06 (**A**) or PRRSV-1 subtype 3 SU1-Bel (**B**). In addition to the six mAbs isolated from a PRRSV-immune animal, a recombinant Nipah virus-glycoprotein specific mAb was tested as a negative control. mAb binding was revealed by addition of a fluorescent secondary antibody and analysis using an Incucyte® SX5 Live-Cell Analysis System.

No significant binding was observed for any of the mAbs tested when staining for PRRSV-1 215-06 infected PAMs, however this was likely the result of poor infection, and not the reactivity of the mAbs, with staining of the SDOW17-A control suggesting significantly lower level of infection than expected. For SU1-

Bel, however, mAb 7 demonstrated significant binding compared to the negative control (adjusted *P* value <0.0001). No significant binding was observed for any of the other mAbs.

Utilising an orthologous recombinant PRRSV-2 VR-2332 sGP3 protein – generated by Dr. Rory Fortes de Brito, PRRS Immunology Group, The Pirbright Institute, as part of a follow-up to this project – cross-reactivity of these mAbs was investigated further by ELISA (**Figure 5.12**).

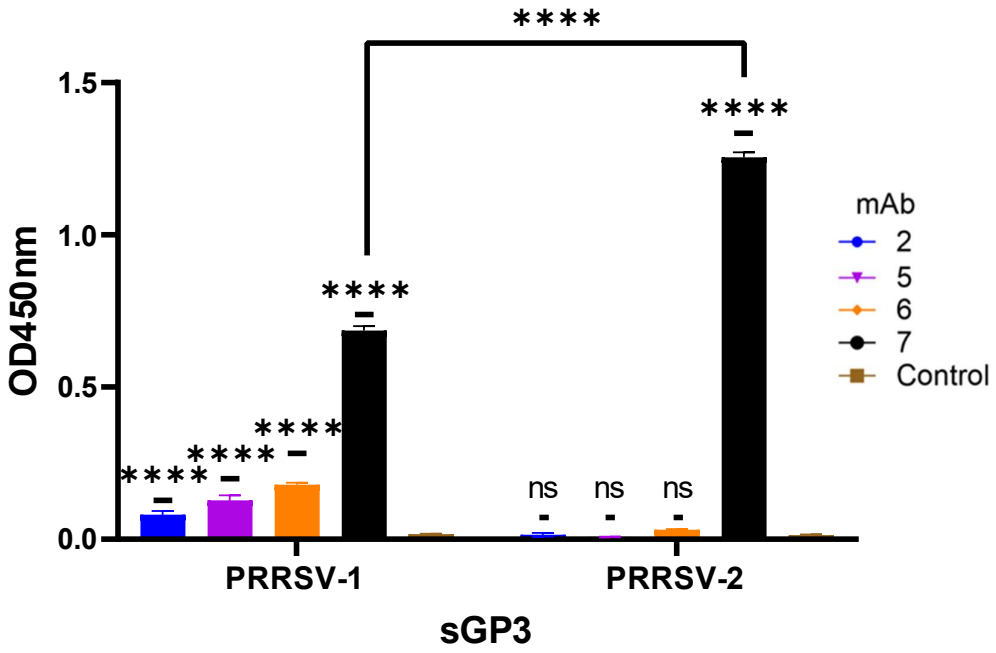


Figure 5.12: Assessment of cross-reactivity of recombinant mAbs using recombinant PRRSV-1 and PRRSV-2 sGP3 by ELISA. Four recombinant mAbs and a negative control mAb, specific to Nipah virus glycoprotein were tested at a concentration of 200 ng/mL. Mean data of three technical replicates ± SD are shown. **** denotes *P* < 0.0001 and ns = not significant.

mAbs 3 and 4 were excluded from this experiment due to insufficient stocks. mAbs 2, 5, 6, and 7 all demonstrated significantly higher binding of PRRSV-1 sGP3 than the control mAb (adjusted *P* value <0.0001), with mAb 7 in turn binding significantly higher than the others. Against PRRSV-2 sGP3, only mAb 7

demonstrated specific binding (adjusted *P* value <0.0001)) above the control. mAb 7, further, demonstrated significantly higher binding of the PRRSV-2 sGP3 than the PRRSV-1 (adjusted *P* value <0.0001).

To greater characterise where these mAbs were binding, some preliminary linear epitope mapping was performed for each of the mAbs utilising a peptide library comprising overlapping sequences (16mers offset by 4 AAs) representing PRRSV-1 sGP3 (**Figure 5.13**).

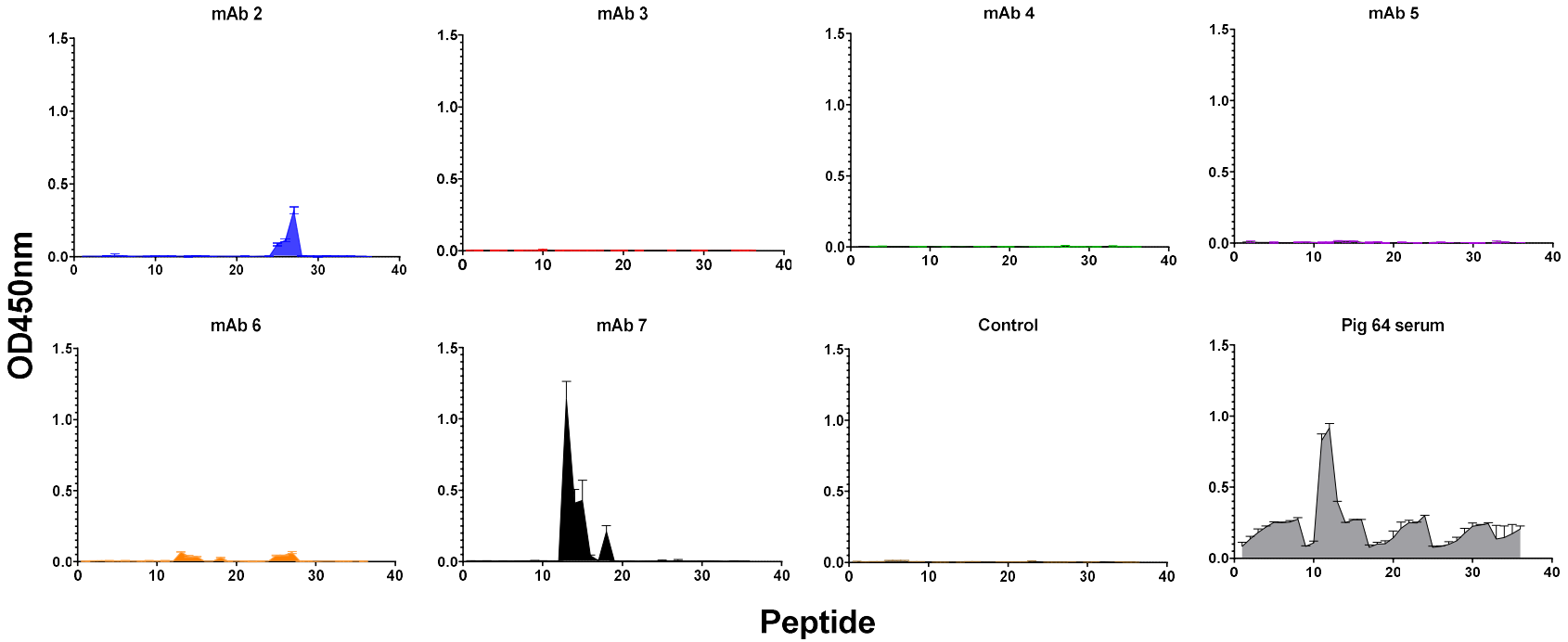


Figure 5.13: Overlapping linear peptides spanning the PRRSV-1 GP3 ectodomain were screened for mAb recognition by ELISA. In addition to the six recombinant mAbs and the control mAb tested, polyclonal sera from pig 64, the animal from which the recombinant mAbs originated, was included. Mean data of two technical replicates ± SD are shown.

Peptides 25 and 28 containing the consensus sequence DKRH (residues 137-141) elicited significant binding from mAb 2, with a clear peak observed from peptide 27. No significant binding was observed from mAb 3, mAb 4, or mAb 5 to any of the peptides tested. Further, peptides 11-13 containing the consensus sequence EERDHDEL (residues 85-93) elicited strong binding from mAb 7, peaking at peptide 13. Significant binding could also be observed against peptide 18, containing the sequence DNLK (residues 87-91). Despite this no significant binding was detected at either peptide 17 or peptide 19. mAb 6, interestingly, also had two distinct binding peaks, appearing to bind similarly to mAb 2 and mAb7 with peaks at peptide 27 and peptide 13. Although low, binding to both was significant compared to the control mAb (adjusted *P* value <0.0001).

Affinity of these mAbs were tested using bio-layer interferometry (BLI). sGP3 was used as a probe for each mAb (**Figure 5.14**) and binding kinetics were calculated (**Table 5.7**).

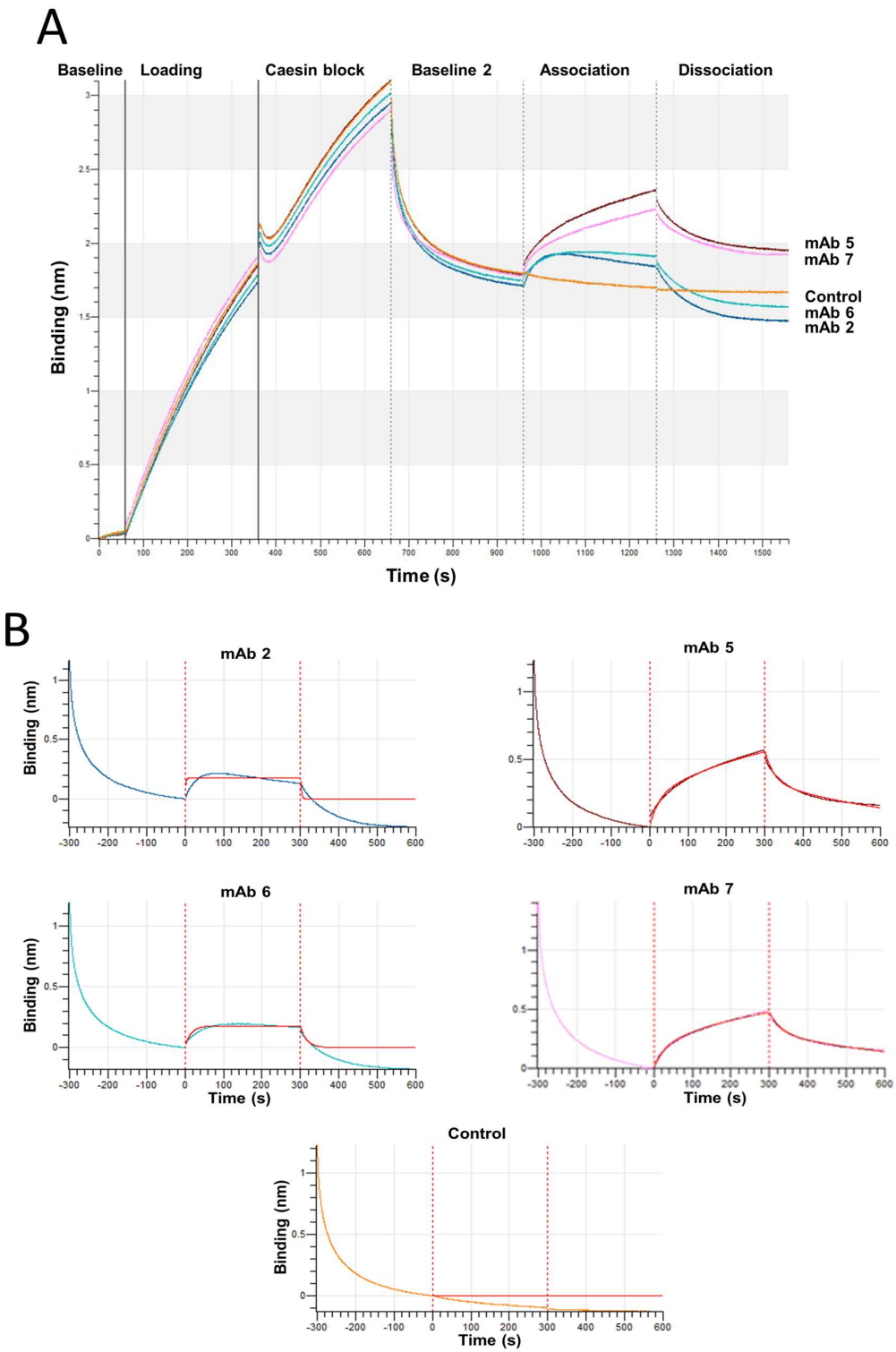


Figure 5.14: Bio-layer interferometry was performed to determine the affinity of recombinant mAbs against PRRSV-1 recombinant sGP3. Overlayed traces (**A**) and individual traces (**B**) with lines show curve fitting by Octet analysis software are shown. 25nM of sGP3 was loaded onto each probe as the ligand and 125nM of each mAb tested as the receptor.

mAb	Response	k_a (1/Ms)	k_a error	k_d (1/s)	k_d error	R^2
2	0.1316	1.336E06	2.761E06	4.004E-01	2.245E-01	0.4578
5	0.5652	1.666E03	7.559E02	2.886E-03	2.798E-05	0.9922
6	0.1663	1.373E04	9.166E04	6.090E-02	9.231E-03	0.6161
7	0.4885	4.843E05	8.426E03	6.659E-03	8.054E-05	0.9798
Control	-9.681E-02	4.000E04	0.000E00	3.357E-05	0.000E00	Null

Table 5.7: Kinetic binding constants for recombinant mAbs binding to recombinant sGP3 were determined by Octet® analysis software. Overall response, the association constant (k_a) and dissociation constant (k_d) as well as their respective errors are shown. R^2 values are also included, indicating confidence in each score.

Due to an error, KD values could not be calculated for these data and, in hindsight, further work was required.

Based on the plots in **Figure 5.14** the control mAb appeared to demonstrate no association to the sGP3 following blocking and the second baseline. No R^2 score could be assigned to the control mAb, explaining the lack of k_a and k_d errors, and so the results detailed in **Table 5.7** should be interpreted with caution.

mAbs 5 and 7 appeared to be high responders, reinforced by the calculated response value detailed in **Table 5.7**. While mAbs 2 and 6 still demonstrated GP3-specific responses, they appeared lower than mAbs 5 and 7, with a significantly lower response values being calculated. Worth noting, is that the R^2 scores assigned to mAbs 2 and 6 were below the 0.9 threshold assigned for this analysis, and so these results should be interpreted with caution.

Finally, to assess the neutralisation capacity, and its breadth, mAbs were also assessed by VNT, utilising both PRRSV-1 and PRRSV-2 (**Figure 5.15**).

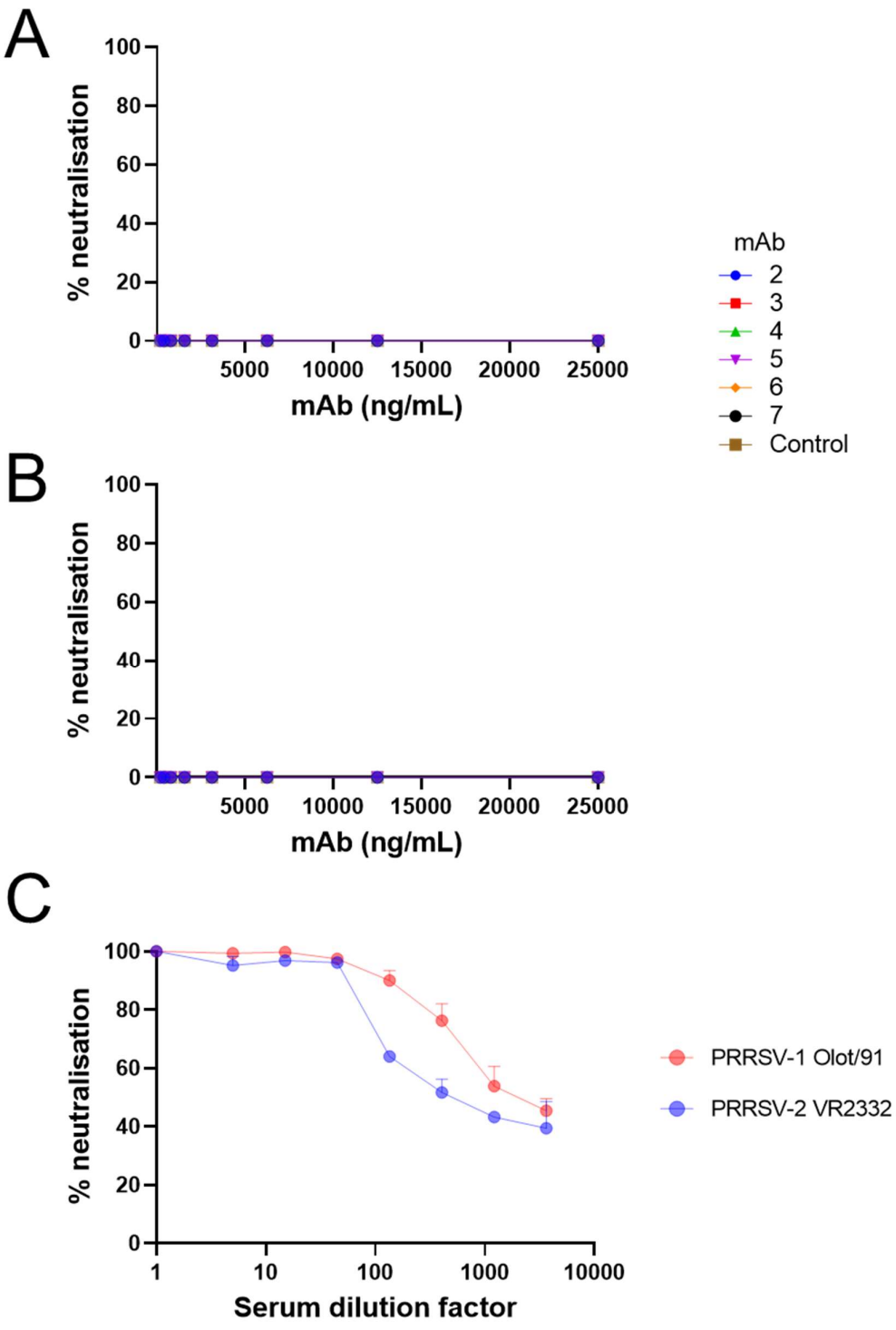


Figure 5.15: Neutralisation capacity of PRRSV sGP3-specific mAbs was tested by VNT. Each mAb was incubated with either PRRSV-1 Olot/91 (**A**) or PRRSV-2 VR-2332 (**B**), before being added to MARC-145 cells. Whole serum from pig 64 was included in both experiments as a positive control for neutralisation (**C**). Percentage neutralisation was calculated based on detection of PRRSV nucleocapsid by immunofluorescence staining.

Despite demonstrating GP3 reactivity and some demonstrating cross-reactivity, none of the mAbs were capable of neutralising either PRRSV-1 or PRRSV-2.

5.6 Whole antibody repertoire analysis

Complementary to other methods employed throughout this project, generation of a whole antibody repertoire across the infection/challenge timeline was attempted, with the aim of assessing of emergence and evolution of antibodies over time. For the six animals described in the heterologous challenge study samples from 0 dpi, and one week post-each challenge: 42, 78, 112 and 147 dpi were isolated. Utilising the same workflow described following the isolation of single cells, cDNA was generated from RNA isolated from whole blood, and VH and VL genes were amplified. In addition to IgG, IgM and IgA VH genes were also amplified. Amplicons were imaged using gel electrophoresis (**Figure 5.16**).

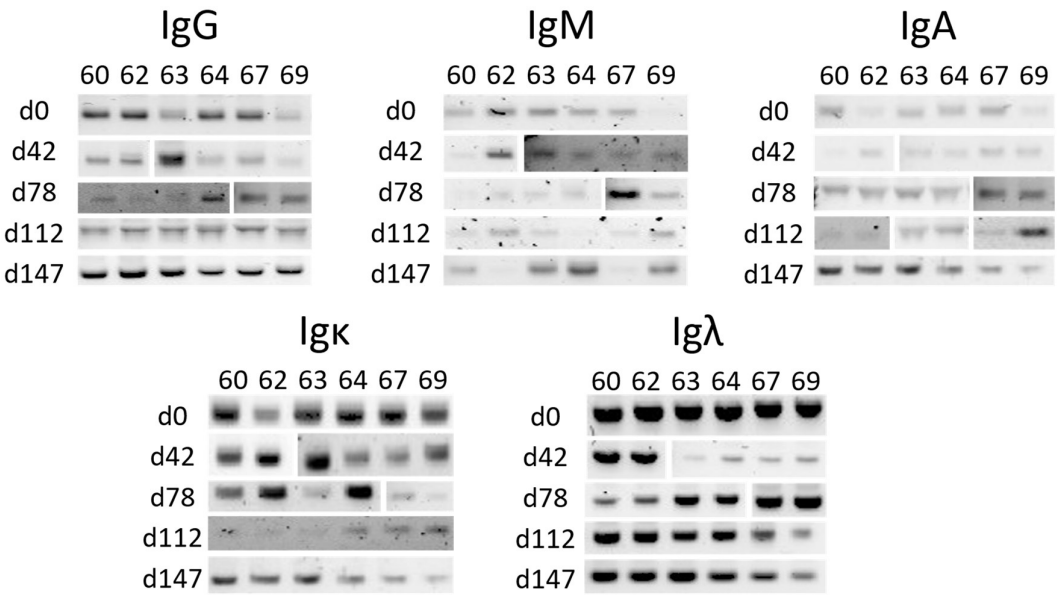


Figure 5.16: VH and VL genes were amplified from RNA isolated from whole blood, from six animals across five timepoints from a heterologous challenge study to establish a library for sequencing. Amplicons were imaged by gel electrophoresis, total library of amplicons, prior to indexing, is shown.

Following VH and VL amplification, all amplicons underwent an additional indexing PCR, and were subsequently pooled prior to Illumina sequencing, before undergoing a final quality control stage. Final quality control revealed issues with multiple bands, hereto undetectable by gel electrophoresis. It was decided, in the face of limited time, that in the first instance only the IgG would be included. All 112 dpi samples, additionally, failed to pass sequencing library QC, and so were excluded from the dataset presented here. Following sequencing, bioinformatic analysis was performed [288], and all sequences clustered with a 97% similarity threshold. For this analysis, the sequences for all 15 mAbs generated from the isolated sGP3-specific single cells were included. Proportion, and total number, of all sequences are detailed (**Table 5.8**) and the associated clusters for each mAb are further detailed (**Table 5.9**).

Chains	Isotypes	Number of sequences	Percentage
All sequences		5,637,048	
VH	All	904,481	
	IgG	902,265	99.8%
VL	All	4,732,567	
	Igλ	3,135,581	66.3%
	Igκ	1,596,458	33.7%

Table 5.8: Summary of whole antibody repertoire sequences generated, including proportions of each isotype, and overall number of sequences.

Cluster	Cluster size	Associated mAb
1	106079	8
9	12562	4
18	2782	1
22	2168	5
24	1684	2
142	276	7
154	265	3
159	256	6
1368	61	9-15

Table 5.9: Summary of which cluster each recombinant mAb described in this chapter was associated with. Cluster size, denoting number of sequences is also shown. Clustering was based on similarity between IgG CDR3 sequences, with a 97% identity threshold.

Analysis revealed a 2:1 proportion of Igλ:Igκ sequences. Further, it was revealed that that while mAbs 1-8 were all within distinct clusters, mAb 9-15 clustered together, reflecting the similarities in sequence identity highlighted earlier in this chapter. These nine clusters were investigated further (**Figure 5.17**).

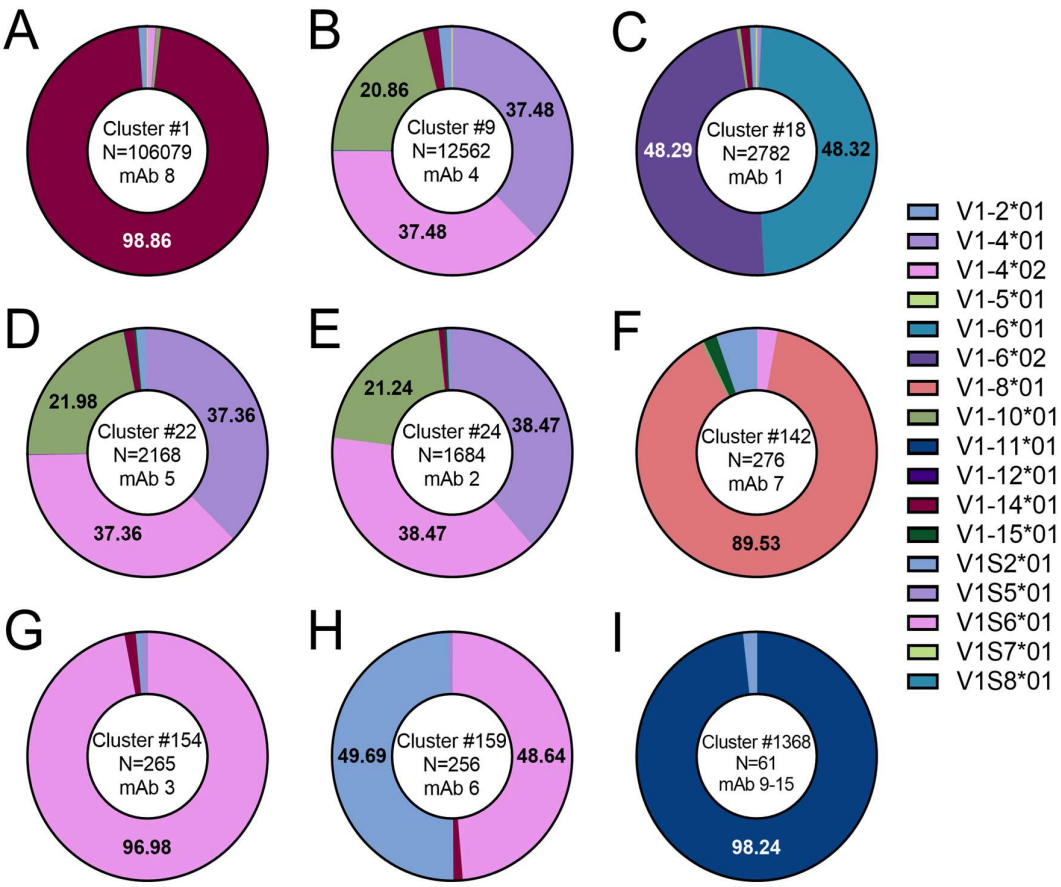


Figure 5.17: Percentage each germline and allele contribute to 9 clusters, seen to represent the 15 antibody sequences investigated. Clustering was based on similarity between IgG CDR3 sequences, with a 97% identity threshold. Germline sequences were identified from the ImMunoGeneTics information system (IMGT®).

These analyses revealed that sequences sharing identity with V gene 1-14, allele 01, comprised the majority of the repertoire, with these sequences composing 98.86% of the largest cluster (cluster 1). Additionally, these analyses revealed a comparable distribution in V gene and allele between cluster 9, 22, and 24, despite representing quite distinct sequences, being largely represented by equal proportions of both alleles of V gene 1-4 (37.36 – 38.47%), and a smaller proportion of V gene 1-10 allele 01 (20.86 - 21.99%). mAb 9 – 15 sequences were all represented by the same cluster, unsurprising given the close identity of

these sequences, as reported in **Section 5.3**. This cluster, further, was most strongly associated with V gene 1-11, allele 01, comprising 98.24% of all sequences in this cluster. No other mAb sequences were observed sharing the same cluster. The number of sequences in each of these clusters was then plotted against time (**Figure 5.18**), to determine the changes in expression following each PRRSV challenge from the heterologous challenge study, detailed in **Chapter 2.17**.

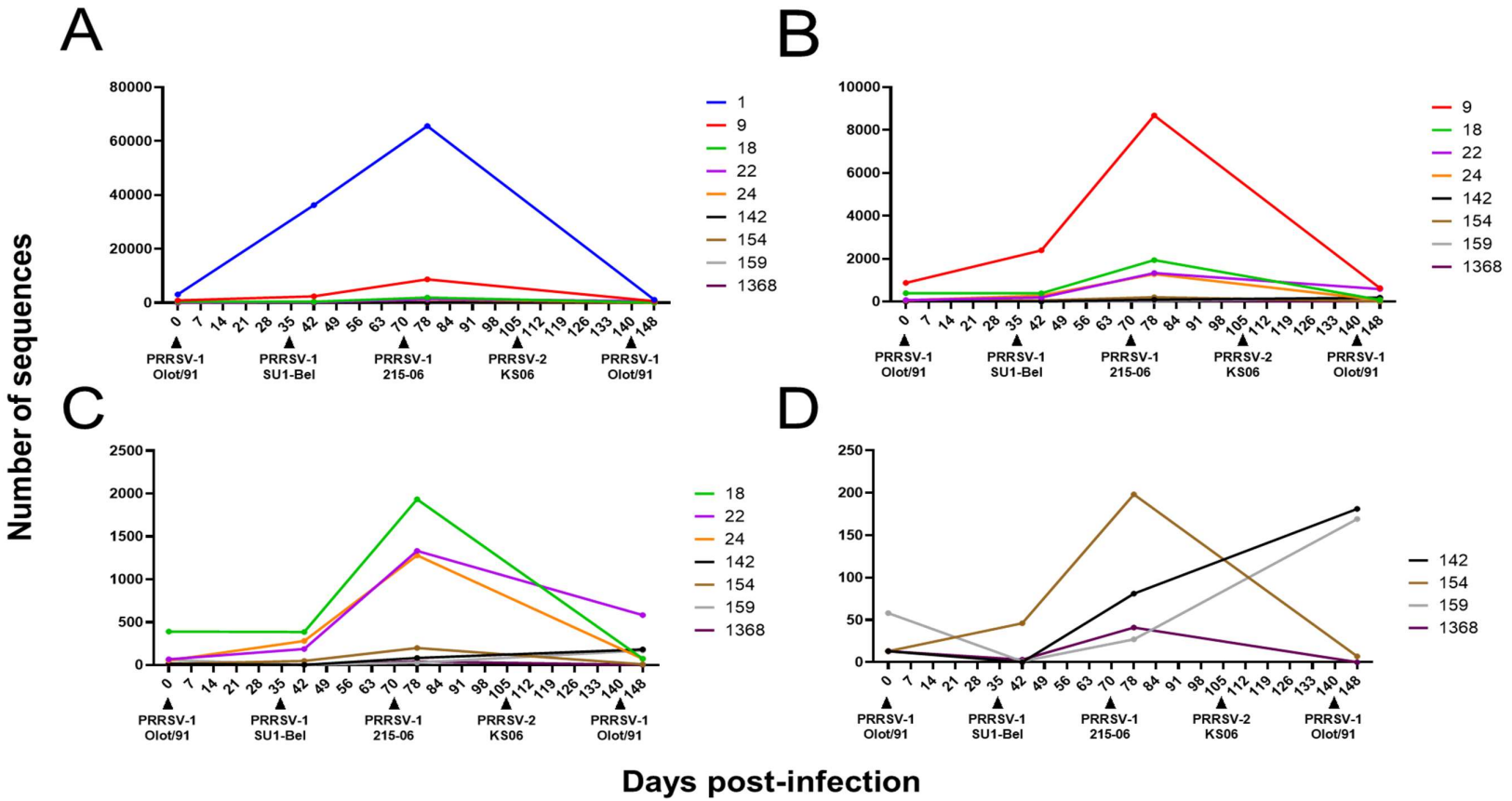


Figure 5.18: The nine clusters associated with each recombinant mAb were investigated over time with sequence numbers reflecting expression. Sequences from 0, 42, 78, and 148 dpi were assessed. Each plot removed the most dominant cluster in each iteration, starting with representation of all mAb-associated clusters (**A**), removal of the top cluster (**B**), removal of the top two clusters (**C**), and removal of all but the bottom clusters (**D**), to assess the dynamics of clusters represented by fewer sequences.

Cluster 1 rose throughout the infection timeline, but was negligible upon termination of the study, suggesting down-regulation of these sequences following PRRSV-2 challenge. The kinetics of cluster 9 were similar, with a slower increase between 0 and 42 dpi, similarly with clusters 18, 22, and 24. Unlike all other clusters examined, clusters 142 and 159, representing mAb 7 and mAb 6 respectively, continue to rise after 78 dpi, suggesting an increase in expression following PRRSV-2 challenge. It is difficult, however, to draw too many conclusions without the additional 112 dpi data set.

5.7 Discussion

Results from this chapter demonstrate the utility of using recombinant sGP3 to isolate PRRSV-specific mAbs.

Worth highlighting is despite the use of an established antibody panel to distinguish between BCR isotypes, and employing the decoy tetramer/two fluorescently tagged sGP3-tetramers to reduce non-specific events, upon back gating the sorted events some of the sorted single cells still appeared to be IgM^{dim}. This could account for some of the cells from which IgG VH genes could not be amplified from, despite GAPDH, or VL chains being successfully amplified.

Worth highlighting as a limitation for the immunostaining assays used in this chapter, is that the cells were required to be fixed with 4% PFA prior to staining. While staining with the mAbs demonstrated binding, an important caveat here is that the fixation of the native GP3 might negatively affect some epitopes, and therefore limit binding of some of these mAbs. A potential resolution for this would

be to conduct immunostaining utilising live cell confocal microscopy, without the need for fixation.

mAb 7 showed significantly higher binding of recombinant PRRSV-2 sGP3, despite appearing to originate before exposure to PRRSV-2. In spite of this, and the cross-reactivity demonstrated from the assays described throughout, mAb 7 showed no neutralisation capacity, even against PRRSV-1. One possible explanation for this is that mAb 7 could be specific against a highly antigenic decoy epitope present within GP3, EERDHDEL, which elicited binding of mAb 7 in the peptide screening assay, has been shown to be a relatively well conserved epitope between PRRSV-1 and PRRSV-2 [223]. In the same study, antibodies raised against this epitope also showed no neutralisation capacity when used against the HP-PRRSV attenuated vaccine strain HuN4 F112, lending support to this hypothesis.

The GP3 peptide RVFVDKRHQF, which elicited binding from mAb 2 in the peptide screening assay, is a documented epitope in PRRSV-1 Lelystad virus [205]. Two peaks in peptide reactivity were observed from mAbs 6 and 7, which persisted between repeat assays. It is possible that this was simply the result of non-specific binding, but statistical analysis showed that these were significant results. Additionally, the lack of binding of mAb 5 in this assay, despite recognition of recombinant sGP3 being demonstrated, suggests this mAb may be specific to a conformational epitope, highlighting a limitation of the use of linear peptides in this assay. While the assay described in this chapter has provided some preliminary epitope mapping, its limitations are clear. Follow up investigation would do well to utilise structural biology methods such as X-ray crystallography.

By generating these mAbs as Fab fragments, and co-crystallising with these peptides may provide more in-depth information on the interactions between these mAbs and these epitopes as has been described previously [289]. Co-crystallising, additionally, with the recombinant sGPs generated as part of this project, could enable greater understanding of the PRRSV antigen-antibody interactions than just linear peptides, enabling study of potential conformational epitopes, as discussed earlier in this thesis. In lieu of generating the structural data discussed above, another method for investigating the interactions between these mAbs and the peptides recognised would be to make use of prediction tools such as SAbPred [290]. While this tool was used to model some of the mAbs detailed in this chapter (**Appendix Figure 9**), utilising this tool to investigate the interactions between these mAbs and the peptide sequences remained unexplored.

The limited number of recombinant mAbs generated makes it difficult to draw too many conclusions regarding broad neutralisation capacity. In the interest of setting a realistic scope for this project, and taking this workflow through as far as possible, the decision was made to push forward with the smaller number of successfully generated mAbs, rather than optimise the generation of a greater number. Improving the throughput of this workflow, would greatly improve the capabilities of screening. The work described in this thesis primarily employed the use of Sanger sequencing for the generation of recombinant mAbs, which greatly limited the number of paired sequences that could be taken forward. This workflow has continued to be optimised, and a higher throughput approach employing the use Illumina sequencing, as was described for **Section 5.6** in the

generation of the whole antibody repertoire analysis, is now a viable method to greatly improve the throughput of this approach. Furthermore, the use of new technologies, such as the Berkley Lights Beacon® system, has enabled vastly higher throughput for isolation of specific B cells, compared to conventional methods such as flow cytometry, as has been highlighted by Young et al., [160], enabling isolation of PRRSV-specific B cells using infected cells as baits. In collaboration with Dr. Jay Calvert and Dr. Jordan Young, as part of an industrial placement at Zoetis Inc., Michigan, USA, utilisation of the Beacon® system with the recombinant GP2, GP3, and GP4 generated as part of this project was planned. By loading the OptoSelect Chips with each rec-GP, B cells with specificity against GP2, GP3, and GP4 could be isolated from material collected from PRRSV hyperimmunised animals. Following isolation, at a significantly higher throughput than those seen by the methods described in this thesis, amplification could be performed utilising the Illumina-based NGS approach as detailed above. Due to shipping issues, the rec-GPs have yet to be received and as such this approach was never fully explored.

Moreover, expanding the workflow described in this chapter into screening with both PRRSV-1 and PRRSV-2 recombinant glycoproteins would facilitate the isolation of cross-reactive (and hopefully cross-neutralising) B cells. This could be approached by staining with PRRSV-1 and PRRSV-2 GP tetramers/loading chips with both PRRSV-1 and PRRSV-2 GPs simultaneously., Greater optimisation would have to be performed, however, and this cannot be approached as simply combining the two rec-GPs. Discrepancies in affinity/specificity between the two species of virus could introduce bias, and

make it difficult to identify true, cross-reactive events. Isolating B cells with PRRSV-1 and PRRSV-2 rec-GP tetramers separately, analysing sequence data by 10x genomics, and comparing frequencies/common sequences between the two could yield great insight into potential conserved targets, but would be limited by the cellular stress caused by flow cytometric sorting.

Despite the limitations discussed here, and that the mAbs isolated ultimately failed to neutralise, the results presented in this chapter demonstrate the potential of these rec-GPs as useful tools for isolating PRRSV-specific B cells.

Chapter 6. Evaluation of the immunogenicity of PRRSV-1 GP3

6.1 Rationale

Results discussed in the previous chapters have demonstrated that recombinant sGP3 elicits strong binding from PRRSV-immune sera, either from sequential heterologous challenge, or from MLV vaccinated and challenged pigs. Recognition by sera from PRRSV-immune pigs demonstrated GP3-binding kinetics that mirrored the neutralising antibody responses, with positive correlations being calculated between the two results. However, the six mAbs generated from sGP3-specific B cells isolated from these animals failed to demonstrate any neutralising capacity. This was not an exhaustive study, given that only a small number of antibodies were characterised, and therefore neutralising GP3 antibodies may not have been captured. To investigate the immunogenicity of sGP3 further, animals were immunised with purified recombinant sGP3, and the response monitored over time.

This pilot study also aimed to assess the immunogenicity of sGP3 using three different vaccine platforms. One limitation of recombinant antigens as potential vaccine candidates, however, is their inherent poor immunogenicity, typically requiring adjuvants to enhance the immune response [291]. Adjuvants serve to enhance and/or shape antigen-specific immune responses [292]. Many diverse classes of compounds have been assessed as adjuvants including cytokines, emulsions, liposomes, microparticles, microbials products, mineral salts, polymers, and saponins [293], and have been demonstrated to enhance both innate and adaptive responses. Particulate adjuvants have been shown to create a local pro-inflammatory environment to recruit immune cells, ultimately leading to an enhanced adaptive responses [293]. Additionally, many adjuvants including

alum, oil-based emulsions, and microparticles act by “targeting” antigens to antigen presenting cells, also resulting in enhanced adaptive responses [293].

To this end, two next-generation vaccine platforms were investigated, and compared to the efficacy of vaccinating with sGP3 delivered in Montanide ISA 201 VG adjuvant (provided by Dr Andra Corder, Seppic, France).

In collaboration with Prof Jonathan Lovell, University at Buffalo, USA, a cobalt porphyrin phospholipid (CoPoP) liposome vaccine delivery technology, adjuvanted by inclusion of 3D (6-acyl)-PHAD® and the saponin QS-21 into the liposome bilayer was evaluated. The CoPoP vaccine system converts soluble his-tagged antigens into liposome-displayed particles, decorating the surface of the colloidal particles with stable, coordinated insertion of the his-tag into the liposome bilayers. All rec-GPs produced as part of this project are hexa-histidine tagged, and so compatible with the CoPoP system. This system has been demonstrated to enhance antibody responses to recombinant antigen derived from several pathogens, i.e., *Plasmodium falciparum* antigen Pfs25 [294], *Borrelia burgdorferi* antigen OspA [295], and influenza A virus haemagglutinin [296], and boasts enhanced thermostability compared to the traditional adjuvanted protein withstanding storage of 60 °C for at least 6 weeks while still inducing functional transmission blocking antibodies [297]. The CoPoP system, however, had not been used for the immunisation of pigs prior to the study reported in this chapter.

The other vaccine platform that was evaluated comprised a self-amplifying (sa)RNA vector, delivered in lipid nanoparticles, expressing membrane displayed

GP3 for cell surface expression in collaboration with Prof. Robin Shattock (Imperial College London, London, UK). The COVID-19 response has demonstrated the power of RNA vaccine technologies, with two licensed mRNA vaccines, including the Pfizer-BioNTech vaccine in use in 156 countries [298]. Antigen expression, however, is proportional to the number of conventional mRNA transcripts successfully delivered during vaccination. Adequate expression for protection may therefore require large/repeated doses [299].

saRNA vaccines address some of these key limitations of conventional mRNA vaccines resulting from their self-replicative activity. Conventional mRNA and saRNA vaccines can be produced using largely identical methods: the target antigenic sequence is flanked by 5' and 3' UTRs, with a 5' cap and poly(A) tail being common to all RNA transcripts [300-302]. saRNA constructs encode additional replicase genes, most often from alphaviruses (i.e. Semliki forest virus, Sindbis virus, and Venezuelan equine encephalitis virus), which form an RNA-dependent RNA polymerase complex, enabling the *in situ* amplification of synthetic transcripts [299, 303]. Generating saRNA vaccines using this approach, rather than using alphavirus viral vectors reduces concerns of viral reactivation, or preexisting immunity to the viral vector [304]. As a result of their self-amplifying capability, saRNA vaccines can be delivered at lower concentrations than conventional mRNA vaccines to achieve comparable antigen expression [303], thereby offering the potential to use lower doses, which might reduce manufacturing costs.

Further, the use of lipid nanoparticles to deliver saRNA vaccines has been shown to increase efficiency of antigen production and immunogenicity in mice and rats

[299, 305]. The relative simplicity of RNA vectors importantly offers the potential for rapid and scalable response to new/emerging pathogen strains.

The study design is detailed fully in **Chapter 2.18**; in summary three groups of pigs were immunised with one of the three vaccine-delivery platforms described above, following a prime-boost regimen, with a 28-day interval, and blood sampled along a 56-day study timeline.

This work, additionally, was performed in close collaboration with Dr. Jane Edwards, PRRS Immunology Group, The Pirbright Institute. Results detailed within this chapter generated from her work will be outlined.

6.2 Vaccine preparation

Ten 300 mL cultures of Expi293F cells were transiently transfected and sGP3 purified from cell culture supernatants as described in **Chapter 3**. Following purification by IMAC, purity of each batch was assessed by western blot (**Figure 6.1A**) and Coomassie staining (**Figure 6.1B**) following SDS-PAGE.

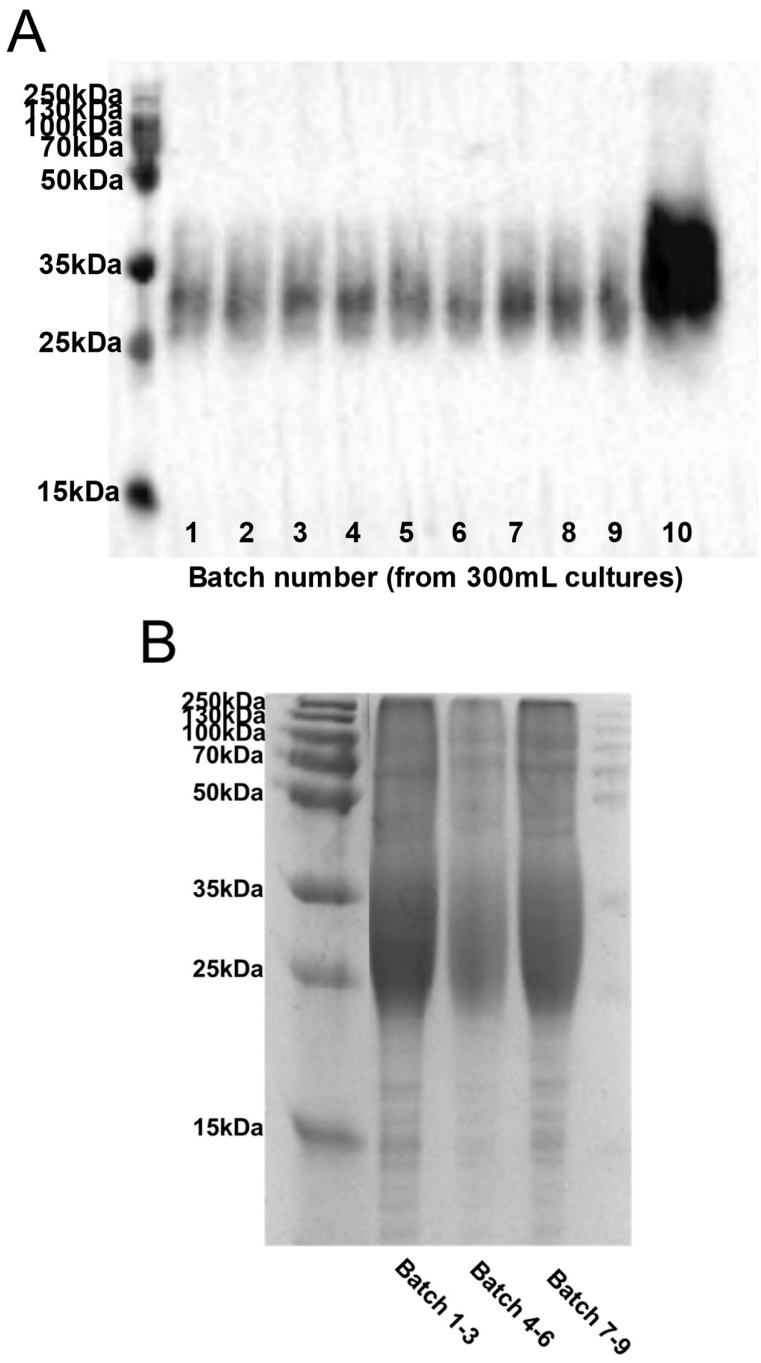


Figure 6.1: Affinity purification of recombinant sGP3 from transfected Expi293F cell culture supernatants was performed using ÄKTA Pure Protein Purification System followed by assessment by SDS-PAGE. Fractions with the strongest bands were taken through concentration and buffer exchange, and purity of the proteins was tested by western blot (**A**) and Coomassie protein stain following concentration (**B**). 1 µg of each sample was loaded.

Analysis of purified baches of sGP3 by western blot showed profiles that were consistent with the results in **Chapter 3**. Batch 10, however, was represented by a far denser band, appearing to span from 30-40 kDa and was therefore excluded from further processing (**Figure 6.1A**). Batches 1-9 were combined into three batches, and buffer exchanged while concentrating to achieve the concentration level required for vaccine formulation, as detailed in **Chapter 2.18**. Coomassie staining of batches 1-9 showed that a major species at 35 kDa consistent with what was seen previous for sGP3 (**Chapter 3**), plus minor contaminants at ~20 to ~12 kDa 100 and ~70 kDa. Batches were pooled and taken through buffer exchange and concentration. All samples were screened for presence of endotoxin, as detailed in **Chapter 2.18**, revealing no significant levels compared to the control (data not shown).

Western blot analysis was performed on the pooled and concentrated batches, using a murine anti-GP3 mAb (Clone HyP10-C40-C1) provided by Dr Barbara Klupp, Friedrich-Loeffler-Institut, Isle of Riems, Germany (**Figure 6.2A**) alongside the standard ant-histidine mAb (**Figure 6.2B**).

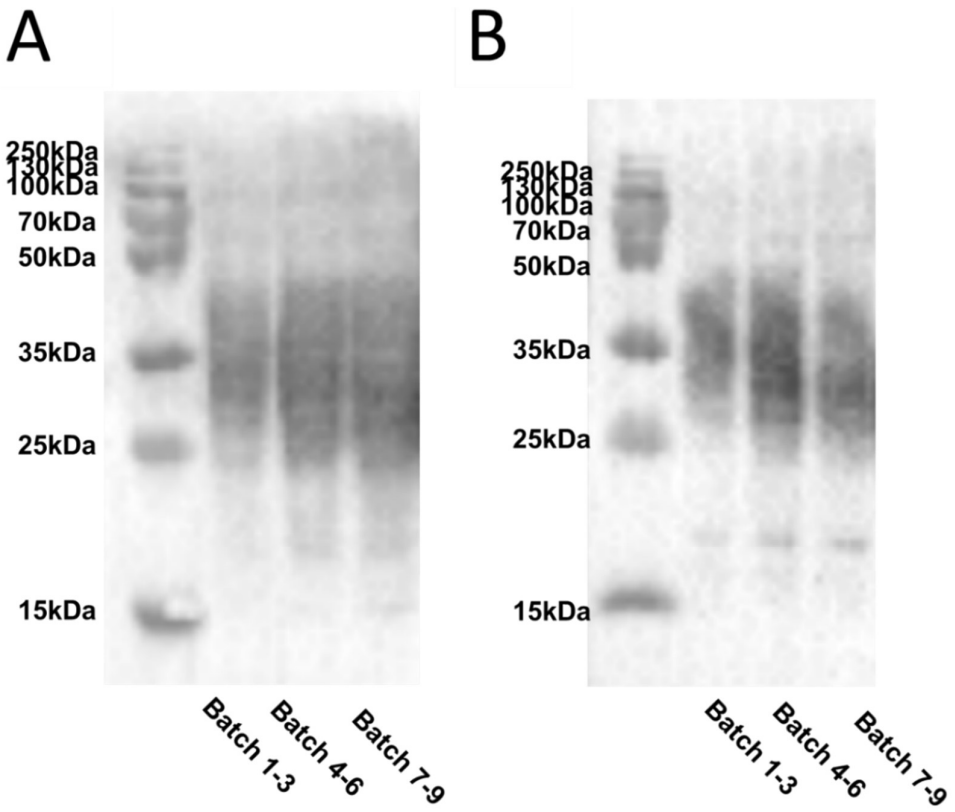


Figure 6.2: Western blot analysis of bulk concentrated sGP3 to assess multiple bands observed by Coomassie staining. 1 µg of protein stock was run through PAGE, before being probed against with either an anti-GP3 mAb (**A**) or an anti-histidine mAb (**B**).

The results demonstrated that the multiple bands observed by Coomassie staining were not only hexa-histidine tagged, but also stained positive with the GP3-specific mAb, indicating these bands may represent a truncated isoform of sGP3. Due to time constraints, and the difficulties in producing such high quantities of this low yield protein, it was decided that this purity was acceptable for a pilot study.

With the sGP3 stock established, vaccine formulation began. Following mixing of the recombinant GP and the liposome, a Ni-NTA competition assay was performed using nickel beads to assess whether sGP3 was being successfully

displayed by the CoPoP liposomes. Analysis revealed that when sGP3 was mixed with PBS, as the negative control, the sGP3 became associated with the nickel beads, however, when sGP3 was mixed with the CoPoP, the sGP3 was retained in the supernatant due to successful display by the CoPoP and therefore was unavailable to bind to the nickel beads. These assays deployed a deglycosylated version of sGP3 since Coomassie was not sufficiently sensitive to detect fully glycosylated sGP3 at the concentration desired for these experiments (**Figure 6.3A**). Following PNGase F digestion, associated of the sGP3 with the CoPoP liposomes was assessed again by Coomassie staining (**Figure 6.3B**). This work was performed by Dr. Jane Edwards, The Pirbright Institute.

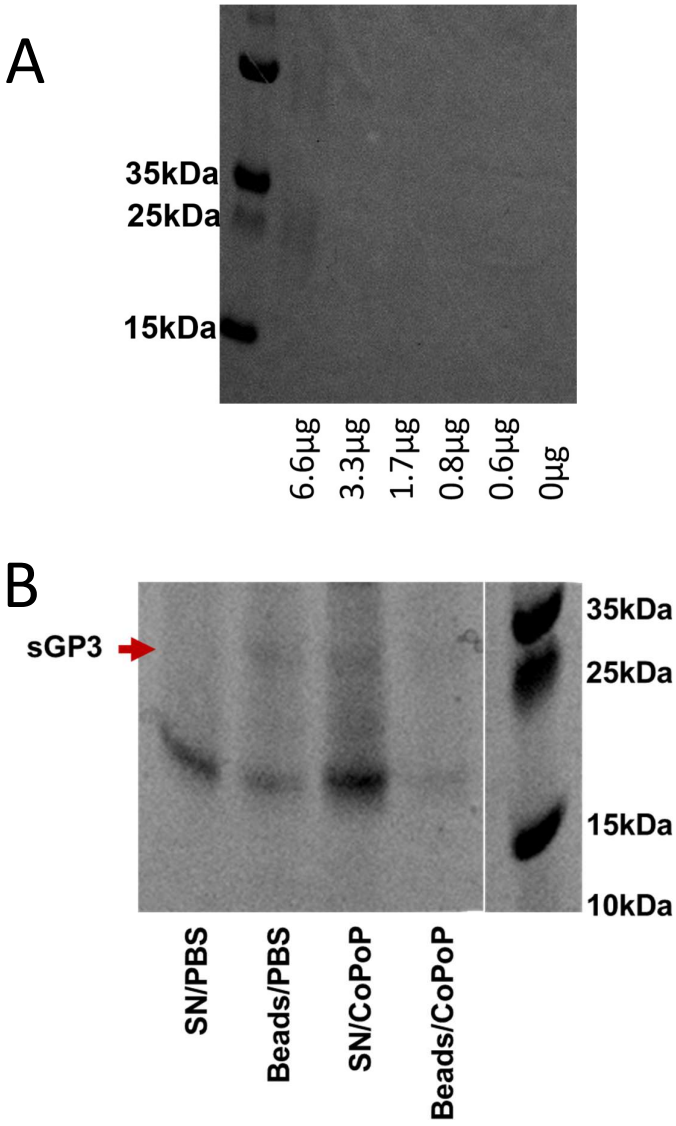


Figure 6.3: CoPoP liposome formation was assessed by Coomassie staining following native-PAGE. A titration of glycosylated sGP3 was performed and assessed by Coomassie staining to assess the limit of detection (**A**). Following deglycosylation of sGP3, association with Ni-NTA beads or the CoPoP liposome was assessed by Coomassie (**B**). 1 µg of sGP3 was added to each condition. Data provided by Dr. Jane Edwards, The Pirbright Institute, UK.

Titration of the sGP3 showed a limit of detection at <6.6 µg, and so alternatives would have to be employed to visualise the CoPoP liposome-associated protein. Deglycosylation enabled detection of the sGP3 by Coomassie, at much lower concentrations than when glycosylated. Further, following association with the

CoPoP liposomes, sGP3 could not be detected associated with beads, demonstrating successful display.

In parallel, construction and formulation of the saRNA-vectored GP3 was performed by Dr. Kostas Paschos, Imperial College London. Both membrane-bound and secreted GP3 were investigated as potential candidates, with the preferred option to have the GP3 displayed on the membrane of transduced cells, thereby increasing exposure to immune cells. The soluble version was made as a back-up in case surface expression of the membrane form was not a viable option. HEK293T were transiently transduced with each saRNA vector, and expression of GP3 was assessed first by western blot (**Figure 6.4A**) and subsequently by flow cytometry (**Figure 6.4B**). In both instances, cells were also transduced with saRNA expressing Gaussia luciferase, to serve as a control population.

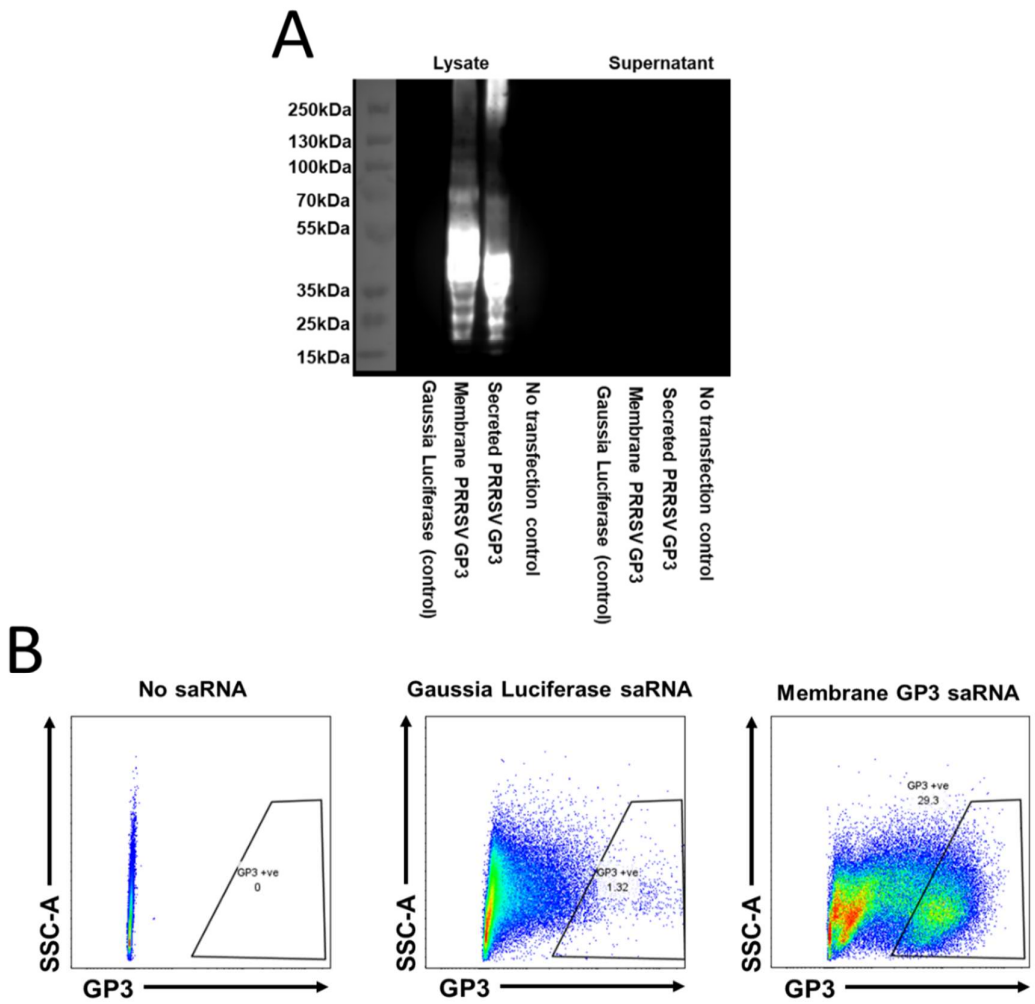


Figure 6.4: saRNA-vectored GP3 expression was assessed in HEK293T cells. Expression was assessed by use of an anti-GP3 mAb by western blot analysis of cell lysate (**A**), or through flow cytometric staining (**B**). Cells transduced with saRNA expressing Gaussia luciferase saRNA were used in both assays as controls. Data provided by Dr. Kostas Paschos, Imperial College London.

Analysis by western blot demonstrated successful expression of both membrane-bound and secreted GP3, with both forms of GP3 being detectable in the whole cell lysate. The secreted GP3, however, could not be detected in the cell supernatant, suggesting the protein was being retained/trapped within the transduced cells. Flow cytometric analysis, further, demonstrated surface expression of the membrane bound GP3, with the proportion of $GP3^{+}$ being significantly higher compared to the no saRNA and Gaussia luciferase saRNA

transduced controls. With the membrane bound GP3 being successfully presented on the cell surface, the saRNA vector was taken forward for vaccine formulation.

Final vaccine formulations for each platform used are detailed in **Chapter 2.18**.

6.3 Characterisation of immune response

Following immunisation of the pigs, serum was taken weekly and PBMCs were isolated every two weeks for analysis of antibody and T cell responses respectively. GP3-specific T cell IFN-γ responses were first assessed by ELISpot (**Figure 6.5**). Media only controls were included and subtracted from the final spot counts. This work was performed by Dr. Jane Edwards, The Pirbright Institute.

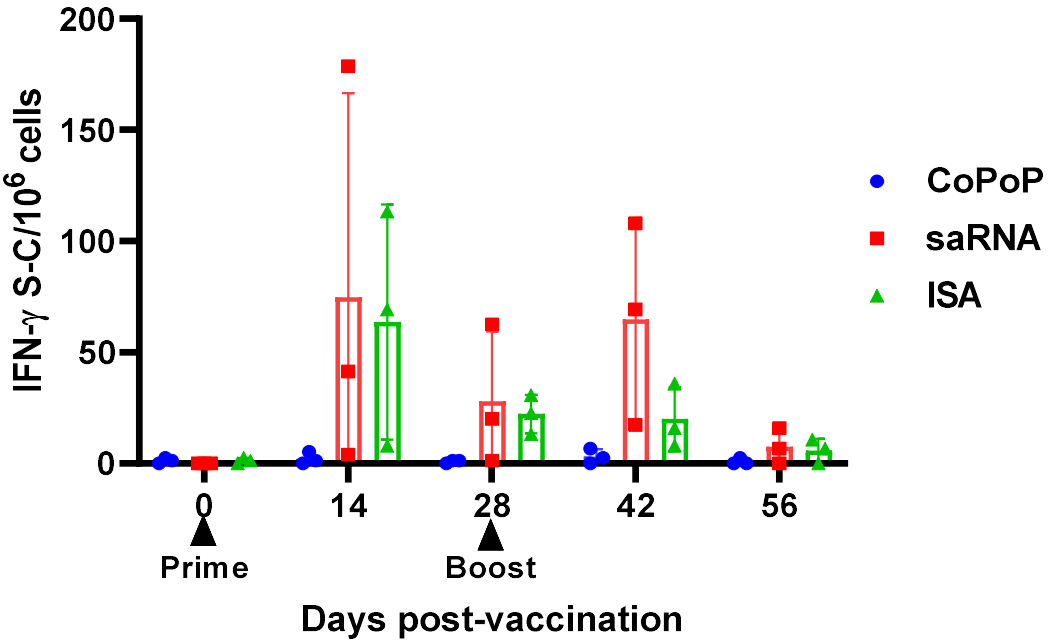


Figure 6.5: GP3-specific T cell IFN-γ responses from animals vaccinated with PRRSV-1 GP3 were assessed by ELISpot assay. PBMC from pigs immunised with sGP3 formulated with Montanide ISA 201 VG adjuvant (ISA), sGP3 displayed on adjuvanted liposomes (CoPoP) or saRNA vectored membrane displayed GP3 (saRNA) were restimulated with a pool of peptides representing sGP3 or were unstimulated. Responses are reported as the unstimulated control-corrected spot count per 1×10^6 cells. Mean data of three biological replicates ± SD are shown. Data provided by Dr. Jane Edwards, The Pirbright Institute.

Tukey's multiple comparisons test revealed a significant increase in average IFN-γ responses in pigs immunised with the saRNA-vectored GP3 at 14 dpv compared to 0 dpv. These responses dropped by 28 dpv, but by 42 dpv were again significantly above those seen at 0 dpv. Responses from the ISA-inoculated animals were only significantly higher at 14 dpv being comparable to those seen by the saRNA-inoculated animals but fading by 28 dpv. By 56 dpv, no significant IFN-γ responses could be detected from any animal, regardless of vaccination approach. No significant responses were observed from the animals vaccinated with the sGP3 displayed on CoPoP at any of the observed timepoints.

To assess the antibody responses induced by vaccination, sera from all nine timepoints were tested by sGP3 ELISA (**Figure 6.6**).

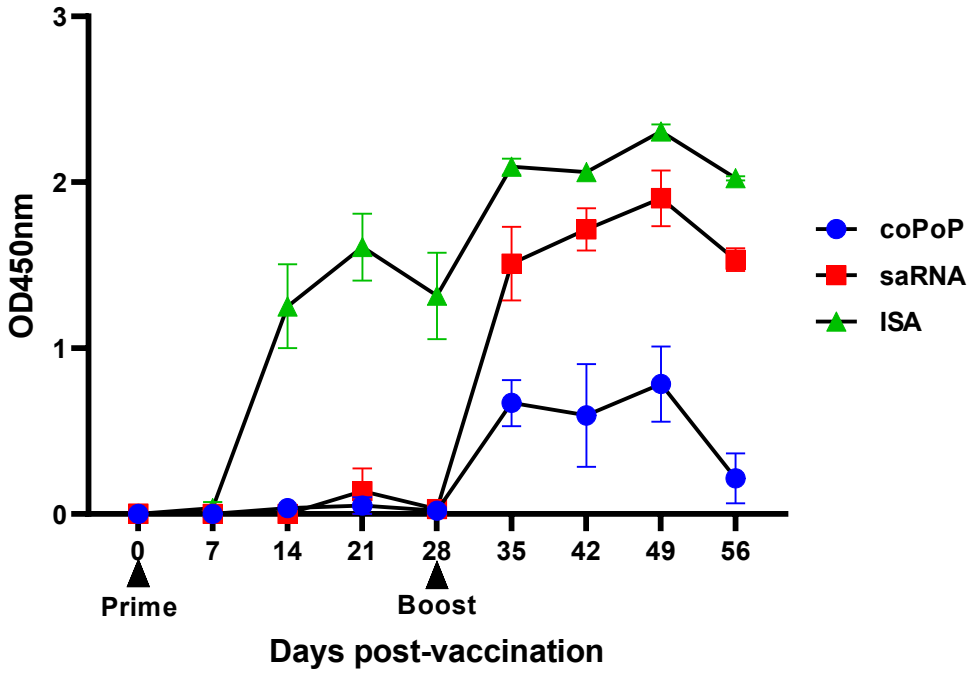


Figure 6.6: Assessment of GP3-specific antibody responses. Reactivity against recombinant sGP3 by sera (diluted at 1:100) from pigs immunised with sGP3 formulated with Montanide ISA 201 VG adjuvant (ISA), sGP3 displayed on adjuvanted liposomes (CoPoP) or saRNA vectored membrane displayed GP3 (saRNA) was measured longitudinally across the course of a 56-day study. Mean data of three biological replicates ± SD are shown.

All three vaccine approaches generated GP3-specific antibody responses which were augmented following the booster immunisation. Significant antibody binding to sGP3 was observed from the sGP3 in Montanide ISA 201 VG adjuvant-inoculated animals by 14 days post-vaccination (dpv) (adjusted *P* value <0.0001), compared to pre-immunisation, with responses remaining significant until termination of the study (56 dpv). Significant sGP3 binding was not seen from animals inoculated with either the saRNA-vectored or CoPoP-delivered GP3 vaccines until 35 dpv (7 days post-boost). The responses from the saRNA-inoculated animals were comparable to those from the ISA-vaccinated animals by 42 dpv, with no significant differences being observed between the two vaccine delivery conditions until termination (56 dpv); responses were significantly lower at 35 dpv (adjusted *P* value = 0.0061). The responses from the CoPoP-inoculated animals were significantly lower (adjusted *P* value <0.0001) than both the saRNA- and ISA-inoculated animals throughout the duration of the study. Furthermore, upon termination at 56 dpv, sGP3 responses from the CoPoP-inoculated animals were not significantly above those observed at 0 dpv.

Antibody end point titres were then calculated following an additional sGP3 ELISA (**Figure 6.7**). Sera from this study was compared to the sera from a known PRRSV-1 Olot/91-reactive animal (detailed in **Chapter 2.17**) as a control. This work was performed by Dr. Jane Edwards, The Pirbright Institute.

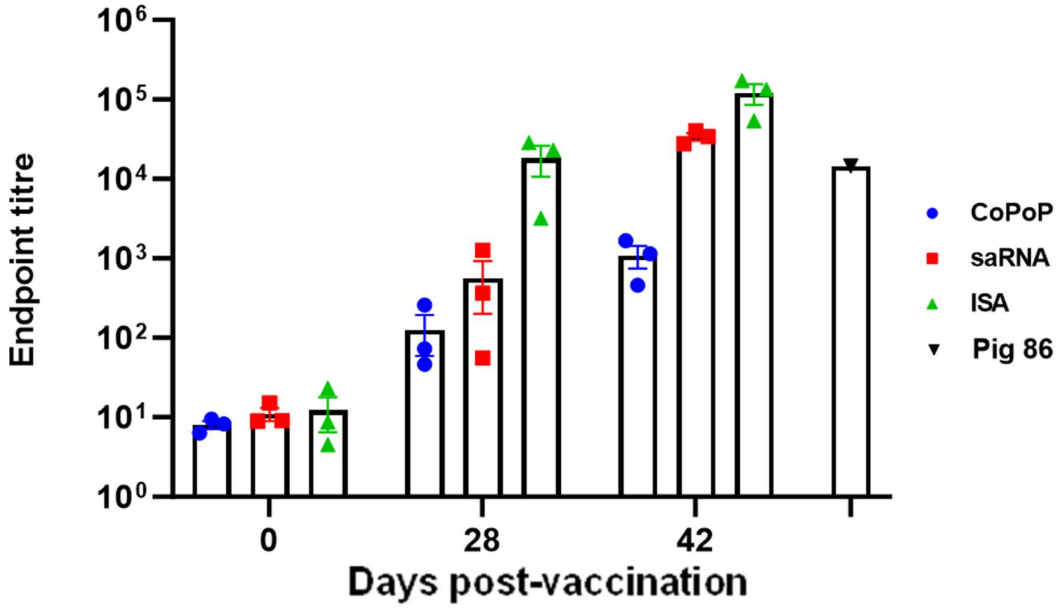


Figure 6.7: Endpoint antibody titres from each serum were calculated following sGP3 ELISA. sGP3 binding antibody titres from pigs immunised with sGP3 formulated with Montanide ISA 201 VG adjuvant (ISA), sGP3 displayed on adjuvanted liposomes (CoPoP) or saRNA vectored membrane displayed GP3 (saRNA) were compared to a known Olot/91-reactive sera (pig 86), as a control. Mean data of three biological replicates ± SD are shown. Data provided by Dr. Jane Edwards, The Pirbright Institute.

Statistical analysis was performed on log transformed data, by two-way ANOVA. By 28 dpv, only sera from the ISA-inoculated animals demonstrated significantly higher titres than those seen at 0 dpv (adjusted *P* value = 0.0005). These titres, furthermore, were comparable to those demonstrated by the Olot/91-reactive pig 86 immune serum, with no significant difference between the two. No significant difference was observed between the CoPoP-inoculated and saRNA-inoculated animals by this timepoint.

By 42 dpv, average antibody titres from all three vaccine delivery platform groups were significantly higher than 0 dpv, with titres from both the CoPoP-inoculated and saRNA-inoculated animals now being comparable to the Olot/91-reactive immune serum. The average titres from the ISA-inoculated sera, conversely,

were higher than that of any other condition tested, with a statistically significant increase compared to the Olot/91-reactive immune serum (adjusted *P* value = 0.0133), the saRNA-inoculated sera (adjusted *P* value = 0.0034), and the CoPoP-inoculated sera (adjusted *P* value = 0.0011).

With the previous ELISA only investigating response against the recombinant GP3, reactivity 56 dpv sera was assessed further by immunostaining of MARC-145 cells infected with PRRSV-1 Olot/91, as described in **Chapter 5.5** (**Figure 6.8**). This work was performed by Dr. Jane Edwards, The Pirbright Institute.

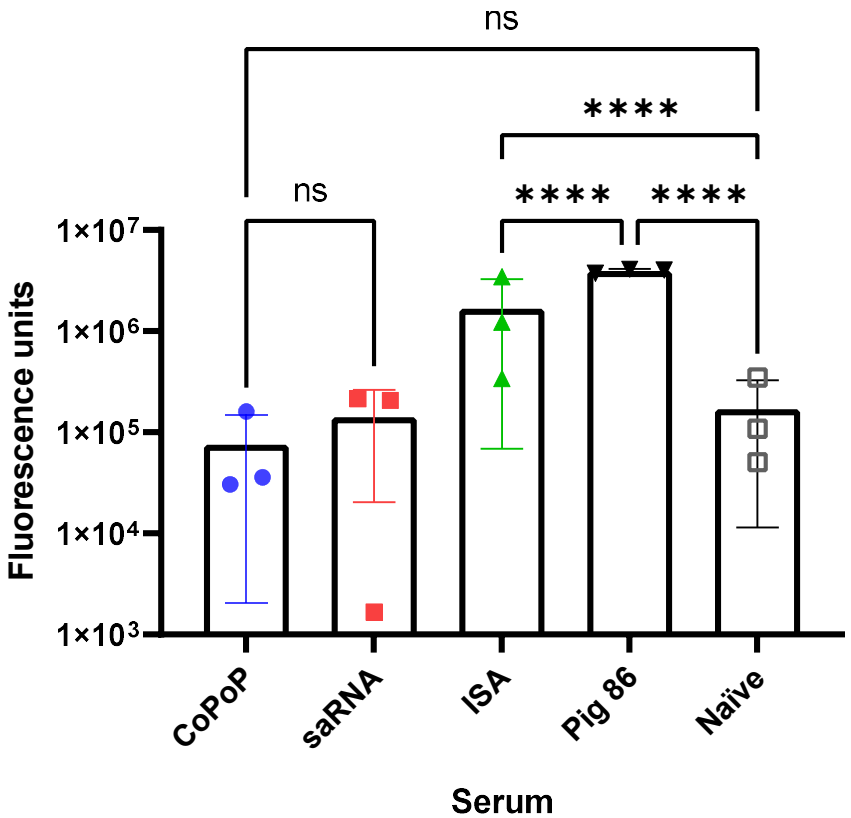


Figure 6.8: Immunostaining of sera from GP3-immunised pigs against PRRSV-1 Olot/91 infected MARC145-cells. Staining of PRRSV-infected cells by 56 dpv sera from pigs immunised with sGP3 formulated with Montanide ISA 201 VG adjuvant (ISA), sGP3 displayed on adjuvanted liposomes (CoPoP) or saRNA vectored membrane displayed GP3 (saRNA) was compared to staining from a known Olot/91-reactive sera (pig 86) and PRRSV-naïve sera, as positive and negative controls, respectively. Mean data of three technical replicates from three biological replicates ± SD are shown. Data provided by Dr. Jane Edwards, The Pirbright Institute.

Analysis by two-way ANOVA revealed that sera from both the CoPoP- and saRNA-inoculated groups did not demonstrate immunostaining of PRRSV-infected cells at a significant level above the PRRSV-naïve negative control serum. On average the ISA-inoculated group demonstrated significantly higher staining than the naïve (adjusted *P* value < 0.0001), though staining observed was significantly lower than the Olot/91-reactive pig 86 serum (adjusted *P* value < 0.0001).

Following immunostaining, linear epitope mapping was performed utilising an overlapping GP3 peptide library (**Figure 6.9**) using the same approach detailed in **Chapter 5.5**. Average responses of 28 and 56 dpv sera from the three pigs from each vaccine group, with technical replicates were assessed.

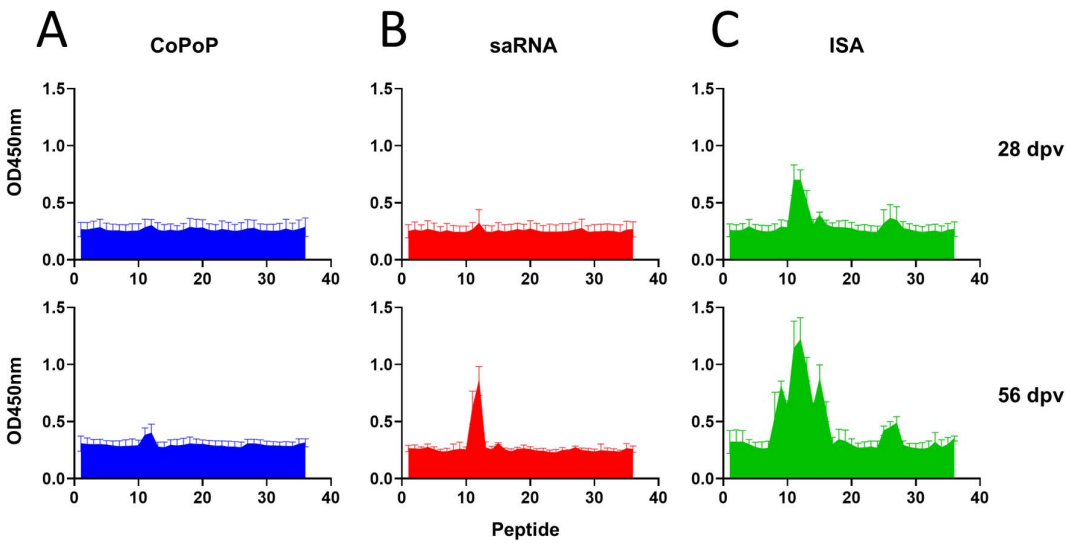


Figure 6.9: ELISA assessing recognition of overlapping GP3 sequence peptides to identify linear epitopes by sera from GP3-immunised pigs. Sera from 28 and 56 dpv from pigs immunised with sGP3 displayed on adjuvanted liposomes (CoPoP) (**A**), saRNA vectored membrane displayed GP3 (saRNA) (**B**), or sGP3 formulated with Montanide ISA 201 VG adjuvant (ISA) (**C**), were compared. Mean data of two technical replicates from three biological replicates ± SD are shown.

No significant binding to any of the peptides tested could be observed from either the CoPoP- or saRNA-inoculated groups at 28 dpv. From the ISA-inoculated group, however, peptides 11-13 containing the consensus sequence RDHD (residues 87-91) elicited significant binding, peaking at peptide 12. Additionally, peptides 25-28 containing the consensus sequence DKRH (residues 137-141) elicited significant binding, with a peak at peptide 27.

At 56 dpv, peptides 11-13 elicited significant binding from all three vaccine groups, with responses again peaking at peptide 12. Binding from the ISA-inoculated animals was significantly higher than either that observed from the CoPoP- or saRNA-inoculated, with the average responses from the saRNA-inoculated group in turn being significantly higher than the CoPoP-inoculated. While no significant binding was observed against any other peptides for the CoPoP- or saRNA-inoculated groups, sera from the ISA-inoculated animals demonstrated significant binding again to peptides 25-28, but also to peptides 8-10, containing the consensus sequence PGRN (residues 69-72), peaking at peptide 9; and peptides 14-17, containing the consensus sequence SMSI (residues 95-97), peaking at peptide 15.

Finally, the capacity of each serum to neutralise PRRSV-1 Olot/91 was assessed by VNT (**Figure 6.10**). Only Olot/91 was used initially, to assess whether these sera could neutralise homologous virus.

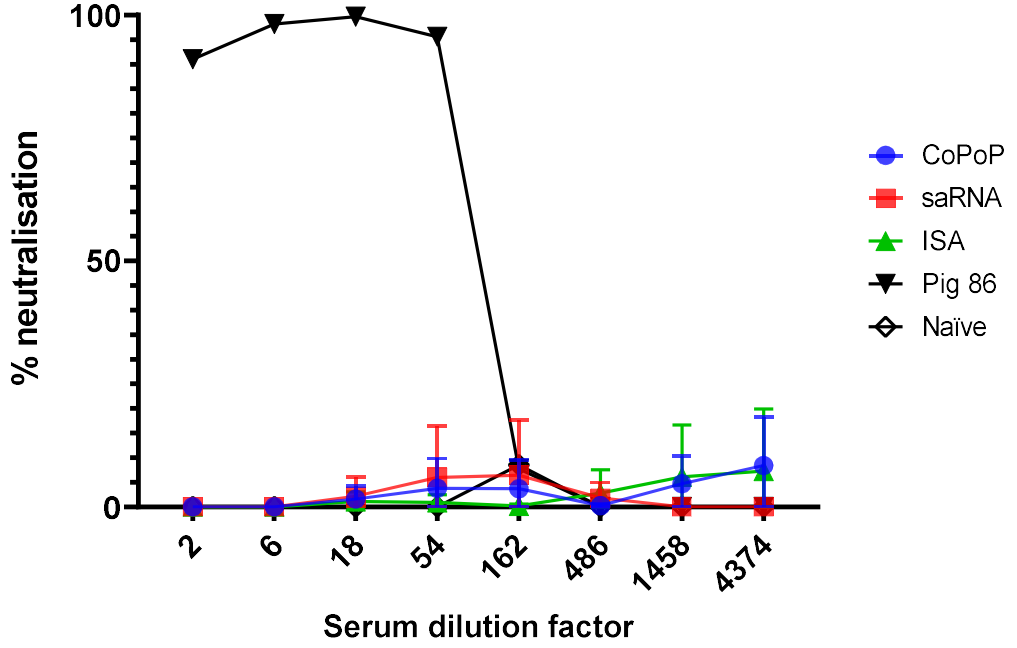


Figure 6.10: Neutralisation capacity of sera from animals vaccinated with PRRSV-1 GP3, using three vaccine delivery platforms, was assessed by VNT. Sera from 56 dpv from pigs immunised with sGP3 formulated with Montanide ISA 201 VG adjuvant (ISA), sGP3 displayed on adjuvanted liposomes (CoPoP) or saRNA vectored membrane displayed GP3 (saRNA) were compared to sera known to neutralise PRRSV-1 Olot/91 (pig 86), and a known negative (PRRSV naïve) serum. Mean data of three biological replicates ± SD are shown.

Sera from all vaccine groups failed to demonstrate the presence of antibodies capable of neutralising PRRSV-1 Olot/91, with no significant neutralisation being observed other than by the control pig 86 serum.

PRRSV GP3 immunisation, particularly ISA-adjuvanted and saRNA-vectored, induced robust antibody responses, but these failed to neutralise PRRSV. As a follow up to this study, an additional series of GP3-depletion experiments were performed. By comparing sGP3-depleted and mock-depleted sera, it was hoped, the contribution of GP3-specific antibodies to neutralisation could be better understood. Two PRRSV-immune sera were selected: pig 64 from the heterologous challenge experiment (detailed thoroughly in **Chapter 4**) and pig 86

from a sequential Olot/91 repeat infection study (also detailed in **Chapter 4**). Both sera were compared to a known naïve serum. All three sera were taken through three separate magnetic depletions, utilising either recombinant PRRSV-1 sGP3, recombinant SARS-CoV-2 S-RBD (as an irrelevant antigen), or a mock depletion with no additional antigen but processing the sera through the same magnetic bead depletion system. Efficacy of depletion was first assessed by sGP3 ELISA (**Figure 6.11**).

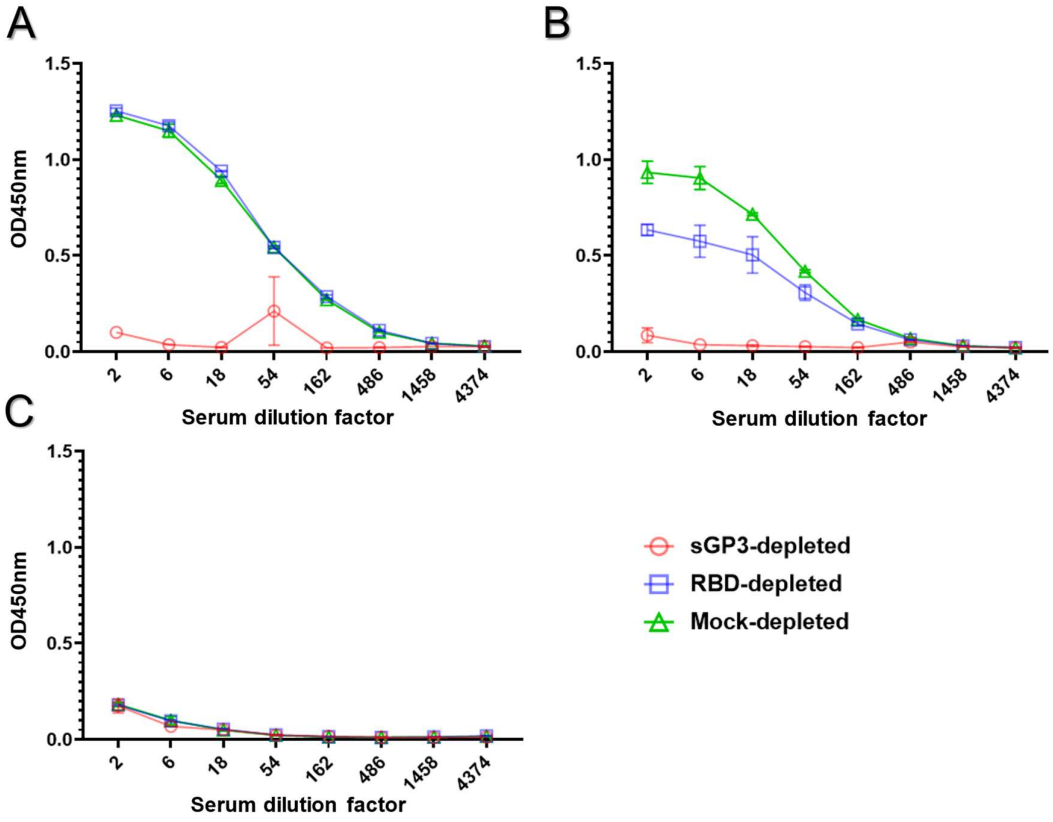


Figure 6.11: Antibody depletion was assessed by ELISA, determining proportion of sGP3 binding from sera depleted using either recombinant PRRSV-1 GP3, recombinant SARS-CoV-2 S-RBD, or with a mock depletion using no antigen. Serum from the hyperimmune pig 64 (**A**), PRRSV-1 Olot/91-reactive pig 86 (**B**) and naïve serum (**C**) were each depleted under three conditions. Mean data of two technical replicates ± SD are shown.

The sGP3 binding demonstrated by the sGP3-depleted sera was significantly lower for both PRRSV-reactive sera compared to the mock depleted. sGP3-depleted serum from pig 64 (**Figure 6.10A**) demonstrated reduced binding up until a 1:486 dilution (adjusted *P* value < 0.0001). For the Olot/91-reactive pig 86 sera (**Figure 6.10B**), this reduction was less significant at a dilution of 1:162 (adjusted *P* value < 0.05), though still significant. At a dilution of 1:486 onwards, significant binding could not be observed.

Following SARS-CoV-2 RDB-depletion a significant reduction in sGP3 binding was observed for the Olot/91-reactive pig 86 sera (**Figure 6.11B**), compared to the mock depleted. Starting at a dilution of 1:2 (adjusted *P* value < 0.0001), this reduction was still significant at 1:18 (adjusted *P* value = 0.0005), however no longer significant with a 1:54 serum dilution. No significant reduction was observed for the pig 64 serum (**Figure 6.11A**) following S-RBD-depletion.

The PRRSV-naïve sera (**Figure 6.11C**) did not demonstrate any significant binding following any depletion condition. Further, there was no significant difference observed between conditions at any dilution.

Based on these data, the same sera were taken forward to assess the effect of depletion on neutralisation capacity. Sera from pig 64 and 86 have demonstrated neutralising capacity against PRRSV-1 Olot/91 (as described in **Chapter 4 and 5**), and so this strain was chosen for assessment by VNT **(Figure 6.12)**.

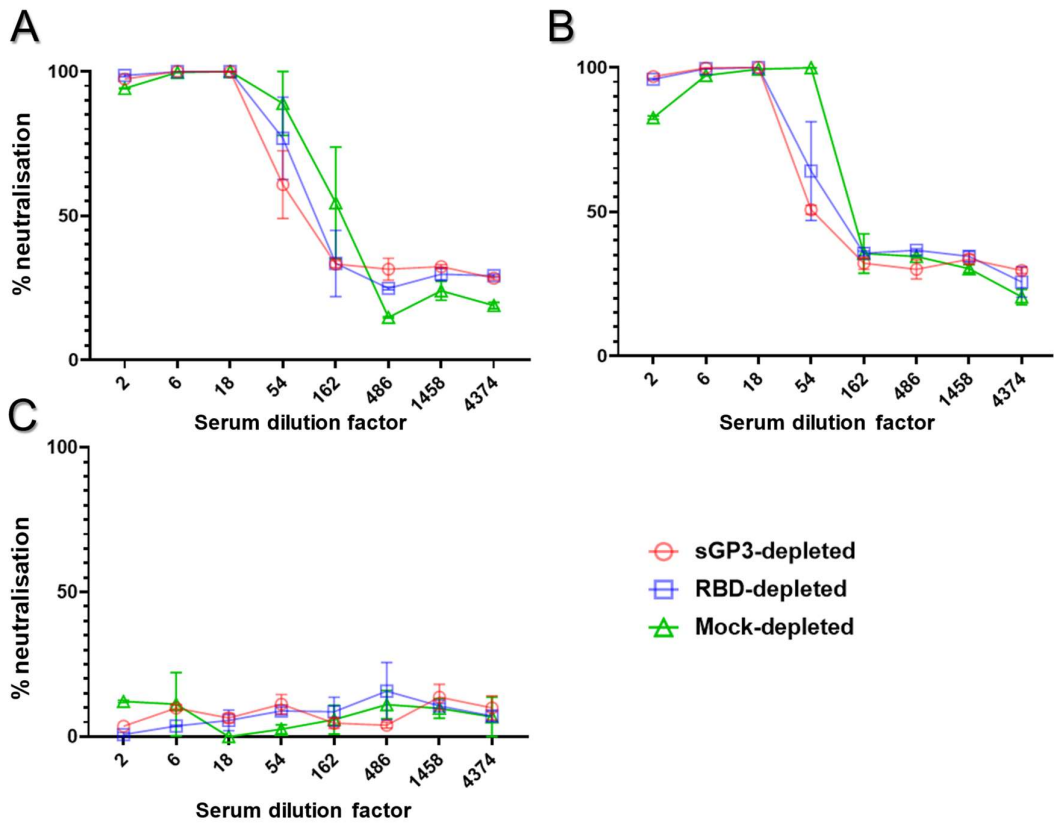


Figure 6.12: The effect of antibody depletion on neutralisation capacity was assessed by VNT. Serum from the hyperimmune pig 64 (**A**), PRRSV-1 Olot/91-reactive pig 86 (**B**) and naïve serum (**C**) were each depleted using either recombinant PRRSV-1 GP3, recombinant SARS-CoV-2 S-RBD, or with a mock depletion using no antigen. Mean data of two technical replicates ± SD are shown.

No significant reduction in neutralisation was observed for the pig 64 serum (**Figure 6.12A**) in either protein condition compared to the mock depleted. There was a significant reduction in neutralisation observed at a dilution of 1:54 from the Olot/91-reactive pig 86 sera (**Figure 6.12B**), following both sGP3- and S-RBD-depletion (adjusted *P* value < 0.0001). This difference was not significant, however, at either the preceding 1:18 dilution, nor the following 1:162 dilution. As with the previous experiment, the PRRSV-naïve sera (**Figure 6.12C**) demonstrated no significant difference between depletion conditions at any

dilution and as expected, did not demonstrate any significant PRRSV-1 Olot/91 neutralisation.

These experiments demonstrated that, despite sGP3 depletion resulting in a significant reduction in sGP3 binding from both PRRSV-reactive sera, there was no significant difference observed in the neutralisation capacity of these sera.

6.4 Discussion

This study set out to investigate the immunogenicity of recombinant GP3, and how different vaccine platforms may improve its immunogenicity. The results described herein have demonstrated that prime-boost immunisation with the saRNA vector successfully induced both antibody and T cell responses to a PRRSV glycoprotein, highlighting its potential for future vaccine development. It is clear, however, that further optimisation is required. The T cell responses observed appeared to vary between time points, fluctuating above and below statistical significance. Further, there appeared to be considerable variation between animals, resulting in large error bars at each time point. This difference in animals was also prevalent for immunostaining experiment detailed in **Figure 6.8**, with one of the three animals demonstrating staining two orders of magnitude below the others in the group, and far below even the negative control serum. While this was not exclusive to the results observed from the saRNA-immunised animals, this does highlight that the study described in this chapter, serving as a pilot study, was limited in the number of animals available. With a larger cohort, a clearer average in responses may have been determined.

Worth highlighting is that, despite immunisation with the saRNA-vectored GP3 resulting in post-boost sGP3 responses comparable to the sGP3 Montanide-ISA adjuvant immunised animals (**Figure 6.6**), the responses were significantly lower by 56 dpv, a trend that was consistent across all subsequent experiments. Previous studies have suggested an estimated half-life of binding antibody responses induced by saRNA-vectored vaccines from 22 – 213 dpv [306, 307], while these studies focus on delivery of SARS-CoV-2 antigens in humans, and so direct parallels cannot be drawn, it is still surprising how short-lasting the immunogenicity demonstrated in this study was. Due to limitations in time, sera from 56 dpv was not included in the calculation of antibody end point titres. In hindsight, it would have been interesting to see if the antibody titres followed this downward trend.

Worth considering is how lipid-complexed mRNA has been shown to induce type I IFN production, limiting the efficacy of mRNA-based vaccines resulting in lower and highly variable antibody titres [308, 309]. This may have contributed to the titres observed in this study. Only IFN-γ was assessed, as a measure for T cell responses, in hindsight including an assay for measuring type I IFNs may have been worth including.

Disappointingly, the CoPoP liposome system failed to induce any T cell responses, and the GP3-specific antibody titres were almost two orders of magnitude lower than the other vaccine groups. Despite the overall poor responses induced by this formulation, sGP3-specific antibody responses could still be detected following the booster immunisation. Similar to the responses against the saRNA-vectored GP3, however, these responses appeared to be on

a downward trend by 56 dpv, though even more dramatically. While no responses could be detected against sGP3 or PRRSV-1 Olot/91 in infected cells, sera from the CoPoP-vaccinated animals still demonstrated binding in the peptide ELISA experiment, suggesting GP3-specific antibodies were still present by 56 dpv, likely represented by very low titres. As discussed above, if time had allowed it would have been interesting to calculate antibody endpoint titres for this timepoint. Worth highlighting is that this study was the first time the CoPoP liposome system has been evaluated in pigs and so further optimisation of this platform is likely still required. It is possible that one reason for the poor responses demonstrated against the CoPoP-formulated sGP3 is that the adjuvants included in the liposome were not optimal for pigs. While the functions of adjuvants are well characterised for use in humans, their mechanisms in veterinary vaccines, particularly in pigs is poorer understood; fewer financial resources are available for research and development of animal vaccines compared with that for human vaccines [310]. Alum is widely used in veterinary vaccines, but is frequently associated with the induction of tissue granulomas and subsequent carcass losses in pigs [311, 312]. Additionally, oil-based liposomes are capable of inducing a strong Th1 response, but are also associated with adverse tissue reactivity, and granuloma formation [312-314]. While there is some recent, limited evidence of the use of QS-21 in pigs [315], there is no documented evidence of 3D (6-acyl)-PHAD® as an adjuvant in pigs. Subsequent studies using this platform should consider designing liposomes with molecular adjuvants known to induce stronger innate immune responses in pigs.

Despite the apparent failure to induce T cell responses, the sGP3 in Montanide ISA 201 VG adjuvant induced the strongest antibody responses overall, consistently resulting in the highest sGP3-specific antibody tires, and binding of sGP3, GP3 peptides, and PRRSV-1 Olot/91 infected cells. Of note is that for the immunostaining assay detailed in **Figure 6.8**, sera from the Olot/91-reactive pig 86 was included as a control. It should not be a surprise that the sera collected as part of the study detailed in this chapter would demonstrate significantly lower staining than this control, as pig 86 had been infected with live virus, and would therefore possess antibody titres against many other immunogenic PRRSV proteins (i.e. NSPs, N protein, major envelope GPs, etc.). While serum from this animal served as a control for the assay, comparing staining between it, and sera from animals only exposed to GP3, would be ill-advised.

There are some questions remaining regarding the sGP3 produced for the purpose of this study, however. As highlighted in **Figures 6.1** and **6.2**, multiple contaminants were observed following affinity purification. These contaminants appeared to be multiple forms of GP3. As previously discussed in **Chapter 3**, a likely explanation for some of these bands observed could be different glycosylation states. This hypothesis is supported by the deglycosylation data presented as part of **Figure 6.3** whereby, following PNGase F digestion, many of these bands disappear. For the smaller bands observed at ~15 kDa, it is possible that these represent potentially truncated forms of the sGP3. This would explain why these bands persist when using the anti-GP3 mAb, as shown in **Figure 6.2**. Further, this may explain why the Montanide ISA adjuvanted sGP3 resulted in antibodies displaying specificity against such a broad range of peptides,

compared to those from the saRNA-vectored group. Some epitopes that would otherwise be obscured/obstructed by glycans [316] and may have been accessible for immune recognition. With the formulation of GP3 being different for the saRNA-vectored vaccine and given the low responses from the CoPoP-vectored group, it is difficult to draw conclusions here.

In addition to the above, due to the limitations of the assays used, it was not possible to confirm that the glycosylated sGP3 had been successfully incorporated into the CoPoP liposome bilayer. The results described herein only demonstrate inclusion of the sGP3 while in a deglycosylated form; for the purpose of this study, it was assumed that the other glycosylated moieties of sGP3 were displayed equally well as the deglycosylated form. Without confirmation, it is unknown whether this was indeed the case, and whether suboptimal inclusion of the fully glycosylated may have contributed to the poor responses induced by the CoPoP-vectored vaccine.

Interestingly, considerable overlap was observed between the peptides eliciting the strongest response of the sGP3-immunised animals, and those eliciting binding from mAb2 and mAb 7, detailed in **Chapter 5.5**. For this study, only response against PRRSV-1 Olot/91 was investigated; it would be interesting to assess whether, like mAb 7, serum from these animals is able to demonstrate cross-reactivity between PRRSV strains. These results, when combined with the results of the depletion experiments detailed herein, **Figures 6.11** and **6.12**, highlight the complexity of the PRRSV minor envelope proteins. Despite numerous literature detailing GP3 as a target for nAbs [129, 191, 218, 220], this study suggests the contrary: that GP3 may not possess neutralising epitopes. An

important caveat to make is that only the ectodomain of GP3 was tested as a part of this study, there still remain question marks over the full length protein, and whether the TM domain onwards may possess neutralising epitopes.

The apparent failure of recombinant GP3 immunisation to induce PRRSV neutralisation is disappointing and suggests the contribution of GP3 to the neutralising responses to PRRSV is more complex than initially thought. As discussed in **Chapter 4** an important caveat is that, as these proteins are recombinant and cannot be directly compared to the native antigen, this should be interpreted with caution. An additional reason why no neutralising responses could be detected is that co-expression of GP3 with GP2 and GP4 may be required to achieve a heterotrimeric complex, which more authentically mimics that present on the PRRSV envelope, and therefore induce neutralising responses, cross-protective or otherwise, and so should be considered for future study. The saRNA vectored construct used for this study demonstrated effective display of GP3 on the surface of transduced cells which, though discussed, could not be achieved as part of this project. The saRNA platform, consequently, could be greatly beneficial in the context of co-expression of PRRSV GPs. This platform is readily amenable for such an evaluation of PRRSV glycoprotein co-expression and should be investigated as a follow-up to this work.

Chapter 7. General discussion

7.1 Summary

PRRSV continues to cause an ever-increasing financial burden to the global pork industry and serves as a major threat to both animal welfare and food security. Existing as two antigenically distinct species, PRRSV-1 and -2 [22], and being prone to mutation and recombination events [51], PRRSV is rapidly evolving and diversifying with highly pathogenic novel strains emerging from both species. Despite decades-long availability of both MLV and inactivated vaccines, protection is often insufficient, conferring little to no protection against more genetically heterologous strains [146]. There is, therefore, an urgent requirement to explore alternative approaches to PRRSV vaccine development. This project aimed to identify novel vaccine targets and to provide a greater understanding of the neutralising antibody response against PRRSV; four primary objectives that were set for this project, to this end, were as follows:

1. Produce novel recombinant PRRSV glycoproteins to use as tools to support mAb isolation and characterisation (**Chapter 3**).
2. Characterise the antigenicity of recombinant PRRSV glycoproteins (**Chapter 4**).
3. Isolate and characterise naturally occurring porcine mAbs capable of neutralising PRRSV (**Chapter 5**).
4. Evaluate the immunogenicity of novel recombinant PRRSV glycoproteins (**Chapter 6**).

The key outcomes of this project presented in this thesis were that: a) a mammalian cell expression system can be used to generate recombinant PRRSV GPs as both full-length forms mimicking the natural proteins, and as artificially

shortened ectodomain-only soluble forms; b) these recombinant GPs are capable of eliciting binding by antibodies and B cells from PRRSV-immune pigs, and are therefore antigenically similar to native PRRSV GPs; c) through tetramerization of these recombinant GPs and utilising them as tools for flow cytometry, PRRSV-specific B cells can be identified and isolated enabling cloning and expression of recombinant mAbs; d) recombinant mAbs derived from sGP3-binding single B cells can be expressed in a mammalian cell system, purified, and demonstrate reactivity against both recombinant and native GP3; e) some mAbs generated through this method displayed promising cross-reactivity, and can be used to identify conserved epitopes shared between PRRSV strains, and species. However, studies detailed throughout this thesis, both of recombinant mAbs and serum from recombinant GP3-immunised animals, suggest that GP3 alone may be insufficient for the generation of broadly neutralising PRRSV antibodies.

7.2 Discussion of limitations and future direction

To the best of my knowledge, **Chapters 3** and **4** describe the first use of a mammalian cell system to produce PRRSV GPs. One limitation highlighted throughout this project is that the full-length rec-GPs remained relatively underexplored compared to the ectodomain only forms. While it was evident that the full-length rec-GPs were not secreted as soluble proteins, as detailed in **Chapter 3**, further work involving lysis of cells and detergent extraction of membrane proteins could generate solubilised full length GP3. However, purification from detergent lysates would also include protein that had not yet undergone proper folding, glycosylation, and other post-translational modifications that would likely serve as contaminants [262]. Nonetheless,

methods for purifying recombinant protein from cell lysate have been described [317], and could be explored for future work.

To focus this project, the role of the additional non-glycosylated proteins of the minor envelope complex, i.e., E and GP5a/ORF5a proteins, were not considered. While the confocal data detailed in **Chapter 3.3** demonstrated that these additional proteins are not required for the co-localisation of GP2, GP3, and GP4, it is unknown whether their presence is required for the complete formation of the minor envelope complex. If so, future work investigating this subject may require the generation of recombinant forms of these proteins also. Additionally, co-expression was not investigated for the ectodomain only forms of the rec-GPs detailed in this thesis. It is unknown whether in their shortened form, they would still be able to form a complex, and whether they would still be secreted when complexed.

Given the difficulties generating recombinant PRRSV GPs, future work intent on identifying potential conserved epitopes may want to focus on alternative approaches. Use of virus like particles (VLPs), for example, has been demonstrated as a successful strategy for isolating mAbs against HIV [318], dengue virus [319], and SARS-CoV-2 [320]. VLPs are virus-derived structures comprised of one or more molecules with the ability to self-assemble, mimicking the size and form of a virus particle but lacking the genetic material and are therefore not pathogenic [321]. VLPs can be engineered to carry antigenic epitopes derived from either the parental virus or foreign sources [322], and make effective vaccine platforms because they possess a number of physical features that enhance their immunogenicity [323]. PRRSV VLPs have been investigated,

and have been demonstrated to induce an immune response, however these have largely focussed on the GP5 and M proteins [324-326]. Use of the minor envelope proteins in PRRSV VLPs, conversely, has been underexplored. The limited studies that have tried to include GP2, GP3, and GP4, in addition to the major envelope proteins, and often report poor representation of the minor proteins in the VLPs, being largely undetectable [207]. Research on PRRSV VLPs is largely in its infancy, but does represent a potential method for identifying antibodies against proteins with such low relative abundance, and apparent low antigenicity in the case of GP2 and GP4, as the PRRSV minor envelope GPs [144].

Another alternative approach to using recombinant antigens for identifying potential conserved epitopes that has historically proven successful for PRRSV is the use of peptide screening/pepscan analysis [327, 328] – the use of overlapping peptides. Detailed throughout this project, for example, was the use of a peptide library for the purpose of epitope mapping using isolated mAbs and material from rec-GP3 immunised animals. Despite 2011 being the earliest example of this approach being used to identify PRRSV epitopes and characterise antigenic regions [205, 328], few neutralising epitopes have been identified within PRRSV GPs, and epitopes responsible for broad neutralisation remain a mystery. As already discussed, these approaches are limited by the use of linear peptides, missing potential conformational, or discontinuous epitopes. As discussed in **Chapter 3**, protein modelling and prediction systems continue to improve, and represent great potential for determining potential epitopes. With more high resolution X-ray structures of antibody-antigen complexes being

deposited into databases such as the Protein Data Bank [329], structure-based methods continue to develop to predict conformational or discontinuous B-cell epitopes, which contain residues that are not necessarily contiguous along the protein sequence. Many of these methods have reported significantly better than random predictive power [330], and in time could be used to identify PRRSV epitopes without the need for recombinant proteins at all.

Highlighted several times throughout the work presented in this thesis is the discrepancy in antigenicity between rec-GP2 and rec-GP4, and rec-GP3. GP3 is well documented as highly antigenic despite its low relative abundance [220-222], which was reflected in the results presented in this thesis. As discussed in **Chapter 4**, while antigenic regions have been identified in both GP2 and GP4 [205], in several instances the rec-GP2 and rec-GP4 failed to elicit, or elicited very poor, binding from PRRSV-reactive sera. Even expanding to a larger cohort than the six heterologous challenge experiment animals that this project largely focussed on demonstrated consistently low binding of rec-GP2 and rec-GP4. As a follow-up already conducted by colleagues in the PRRS Immunology Group at The Pirbright Institute and Prof Lorenzo Fraile, University of Lleida, Spain, these rec-GPs have been used to assess responses of sera collected from Spanish sow herds that were repeatedly vaccinated with PRRSV MLV and naturally exposed to circulating PRRSV-1 strains. These animals demonstrated cross-neutralising antibody titres against PRRSV-2, despite lack of exposure to this viral species. Sera from these animals exhibited significantly higher binding of rec-GP2 and rec-GP4 than any experiment detailed in this thesis. It is possible, therefore, that repeated exposure of multiple strains is necessary to induce

significant GP2/GP4-specific responses. Performing the workflow detailed throughout this thesis, utilising sGP2 and sGP4 to isolate PRRSV-specific B cells from these animals and assessing their capacity for neutralisation would be of great interest.

This suggests another potential limitation of the work presented in this thesis; a large proportion of the characterisation of the rec-GP-specific responses were determined through indirect ELISA which may not have been sufficiently sensitive. With the above data suggesting that rec-GP2 and rec-GP4 could elicit binding from hyperimmunised pig sera, it's possible that the responses from the sera tested in **Chapter 4** were below the limit of sensitivity, rather than being absent. This hypothesis is supported by the flow cytometry data presented later in **Chapter 4** which demonstrated that, while infrequent compared to rec-GP3-specific events, rec-GP2 and rec-GP4 specific cells could be detected using this method. To compensate, future studies could aim to isolate GP2/GP4-specific cells from a larger pool of cells.

To be realistic in the scope of this project, the design of these rec-GPs was limited to PRRSV-1 Olot/91. Follow on work should investigate not only more diverse PRRSV-1 strains, but also investigate PRRSV-2 strains. As mentioned in **Chapter 5**, work in the PRRS Immunology Group at The Pirbright Institute has already begun in this regard. Using the methods detailed throughout this thesis, recombinant proteins based on PRRSV-2 VR-2332 sequence data have been generated for sGP2, sGP3, and sGP4, in addition to recombinant GP5 based on both the PRRSV-1 Olot/91 and PRRSV-2 VR2332 sequences. Characterisation of these rec-GPs is underway.

Further to the above, **Chapter 4** detailed the identification of PRRSV-specific single B cells using two tetramers of each rec-GP. In future work, staining cells with tetramers assembled from rec-GPs based on both PRRSV-1 and PRRSV-2 sequences simultaneously could greatly increase the efficiency of this workflow, enabling identification of cross-reactive cells before undergoing the laborious process of recombinant mAb generation.

Chapter 5 described how these GPs could be used to isolate B cells, enabling generation of recombinant mAbs. While the workflow detailed in this thesis did enable generation and characterisation of PRRSV-specific mAbs, there were some key limitations worth highlighting; each step of processing revealed increasingly poor overall recovery rates of the VH and VL genes. Sanger sequencing resulted in loss of some sequences, that were unable to be properly sequenced despite amplification. Following sequencing, furthermore, roughly half of the recombinant mAbs failed to express and, due to limitations in time, were not revisited. Those that were expressed were few in number, and the following assays detailed later in **Chapter 5** revealed some of these failed to recognise GP3.

Still, some of these mAbs demonstrated impressive cross-reactivity and despite their inability to neutralise could still serve as useful research tools. One limitation discussed in **Chapter 3** was the lack of available GP-specific antibodies preventing immunolabelling, which these cross-reactive sGP3-specific mAbs can now help to address. An additional possible use for these recombinant GP3-specific mAbs is as adjuvants to improve the efficacy of existing vaccines. Recent studies have shown successful use of a GP3-specific IgM mAb isolated from mice

hybridomas to adjuvant both inactivated and MLV PRRSV vaccines [331]. Furthermore, the results presented in this study suggest that the antibody-mediated neutralisation of PRRSV may involve multiple PRRSV structural proteins, highlighting GP3 and GP4 in particular, and is not determined by a single protein. This aligns with the new hypothesis formed based on the results presented in this thesis: that GP3 alone is insufficient for neutralisation, broad or otherwise.

The data presented herein focussed only on B cells isolated from PBMCs. As the lungs are the primary site of PRRSV infection and therefore the early immune response, further work comprising an in-depth analysis of the immune response in the lung, in addition to the draining lymph nodes, over the course of infection should be conducted. Material from these tissues is also available from the heterologous PRRSV challenge study, in addition to spleen and tonsils, and so could be a focus of future investigation.

For this project, only one animal – pig 64 – was selected to take forward for isolation of B cells. Previous studies indicated that approximately 1 % of experimentally infected pigs could produce bnAbs [47, 74]. Though ELISA and tetramer data demonstrated a strong response to the rec-GPs in pig 64, it is still possible that this animal did not possess a high titre of broadly neutralising antibodies. For the heterologous challenge experiment, PRRSV-2 neutralisation was only seen following PRRSV-2 challenge [251]. While it was hypothesised that the sequential heterologous challenge would promote the maturation of bnAbs, there is no conclusive evidence that any of these animals did possess bnAbs. The whole antibody repertoire data does suggest likelihood for cross-

reactive Abs within the repertoire of these animals, as described in **Chapter 5.6**. The kinetics observed of certain clusters of VH genes arising prior to PRRSV-2 challenge, and continuing to rise until termination is suggestive of cross-reactive Abs [332]. However, without a complete set of data, and the observation that recombinant anti-GP3 mAbs associated with these clusters failed to neutralise, it is difficult to come to firm conclusions. Follow-up work based on this project should aim to complete the repertoire sequencing dataset for the day 112 timepoint. Estimating repertoire diversity and linking changes in diversity with the timeline of viral challenge, clinical status, and outcomes could provide great insight into vaccine profiling, and the accurate/early detection of disease and infection [333, 334].

The sGP3 vaccine formulations described in **Chapter 6** demonstrated that it was possible to induce both Ab and T cell immune responses using rec-GPs. Though high rec-GP3-specific antibody titres were demonstrated, rec-GP3 immunisation failed to induce detectable nAb titres, regardless of the vaccine delivery platform investigated. Further experiments should broaden investigation beyond only GP3, assessing the immunogenicity of GP2, GP3, and GP4 proteins simultaneously. There is evidence that these proteins might act synergistically to induce neutralising responses with broad capacity against PRRSV [155, 335]. It is conceivable that neutralising epitopes within these proteins are conformational, and only presented when the minor GPs are assembled as a multimer. Therefore, inoculating with individual rec-GPs may not be sufficient to generate a neutralising response. The use of polycistronic vectors was discussed in both **Chapter 3** and **Chapter 6** as an approach to achieve this. Considering the results presented as

part of the immunogenicity study detailed in **Chapter 6**, there is a good case for using a polycistronic saRNA vector to enable surface expression of all three GPs and could result in the presentation/conformation of these rec-GPs in a way that is much more representative of their natural form, the benefits of which have already been discussed in previous chapters.

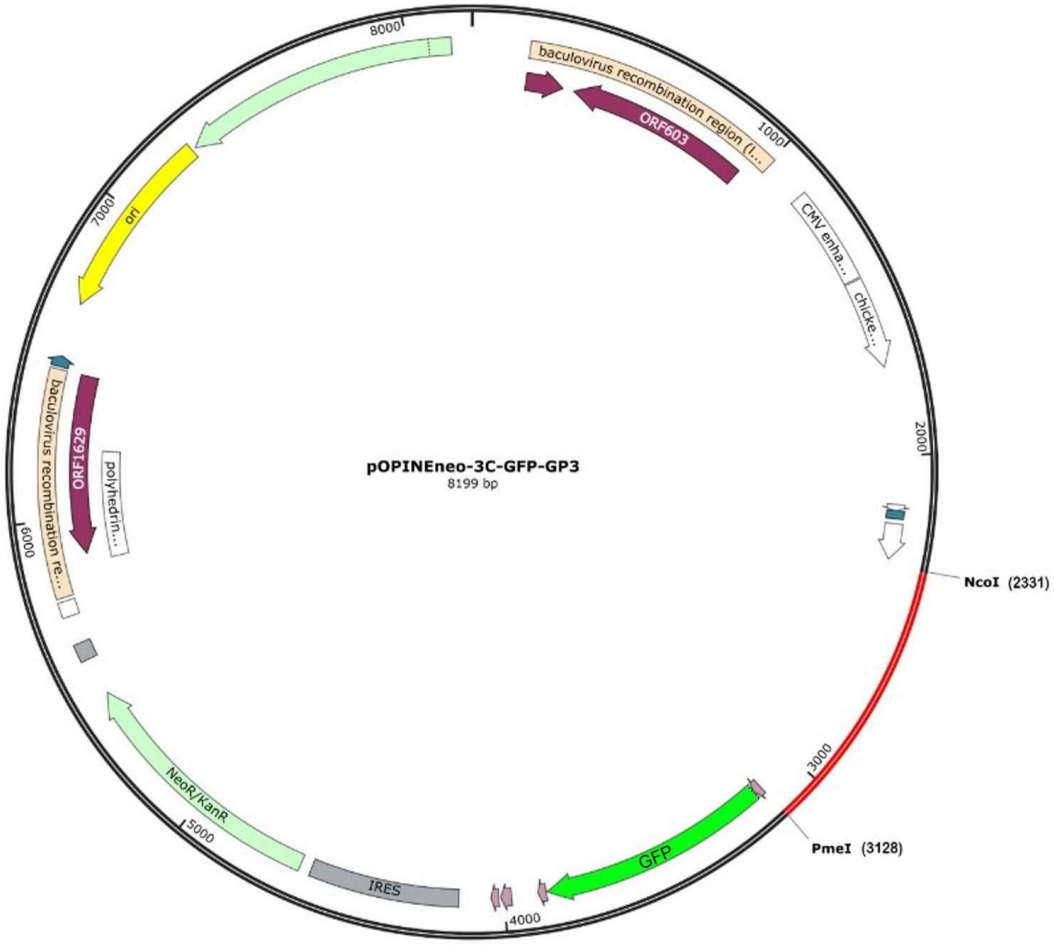
The work presented in **Chapter 6** especially highlighted the challenges in producing the rec-GPs which are highly glycosylated and expressed at relatively low levels. Heterogeneity due to multiple glycoforms, and potentially truncated isoforms of each protein, were observed throughout this thesis. The minor GPs of PRRSV are clearly difficult proteins to produce, and going forward co-expression in mammalian or insect cells could be explored to increase protein levels which would enable additional purification steps size such as exclusion chromatography to be carried out leading to increased sample homogeneity.

7.3 Conclusion

In summary, the work presented in this thesis suggests PRRSV sGP3 is antigenic, immunogenic, and possesses conserved antibody epitopes, though alone may be insufficient to elicit a neutralising antibody response. This work, in combination with the future work described, provide groundwork for subsequent research into the PRRSV minor envelope proteins, and the role they play in the immune response against PRRSV. It is hoped that these data will aid in the development of next generation PRRSV vaccines that are urgently required to improve control of the disease.

Appendix

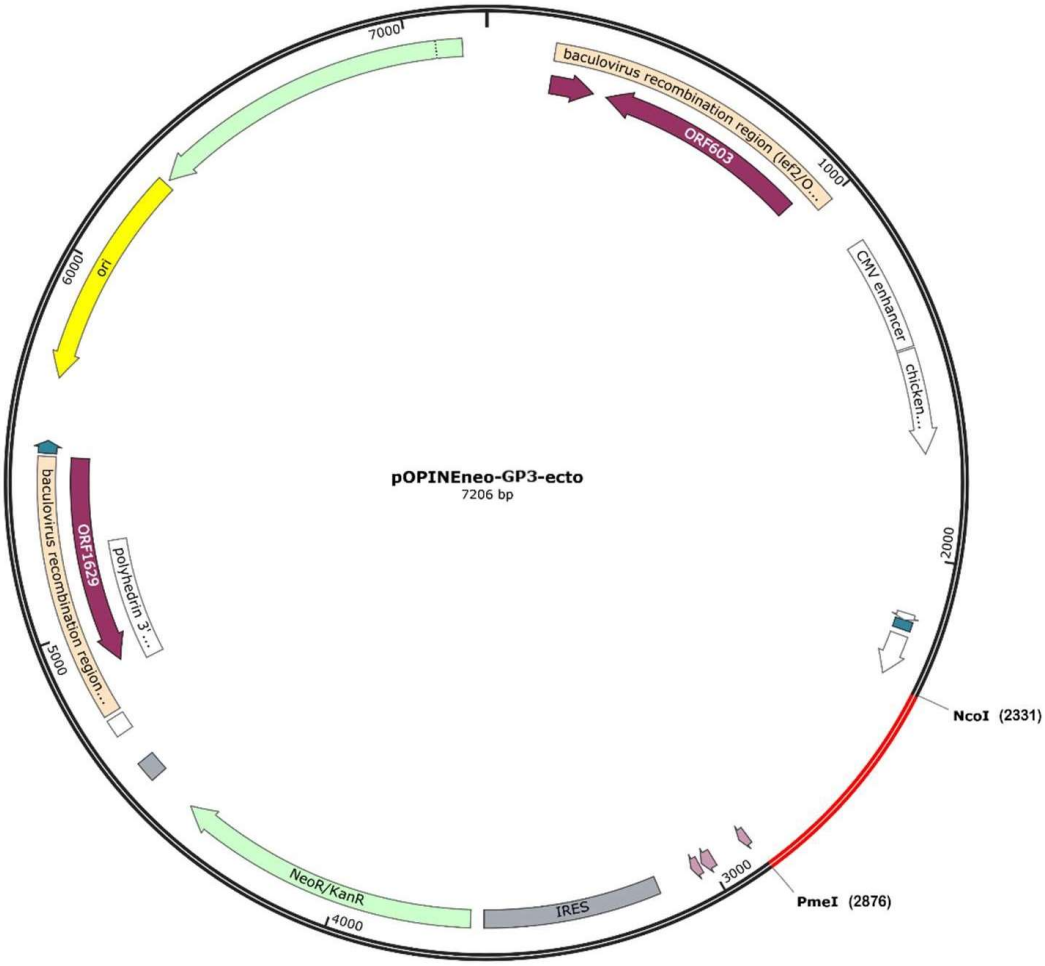
Appendix Figure 1: pOPINEneo-3c-GFP plasmid map. Used for generating recombinant PRRSV GP-GFP fluorescent fusions. Inserts are represented in **red**, flanked by respective cutting restriction endonucleases.GP3-cloned plasmids are shown as example. This plasmid was kindly provided by the Ray Owens Group, PPUK, Rosalind Franklin Institute/University of Oxford.



A.1.2 Position of elements

	bp
Vector size	8199
Insert size	552-798

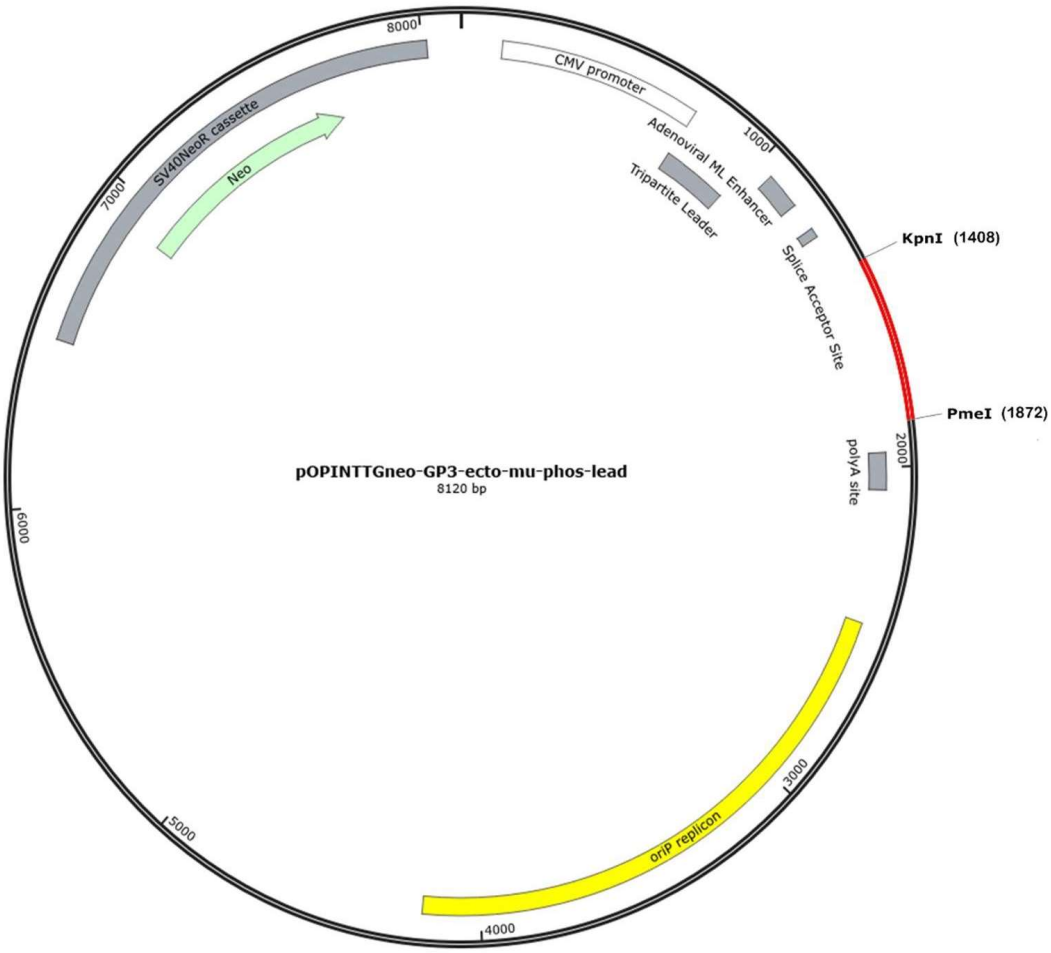
Appendix Figure 2: pOPINEneo plasmid map. Used for generating both full length and forms with the first transmembrane domain onwards removed of each recombinant PRRSV GP. Inserts are represented in **red**, flanked by respective cutting restriction endonucleases.GP3-cloned plasmids are shown as example. This plasmid was kindly provided by the Ray Owens Group, PPUK, Rosalind Franklin Institute/University of Oxford.



A.2.2 Position of elements

	bp
Vector size……..……...7206	
Insert size……....408-798	

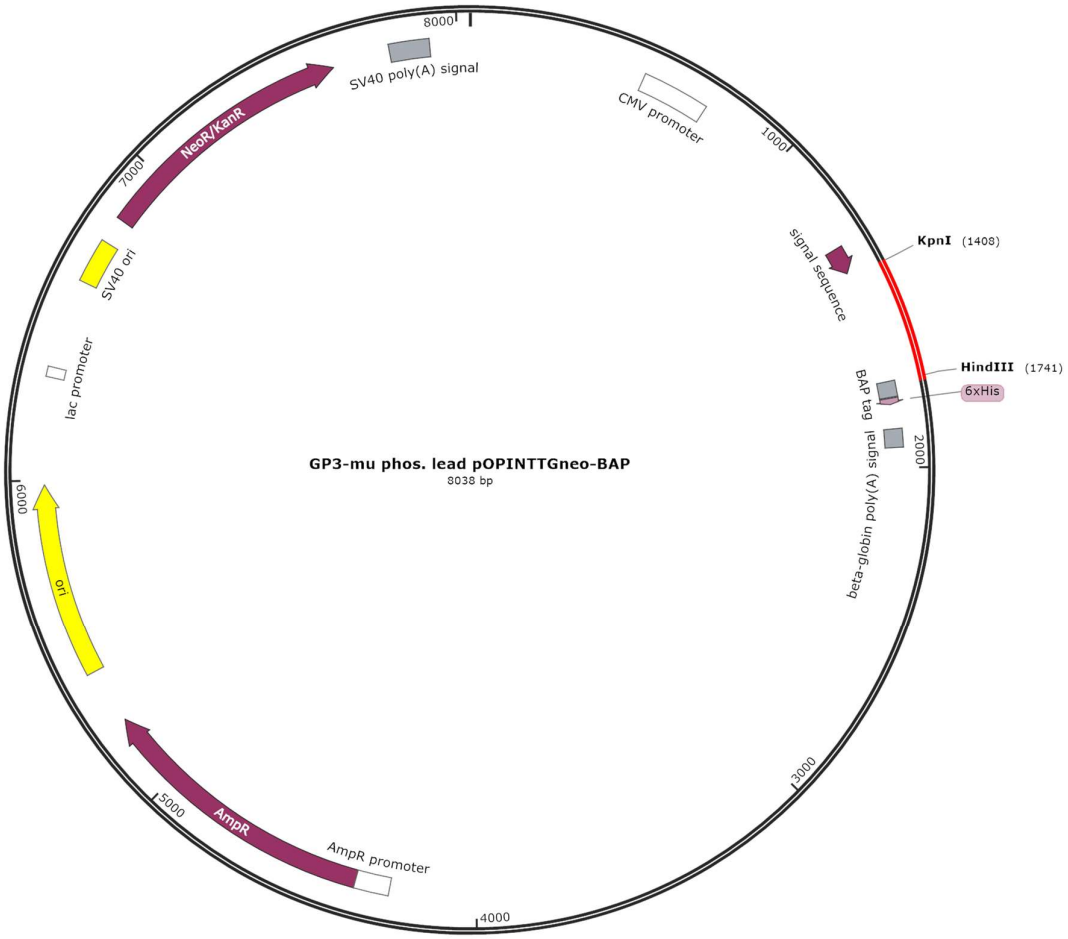
Appendix Figure 3: pOPINTTneo plasmid map. Used for generating recombinant PRRSV GPs with receptor-type protein-tyrosine phosphatase μ leader sequences, with the first transmembrane domain onwards removed. Inserts are represented in **red**, flanked by respective cutting restriction endonucleases.GP3-cloned plasmids are shown as example. This plasmid was kindly provided by the Ray Owens Group, PPUK, Rosalind Franklin Institute/University of Oxford.



A.3.2 Position of elements

	bp
Vector size	8120
Insert size	408-798

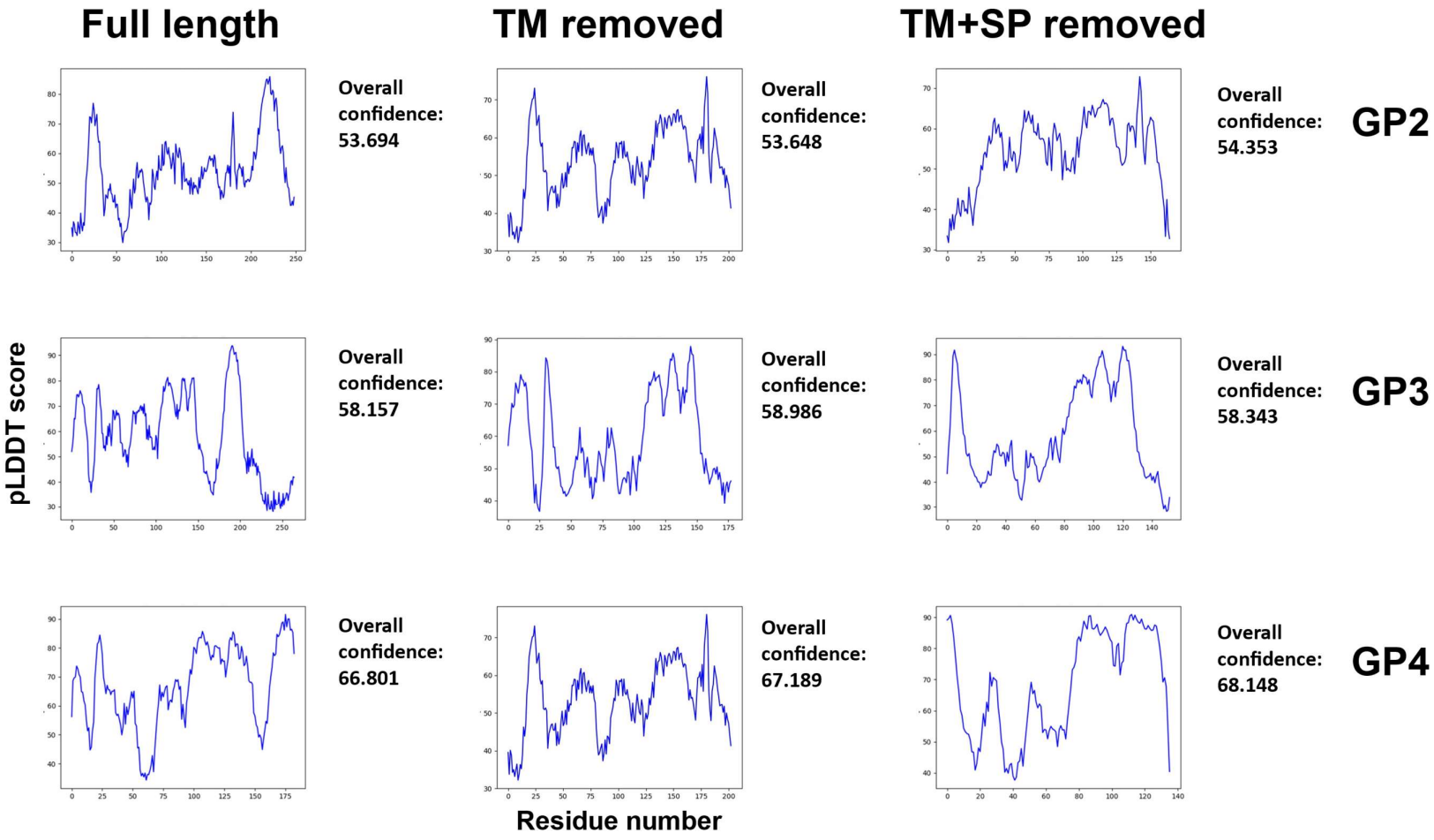
Appendix Figure 4: pOPINTTneo plasmid map also encoding for a biotin acceptor peptide tag. Used for generating recombinant PRRSV GPs with receptor-type protein-tyrosine phosphatase μ leader sequences, with the first transmembrane domain onwards removed, and an additional BAP tag. Inserts are represented in **red**, flanked by respective cutting restriction endonucleases.GP3-cloned plasmids are shown as example. This plasmid was kindly provided by the Ray Owens Group, PPUK, Rosalind Franklin Institute/University of Oxford.



A.4.2 Position of elements

	bp
Vector size…….…...8038	
Insert size…….408-798	

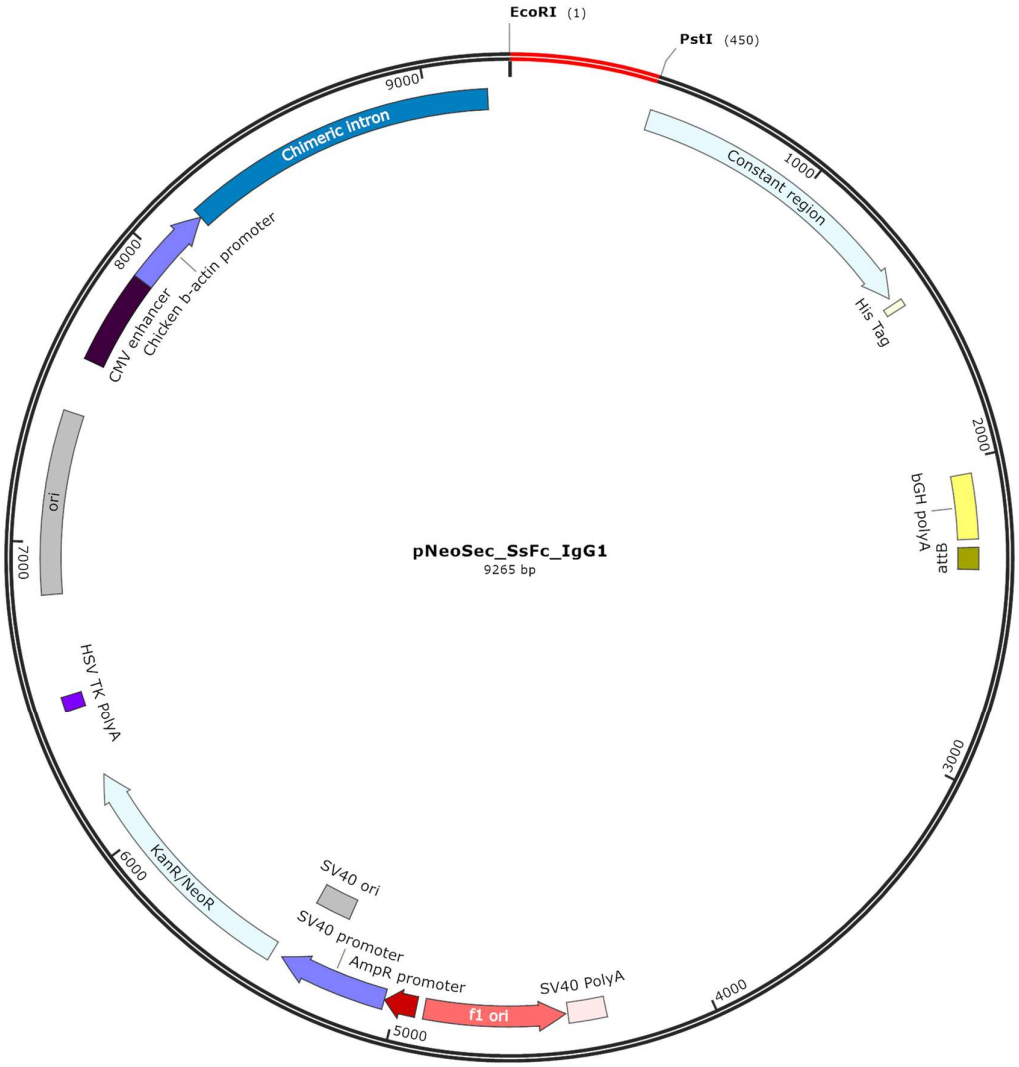
Appendix Figure 5: Overall pLDDT confidence scores of AlphaFold predictions from Figure 3.3. Recombinant PRRSV GP sequences as either full length, with the transmembrane domain onwards removed, or the transmembrane domain onwards, and signal peptides removed were modelled. n = 5 predictions were made per sequence, confidence scores are given out of 100.



Appendix Table 1: List of primers kindly provided by the Immunological Toolbox, The Pirbright Institute, UK, enabling amplification of VH and VL genes. Cells highlighted in **green** were used in the first round of PCR, and those in **blue** were used for subsequent rounds and for the addition of overhangs for cloning.

Primer name	Sequence (5' to 3')	Target sequence
235	AACTGGGTGGTCTTGTTTGC	ssIGHV_L1_F
236	GGAGTAGAGCCCTGACGG	ssIGHG-R
237	ATGCTCACAGAGGGTAGGAG	ssIgM_GSP3
238	CTCCAGGTTACTGTCAGGGG	ssIgA_GSP2
246	GCCTCYTGCTGCTCTGG	IGKV1-F
247	TTCCCTGCTCAGCTCCTG	IGKV2-F
248	GACCACCCCATCCACTTTC	IGKC-R
251	CCTTGTCACCCTCCTCACTC	IGLV2-F
252	CTGGAYCCCTCTCCTGCTC	IGLV3-F
253	CCTGGACGGTGCTTCTGAT	IGLV8-F
300	GCGTCACTGTCTTCTCCACA	ssCL4_R
256	TCGTCGGCAGCGTCAGATGTGTATAAGAGACAGG AGGWGAAGCTGGTGGAGTCTG	ssIGHV-F_OH
260	GTCTCGTGGGCTCGGAGATGTGTATAAGAGACAG GTAGACCGATGGAGCTGTGTTGT	ssIgG3_1-R_OH
262	GTCTCGTGGGCTCGGAGATGTGTATAAGAGACAG CAGAGGGTAGACCGATGGGG	ssIgG156n_1-R_OH
258	GTCTCGTGGGCTCGGAGATGTGTATAAGAGACAG GGAAGAGATTCGGGGCAGA	ssIgM_GSP1_OH
259	GTCTCGTGGGCTCGGAGATGTGTATAAGAGACAG TGGGAAGATTTTGGGGCTGG	ssIgA_GSP2_OH
264	TCGTCGGCAGCGTCAGATGTGTATAAGAGACAGG CCTCYTGCTGCTCTGG	IGKV1-F_OH
266	GTCTCGTGGGCTCGGAGATGTGTATAAGAGACAG GGGTCTCTAACTGCTCCTTCG	ssIGKC2_R _OH
267	TCGTCGGCAGCGTCAGATGTGTATAAGAGACAGC CTTGTCACCCTCCTCACTC	IGLV2-F_OH
268	TCGTCGGCAGCGTCAGATGTGTATAAGAGACAGC TGGAYCCCTCTCCTGCTC	IGLV3-F_OH
270	TCGTCGGCAGCGTCAGATGTGTATAAGAGACAGC CTGGACGGTGCTTCTGAT	IGLV8-F_OH
272	GTCTCGTGGGCTCGGAGATGTGTATAAGAGACAG GYGGCCTTGGGCTGAC	ssCL1_R_OH

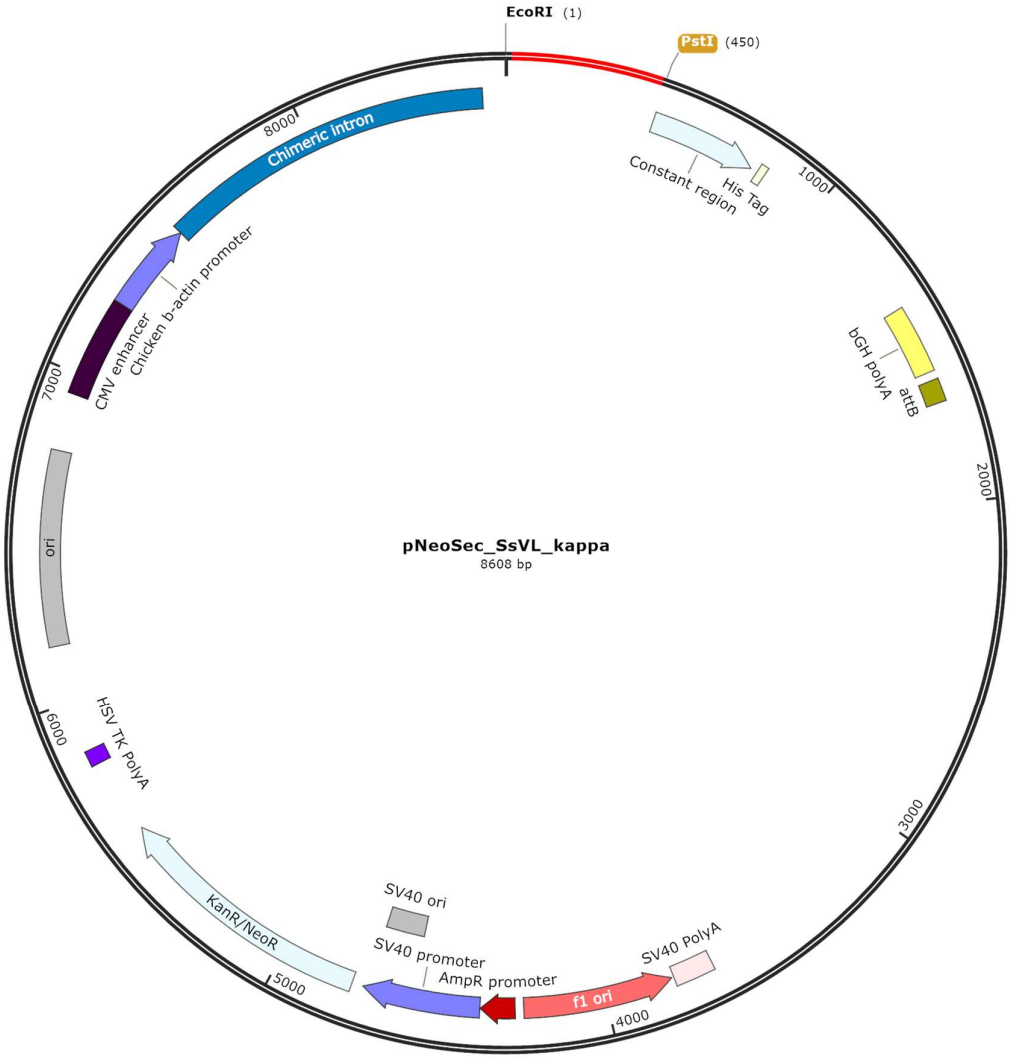
Appendix Figure 6: pNeoSec_SsFc_IgG1 plasmid map. Used for generating recombinant VH IgG1 genes for recombinant mAb expression. Inserts are represented in **red**, flanked by respective cutting restriction endonucleases. This plasmid was kindly provided by the Immunological Toolbox, The Pirbright Institute, UK.



A.6.2 Position of elements

	bp
Vector size	9265
Insert size	472

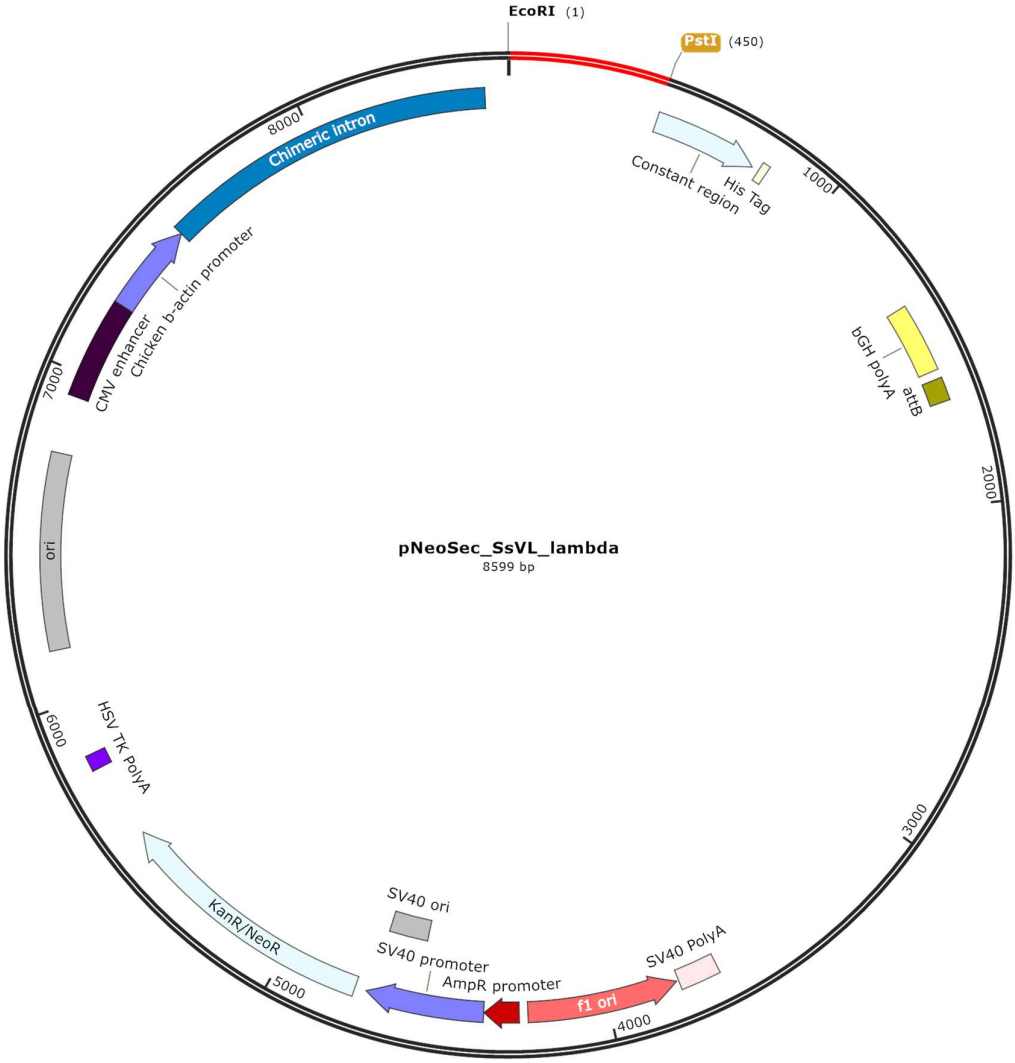
Appendix Figure 7: pNeoSec_SsFc_IgG1 plasmid map. Used for generating recombinant VL Igκ genes for recombinant mAb expression. Inserts are represented in **red**, flanked by respective cutting restriction endonucleases. This plasmid was kindly provided by the Immunological Toolbox, The Pirbright Institute, UK.



A.7.2 Position of elements

	bp
Vector size	8608
Insert size	477-512

Appendix Figure 8: pNeoSec_SsFc_IgG1 plasmid map. Used for generating recombinant VL Igλ genes for recombinant mAb expression. Inserts are represented in **red**, flanked by respective cutting restriction endonucleases. This plasmid was kindly provided by the Immunological Toolbox, The Pirbright Institute, UK.



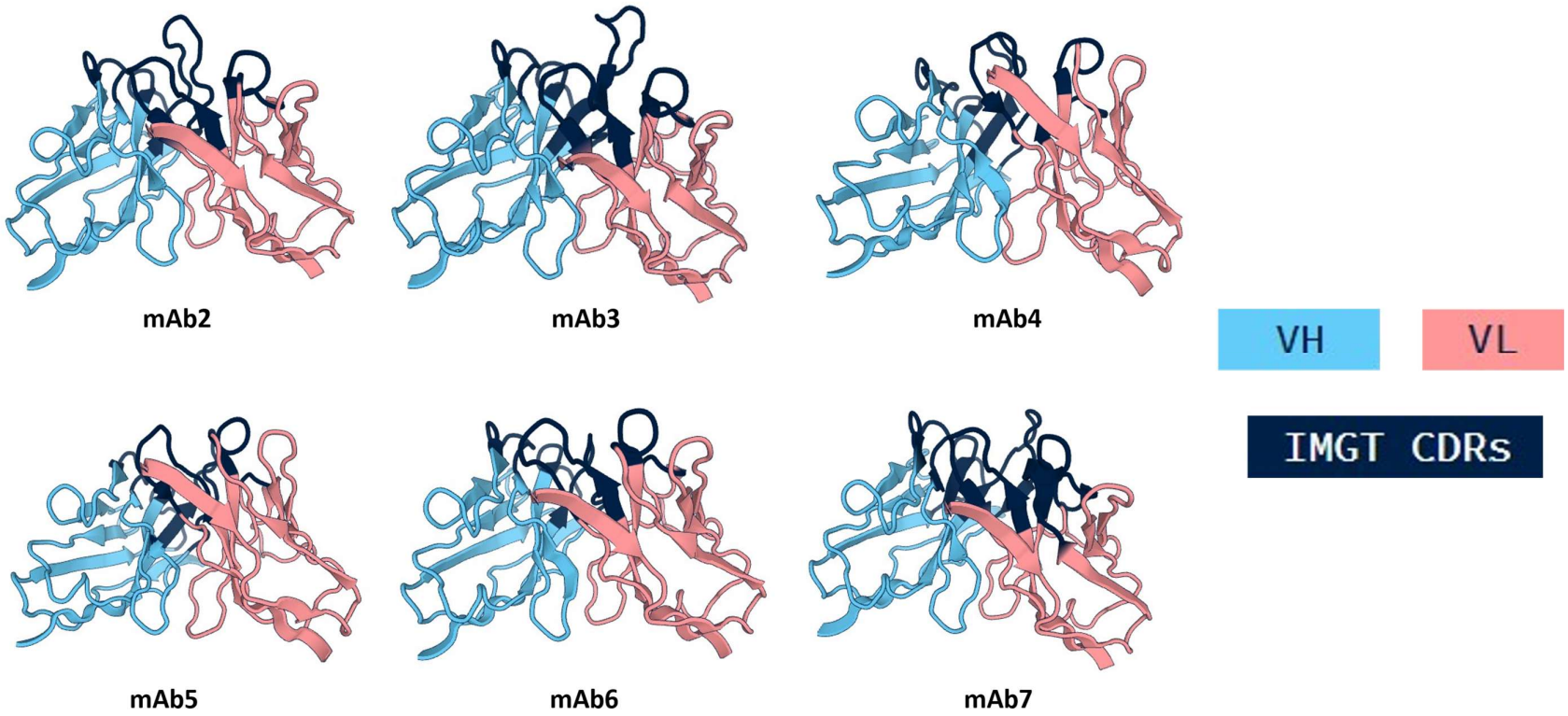
A.8.2 Position of elements

	bp
Vector size	8599
Insert size	422-477

Appendix Table 2: Peptide library comprising overlapping sequences (16mers offset by 4 amino acids) representing PRRSV-1 Olot/91 GP3, up to the first transmembrane domain. Synthetic biotinylated peptides were used for epitope screening assays detailed in Chapters 5 and 6. *The hydrophilic tetrapeptide SGSG was added between the biotin and the sequence of interest, to prevent steric hindrance.

Peptide number	Sequence*
1	SGSGNSNSTLCFWFPLAHGN
2	SGSGTLCFWFPLAHGNTSFE
3	SGSGWFPLAHGNTSFELTIN
4	SGSGAHGNTSFELTINYTIC
5	SGSGTSFELTINYTICMPCS
6	SGSGLTINYTICMPCSTSQA
7	SGSGYTICMPCSTSQAAHQR
8	SGSGMPCSTSQAAHQRLEPG
9	SGSGTSQAAHQRLEPGRNMW
10	SGSGAHQRLEPGRNMWCRIG
11	SGSGLEPGRNMWCRIGHDRC
12	SGSGRNMWCRIGHDRCEERD
13	SGSGCRIGHDRCEERDHDEL
14	SGSGHDRCEERDHDELSMSI
15	SGSGEERDHDELSMSIPSGY
16	SGSGHDELSMSIPSGYDNLK
17	SGSGSMSIPSGYDNLKLEGY
18	SGSGPSGYDNLKLEGYYAWL
19	SGSGDNLKLEGYYAWLAFLS
20	SGSGLEGYYAWLAFLSFSYA
21	SGSGYAWLAFLSFSYAAQFH
22	SGSGAFLSFSYAAQFHPELF
23	SGSGFSYAAQFHPELFGIGN
24	SGSGAQFHPELFGIGNVSRV
25	SGSGPELFGIGNVSRVFVDK
26	SGSGGIGNVSRVFVDKQHQF
27	SGSGVSRVFVDKQHQFICAE
28	SGSGFVDKQHQFICAEHDGR
29	SGSGQHQFICAEHDGRNSTI
30	SGSGICAEHDGRNSTISTEY
31	SGSGHDGRNSTISTEYNISA
32	SGSGNSTISTEYNISALYAV
33	SGSGSTEYNISALYAVYYHH
34	SGSGNISALYAVYYHHQIDG
35	SGSGLYAVYYHHQIDGGNWF
36	SGSGVYYHHQIDGGNWFHLE

Appendix Figure 9: Structure of the six mAbs that were characterised throughout Chapter 5 was predicted using SAbPred. VH chains are represented in blue, VL represented in pink, and the complementarity determining regions, as annotated using the international ImMunoGeneTics information system®, represented in black.



Appendix Table 3: List of Illumina i7 and i5 index primer sequences used for whole antibody repertoire VH and VL sequence indexing.

Index primer	Sequence
i7_701	CAAGCAGAAGACGGCATACGAGATTCGCCTTAGTCTCGTGGGCTCGG
i7_702	CAAGCAGAAGACGGCATACGAGATCTAGTACGGTCTCGTGGGCTCGG
i7_703	CAAGCAGAAGACGGCATACGAGATTTCTGCCTGTCTCGTGGGCTCGG
i7_704	CAAGCAGAAGACGGCATACGAGATGCTCAGGAGTCTCGTGGGCTCGG
i7_705	CAAGCAGAAGACGGCATACGAGATAGGAGTCCGTCTCGTGGGCTCGG
i7_706	CAAGCAGAAGACGGCATACGAGATCATGCCTAGTCTCGTGGGCTCGG
i5_S502	AATGATACGGCGACCACCGAGATCTACACCTCTCTATTCGTCGGCAGCGTC
i5_S503	AATGATACGGCGACCACCGAGATCTACACTATCCTCTTCGTCGGCAGCGTC
i5_S505	AATGATACGGCGACCACCGAGATCTACACGTAAGGAGTCGTCGGCAGCGTC
i5_S506	AATGATACGGCGACCACCGAGATCTACACACTGCATATCGTCGGCAGCGTC
i5_S507	AATGATACGGCGACCACCGAGATCTACACAAGGAGTATCGTCGGCAGCGTC

Bibliography

1. Holtkamp, D.J., et al., *Assessment of the economic impact of porcine reproductive and respiratory syndrome virus on United States pork producers*. 2013. p. 72-84.
2. Lunney, J.K., et al., *Porcine reproductive and respiratory syndrome virus (PRRSV): Pathogenesis and interaction with the immune system*. 2016, Annu Rev Anim Biosci. p. 129-154.
3. Iowa State University, C.o.V.M. *Swine Manual index - Porcine Reproductive and Respiratory Syndrome (PRRS)*. [Webpage] 2023 [cited 2023 08/01/2024]; Available from: https://vetmed.iastate.edu/vdpam/FSVD/swine/index-diseases/porcine-reproductive.
4. Pena, R.N., et al., *Genetic Markers Associated with Field PRRSV-Induced Abortion Rates.* Viruses, 2019/08. **11**(8).
5. Christianson, W.T., et al., *Pathogenesis of porcine reproductive and respiratory syndrome virus infection in mid-gestation sows and fetuses.* 1993, Canadian Veterinary Medical Association. p. 262-268.
6. Opriessnig, T., et al., *Comparison of Molecular and Biological Characteristics of a Modified Live Porcine Reproductive and Respiratory Syndrome Virus (PRRSV) Vaccine (Ingelvac PRRS MLV), the Parent Strain of the Vaccine (ATCC VR2332), ATCC VR2385, and Two Recent Field Isolates of PRRSV.* Journal of Virology, 2002/12. **76**(23).
7. Rossow, K.D., *Porcine reproductive and respiratory syndrome.* Veterinary pathology, 1998 Jan. **35**(1).
8. Opriessnig, T., et al., *A PCV2 vaccine based on genotype 2b is more effective than a 2a-based vaccine to protect against PCV2b or combined PCV2a/2b viremia in pigs with concurrent PCV2, PRRSV and PPV infection.* Vaccine, 2013/01/07. **31**(3).
9. Thacker, E.L., et al., *Mycoplasma hyopneumoniae Potentiation of Porcine Reproductive and Respiratory Syndrome Virus-Induced Pneumonia.* Journal of Clinical Microbiology, 1999/03. **37**(3).
10. Galina, L., et al., *Interaction between Streptococcus suis serotype 2 and porcine reproductive and respiratory syndrome virus in specific pathogen-free piglets - PubMed.* The Veterinary record, 01/15/1994. **134**(3).
11. Feng, W.-h., et al., *In Utero Infection by Porcine Reproductive and Respiratory Syndrome Virus Is Sufficient To Increase Susceptibility of Piglets to Challenge by Streptococcus suis Type II.* Journal of Virology, 2001-5-15.
12. Pileri, E., et al., *Review on the transmission porcine reproductive and respiratory syndrome virus between pigs and farms and impact on vaccination.* Veterinary Research 2016 47:1, 2016-10-28. **47**(1).
13. Clilverd, H., et al., *Infection dynamics, transmission, and evolution after an outbreak of porcine reproductive and respiratory syndrome virus.* Front Microbiol, 2023. **14**: p. 1109881.
14. More, S., et al., *Assessment of listing and categorisation of animal diseases within the framework of the Animal Health Law (Regulation (EU) No 2016/429): porcine reproductive and respiratory syndrome (PRRS).* EFSA Journal, 2017/07/01. **15**(7).
15. Halbur, P.G., et al., *Comparison of the Pathogenicity of Two US Porcine Reproductive and Respiratory Syndrome Virus Isolates with that of the Lelystad Virus.* Veterinary Pathology, 1995-11-01. **32**(6).
16. Franzo, G., et al., *Phylodynamic and phylogeographic reconstruction of porcine reproductive and respiratory syndrome virus (PRRSV) in Europe: Patterns and determinants.* Transbound Emerg Dis, 2022. **69**(5): p. e2175-e2184.
17. Albina, E., *Epidemiology of porcine reproductive and respiratory syndrome (PRRS): An overview.* Veterinary Microbiology, 1997/04/01. **55**(1-4).

18. Cavanagh, D., *Nidovirales: a new order comprising Coronaviridae and Arteriviridae.* Arch Virol., 1994. **142**(3): p. 629-33.
19. Ruedas-Torres, I., et al., *The jigsaw of PRRSV virulence.* Veterinary Microbiology, 2021/09/01. **260**.
20. Allende, R., et al., *North American and European porcine reproductive and respiratory syndrome viruses differ in non-structural protein coding regions*. 1999, J Gen Virol. p. 307-315.
21. Kuhn, J.H., et al., *Reorganization and expansion of the nidoviral family Arteriviridae.* Archives of Virology 2015 161:3, 2015-11-25. **161**(3).
22. Forsberg, R., *Divergence Time of Porcine Reproductive and Respiratory Syndrome Virus Subtypes*. 2005, Oxford Academic. p. 2131-2134.
23. Hanada, K., et al., *The Origin and Evolution of Porcine Reproductive and Respiratory Syndrome Viruses.* Molecular Biology and Evolution, 2005/04. **22**(4).
24. Murtaugh, M.P., M.R. Elam, and L.T. Kakach, *Comparison of the structural protein coding sequences of the VR-2332 and Lelystad virus strains of the PRRS virus*. 1995, Springer-Verlag. p. 1451-1460.
25. Nelsen, C.J., M.P. Murtaugh, and K.S. Faaberg, *Porcine Reproductive and Respiratory Syndrome Virus Comparison: Divergent Evolution on Two Continents.* Journal of Virology, 1999/01. **73**(1).
26. Shi, M., et al., *Molecular epidemiology of PRRSV: a phylogenetic perspective - PubMed.* Virus research, 2010 Dec. **154**(1-2).
27. Shi, M., et al., *Phylogeny-Based Evolutionary, Demographical, and Geographical Dissection of North American Type 2 Porcine Reproductive and Respiratory Syndrome Viruses.* Journal of Virology, 2010-September-1. **84**(17).
28. Zimmerman, J., et al., *Porcine reproductive and respiratory syndrome virus (porcine arterivirus) In: Straw*. 9th ed. Diseases of Swine. 2006: Blackwell Publishing Professional.
29. Aiki-Raji, C.O., et al., *Prevalence of porcine reproductive and respiratory syndrome virus and porcine parvovirus antibodies in commercial pigs, southwest Nigeria.* Beni-Suef University Journal of Basic and Applied Sciences, 2018/03/01. **7**(1).
30. Oba, P., et al., *Molecular characterization of porcine reproductive and respiratory syndrome virus (PRRSv) identified from slaughtered pigs in northern Uganda.* BMC Veterinary Research 2022 18:1, 2022-05-13. **18**(1).
31. Zhou, L., et al., *Whole Genome Analysis of Two Novel Type 2 Porcine Reproductive and Respiratory Syndrome Viruses with Complex Genome Recombination between Lineage 8, 3, and 1 Strains Identified in Southwestern China.* Viruses, 2018/06. **10**(6).
32. Deng, M.-C., et al., *Molecular epidemiology of porcine reproductive and respiratory syndrome viruses isolated from 1991 to 2013 in Taiwan.* Archives of Virology 2015 160:11, 2015-08-06. **160**(11).
33. Paploski, I.A.D., et al., *Phylogenetic Structure and Sequential Dominance of Sub-Lineages of PRRSV Type-2 Lineage 1 in the United States.* Vaccines 2021, Vol. 9, Page 608, 2021-06-05. **9**(6).
34. Sun, Y.-K., et al., *Insights into the evolutionary history and epidemiological characteristics of the emerging lineage 1 porcine reproductive and respiratory syndrome viruses in China.* Transboundary and Emerging Diseases, 2020/11/01. **67**(6).
35. Ramírez, M., et al., *Detection of porcine reproductive and respiratory syndrome virus (PRRSV) 1-7-4-type strains in Peru.* Transboundary and Emerging Diseases, 2019/05/01. **66**(3).
36. Xu, H., et al., *Novel characteristics of Chinese NADC34-like PRRSV during 2020–2021.* Transboundary and Emerging Diseases, 2022/09/01. **69**(5).

37. Gao, F., et al., *Replacement of the heterologous 5' untranslated region allows preservation of the fully functional activities of type 2 porcine reproductive and respiratory syndrome virus.* Virology, 2013. **439**(1): p. 1-12.
38. Oleksiewicz, M.B., et al., *Determination of 5'-leader sequences from radically disparate strains of porcine reproductive and respiratory syndrome virus reveals the presence of highly conserved sequence motifs.* Archives of Virology 1999 144:5, 2014-05-18. **144**(5).
39. Lunney, J.K., et al., *Porcine reproductive and respiratory syndrome virus (PRRSV): Pathogenesis and interaction with the immune system*. 2016, Annu Rev Anim Biosci. p. 129-154.
40. Han, M. and D. Yoo, *Engineering the PRRS virus genome: Updates and perspectives.* Veterinary Microbiology, 2014/12/12. **174**(3).
41. Van Breedam, W., et al., *The M/GP5 glycoprotein complex of porcine reproductive and respiratory syndrome virus binds the sialoadhesin receptor in a sialic acid-dependent manner*. 2010, Public Library of Science.
42. Kappes, M.A. and K.S. Faaberg, *PRRSV structure, replication and recombination: Origin of phenotype and genotype diversity.* Virology, 2015/05/01. **479-480**.
43. Johnson, C.R., et al., *Novel structural protein in porcine reproductive and respiratory syndrome virus encoded by an alternative ORF5 present in all arteriviruses.* Journal of General Virology, 2011/05/01. **92**(5).
44. Snijder, E.J., J.C. Dobbe, and W.J.M. Spaan, *Heterodimerization of the Two Major Envelope Proteins Is Essential for Arterivirus Infectivity*. 2003, American Society for Microbiology (ASM). p. 97.
45. Mardassi, H., S. Mounir, and S. Dea, *Molecular analysis of the ORFs 3 to 7 of porcine reproductive and respiratory syndrome virus, Quebec reference strain**. 1995. p. 1405-1418.
46. Wissink, E.H.J., et al., *Envelope Protein Requirements for the Assembly of Infectious Virions of Porcine Reproductive and Respiratory Syndrome Virus*. 2005, American Society for Microbiology. p. 12495-12506.
47. Trible, B.R., et al., *A Single Amino Acid Deletion in the Matrix Protein of Porcine Reproductive and Respiratory Syndrome Virus Confers Resistance to a Polyclonal Swine Antibody with Broadly Neutralizing Activity*. 2015, American Society for Microbiology (ASM). p. 6515.
48. Le Gall, A., et al., *Molecular variation in the nucleoprotein gene (ORF7) of the porcine reproductive and respiratory syndrome virus (PRRSV) - PubMed.* Virus research, 1998 Mar. **54**(1).
49. Snijder, E.J., et al., *The molecular biology of arteriviruses.* Journal of General Virology, 1998/05/01. **79**(5).
50. Xiong, J., et al., *A Novel Motif in the 3'-UTR of PRRSV-2 Is Critical for Viral Multiplication and Contributes to Enhanced Replication Ability of Highly Pathogenic or L1 PRRSV.* Viruses, 2022. **14**(2).
51. Kappes, M.A. and K.S. Faaberg, *PRRSV structure, replication and recombination: Origin of phenotype and genotype diversity*. 2015, Academic Press. p. 475-486.
52. Risser, J., et al., *Porcine reproductive and respiratory syndrome virus genetic variability a management and diagnostic dilemma.* Virology Journal 2021 18:1, 2021-10-18. **18**(1).
53. Dorp, L.v., et al., *Emergence of genomic diversity and recurrent mutations in SARS-CoV-2.* Infection, Genetics and Evolution, 2020/09. **83**.
54. Egeren, D.V., et al., *Risk of rapid evolutionary escape from biomedical interventions targeting SARS-CoV-2 spike protein.* PLoS ONE, 2021. **16**(4).

55. Nobusawa, E. and K. Sato, *Comparison of the Mutation Rates of Human Influenza A and B Viruses.* Journal of Virology, 2006/04. **80**(7).
56. Robinson, S.R., et al., *Porcine reproductive and respiratory syndrome virus neutralizing antibodies provide in vivo cross-protection to PRRSV1 and PRRSV2 viral challenge.* Virus research, 2018/03/03. **248**.
57. Brar, M.S., et al., *Evolutionary diversification of type 2 porcine reproductive and respiratory syndrome virus.* Journal of General Virology, 2015/07/01. **96**(7).
58. An, T., et al., *Highly Pathogenic Porcine Reproductive and Respiratory Syndrome Virus, Asia.* Emerging Infectious Diseases, 2011. **17**: p. 1782-1784.
59. Tian, K., et al., *Emergence of Fatal PRRSV Variants: Unparalleled Outbreaks of Atypical PRRS in China and Molecular Dissection of the Unique Hallmark.* PLOS ONE, Jun 13, 2007. **2**(6).
60. Martinez-Lobo, F.J., et al., *Comparative pathogenicity of type 1 and type 2 isolates of porcine reproductive and respiratory syndrome virus (PRRSV) in a young pig infection model.* Veterinary Microbiology, 2011/12/29. **154**(1-2).
61. Rodríguez-Gómez, I.M., et al., *Virulent Lena strain induced an earlier and stronger downregulation of CD163 in bronchoalveolar lavage cells.* Veterinary Microbiology, 2019/08/01. **235**.
62. Weesendorp, E., et al., *Lung pathogenicity of European genotype 3 strain porcine reproductive and respiratory syndrome virus (PRRSV) differs from that of subtype 1 strains.* Veterinary Microbiology, 2014/11/11. **174**(1).
63. Morgan, S.B., et al., *Increased pathogenicity of European porcine reproductive and respiratory syndrome virus is associated with enhanced adaptive responses and viral clearance*. 2013, Vet Microbiol. p. 13-22.
64. Martín-Valls, G.E., et al., *Description of a New Clade within Subtype 1 of Betaarterivirus suid 1 Causing Severe Outbreaks in Spain.* Microbiology Resource Announcements, 2022-6-2. **11**(7).
65. Canelli, E., et al., *Phenotypic characterization of a highly pathogenic Italian porcine reproductive and respiratory syndrome virus (PRRSV) type 1 subtype 1 isolate in experimentally infected pigs - PubMed.* Veterinary microbiology, 2017. **210**.
66. Martín-Valls, G.E., et al., *Introduction of a PRRSV-1 strain of increased virulence in a pig production structure in Spain: virus evolution and impact on production.* Porcine Health Management 2023 9:1, 2023-01-03. **9**(1).
67. Breedam, V., et al., *Porcine reproductive and respiratory syndrome virus entry into the porcine macrophage*. 2010.
68. Wang, L., et al., *Porcine alveolar macrophage polarization is involved in inhibition of porcine reproductive and respiratory syndrome virus (PRRSV) replication.* J Vet Med Sci, 2017. **79**(11): p. 1906-1915.
69. Singleton, H., et al., *Establishing Porcine Monocyte-Derived Macrophage and Dendritic Cell Systems for Studying the Interaction with PRRSV-1.* Frontiers in Microbiology, 2016/06/02. **7**.
70. Wahyuningtyas, R., et al., *Recombinant Antigen of Type 2 Porcine Reproductive and Respiratory Syndrome Virus (PRRSV-2) Promotes M1 Repolarization of Porcine Alveolar Macrophages and Th1 Type Response.* Vaccines, 2021. **9**(9): p. 1009.
71. Hernández, J., Y. Li, and E. Mateu, *Swine Dendritic Cell Response to Porcine Reproductive and Respiratory Syndrome Virus: An Update.* Front Immunol, 2021. **12**: p. 712109.
72. Yun, S.I. and Y.M. Lee, *Overview: Replication of porcine reproductive and respiratory syndrome virus.* J Microbiol, 2013. **51**(6): p. 711-23.

73. Delputte, P.L., et al., *Involvement of the matrix protein in attachment of porcine reproductive and respiratory syndrome virus to a heparinlike receptor on porcine alveolar macrophages - PubMed.* Journal of virology, 2002 May. **76**(9).
74. Popescu, L.N., et al., *GP5 of porcine reproductive and respiratory syndrome virus (PRRSV) as a target for homologous and broadly neutralizing antibodies*. 2017, Elsevier B.V. p. 90-96.
75. Bordet, E., et al., *Porcine Reproductive and Respiratory Syndrome Virus Type 1.3 Lena Triggers Conventional Dendritic Cells 1 Activation and T Helper 1 Immune Response Without Infecting Dendritic Cells.* Frontiers in Immunology, 2018. **9**.
76. Prather, R.S., et al., *An Intact Sialoadhesin (Sn/SIGLEC1/CD169) Is Not Required for Attachment/Internalization of the Porcine Reproductive and Respiratory Syndrome Virus.* Journal of Virology, 2013-9-1.
77. M, Y., et al., *Splenic CD163+ macrophages as targets of porcine reproductive and respiratory virus: Role of Siglecs.* Veterinary Microbiology, 2017/01/01. **198**.
78. Su, C.-M., R.R.R. Rowland, and D. Yoo, *Recent Advances in PRRS Virus Receptors and the Targeting of Receptor–Ligand for Control.* Vaccines, 2021/04. **9**(4).
79. An, T.-Q., et al., *Molecular and Cellular Mechanisms for PRRSV Pathogenesis and Host Response to Infection.* Virus Research, 2020/09. **286**.
80. Welch, S.-K.W. and J.G. Calvert, *A brief review of CD163 and its role in PRRSV infection - PubMed.* Virus research, 2010 Dec. **154**(1-2).
81. Gorp, H.V., et al., *Sialoadhesin and CD163 join forces during entry of the porcine reproductive and respiratory syndrome virus.* Journal of General Virology, 2008/12/01. **89**(12).
82. Calvert, J.G., et al., *CD163 Expression Confers Susceptibility to Porcine Reproductive and Respiratory Syndrome Viruses*. 2007, American Society for Microbiology (ASM). p. 7371.
83. Burkard, C., et al., *Precision engineering for PRRSV resistance in pigs: Macrophages from genome edited pigs lacking CD163 SRCR5 domain are fully resistant to both PRRSV genotypes while maintaining biological function.* PLOS Pathogens, Feb 23, 2017. **13**(2).
84. Whitworth, K.M., et al., *Gene-edited pigs are protected from porcine reproductive and respiratory syndrome virus.* Nature Biotechnology 2016 34:1, 2016-01-01. **34**(1).
85. Xu, K., et al., *CD163 and pAPN double-knockout pigs are resistant to PRRSV and TGEV and exhibit decreased susceptibility to PDCoV while maintaining normal production performance.* eLife, 2020. **9**.
86. Yang, H., et al., *CD163 knockout pigs are fully resistant to highly pathogenic porcine reproductive and respiratory syndrome virus.* Antiviral Research, 2018/03/01. **151**.
87. Snijder, E.J., et al., *Arterivirus molecular biology and pathogenesis.* Journal of General Virology, 2013/10/01. **94**(10).
88. Fang, Y. and E.J. Snijder, *The PRRSV replicase: exploring the multifunctionality of an intriguing set of nonstructural proteins.* Virus Res, 2010. **154**(1-2): p. 61-76.
89. Tijms, M.A., Y. van der Meer, and E.J. Snijder, *Nuclear localization of non-structural protein 1 and nucleocapsid protein of equine arteritis virus.* J Gen Virol, 2002. **83**(Pt 4): p. 795-800.
90. Pol, J.M.A., F. Wagenaar, and J.E.G. Reus, *Comparative morphogenesis of three PRRS virus strains.* Veterinary Microbiology, 1997. **55**(1): p. 203-208.
91. Dea, S., et al., *Ultrastructural characteristics and morphogenesis of porcine reproductive and respiratory syndrome virus propagated in the highly permissive MARC-145 cell clone.* Adv Exp Med Biol, 1995. **380**: p. 95-8.

92. Xiao, Z., et al., *The Level of Virus-Specific T-Cell and Macrophage Recruitment in Porcine Reproductive and Respiratory Syndrome Virus Infection in Pigs Is Independent of Virus Load.* Journal of Virology, 2004/06. **78**(11).
93. Wu, C., et al., *Broad neutralization activity against both PRRSV-1 and PRRSV-2 and enhancement of cell mediated immunity against PRRSV by a novel IgM monoclonal antibody*. 2020, Antiviral Res.
94. Lopez, O.J. and F. Osorio, *Effect of virus-specific antibodies on attachment, internalization and infection of porcine reproductive and respiratory syndrome virus in primary macrophages - PubMed.* Veterinary immunology and immunopathology, 2004. **102**(3).
95. Labarque, G.G., et al., *Effect of cellular changes and onset of humoral immunity on the replication of porcine reproductive and respiratory syndrome virus in the lungs of pigs.* Journal of General Virology, 2000/05/01. **81**(5).
96. Butler, J.E., et al., *Porcine reproductive and respiratory syndrome (PRRS): an immune dysregulatory pandemic.* Immunologic Research 2014 59:1, 2014-07-01. **59**(1).
97. Crisci, E., L. Fraile, and M. Montoya, *Cellular Innate Immunity against PRRSV and Swine Influenza Viruses.* Veterinary Sciences, 2019/03. **6**(1).
98. Li, H., et al., *The cysteine protease domain of porcine reproductive and respiratory syndrome virus non-structural protein 2 antagonizes interferon regulatory factor 3 activation.* Journal of General Virology, 2010/12/01. **91**(12).
99. Yang, L. and Y.-J. Zhang, *Antagonizing cytokine-mediated JAK-STAT signaling by porcine reproductive and respiratory syndrome virus.* Veterinary Microbiology, 2017/09. **209**.
100. Sagong, M. and C. Lee, *Porcine reproductive and respiratory syndrome virus nucleocapsid protein modulates interferon-β production by inhibiting IRF3 activation in immortalized porcine alveolar macrophages.* Archives of Virology, 2011. **156**(12).
101. Cao, J., et al., *Suppression of NK cell-mediated cytotoxicity against PRRSV-infected porcine alveolar macrophages in vitro - PubMed.* Veterinary microbiology, 06/28/2013. **164**(3-4).
102. Li, Y., et al., *Systemic CD4 cytotoxic T cells improve protection against PRRSV-1 transplacental infection.* Frontiers in Immunology, 2023/01/17. **13**.
103. Proctor, J., et al., *Heterologous vaccine immunogenicity, efficacy, and immune correlates of protection of a modified-live virus porcine reproductive and respiratory syndrome virus vaccine.* Frontiers in Microbiology, 2022/09/23. **13**.
104. Wongyanin, P., et al., *Role of porcine reproductive and respiratory syndrome virus nucleocapsid protein in induction of interleukin-10 and regulatory T-lymphocytes (Treg).* Journal of General Virology, 2012/06/01. **93**(6).
105. Sang, Y., R.R. Rowland, and F. Blecha, *Porcine type I interferons: polymorphic sequences and activity against PRRSV.* BMC Proceedings, 2011. **5**(Suppl 4).
106. Hernández, J., Y. Li, and E. Mateu, *Swine Dendritic Cell Response to Porcine Reproductive and Respiratory Syndrome Virus: An Update.* Frontiers in Immunology, 2021/07/28. **12**.
107. Chang, H.-C., et al., *Phenotypic and functional modulation of bone marrow-derived dendritic cells by porcine reproductive and respiratory syndrome virus.* Veterinary Microbiology, 2008/06/22. **129**(3-4).
108. Loving, C.L., S.L. Brockmeier, and R.E. Sacco, *Differential type I interferon activation and susceptibility of dendritic cell populations to porcine arterivirus.* Immunology, 2007/02. **120**(2).
109. Lamontagne, L., et al., *Porcine Reproductive and Respiratory Syndrome Virus Persistence in Blood, Spleen, Lymph Nodes, and Tonsils of Experimentally*

Infected Pigs Depends on the Level of CD8high T Cells. https://home.liebertpub.com/vim, 2004-07-09. **16**(3).
110. Zignego, A.L., et al., *Hepatitis C virus infection in the immunocompromised host: a complex scenario with variable clinical impact.* Journal of Translational Medicine 2012 10:1, 2012-08-03. **10**(1).
111. López-Abente, J., R. Correa-Rocha, and M. Pion, *Functional Mechanisms of Treg in the Context of HIV Infection and the Janus Face of Immune Suppression.* Frontiers in Immunology, 2016. **7**.
112. Silva-Campa, E., et al., *Porcine reproductive and respiratory syndrome virus induces CD4+CD8+CD25+Foxp3+ regulatory T cells (Tregs) - PubMed.* Virology, 08/15/2012. **430**(1).
113. Nedumpun, T., et al., *Induction of porcine reproductive and respiratory syndrome virus (PRRSV)-specific regulatory T lymphocytes (Treg) in the lungs and tracheobronchial lymph nodes of PRRSV-infected pigs - PubMed.* Veterinary microbiology, 2018 Mar. **216**.
114. C.A., J., et al., *Immunobiology: The Immune System in Health and Disease.* 2001, New York: Garland Science.
115. Boyd Scott, D. and A. Joshi Shilpa, *High-Throughput DNA Sequencing Analysis of Antibody Repertoires.* Microbiology Spectrum, 2014. **2**(5): p. 10.1128/microbiolspec.aid-0017-2014.
116. Lopez, O.J., et al., *Protection against porcine reproductive and respiratory syndrome virus (PRRSV) infection through passive transfer of PRRSV-neutralizing antibodies is dose dependent*. 2007, Clin Vaccine Immunol. p. 269-275.
117. Osorio, F., et al., *Passive transfer of virus-specific antibodies confers protection against reproductive failure induced by a virulent strain of porcine reproductive and respiratory syndrome virus and establishes sterilizing immunity - PubMed.* Virology, 2002. **302**(1).
118. Loving, C.L., et al., *Innate and adaptive immunity against Porcine Reproductive and Respiratory Syndrome Virus.* Vet Immunol Immunopathol, 2015. **167**(1-2): p. 1-14.
119. Kick, A.R., et al., *The Local and Systemic Humoral Immune Response Against Homologous and Heterologous Strains of the Type 2 Porcine Reproductive and Respiratory Syndrome Virus.* Front Immunol, 2021. **12**: p. 637613.
120. Bautista, E.M., et al., *Functional Properties of the Predicted Helicase of Porcine Reproductive and Respiratory Syndrome Virus.* Virology, 2002/07/07. **298**(2).
121. Wills, R.W., et al., *Porcine reproductive and respiratory syndrome virus: a persistent infection - PubMed.* Veterinary microbiology, 1997 Apr. **55**(1-4).
122. Rowland, R.R.R., et al., *Lymphoid tissue tropism of porcine reproductive and respiratory syndrome virus replication during persistent infection of pigs originally exposed to virus in utero.* Veterinary Microbiology, 2003/10/10. **96**(3).
123. Romeo, C., et al., *Complex interplay between PRRSV-1 genetic diversity, coinfections and antimicrobial use influences performance parameters in post-weaning pigs.* Veterinary Microbiology, 2023. **284**.
124. Robinson, S.R., et al., *Broadly neutralizing antibodies against the rapidly evolving porcine reproductive and respiratory syndrome virus*. 2015, Virus Res. p. 56-65.
125. Martínez-Lobo, F.J., et al., *The Ability of Porcine Reproductive and Respiratory Syndrome Virus Isolates to Induce Broadly Reactive Neutralizing Antibodies Correlates With In Vivo Protection.* Frontiers in Immunology, 2021/07/26. **12**.
126. Thaa, B., et al., *Signal Peptide Cleavage from GP5 of PRRSV: A Minor Fraction of Molecules Retains the Decoy Epitope, a Presumed Molecular Cause for Viral Persistence*. 2013, Public Library of Science. p. 65548.

127. Vanhee, M., et al., *A Variable region in GP4 of european-type porcine reproductive and respiratory syndrome virus induces neutralizing antibodies against homologous but not heterologous virus strains*. 2010, Mary Ann Liebert, Inc. 140 Huguenot Street, 3rd Floor New Rochelle, NY 10801 USA. p. 403-413.
128. Das, P.B., et al., *The Minor Envelope Glycoproteins GP2a and GP4 of Porcine Reproductive and Respiratory Syndrome Virus Interact with the Receptor CD163*. 2010, American Society for Microbiology. p. 1731-1740.
129. Vu, H.L.X., et al., *Immune Evasion of Porcine Reproductive and Respiratory Syndrome Virus through Glycan Shielding Involves both Glycoprotein 5 as Well as Glycoprotein 3*. 2011, American Society for Microbiology. p. 5555-5564.
130. Choi, J.-C., et al., *Porcine Reproductive and Respiratory Syndrome Virus Engineered by Serine Substitution on the 44th Amino Acid of GP5 Resulted in a Potential Vaccine Candidate with the Ability to Produce High Levels of Neutralizing Antibody.* Veterinary Sciences, 2023/03. **10**(3).
131. Fan, B., et al., *Influence of the amino acid residues at 70 in M protein of porcine reproductive and respiratory syndrome virus on viral neutralization susceptibility to the serum antibody*. 2016, BioMed Central Ltd. p. 1-11.
132. Costers, S., et al., *GP4 of porcine reproductive and respiratory syndrome virus contains a neutralizing epitope that is susceptible to immunoselection in vitro*. 2010, Springer. p. 371-378.
133. Seuberlich, T., et al., *Nucleocapsid Protein-Based Enzyme-Linked Immunosorbent Assay for Detection and Differentiation of Antibodies against European and North American Porcine Reproductive and Respiratory Syndrome Virus.* Clinical and Vaccine Immunology, 2002. **9**(6): p. 1183-1191.
134. Zimmerman, J.J., et al., *Porcine reproductive and respiratory syndrome viruses (porcine arteriviruses)*. 2019/03/29.
135. Amadori, M., V. Listorti, and E. Razzuoli, *Reappraisal of PRRS Immune Control Strategies: The Way Forward.* Pathogens, 2021/09. **10**(9).
136. Papatsiros, V.G., *Impact of a killed PRRSV vaccine on sow longevity in a PRRSV infected swine herd.* Journal of Applied Animal Research, 2012-12-1. **40**(4).
137. Gao, J., et al., *MYH9 is an Essential Factor for Porcine Reproductive and Respiratory Syndrome Virus Infection.* Scientific Reports 2016 6:1, 2016-04-26. **6**(1).
138. Vreman, S., et al., *Immune responses induced by inactivated porcine reproductive and respiratory syndrome virus (PRRSV) vaccine in neonatal pigs using different adjuvants - PubMed.* Veterinary immunology and immunopathology, 2021 Feb. **232**.
139. Wang, D., et al., *MiR-125b Reduces Porcine Reproductive and Respiratory Syndrome Virus Replication by Negatively Regulating the NF-κB Pathway.* PLoS ONE, 2013. **8**(2).
140. Chen, J., et al., *MicroRNA 373 Facilitates the Replication of Porcine Reproductive and Respiratory Syndrome Virus by Its Negative Regulation of Type I Interferon Induction.* Journal of Virology, 2017/02/02. **91**(3).
141. Chae, C. and C. Chae, *Commercial PRRS Modified-Live Virus Vaccines.* Vaccines 2021, Vol. 9, Page 185, 2021-02-22. **9**(2).
142. Kimman, T.G., et al., *Challenges for porcine reproductive and respiratory syndrome virus (PRRSV) vaccinology.* Vaccine, 2009/06/08. **27**(28).
143. Murtaugh, M.P., Z. Xiao, and F. Zuckerman, *Immunological responses of swine to porcine reproductive and respiratory syndrome virus infection.* Viral immunology, 2002. **15**(4).
144. Zhang, H., et al., *Research Progress on the Development of Porcine Reproductive and Respiratory Syndrome Vaccines.* Vet Sci, 2023. **10**(8).

145. Zhou, L., X. Ge, and H. Yang, *Porcine Reproductive and Respiratory Syndrome Modified Live Virus Vaccine: A "Leaky" Vaccine with Debatable Efficacy and Safety.* Vaccines (Basel), 2021. **9**(4).
146. Charerntantanakul, W., *Porcine reproductive and respiratory syndrome virus vaccines: Immunogenicity, efficacy and safety aspects*. 2012, Baishideng Publishing Group Inc. p. 23.
147. Lee, S.-C., et al., *Pathogenicity and genetic characteristics associated with cell adaptation of a virulent porcine reproductive and respiratory syndrome virus nsp2 DEL strain CA-2.* Veterinary Microbiology, 2016. **186**: p. 174-188.
148. Wang, J., et al., *Attenuated Porcine Reproductive and Respiratory Syndrome Virus Regains Its Fatal Virulence by Serial Passaging in Pigs or Porcine Alveolar Macrophages To Increase Its Adaptation to Target Cells.* Microbiol Spectr, 2022. **10**(6): p. e0308422.
149. Wang, A., et al., *Recombination between Vaccine and Field Strains of Porcine Reproductive and Respiratory Syndrome Virus.* Emerging Infectious Diseases, 2019/12. **25**(12).
150. Nielsen, H.S., et al., *Reversion of a live porcine reproductive and respiratory syndrome virus vaccine investigated by parallel mutations.* Journal of General Virology, 2001/06/01. **82**(6).
151. Renson, P., et al., *Maternally-derived neutralizing antibodies reduce vaccine efficacy against porcine reproductive and respiratory syndrome virus infection.* Vaccine, 2019/07/07. **37**(31).
152. Fablet, C., et al., *Factors associated with herd-level PRRSV infection and age-time to seroconversion in farrow-to-finish herds - PubMed.* Veterinary microbiology, 2016. **192**.
153. Sanders, B., M. Koldijk, and H. Schuitemaker, *Inactivated Viral Vaccines.* Vaccine Analysis: Strategies, Principles, and Control, 2015.
154. Kim, H., et al., *The assessment of efficacy of porcine reproductive respiratory syndrome virus inactivated vaccine based on the viral quantity and inactivation methods*. 2011, BioMed Central. p. 323.
155. Li, C., et al., *Efficacy of the Synergy Between Live-Attenuated and Inactivated PRRSV Vaccines Against a NADC30-Like Strain of Porcine Reproductive and Respiratory Syndrome Virus in 4-Week Piglets.* Frontiers in Veterinary Science, 2022/02/02. **9**.
156. Zhao, J., et al., *The Construction and Immunogenicity Analyses of Recombinant Pseudorabies Virus With NADC30-Like Porcine Reproductive and Respiratory Syndrome Virus-Like Particles Co-expression.* Frontiers in Microbiology, 2022/03/02. **13**.
157. Renukaradhya, G.J., et al., *Inactivated and subunit vaccines against porcine reproductive and respiratory syndrome: Current status and future direction.* Vaccine, 2015. **33**(27).
158. Cui, J., et al., *A PRRSV GP5-Mosaic vaccine: Protection of pigs from challenge and ex vivo detection of IFNγ responses against several genotype 2 strains.* PLoS ONE, 2019. **14**(1).
159. Graham, B.S., M.S.A. Gilman, and J.S. McLellan, *Structure-Based Vaccine Antigen Design.* Annual review of medicine, 2019/01/01. **70**(1).
160. Young, J.E., et al., *Isolation of Porcine Reproductive and Respiratory Syndrome Virus GP5-Specific, Neutralizing Monoclonal Antibodies From Hyperimmune Sows*. 2021, Frontiers Media S.A. p. 1.
161. Kulp, D.W. and W.R. Schief, *Advances in structure-based vaccine design.* Current Opinion in Virology, 2013/06/01. **3**(3).
162. Sesterhenn, F., et al., *De novo protein design enables the precise induction of RSV-neutralizing antibodies.* Science, 2020-05-15. **368**(6492).

163. KIM, H.W., et al., *RESPIRATORY SYNCYTIAL VIRUS DISEASE IN INFANTS DESPITE PRIOR ADMINISTRATION OF ANTIGENIC INACTIVATED VACCINE12.* American Journal of Epidemiology, 1969/04/01. **89**(4).
164. CHIN, J., et al., *FIELD EVALUATION OF A RESPIRATORY SYNCYTIAL VIRUS VACCINE AND A TRIVALENT PARAINFLUENZA VIRUS VACCINE IN A PEDIATRIC POPULATION1.* American Journal of Epidemiology, 1969/04/01. **89**(4).
165. *Respiratory syncytial virus (RSV) immunisation programme: JCVI advice*, J.C.o.V.a. Immunisation, Editor. 2023, UK Department of Health & Social Care: https://www.gov.uk/government/publications/rsv-immunisation-programme-jcvi-advice-7-june-2023/respiratory-syncytial-virus-rsv-immunisation-programme-jcvi-advice-7-june-2023.
166. Kaufmann, B., et al., *Neutralization of West Nile virus by cross-linking of its surface proteins with Fab fragments of the human monoclonal antibody CR4354.* Proceedings of the National Academy of Sciences, 2010-11-2. **107**(44).
167. Lee, P.S., et al., *Design and Structure of an Engineered Disulfide-Stabilized Influenza Virus Hemagglutinin Trimer.* Journal of Virology, 2015-4-29. **89**(14).
168. Schroeder, M., et al., *In silico Design, Synthesis, and Screening of Novel Deoxyhypusine Synthase Inhibitors Targeting HIV-1 Replication.* ChemMedChem, 2014/05/01. **9**(5).
169. Nan, Y., et al., *Improved Vaccine against PRRSV: Current Progress and Future Perspective.* Frontiers in Microbiology, 2017. **8**.
170. Spilman, M.S., et al., *Cryo-electron tomography of porcine reproductive and respiratory syndrome virus: organization of the nucleocapsid.* Journal of General Virology, 2009/03/01. **90**(3).
171. Murtaugh, M.P. and M. Genzow, *Immunological solutions for treatment and prevention of porcine reproductive and respiratory syndrome (PRRS)*. Vaccine, 10/26/2011. **29**(46).
172. Darwich, L., I. Díaz, and E. Mateu, *Certainties, doubts and hypotheses in porcine reproductive and respiratory syndrome virus immunobiology.* Virus Res, 2010. **154**(1-2): p. 123-32.
173. Xu, H., et al., *[Screening of polypeptides binding to porcine reproductive and respiratory syndrome virus by phage display library].* Wei Sheng Wu Xue Bao, 2011. **51**(1): p. 127-33.
174. Oleksiewicz, M.B., et al., *Epitope mapping porcine reproductive and respiratory syndrome virus by phage display: the nsp2 fragment of the replicase polyprotein contains a cluster of B-cell epitopes.* J Virol, 2001. **75**(7): p. 3277-90.
175. Li, K., et al., *Generation of porcine monoclonal antibodies based on single cell technologies.* Vet Immunol Immunopathol, 2019. **215**: p. 109913.
176. Stadejek, T., et al., *Molecular evolution of PRRSV in Europe: current state of play.* Vet Microbiol, 2013. **165**(1-2): p. 21-8.
177. Meng, X.J., *Heterogeneity of porcine reproductive and respiratory syndrome virus: implications for current vaccine efficacy and future vaccine development.* Vet Microbiol, 2000. **74**(4): p. 309-29.
178. de Lima, M., et al., *Serologic marker candidates identified among B-cell linear epitopes of Nsp2 and structural proteins of a North American strain of porcine reproductive and respiratory syndrome virus*. 2006, Academic Press. p. 410-421.
179. Cao, S., et al., *The tail domain of PRRSV NSP2 plays a key role in aggrephagy by interacting with 14-3-3ε.* Veterinary Research, 2020. **51**(1): p. 104.
180. Su, J., et al., *Nsp2 and GP5-M of Porcine Reproductive and Respiratory Syndrome Virus Contribute to Targets for Neutralizing Antibodies.* Virol Sin, 2019. **34**(6): p. 631-640.

181. Yin, B., et al., *Molecular Characterization of the Nsp2 and ORF5 (ORF5a) Genes of PRRSV Strains in Nine Provinces of China During 2016–2018.* Frontiers in Veterinary Science, 2021/03/04. **8**.
182. Bai, W., et al., *The molecular characteristic analysis of PRRSV GSWW/2015 strain and its pathogenicity to pigs.* BMC Veterinary Research 2018 14:1, 2018-08-17. **14**(1).
183. Dea, S., et al., *Current knowledge on the structural proteins of porcine reproductive and respiratory syndrome (PRRS) virus: Comparison of the North American and European isolates*. 2000, Springer Wien. p. 659-688.
184. Wootton, S.K., R.R.R. Rowland, and D. Yoo, *Phosphorylation of the Porcine Reproductive and Respiratory Syndrome Virus Nucleocapsid Protein.* Journal of Virology, 2002/10. **76**(20).
185. Wootton, S.K. and D. Yoo, *Homo-Oligomerization of the Porcine Reproductive and Respiratory Syndrome Virus Nucleocapsid Protein and the Role of Disulfide Linkages.* Journal of Virology, 2003/04. **77**(8).
186. Lee, C., et al., *Mutations within the nuclear localization signal of the porcine reproductive and respiratory syndrome virus nucleocapsid protein attenuate virus replication.* Virology, 2006/03/03. **346**(1).
187. Meulenberg, J.J.M., et al., *Lelystad Virus, the Causative Agent of Porcine Epidemic Abortion and Respiratory Syndrome (PEARS), Is Related to LDV and EAV.* Virology, 1993. **192**(1): p. 62-72.
188. Veit, M., et al., *Membrane proteins of arterivirus particles: Structure, topology, processing and function*. 2014, Elsevier. p. 16.
189. Wissink, E.H.J., et al., *The major envelope protein, GP5, of a European porcine reproductive and respiratory syndrome virus contains a neutralization epitope in its N-terminal ectodomain*. 2003, Microbiology Society. p. 1535-1543.
190. Wissink, E.H.J., et al., *Significance of the oligosaccharides of the porcine reproductive and respiratory syndrome virus glycoproteins GP2a and GP5 for infectious virus production*. 2004, Microbiology Society. p. 3715-3723.
191. Ansari, I.H., et al., *Influence of N-Linked Glycosylation of Porcine Reproductive and Respiratory Syndrome Virus GP5 on Virus Infectivity, Antigenicity, and Ability To Induce Neutralizing Antibodies*. 2006, American Society for Microbiology. p. 3994-4004.
192. Luo, Q., et al., *Genetic variation and recombination analysis of the GP5 (GP5a) gene of PRRSV-2 strains in China from 1996 to 2022.* Front Microbiol, 2023. **14**: p. 1238766.
193. Fan, B., et al., *The amino acid residues at 102 and 104 in GP5 of porcine reproductive and respiratory syndrome virus regulate viral neutralization susceptibility to the porcine serum neutralizing antibody.* Virus Res, 2015. **204**: p. 21-30.
194. Ostrowski, M., et al., *Identification of Neutralizing and Nonneutralizing Epitopes in the Porcine Reproductive and Respiratory Syndrome Virus GP5 Ectodomain*. 2002, American Society for Microbiology. p. 4241-4250.
195. Delisle, B., et al., *Porcine reproductive and respiratory syndrome virus diversity of Eastern Canada swine herds in a large sequence dataset reveals two hypervariable regions under positive selection.* Infection, Genetics and Evolution, 2012. **12**(5): p. 1111-1119.
196. Kim, W.I., et al., *Significance of genetic variation of PRRSV ORF5 in virus neutralization and molecular determinants corresponding to cross neutralization among PRRS viruses.* Vet Microbiol, 2013. **162**(1): p. 10-22.
197. Li, J. and M.P. Murtaugh, *Dissociation of porcine reproductive and respiratory syndrome virus neutralization from antibodies specific to major envelope protein surface epitopes.* Virology, 2012. **433**(2): p. 367-76.

198. Leng, X., et al., *Evaluation of the efficacy of an attenuated live vaccine against highly pathogenic porcine reproductive and respiratory syndrome virus in young pigs.* Clin Vaccine Immunol, 2012. **19**(8): p. 1199-206.
199. Meng, X.J., et al., *Sequence comparison of open reading frames 2 to 5 of low and high virulence United States isolates of porcine reproductive and respiratory syndrome virus.* J Gen Virol, 1995. **76 (Pt 12)**: p. 3181-8.
200. de Vries, A.A., et al., *Structural proteins of equine arteritis virus.* J Virol, 1992. **66**(11): p. 6294-303.
201. Zhao, G., et al., *Immunological evaluation of recombination PRRSV GP3 and GP5 DNA vaccines in vivo.* Front Cell Infect Microbiol, 2022. **12**: p. 1016897.
202. Meulenberg, J.J.M., et al., *Posttranslational Processing and Identification of a Neutralization Domain of the GP 4 Protein Encoded by ORF4 of Lelystad Virus*. 1997. p. 6061-6067.
203. Das, P.B., et al., *Glycosylation of minor envelope glycoproteins of porcine reproductive and respiratory syndrome virus in infectious virus recovery, receptor interaction, and immune response*. 2011, Academic Press. p. 385-394.
204. Meulenberg, J.J.M., et al., *Characterization of proteins encoded by ORFs 2 to 7 of Lelystad virus*. 1995. p. 155-163.
205. Vanhee, M., et al., *Characterization of antigenic regions in the porcine reproductive and respiratory syndrome virus by the use of peptide-specific serum antibodies*. 2011, Elsevier. p. 4794-4804.
206. Wu, W.H., et al., *A 10-kDa structural protein of porcine reproductive and respiratory syndrome virus encoded by ORF2b.* Virology, 2001. **287**(1): p. 183-91.
207. García Durán, M., et al., *Generation of porcine reproductive and respiratory syndrome (PRRS) virus-like-particles (VLPs) with different protein composition.* J Virol Methods, 2016. **236**: p. 77-86.
208. Lee, C. and D. Yoo, *The small envelope protein of porcine reproductive and respiratory syndrome virus possesses ion channel protein-like properties.* Virology, 2006. **355**(1): p. 30-43.
209. Wu, W.H., et al., *The 2b protein as a minor structural component of PRRSV.* Virus Res, 2005. **114**(1-2): p. 177-81.
210. Lalonde, C., C. Provost, and C.A. Gagnon, *Whole-Genome Sequencing of Porcine Reproductive and Respiratory Syndrome Virus from Field Clinical Samples Improves the Genomic Surveillance of the Virus.* J Clin Microbiol, 2020. **58**(11).
211. van Dinten, L.C., et al., *An infectious arterivirus cDNA clone: identification of a replicase point mutation that abolishes discontinuous mRNA transcription.* Proc Natl Acad Sci U S A, 1997. **94**(3): p. 991-6.
212. Firth, A.E., et al., *Discovery of a small arterivirus gene that overlaps the GP5 coding sequence and is important for virus production.* J Gen Virol, 2011. **92**(Pt 5): p. 1097-1106.
213. Jeong, H.J., et al., *Comparative measurement of cell-mediated immune responses of swine to the M and N proteins of porcine reproductive and respiratory syndrome virus.* Clin Vaccine Immunol, 2010. **17**(4): p. 503-12.
214. Hedges, J.F., U.B.R. Balasuriya, and N.J. MacLachlan, *The Open Reading Frame 3 of Equine Arteritis Virus Encodes an Immunogenic Glycosylated, Integral Membrane Protein.* Virology, 1999. **264**(1): p. 92-98.
215. Faaberg, K.S. and P.G.W. Plagemann, *ORF 3 of Lactate Dehydrogenase-Elevating Virus Encodes a Soluble, Nonstructural, Highly Glycosylated, and Antigenic Protein.* Virology, 1997. **227**(1): p. 245-251.
216. Dokland, T., *The structural biology of PRRSV*. 2010, Elsevier. p. 86-97.

217. Mardassi, H., et al., *A Subset of Porcine Reproductive and Respiratory Syndrome Virus GP 3 Glycoprotein Is Released into the Culture Medium of Cells as a Non-Virion-Associated and Membrane-Free (Soluble) Form †*. 1998, American Society for Microbiology (ASM). p. 6298-6306.
218. Zhang, M., et al., *Glycoprotein 3 of porcine reproductive and respiratory syndrome virus exhibits an unusual hairpin-like membrane topology*. 2018, American Society for Microbiology. p. 660-678.
219. Luong, H.Q., et al., *Evaluation of Antibody Response Directed against Porcine Reproductive and Respiratory Syndrome Virus Structural Proteins.* Vaccines 2020, Vol. 8, Page 533, 2020-09-16. **8**(3).
220. Wang, Q., et al., *Unique Epitopes Recognized by Monoclonal Antibodies against HP-PRRSV: Deep Understanding of Antigenic Structure and Virus-Antibody Interaction*. 2014, Public Library of Science. p. e111633.
221. Music, N. and C.A. Gagnon, *The role of porcine reproductive and respiratory syndrome (PRRS) virus structural and non-structural proteins in virus pathogenesis.* Anim Health Res Rev, 2010. **11**(2): p. 135-63.
222. de Lima, M., et al., *GP3 is a structural component of the PRRSV type II (US) virion*. 2009, Academic Press. p. 31-36.
223. Chen, J.z., et al., *Identification of two dominant linear epitopes on the GP3 protein of highly pathogenic porcine reproductive and respiratory syndrome virus (HP-PRRSV)*. 2014, Elsevier B.V. p. 238-243.
224. Zhou, Y.J., et al., *Antigenic structure analysis of glycosylated protein 3 of porcine reproductive and respiratory syndrome virus*. 2006, Elsevier. p. 98-104.
225. Oleksiewicz, M.B., A. Bøtner, and P. Normann, *Porcine B-cells recognize epitopes that are conserved between the structural proteins of American- and European-type porcine reproductive and respiratory syndrome virus*. 2002, Society for General Microbiology. p. 1407-1418.
226. Stoian, A.M.M. and R.R.R. Rowland, *Challenges for porcine reproductive and respiratory syndrome (PRRS) vaccine design: Reviewing virus glycoprotein interactions with CD163 and targets of virus neutralization*. 2019, MDPI Multidisciplinary Digital Publishing Institute.
227. Sun, Q., et al., *Recent Progress in Studies of Porcine Reproductive and Respiratory Syndrome Virus 1 in China.* Viruses, 2023. **15**(7).
228. Chen, N., et al., *ORF5 of porcine reproductive and respiratory syndrome virus (PRRSV) is a target of diversifying selection as infection progresses from acute infection to virus rebound.* Infect Genet Evol, 2016. **40**: p. 167-175.
229. Evans, A.B., et al., *Antigenic and Biological Characterization of ORF2-6 Variants at Early Times Following PRRSV Infection.* Viruses, 2017. **9**(5).
230. Zhang, Z., et al., *A broadly neutralizing monoclonal antibody induces broad protection against heterogeneous PRRSV strains in piglets*. 2021, BioMed Central Ltd. p. 1-23.
231. Van Nieuwstadt, A.P., et al., *Proteins Encoded by Open Reading Frames 3 and 4 of the Genome of Lelystad Virus (Arteriviridae) Are Structural Proteins of the Virion*. 1996. p. 4767-4772.
232. Oleksiewicz, M.B., et al., *RAPID COMMUNICATION Emergence of Porcine Reproductive and Respiratory Syndrome Virus Deletion Mutants: Correlation with the Porcine Antibody Response to a Hypervariable Site in the ORF 3 Structural Glycoprotein*. 2000.
233. Costers, S., et al., *GP4-specific neutralizing antibodies might be a driving force in PRRSV evolution*. 2010, Virus Res. p. 104-113.
234. Kelley, L.A., et al., *The Phyre2 web portal for protein modeling, prediction and analysis.* Nature Protocols, 2015. **10**(6): p. 845-858.

235. Almagro Armenteros, J.J., et al., *SignalP 5.0 improves signal peptide predictions using deep neural networks.* Nat Biotechnol, 2019. **37**(4): p. 420-423.
236. Krogh, A., et al., *Predicting transmembrane protein topology with a hidden Markov model: application to complete genomes.* J Mol Biol, 2001. **305**(3): p. 567-80.
237. Jumper, J., et al., *Highly accurate protein structure prediction with AlphaFold.* Nature, 2021. **596**(7873): p. 583-589.
238. Rose, A.S., et al., *NGL viewer: web-based molecular graphics for large complexes.* Bioinformatics, 2018. **34**(21): p. 3755-3758.
239. Luger, K., et al., *Crystal structure of the nucleosome core particle at 2.8 A resolution.* Nature, 1997. **389**(6648): p. 251-60.
240. Berrow, N.S., et al., *A versatile ligation-independent cloning method suitable for high-throughput expression screening applications.* Nucleic Acids Res, 2007. **35**(6): p. e45.
241. Kim, H.S., et al., *Enhanced replication of porcine reproductive and respiratory syndrome (PRRS) virus in a homogeneous subpopulation of MA-104 cell line.* Arch Virol, 1993. **133**(3-4): p. 477-83.
242. Wu, X., et al., *Establishment and Characterization of a High and Stable Porcine CD163-Expressing MARC-145 Cell Line.* BioMed Research International, 2018. **2018**: p. 4315861.
243. Tan, T.K., et al., *A COVID-19 vaccine candidate using SpyCatcher multimerization of the SARS-CoV-2 spike protein receptor-binding domain induces potent neutralising antibody responses.* Nat Commun, 2021. **12**(1): p. 542.
244. Lefranc, M.-P., *IMGT, the International ImMunoGeneTics Information System.* Cold Spring Harbor Protocols, 2011-06-01. **2011**(6).
245. Manso, T., et al., *IMGT® databases, related tools and web resources through three main axes of research and development.* Nucleic Acids Research, 2022/01/07. **50**(D1).
246. Lefranc, M.-P., et al., *IMGT®, the international ImMunoGeneTics information system® 25 years on.* Nucleic Acids Research, 2015/01/28. **43**(D1).
247. Plana, J., et al., *Porcine epidemic abortion and respiratory syndrome (mystery swine disease). Isolation in Spain of the causative agent and experimental reproduction of the disease.* Veterinary Microbiology, 1992. **33**(1): p. 203-211.
248. Weesendorp, E., et al., *Comparative analysis of immune responses following experimental infection of pigs with European porcine reproductive and respiratory syndrome virus strains of differing virulence.* Vet Microbiol, 2013. **163**(1-2): p. 1-12.
249. Morgan, S.B., et al., *Increased pathogenicity of European porcine reproductive and respiratory syndrome virus is associated with enhanced adaptive responses and viral clearance.* Veterinary Microbiology, 2013/04/12. **163**(1-2).
250. Collins, J.E., et al., *Isolation of swine infertility and respiratory syndrome virus (isolate ATCC VR-2332) in North America and experimental reproduction of the disease in gnotobiotic pigs.* J Vet Diagn Invest, 1992. **4**(2): p. 117-26.
251. Goldeck, D., et al., *Establishment of Systems to Enable Isolation of Porcine Monoclonal Antibodies Broadly Neutralizing the Porcine Reproductive and Respiratory Syndrome Virus*. 2019.
252. Mokhtar, H., et al., *The Non-structural Protein 5 and Matrix Protein Are Antigenic Targets of T Cell Immunity to Genotype 1 Porcine Reproductive and Respiratory Syndrome Viruses.* Frontiers in Immunology, 2016/02/16. **7**.
253. Edgar, R.C., *Search and clustering orders of magnitude faster than BLAST.* Bioinformatics, 2010. **26**(19): p. 2460-1.

254. Tamura, K., G. Stecher, and S. Kumar, *MEGA11: Molecular Evolutionary Genetics Analysis Version 11.* Mol Biol Evol, 2021. **38**(7): p. 3022-3027.
255. Zost, S.J., et al., *Rapid isolation and profiling of a diverse panel of human monoclonal antibodies targeting the SARS-CoV-2 spike protein.* Nature Medicine, 2020. **26**(9): p. 1422-1427.
256. Fairhead, M. and M. Howarth, *Site-specific biotinylation of purified proteins using BirA.* Methods Mol Biol, 2015. **1266**: p. 171-84.
257. Fitzpatrick, K.S., et al., *Validation of antigen tetramers for the detection of antigen-specific B cells.* bioRxiv, 2022: p. 2022.10.24.513230.
258. Franz, B., et al., *Ex vivo characterization and isolation of rare memory B cells with antigen tetramers.* Blood, 2011. **118**(2): p. 348-57.
259. Howarth, M. and A.Y. Ting, *Imaging proteins in live mammalian cells with biotin ligase and monovalent streptavidin.* Nat Protoc, 2008. **3**(3): p. 534-45.
260. Meulenberg, J.J., et al., *Nucleocapsid protein N of Lelystad virus: expression by recombinant baculovirus, immunological properties, and suitability for detection of serum antibodies.* Clin Diagn Lab Immunol, 1995. **2**(6): p. 652-6.
261. Kreutz, L.C. and W.L. Mengeling, *Baculovirus expression and immunological detection of the major structural proteins of porcine reproductive and respiratory syndrome virus.* Veterinary Microbiology, 1997. **59**(1): p. 1-13.
262. Khan, K.H., *Gene expression in Mammalian cells and its applications.* Adv Pharm Bull, 2013. **3**(2): p. 257-63.
263. Lu, Z.H., A.L. Archibald, and T. Ait-Ali, *Beyond the whole genome consensus: unravelling of PRRSV phylogenomics using next generation sequencing technologies.* Virus Res, 2014. **194**: p. 167-74.
264. EMBL-EBI. *Frequently asked questions*. 2023 09/10/2023].
265. Ye, Y. and A. Godzik, *Flexible structure alignment by chaining aligned fragment pairs allowing twists.* Bioinformatics, 2003. **19**(suppl_2): p. ii246-ii255.
266. Li, Z., et al., *FATCAT 2.0: towards a better understanding of the structural diversity of proteins.* Nucleic Acids Research, 2020. **48**(W1): p. W60-W64.
267. Ellgaard, L. and A. Helenius, *Quality control in the endoplasmic reticulum.* Nat Rev Mol Cell Biol, 2003. **4**(3): p. 181-91.
268. Kufareva, I. and R. Abagyan, *Methods of protein structure comparison.* Methods Mol Biol, 2012. **857**: p. 231-57.
269. Zhang, W., et al., *An integrated analysis of membrane remodeling during porcine reproductive and respiratory syndrome virus replication and assembly.* PLOS ONE, 2018. **13**(7): p. e0200919.
270. Yang, Q., et al., *Lipid rafts both in cellular membrane and viral envelope are critical for PRRSV efficient infection.* Virology, 2015. **484**: p. 170-180.
271. Matczuk, A.K., et al., *Expression of the Heterotrimeric GP2/GP3/GP4 Spike of an Arterivirus in Mammalian Cells.* Viruses, 2022. **14**(4).
272. Li, J., et al., *N-glycosylation profiling of porcine reproductive and respiratory syndrome virus envelope glycoprotein 5.* Virology, 2015. **478**: p. 86-98.
273. Wei, Z., et al., *Influence of N-linked glycosylation of minor proteins of porcine reproductive and respiratory syndrome virus on infectious virus recovery and receptor interaction*. 2012, Academic Press. p. 1-11.
274. Zucchelli, S., et al., *SINEUPs are modular antisense long non-coding RNAs that increase synthesis of target proteins in cells.* Front Cell Neurosci, 2015. **9**: p. 174.
275. Reddy Chichili, V.P., V. Kumar, and J. Sivaraman, *Linkers in the structural biology of protein-protein interactions.* Protein Sci, 2013. **22**(2): p. 153-67.
276. Chen, X., J.L. Zaro, and W.C. Shen, *Fusion protein linkers: property, design and functionality.* Adv Drug Deliv Rev, 2013. **65**(10): p. 1357-69.

277. Rahe, M.C., et al., *The PRRSV-Specific Memory B Cell Response Is Long-Lived in Blood and Is Boosted During Live Virus Re-exposure.* Front Immunol, 2020. **11**: p. 247.
278. Rahe, M.C., K.L. Gustafson, and M.P. Murtaugh, *B Cell Tetramer Development for Veterinary Vaccinology.* Viral Immunol, 2018. **31**(1): p. 1-10.
279. Rahe, M.C. and M.P. Murtaugh, *Mechanisms of Adaptive Immunity to Porcine Reproductive and Respiratory Syndrome Virus.* Viruses, 2017. **9**(6).
280. Mulupuri, P., et al., *Antigen-specific B-cell responses to porcine reproductive and respiratory syndrome virus infection.* J Virol, 2008. **82**(1): p. 358-70.
281. Wilson, H.L. and M.R. Obradovic, *Evidence for a common mucosal immune system in the pig.* Mol Immunol, 2015. **66**(1): p. 22-34.
282. Mardassi, H., et al., *A subset of porcine reproductive and respiratory syndrome virus GP3 glycoprotein is released into the culture medium of cells as a non-virion-associated and membrane-free (soluble) form*. 1998, J Virol. p. 6298-6306.
283. *Recombinant Protein - an overview | ScienceDirect Topics.* Enzymes, 2011.
284. Mukhopadhyay, A., P.K. Bhatia, and S.S. Majumdar, *Preliminary studies with recombinant chorionic gonadotropin beta-subunit produced in Escherichia coli for use as an antigen in a birth control vaccine.* Am J Reprod Immunol, 1998. **39**(3): p. 172-82.
285. Gristick, H.B., et al., *Natively glycosylated HIV-1 Env structure reveals new mode for antibody recognition of the CD4-binding site.* Nat Struct Mol Biol, 2016. **23**(10): p. 906-915.
286. Wu, X., et al., *Rational design of envelope identifies broadly neutralizing human monoclonal antibodies to HIV-1.* Science, 2010. **329**(5993): p. 856-61.
287. Holzer, B., et al., *Protective porcine influenza virus-specific monoclonal antibodies recognize similar haemagglutinin epitopes as humans.* PLoS Pathog, 2021. **17**(3): p. e1009330.
288. Ramirez Valdez, K., et al., *A Customizable Suite of Methods to Sequence and Annotate Cattle Antibodies.* Vaccines, 2023. **11**(6): p. 1099.
289. Wu, S., et al., *Fabs enable single particle cryoEM studies of small proteins.* Structure, 2012. **20**(4): p. 582-92.
290. Dunbar, J., et al., *SAbPred: a structure-based antibody prediction server.* Nucleic Acids Res, 2016. **44**(W1): p. W474-8.
291. Bradley, J.E. and T.R. Unnasch, *Molecular approaches to the diagnosis of onchocerciasis.* Adv Parasitol, 1996. **37**: p. 57-106.
292. Reed, S.G., M.T. Orr, and C.B. Fox, *Key roles of adjuvants in modern vaccines.* Nature Medicine, 2013. **19**(12): p. 1597-1608.
293. Awate, S., L.A. Babiuk, and G. Mutwiri, *Mechanisms of action of adjuvants.* Front Immunol, 2013. **4**: p. 114.
294. Huang, W.C., et al., *A malaria vaccine adjuvant based on recombinant antigen binding to liposomes.* Nat Nanotechnol, 2018. **13**(12): p. 1174-1181.
295. Federizon, J., et al., *Immunogenicity of the Lyme disease antigen OspA, particleized by cobalt porphyrin-phospholipid liposomes.* Vaccine, 2020. **38**(4): p. 942-950.
296. Sia, Z.R., et al., *A liposome-displayed hemagglutinin vaccine platform protects mice and ferrets from heterologous influenza virus challenge.* Proc Natl Acad Sci U S A, 2021. **118**(22).
297. Mabrouk, M.T., et al., *Lyophilized, antigen-bound liposomes with reduced MPLA and enhanced thermostability.* Int J Pharm, 2020. **589**: p. 119843.
298. Soheili, M., et al., *The efficacy and effectiveness of COVID-19 vaccines around the world: a mini-review and meta-analysis.* Annals of Clinical Microbiology and Antimicrobials, 2023. **22**(1): p. 42.

299. Bloom, K., F. van den Berg, and P. Arbuthnot, *Self-amplifying RNA vaccines for infectious diseases.* Gene Therapy, 2021. **28**(3): p. 117-129.
300. Jackson, N.A.C., et al., *The promise of mRNA vaccines: a biotech and industrial perspective.* NPJ Vaccines, 2020. **5**: p. 11.
301. Beckert, B. and B. Masquida, *Synthesis of RNA by in vitro transcription.* Methods Mol Biol, 2011. **703**: p. 29-41.
302. Pardi, N., et al., *In vitro transcription of long RNA containing modified nucleosides.* Methods Mol Biol, 2013. **969**: p. 29-42.
303. Vogel, A.B., et al., *Self-Amplifying RNA Vaccines Give Equivalent Protection against Influenza to mRNA Vaccines but at Much Lower Doses.* Mol Ther, 2018. **26**(2): p. 446-455.
304. Tews, B.A. and G. Meyers, *Self-Replicating RNA.* Methods Mol Biol, 2017. **1499**: p. 15-35.
305. Geall, A.J., et al., *Nonviral delivery of self-amplifying RNA vaccines.* Proc Natl Acad Sci U S A, 2012. **109**(36): p. 14604-9.
306. Komori, M., et al., *saRNA vaccine expressing membrane-anchored RBD elicits broad and durable immunity against SARS-CoV-2 variants of concern.* Nature Communications, 2023. **14**(1): p. 2810.
307. Elliott, T., et al., *Enhanced immune responses following heterologous vaccination with self-amplifying RNA and mRNA COVID-19 vaccines.* PLOS Pathogens, Oct 4, 2022. **18**(10).
308. Liu, Y., Y. Li, and Q. Hu, *Advances in saRNA Vaccine Research against Emerging/Re-Emerging Viruses.* Vaccines (Basel), 2023. **11**(7).
309. Pollard, C., et al., *Type I IFN counteracts the induction of antigen-specific immune responses by lipid-based delivery of mRNA vaccines.* Mol Ther, 2013. **21**(1): p. 251-9.
310. Burakova, Y., et al., *Adjuvants for Animal Vaccines.* Viral Immunology, 2017. **31**(1): p. 11-22.
311. Valtulini, S., et al., *Aluminium hydroxide-induced granulomas in pigs.* Vaccine, 2005. **23**(30): p. 3999-4004.
312. Wilson-Welder, J.H., et al., *Vaccine adjuvants: current challenges and future approaches.* J Pharm Sci, 2009. **98**(4): p. 1278-316.
313. Straw, B.E., et al., *Comparison of tissue reactions produced by Haemophilus pleuropneumoniae vaccines made with six different adjuvants in swine.* Can J Comp Med, 1985. **49**(2): p. 149-51.
314. Aucouturier, J., et al., *Assessment of efficacy and safety of various adjuvant formulations with a total soluble extract of Trichinella spiralis.* Parasite, 2001. **8**(2 Suppl): p. S126-32.
315. Shi, J., *Q-Vant Biosciences Announces Positive Study Results for Its Sustainable Quillaja-Based Vaccine Adjuvant, Q-VET-S®, in Kansas State's Classic Swine Fever Vaccine*. 2023, Q-VANT Biosciences: https://q-vant.com/q-vant-biosciences-announces-positive-study-results-for-its-sustainable-quillaja-based-vaccine-adjuvant-q-vet-s-in-kansas-states-classic-swine-fever-vaccine/.
316. Zhang, A., et al., *Beyond neutralization: Fc-dependent antibody effector functions in SARS-CoV-2 infection.* Nature Reviews Immunology, 2023. **23**(6): p. 381-396.
317. Wingfield, P.T., *Overview of the purification of recombinant proteins.* Curr Protoc Protein Sci, 2015. **80**: p. 6.1.1-6.1.35.
318. Wang, Z., et al., *Isolation of single HIV-1 Envelope specific B cells and antibody cloning from immunized rhesus macaques.* J Immunol Methods, 2020. **478**: p. 112734.
319. Woda, M., et al., *Dynamics of Dengue Virus (DENV)-Specific B Cells in the Response to DENV Serotype 1 Infections, Using Flow Cytometry With Labeled Virions.* J Infect Dis, 2016. **214**(7): p. 1001-9.

320. Sullivan, E., et al., *SARS-CoV-2 Virus-like Particles Produced by a Single Recombinant Baculovirus Generate Anti-S Antibody and Protect against Variant Challenge.* Viruses, 2022. **14**(5).
321. Nooraei, S., et al., *Virus-like particles: preparation, immunogenicity and their roles as nanovaccines and drug nanocarriers.* Journal of Nanobiotechnology, 2021. **19**(1): p. 59.
322. Tagliamonte, M., et al., *Chapter Eleven - Virus-Like Particles*, in *Micro and Nanotechnology in Vaccine Development*, M. Skwarczynski and I. Toth, Editors. 2017, William Andrew Publishing. p. 205-219.
323. Jennings, G.T. and M.F. Bachmann, *The coming of age of virus-like particle vaccines.* Biological Chemistry, 2008. **389**(5): p. 521-536.
324. Uribe-Campero, L., et al., *Plant-based porcine reproductive and respiratory syndrome virus VLPs induce an immune response in mice.* Research in Veterinary Science, 2015. **102**: p. 59-66.
325. VanderBurgt, J.T., et al., *Plant production of a virus-like particle-based vaccine candidate against porcine reproductive and respiratory syndrome.* Frontiers in Plant Science, 2023. **14**.
326. Van Noort, A., et al., *Intranasal immunization of pigs with porcine reproductive and respiratory syndrome virus-like particles plus 2', 3'-cGAMP VacciGrade™ adjuvant exacerbates viremia after virus challenge.* Virology Journal, 2017. **14**(1): p. 76.
327. Mokhtar, H., et al., *Proteome-wide screening of the European porcine reproductive and respiratory syndrome virus reveals a broad range of T cell antigen reactivity.* Vaccine, 2014. **32**(50): p. 6828-37.
328. Zhao, J., et al., *Establishment of a peptide-based enzyme-linked immunosorbent assay for detecting antibodies against PRRSV M protein.* BMC Vet Res, 2021. **17**(1): p. 355.
329. Berman, H.M., et al., *The Protein Data Bank.* Nucleic Acids Research, 2000. **28**(1): p. 235-242.
330. Cia, G., F. Pucci, and M. Rooman, *Critical review of conformational B-cell epitope prediction methods.* Brief Bioinform, 2023. **24**(1).
331. Chen, R., et al., *A porcine reproductive and respiratory syndrome virus (PRRSV)-specific IgM as a novel adjuvant for an inactivated PRRSV vaccine improves protection efficiency and enhances cell-mediated immunity against heterologous PRRSV challenge.* Vet Res, 2022. **53**(1): p. 65.
332. Montague, Z., et al., *Dynamics of B-cell repertoires and emergence of cross-reactive responses in COVID-19 patients with different disease severity.* medRxiv, 2021.
333. Greiff, V., et al., *A bioinformatic framework for immune repertoire diversity profiling enables detection of immunological status.* Genome Medicine, 2015. **7**(1): p. 49.
334. Yaari, G. and S.H. Kleinstein, *Practical guidelines for B-cell receptor repertoire sequencing analysis.* Genome Medicine, 2015. **7**(1): p. 121.
335. Han, K., et al., *Comparative Virulence of Reproductive Diseases Caused by Type 1 (European-like) and Type 2 (North American-like) Porcine Reproductive and Respiratory Syndrome Virus in Experimentally Infected Pregnant Gilts.* Journal of Comparative Pathology, 2014. **150**(2): p. 297-305.